P4/US/1/68

Proceedings of the
Symposium on

CORRELATION OF MATERIAL CHARACTERISTICS WITH SYSTEMS PERFORMANCE

held at

Have Vol I as #11351

USAF CONFERENCE FACILITY
Orlando Air Force Base, Florida

May 10-12, 1967

Sponsored by

The Technical Cooperation Program

Arranged by

Air Force Materials Laboratory

Wright-Patterson Air Force Base, Ohio

VOLUM

ACKNOWLEDGEMENT:

On behalf of the Working Group "Methods of Testing and Evaluation of Materials", the conference committee takes this opportunity to express its appreciation to the following:

The Air Force Materials Laboratory for arranging the use of the USAF Conference Facility at Orlando, Florida and for funding the support of the symposium.

Mr. W. J. Trapp, AFML, for organizing and conducting the symposium and for editing the proceedings.

The Research Institute of the University of Dayton for their assistance in conducting the symposium and printing of the proceedings.

The personnel of the USAF Conference Facility for their competent and thoughtful assistance at the conference site.

Symposium Committee

W. J. Trapp, Chairman
F. H. Edwards
J. A. Kies
Katharine Mather
P. J. Todkill

Date Recd: 3/17/69 DISPOSITION:

On Dist. List ( ) PLASTEC Destroy

	TO:		
( )	Pebly	( )	( )
( )	Baldanza	( )	( )
( )	Beach	( )	( )
( )	Landrock	( )	( )
( )	Molzon	( )	( )
( )	Shibley	( )	( )
( )	Titus	( )	( )
( )	Anzalone	(X)	( )

COMMENTS:

SITCO / We have Vol 1 on this as # 1135, This one Vol 2 was just located.

P4/US/1/68

Proceedings of the Symposium on

CORRELATION OF MATERIAL CHARACTERISTICS WITH SYSTEMS PERFORMANCE

held at

USAF CONFERENCE FACILITY

Orlando Air Force Base, Florida

May 10-12, 1967

Sponsored by

The Technical Cooperation Program

Arranged by

Air Force Materials Laboratory

Wright-Patterson Air Force Base, Ohio

VOLUME 2

TABLE OF CONTENTS

11829

APPENDIXES

AUTHOR INDEX

PREFACE

F. S. Williams and W. Trapp*

In 1957, the President of the United States and the Prime Minister of Great Britain made a "Declaration of Common Purpose". Subsequently the Canadian and Australian governments also subscribed to this document. The Declaration emphasized the principle of interdependence, based on the concept that the resources of the three countries, and in particular their skilled scientific and technical manpower, could be used to much greater advantage if closer collaboration could be achieved. Accordingly, provisions were made under this Declaration to exchange non-atomic information exchange considerations.

From this Declaration of Common Purpose there has emerged "The Technical Cooperation Program", the primary objectives of which is to eliminate wasteful duplication of Defense research and development effort. A sub-committee reviews the objectives, the resources employed, and the progress achieved in the four countries. It formulates proposals designed to obtain the maximum cooperation and optimum employment of the resources at hand. It also tries to insure complete and continuous interchange of information among the four countries in the specified fields of research and development.

As part of the organization of the TTCP, a Sub-Group on Materials was established which has within it the Working Panel on Methods of Test and Evaluation, the sponsor of the symposium described in these proceedings. The establishment of the Sub-Group on Materials derived from full recognition that advances in performance of weapon systems and supporting equipment were increasingly dependent upon the improvement in the knowledge of the properties and applications of materials and on the improvement of the materials themselves. The ability, however, to readily translate improvements in properties of materials into improvements in the performance of a system is dependent upon the validity of the method of characterizing or testing the material.

While there is an almost limitless variety of test methods in use for characterizing a material, there is very limited information available to show the significance of the test by relating variations in the material property to variations in the service performance of the component or system. Improvements in techniques of correlation would do much to stem the rising cost of test and evaluation.

*F. S. Williams, Chairman Working Panel on Methods of Test and Evaluation

W. Trapp, Chairman, Symposium Committee

The Panel came to the conclusion that it should solicit examples of efforts expended to relate material properties to systems performance as a means of establishing the "state-of-the-art, in this area and through this, to stimulate scientists and engineers in materials and materials application oriented organizations to seek more meaningful relationships, or correlations between laboratory tests and service performance.

With the foregoing as a background, the symposium was planned with a view to presenting papers on testing and evaluation, as applied to a broad spectrum of materials - metallic, non-metallic, and composite. The essential unifying theme or common denomination was the "correlation of material characteristics with system performance".

The Working Panel on Methods of Test and Evaluation desire to express its appreciation to all the participants of the symposium for their important contributions.

RELATIONSHIPS BETWEEN SPECIMEN PERFORMANCE AND STRUCTURE PERFORMANCE IN LOW-CYCLE FATIGUE

M. R. Gross
U. S. Navy Marine Engineering Laboratory
Annapolis, Maryland

Introduction

The existence of a correlation between the behavior of simple laboratory specimens and the performance of complicated engineering structures is often assumed but infrequently demonstrated. It is the purpose of this paper to compare the low-cycle fatigue behavior of laboratory specimens with that of more complex structures and components to demonstrate the existence and extent of correlation.

Tests and Results

The dimensions of the simple laboratory specimen, results from which are used in the comparisons, are shown in Figure 1. A series of these specimens was tested in flexure as cantilever beams. The short end of the specimen was held stationary, while the long end was flexed between fixed stops by a hydraulic piston. A strain gage (0.25-inch gage length) was attached to the minimum test section of the specimen to record the longitudinal strains. The applied loads were obtained from weigh-bars placed in the loading system. Specimens were tested at various strain levels in an air environment under completely reversed conditions. Information recorded during the test was load range, total strain range, and number of cycles to failure. Failure was defined as the development of one or more surface cracks 3/16- to 1/4-inch in length.

There is general agreement that low- and intermediate-cycle fatigue life is total-strain-range dependent.[1, 2, 3] Figure 2 is a log-log plot of total strain range (ε_T) versus number of cycles to failure (N_f) for a wide variety of wrought specimens which differ greatly in basic alloy composition and strength level. The results show that in the life range of about 100 to 50,000 cycles, the low-cycle fatigue lives of many common constructional alloys are similar when compared on the basis of total strain range.

Figure 3 is an internally pressurized box which was developed by MEL to study the low-cycle fatigue behavior of a structural component of greater complexity than a simple laboratory specimen. Boxes have been fabricated from a variety of materials including both ferrous and nonferrous alloys. The internal dimensions of the box are 5 x 5 x 15 inches. They are constructed

from 1-inch thick plate welded together to form the necessary dimensions. The boxes are cyclically pressurized at a constant peak pressure sufficiently high to cause low-cycle fatigue failure.

Figure 4 compares the box test results with those shown in Figure 2. A regression line having the same slope and confidence limits as the specimen data has been constructed through the geometric mean of the box data. It is apparent that the trend and dispersion of the box data are similar to the specimen data despite differences in complexity and failure criteria.

Figure 5 is a photograph of one of the pressure vessels used by the Pressure Vessel Research Committee of the Welding Research Council to study low-cycle fatigue.[4] The results of these tests are compared with MEL specimen data in Figure 6. Included are some data obtained by the Babcock and Wilcox Company in Great Britain. Except for a "tailing-off" at high-cycle lives, the pressure vessels follow the same general trend and dispersion as those of the specimens. As for the specimens and boxes, the low-cycle fatigue behavior of the pressure vessels seems to be independent of variations in composition and/or strength level.

Figure 7 shows the MEL low-cycle fatigue test facility used to evaluate various 70-30 cupronickel piping configurations in pure bending. The pipe size is 4 inches. The piping test results are compared with the specimen results in Figure 8. As in the two previous cases, the trends and dispersions of the results are similar.

Discussion

The results serve to demonstrate the enhancement to be gained in the understanding and analysis of low-cycle fatigue problems when dealing in terms of strain rather than stress. All of the strain data presented for the structures were obtained by dividing the nominal stress by the modulus of elasticity. It is apparent that this simple normalization serves to place specimens and structures on a common basis over a rather broad range of fatigue life.

It should be recognized that the positions of the relationships in the graphs are relative, and any coincidence of specimen and structure results could only be fortuitous. One could shift the relative position in a relationship merely by changing the criterion for failure. For example, if failure of a structure were defined as crack initiation rather than leakage, the relationship would be shifted to the left. From the present state-of-the-art, it is impossible to establish with any degree of certainty the location of the structure relationship relative to that of the specimen without actually conducting a fatigue test of a single structure or model. On the other hand, it would appear that once having

obtained a "fix" from a single test, one then could predict with reasonable accuracy the expected low-cycle fatigue life of a similar structure under different conditions of stress and strain.

Conclusions

On the basis of the correlations examined, it is concluded that complex structural configurations follow the same general low-cycle fatigue relationships as those of simple laboratory specimens. When compared on the basis of total strain range, the low-cycle fatigue life of both specimens and structures appears to be essentially independent of alloy composition and/or yield strength in the life range of about 10^3 to 10^5 cycles. From the observed correlations, it appears that if one were able to obtain a "fix" from a single structural or model test, it would then be possible to predict with reasonable accuracy the low-cycle fatigue life of similar structures under different conditions of stress or strain.

References

1. Langer, B. F., "Design of Pressure Vessels for Low-Cycle Fatigue," Journal of Basic Engineering, ASME Trans., Vol. 84, Series D, No. 3, September 1962, pp 389-402.

2. Gross, M. R., "Low-Cycle Fatigue of Materials for Submarine Construction," Naval Engineers Journal, Vol. 75, No. 5, October 1963, pp 783-797.

3. Manson, S. S. and Hirschberg, M. H., "Fatigue Behavior in Strain Cycling in the Low and Intermediate Cycle Range," Fatigue - An Interdisciplinary Approach, Syracuse University Press (1964).

4. Kooistra, L. F., Lange, E. A., and Pickett, A. G., "Full-Size Pressure Vessel Testing and Its Application to Design," Journal of Engineering for Power, ASME Trans., Vol. 86, Series A, October 1964, pp 419-428.

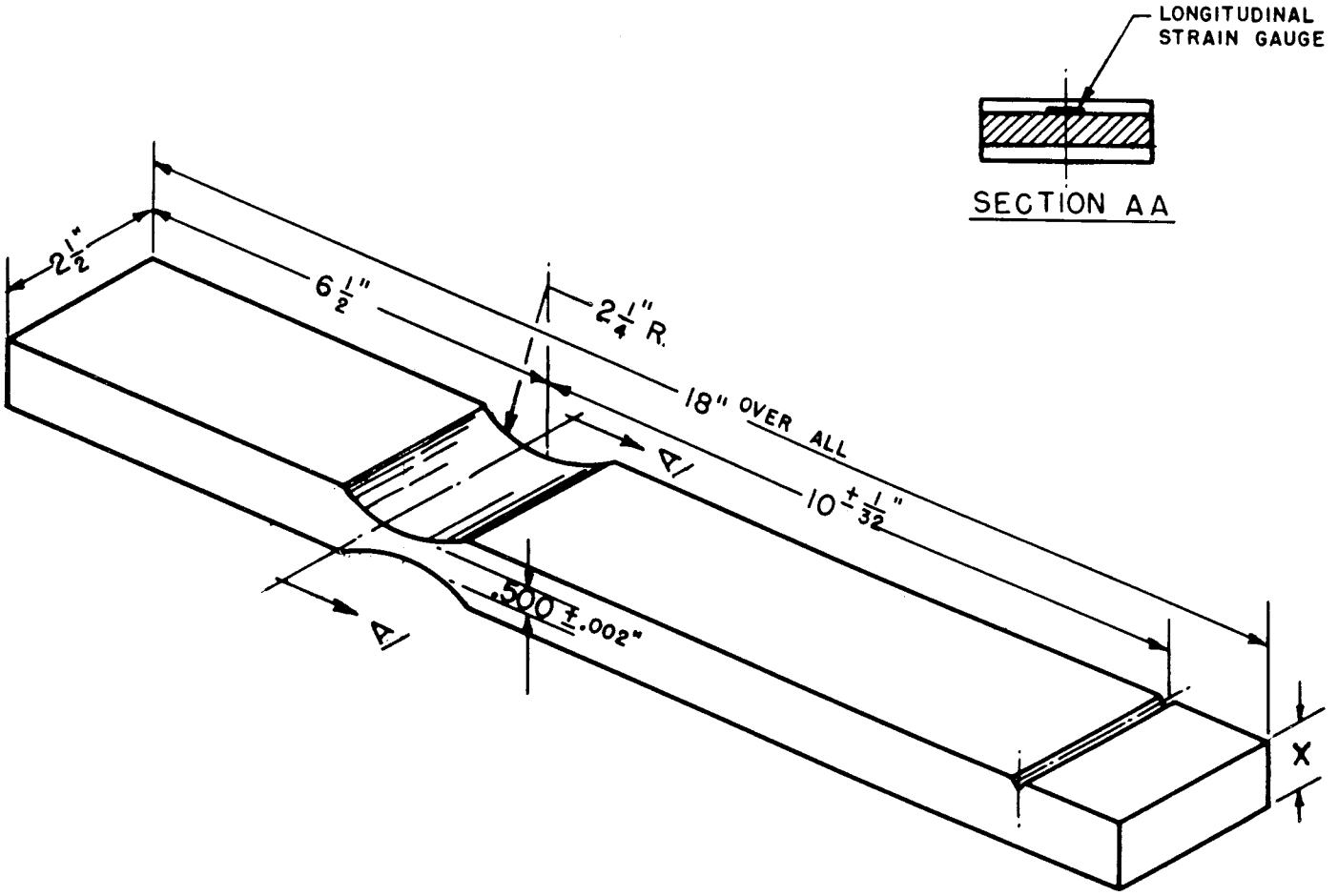

Fig. 1 - Smooth Plastic Strain Fatigue Specimen

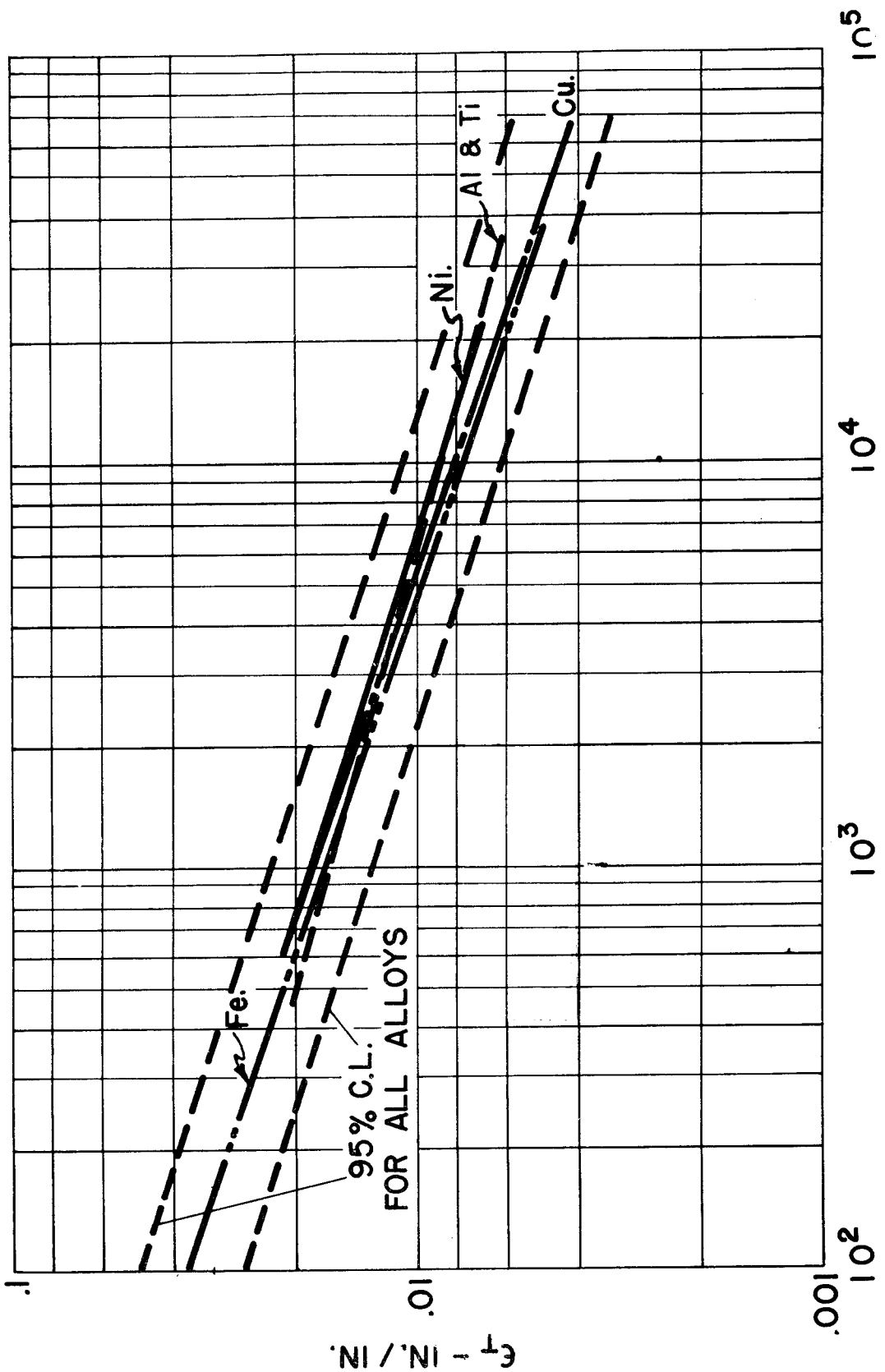

Fig. 2 - Total Strain Range Vs. Cycles to Failure for Wrought Alloys in Air

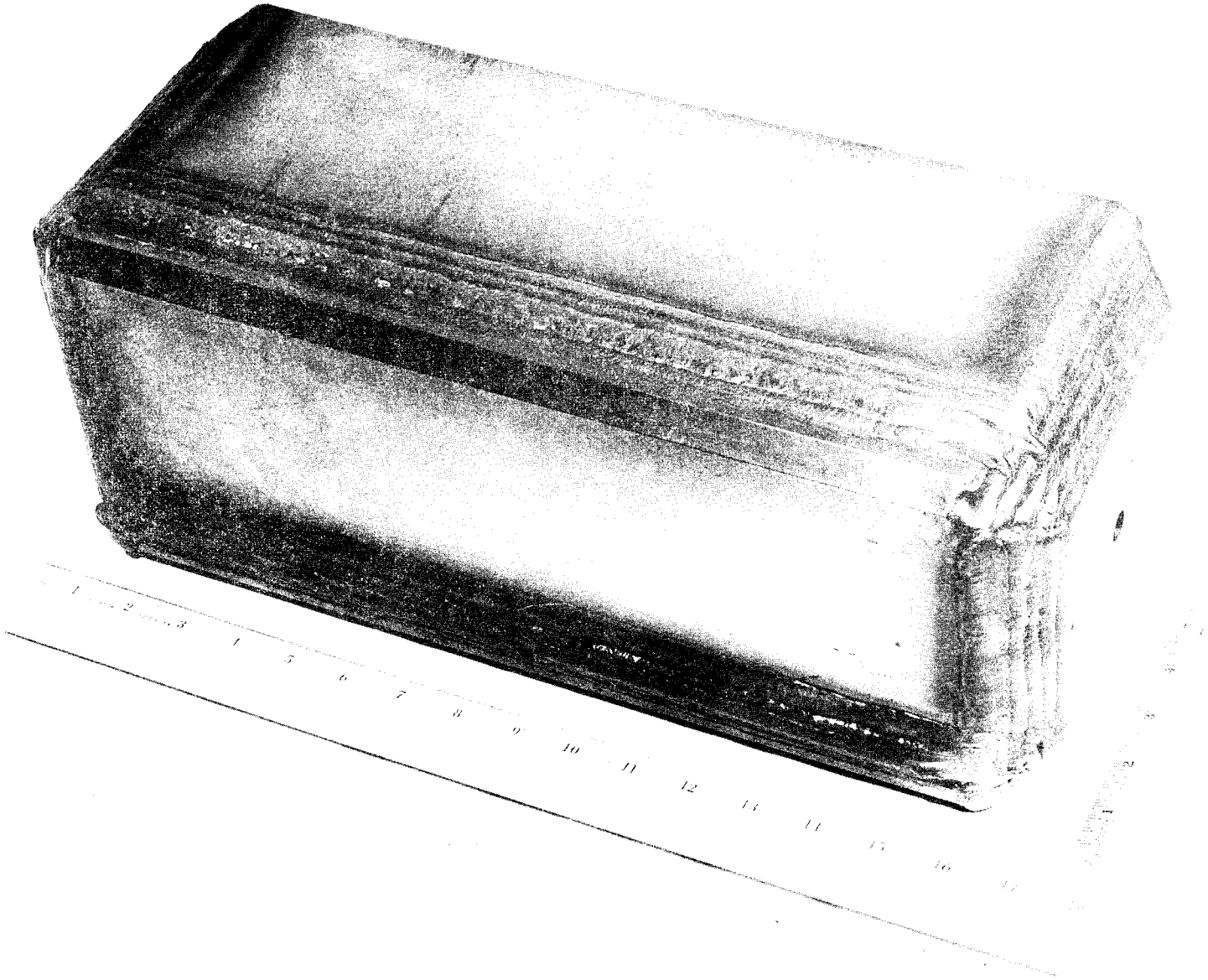

Fig. 3 - J-Weld Box Prior to Test

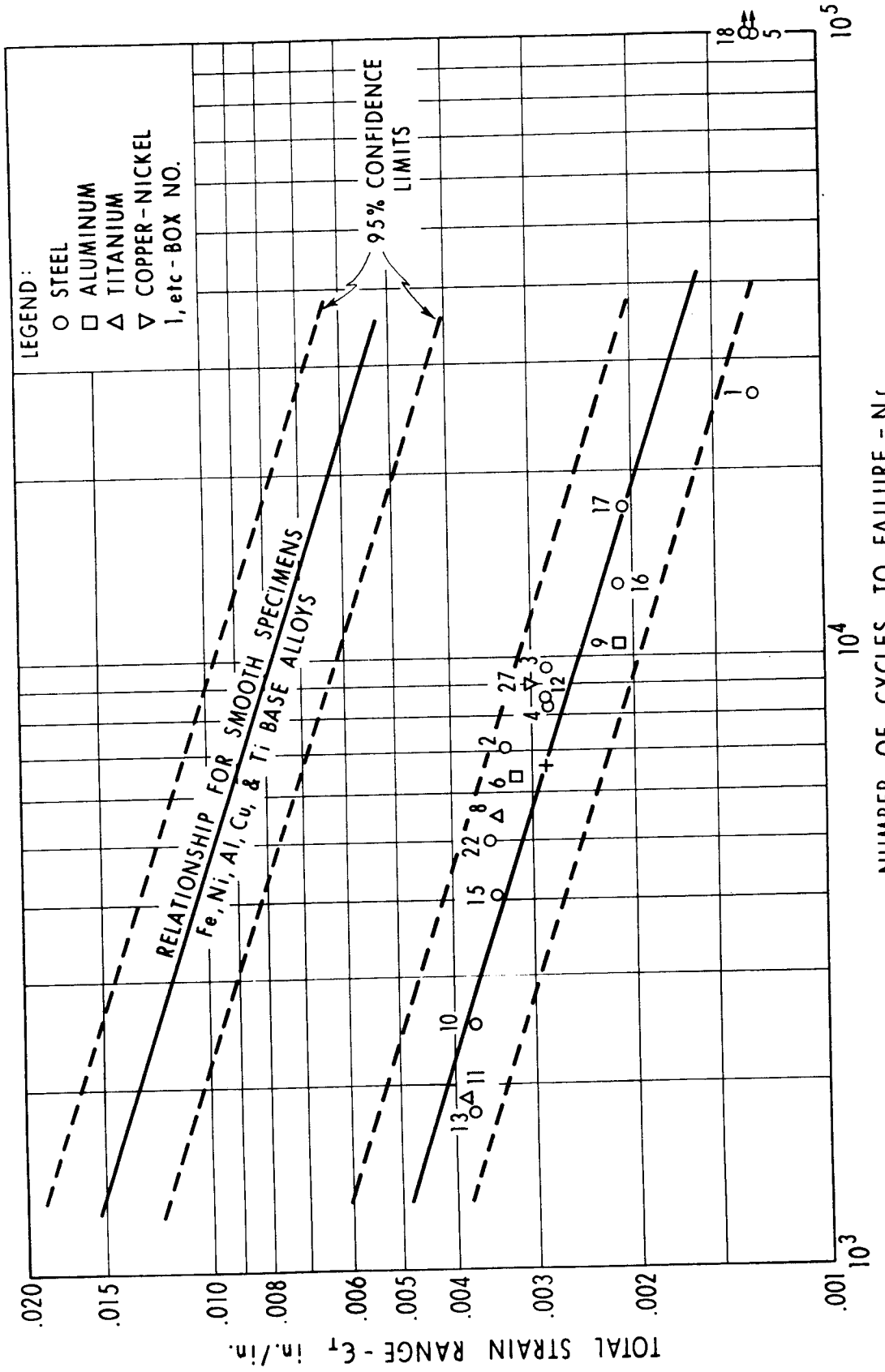

Fig. 4 - Comparison of Box Test Fatigue Results With Specimen Results

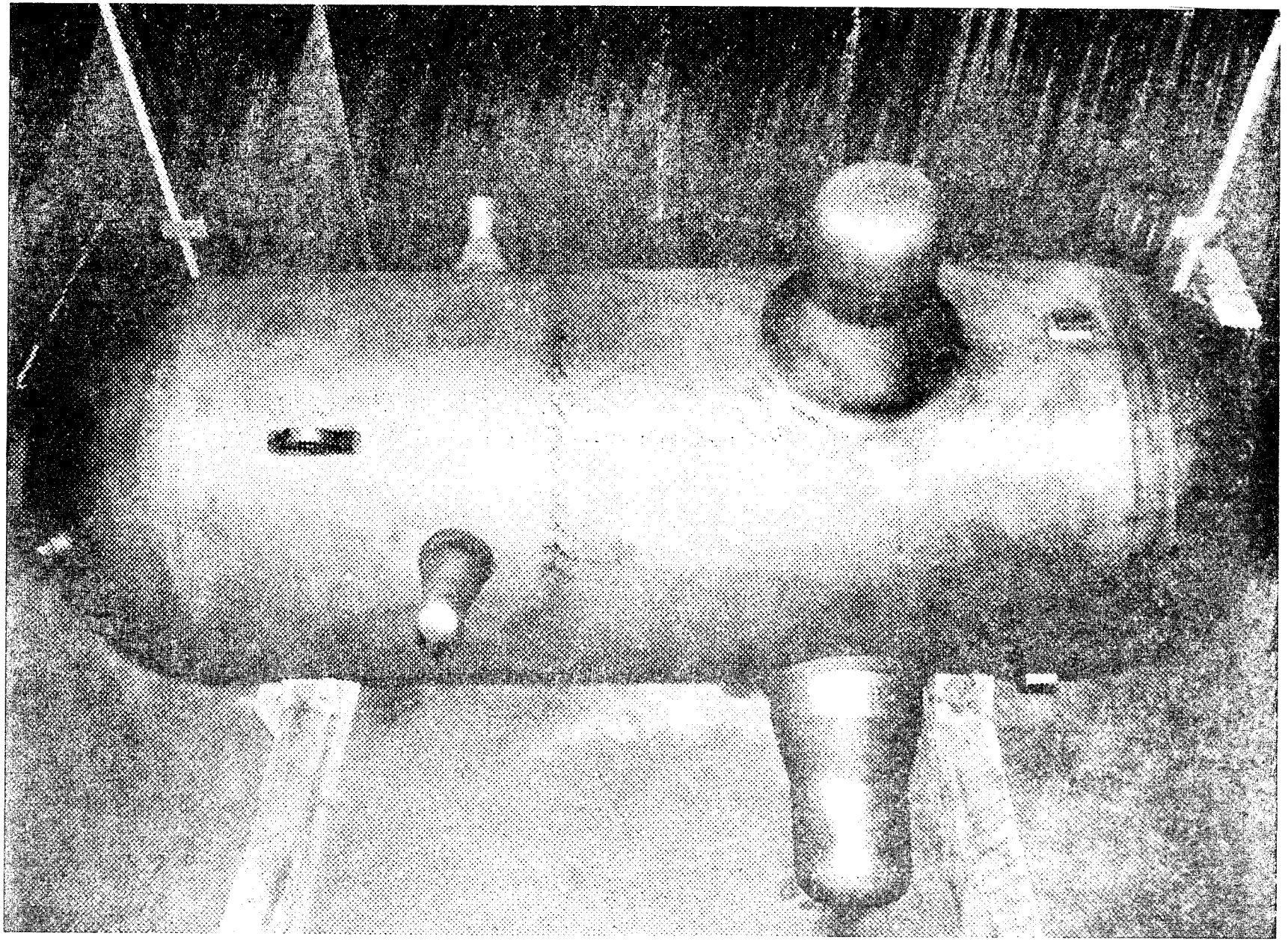

Fig. 5 - Full-Size Pressure Vessel Used in Plastic Fatigue Tests. Materials: A-201, A-302, T-1 (Dimensions: ID = 3 ft, t = 2 in., L = 7 ft).

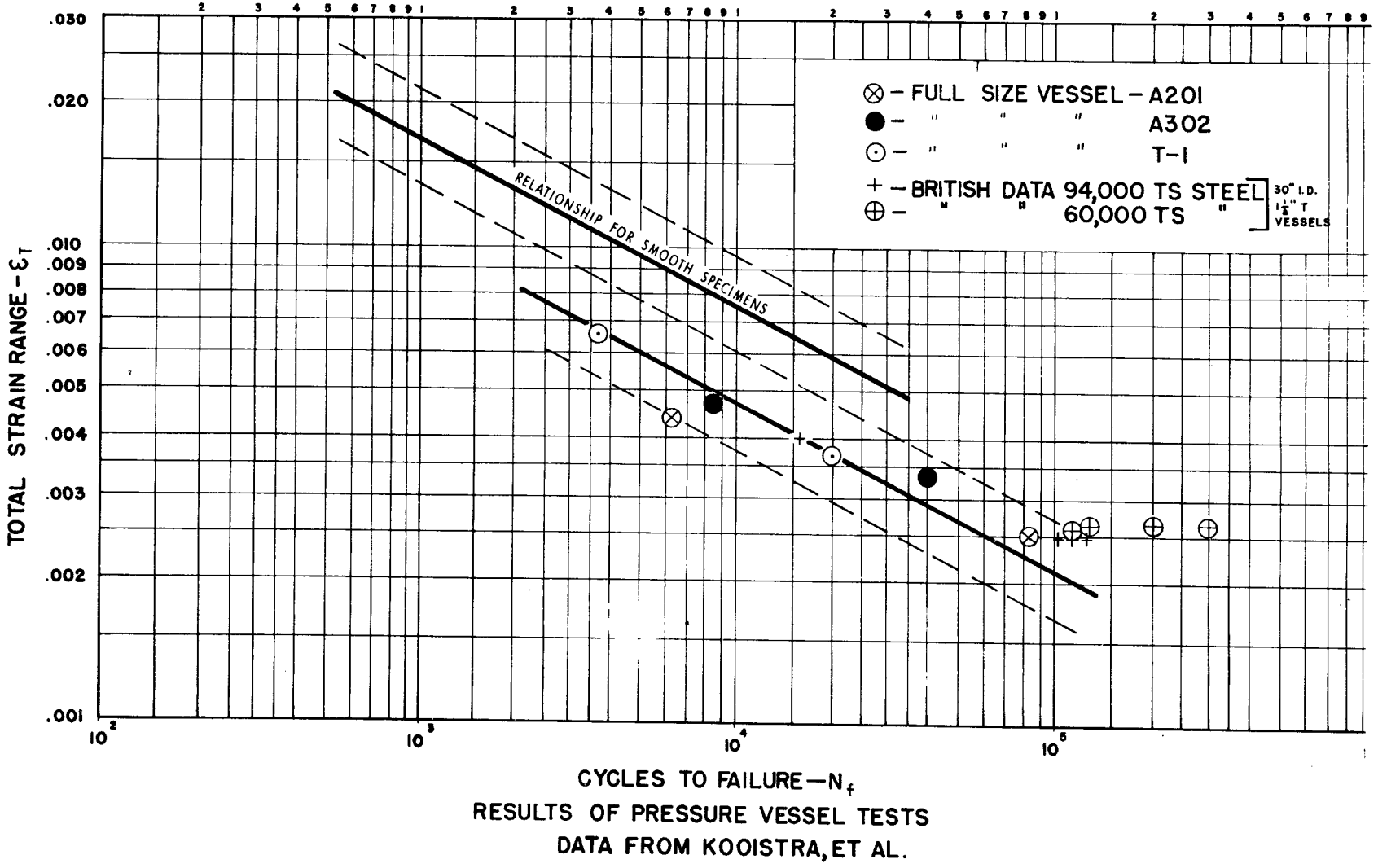

Fig. 6 - Comparison of Pressure Vessel Fatigue Results With Specimen Results

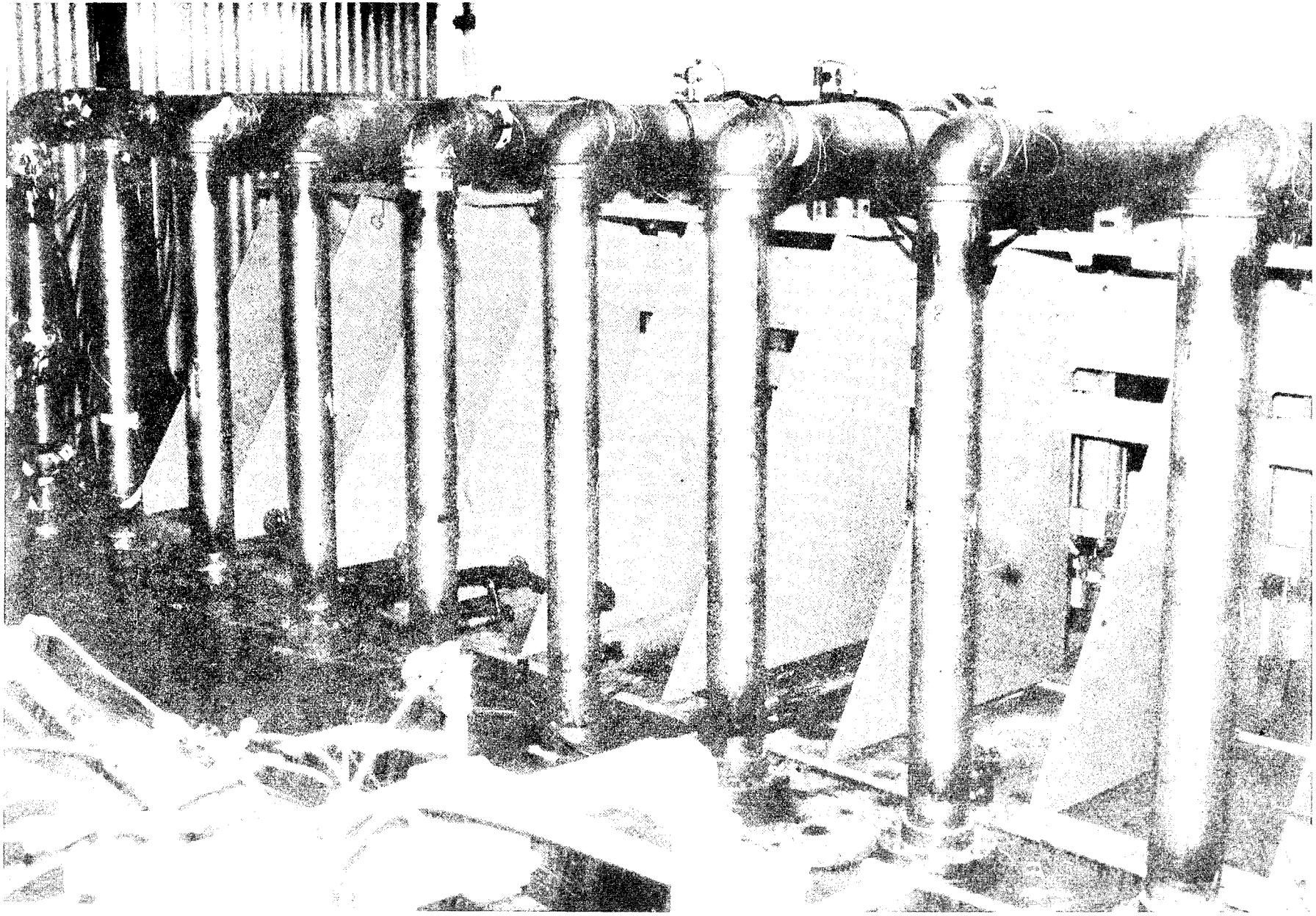

Fig. 7 - Low-Cycle Fatigue Evaluation Facility for Pipe Configurations

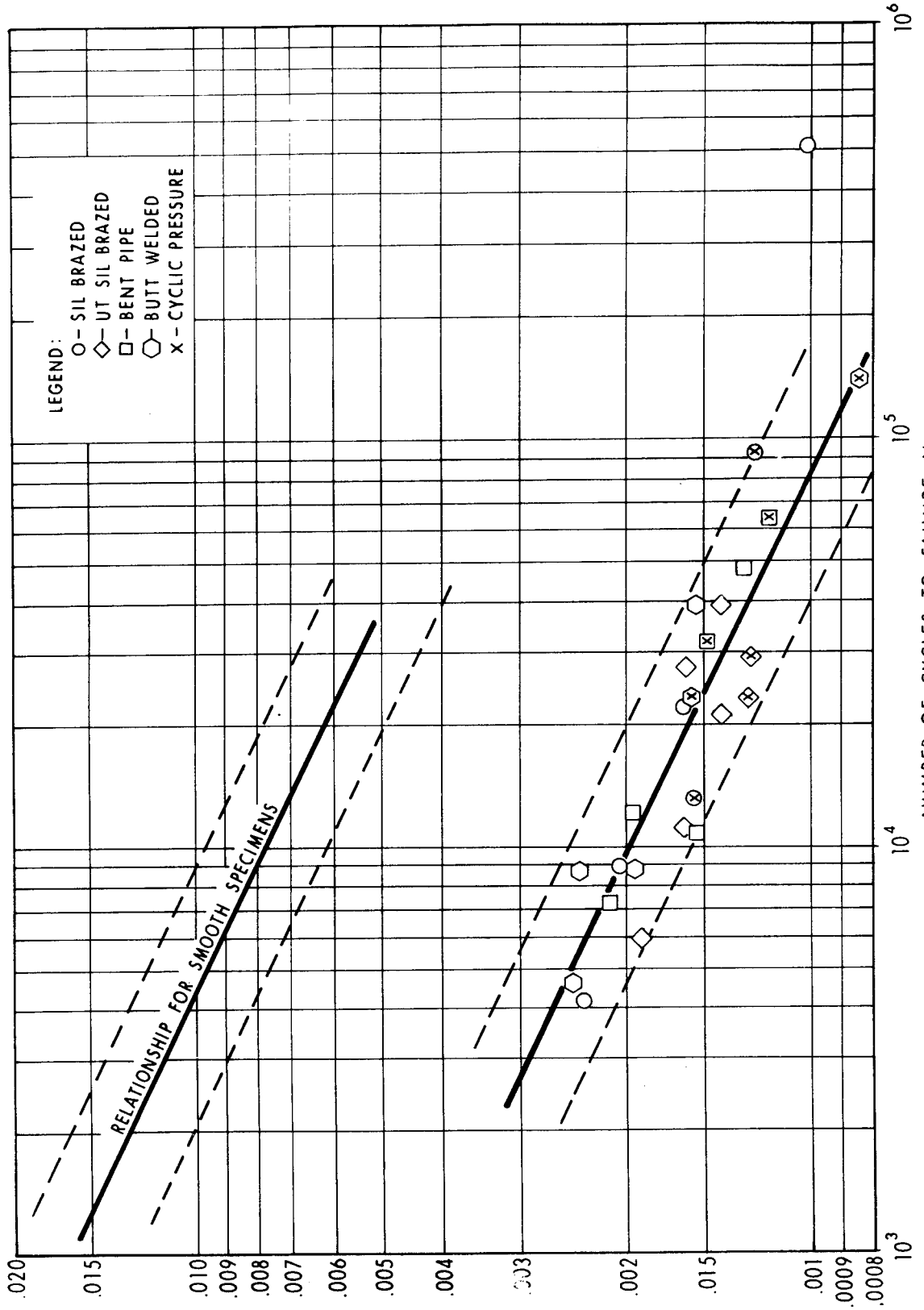

Fig. 8 - Comparison of 4-Inch 70-30 Cu-Ni Pipe Fatigue Results With Specimen Results

EVALUATION OF HIGH PERFORMANCE ROCKET MOTOR CASES USING SUB-SCALE PRECRACKED MODELS

C. M. Carman

Pitman-Dunn Research Laboratories

Frankford Arsenal, Philadelphia, Pa.

INTRODUCTION

Solid propellant rocket motor cases are, in essence, pressure vessels made of high quality materials. For best performance, it is necessary that these pressure vessels be made of high strength materials (yield strength $\gtrsim$ 200,000 psi steel equivalent). This strength may be achieved by heat treatment alone or by a combination of both cold rolling and heat treatment. Such materials are subject to brittle failures as exemplified by early attempts to use them in certain rocket motor cases.

To properly design and fabricate these pressure vessels, the designer must have some insight as to how these materials will behave under service conditions. The standard "V" notch Charpy impact test, used successfully for studying lower strength materials, fails to give meaningful data when applied to these higher strength materials. The Charpy impact values are uniformly low and the transition temperature becomes ill-defined.

Since one of the primary considerations in selecting high strength materials for these pressure vessels is their ability to resist crack propagation, a material strength concept involving the effects of flaws on structural integrity would be very helpful. Fracture mechanics as developed by Irwin[1] is such a concept. A brief description of this theory is as follows.

In 1920, Griffith[2] proposed that brittle bodies fail because of the presence of numerous internal cracks or flaws which produce local stress concentrations. Griffith also stated that the elastic body under stress must pass from the unbroken state to the broken state by a process during which a decrease of potential (elastic) energy takes place. He proposed that the condition for fracture is reached when the increase in free surface energy (surface tension), caused by the extension of the crack, is balanced by the release of elastic strain energy in the volume surrounding the crack. Mathematically, this may be expressed:

$$\frac{d\ (\epsilon\epsilon RR)}{Bda} \geq \frac{d\ (2T)}{Bda} \qquad (1)$$

In ceramics, and especially in glasses, hardly any deformation accompanies fracture. This led to the surface tension concept of brittle fracture. However, in metals, plastic deformation always takes place and Griffith's surface tension concept is not suitable. Both Irwin[3] and Orowan[4] independently came to the conclusion that the

slight plastic flow which occurs in the brittle fracture zone absorbs a large amount of additional energy, and must be considered in determining the energy required to create new fracture surfaces. On this basis, it was proposed that a work function be substituted for the surface tension terms as in equation 2

$$\frac{d\ (\epsilon\epsilon RR)_c}{Bda} = \frac{dW}{BdA} \tag{2}$$

where W = work function which is composed of two terms: (1) surface tension and (2) plastic deformation.

Inglis[5] developed the stress analysis for a through-crack in an infinite plate so that equation 2 becomes:

$$\frac{dW}{dA} = G = \frac{\pi\sigma^2 a}{E} \tag{3}$$

Recently, Irwin[6] has proposed that the events at the leading edge of a crack can be described in terms of a parameter, K, which is a function of the local elevation of the elastic stress field ahead of the crack. It may be shown that:

$$EG = K^2 \tag{4}$$

This high elevation of stresses near the tip of a crack should receive the greatest attention since it is at that point that additional growth of the crack takes place. Small amounts of plasticity and other non-linear effects may be viewed as taking place within the crack tip stress field and, hence, may be neglected in the presentation of the gross features.

The surfaces of a crack, since they are stress-free boundaries of the body near the crack tip, are the dominating influence on the distributions of stresses in that vicinity. Other remote boundaries and loading forces effect only the intensity of the local stress field.

The stress fields near the crack tip can be divided into three basic types, each associated with a local mode of deformation as illustrated in Figure 1. The opening mode, I, is associated with local displacement in which the crack surfaces move directly apart (symmetric with respect to the x-y and x-z planes). The edge sliding mode, II, is characterized by displacements in which the crack surfaces slide over one another perpendicular to the leading edge of the crack (symmetrical with respect to the x-y plane and skew symmetric with respect to the x-z plane). Mode III, tearing, finds the crack surfaces

sliding with respect to one another parallel to the leading edge (skew symmetric with respect to the x-y and x-z planes).

The stress and displacement fields associated with Mode I have been derived by Irwin[7,8] based on the method of Westergaard[9]. These expressions are given in equation 5:

$$\sigma_x = \frac{K_I}{\sqrt{2\pi r}} \cos\frac{\theta}{2}\left[1 - \sin\frac{\theta}{2}\sin\frac{3\theta}{2}\right]$$

$$\sigma_y = \frac{K_I}{\sqrt{2\pi r}} \cos\frac{\theta}{2}\left[1 + \sin\frac{\theta}{2}\sin\frac{3\theta}{2}\right]$$

$$\tau_{xy} = \frac{K_I}{\sqrt{2\pi r}} \sin\frac{\theta}{2}\cos\frac{\theta}{2}\cos\frac{3\theta}{2}$$

$$\sigma_z = \gamma\,(\sigma_x + \sigma_y),\ \tau_{xz} = \tau_{yz} = 0 \qquad (5)$$

$$\mu = \frac{K_I}{G}\sqrt{r/2\pi}\cos\frac{\theta}{2}\left[1 - 2\gamma + \sin^2\frac{\theta}{2}\right]$$

$$\nu = \frac{K_I}{G}\sqrt{r/2\pi}\sin\frac{\theta}{2}\left[2 - 2\gamma - \cos^2\frac{\theta}{2}\right]$$

$$\omega = 0$$

Similar equations may be developed for Modes II and III but, in general, specific crack tip stress field analyses are not available for these modes of failure.

However, fracture failures of structural components are associated primarily with tensile (or opening mode) type stress system. When the fracture is entirely a flat transverse tensile break with negligible plastic contraction parallel to the leading edge of the crack, use of the parameters G_I and K_I is appropriate.

For a crack traversing a plate under conditions such that plastic contraction of the plate thickness accompanies crack extension, oblique shear fractures form adjacent to the free surfaces and, in the absence of a strain rate sensitivity in the flow stress, these tend to grow in proportion to the G value as the crack lengthens. For a relatively high degree of crack toughness, several plate thicknesses of crack extension from a sharp notch or fatigue crack produce enough growth of the shear lip borders so that a single oblique shear fracture thereafter covers the entire fracture surface.

The mathematical representation must, for simplicity, consist of a linear elasticity crack stress field analysis. Thus, the plastic

yielding itself is not representable in the stress field of the basic model. The best that can be done is to assume a tensile crack whose length is such that the stress field of the model most nearly fits the real crack stress field in the elastic region surrounding the crack. Recent work by McClintock and Irwin[10] has shown the original estimate of the plastic zone size ($r_{ys} = \frac{K^2}{2\pi\sigma_{ys}^2}$) to be an accurate description.

The accuracy with which the idealized stress field can be fitted to the real stress field increases with the decrease of plastic zone size relative to crack and specimen dimensions. Thus, conceptually, the misfit at any fixed fraction of crack length relative to specimen width can be made as small as desired by increasing crack and specimen dimensions. When the fracture mechanics is applied to "mixed mode" tensile fractures, the fracture mode subscript (I, II, or III) is omitted from the $\mathcal{G}$ and K symbols.

The U. S. Army Materiel Command recently completed a program directed toward developing improved techniques for the fabrication of high performance, solid propellant rocket motors. As a result of this study, cases were fabricated from materials having intermediate and limited fracture toughness. The preliminary experimental data are discussed in these terms.

EXPERIMENTAL PROCEDURE AND RESULTS

Pressure Vessels Fabricated from Materials of Intermediate Fracture Toughness.

Of particular practical concern is the situation in which the fracture toughness is not quite sufficient to affect fracture arrest. This condition represents the highest strength-to-weight pressure vessels which can be made today with a reasonable assurance of reliability. The behavior of two pressure vessels will be used to illustrate the influence of fracture toughness on pressure vessel performance under these conditions.

The first example is the production of the second-stage Pershing rocket motor case from D6A steel by the Curtiss-Wright Corporation. The general configuration of this rocket motor case is shown in Figure 2.

The manufacturing procedure consisted of forming the center section by shear spinning from a roll ring forging. The forward dome and aft closure are machined forgings. Two girth welds complete the assembly

of the ends to the center body. The rocket motor cases were heat treated to a yield strength of 199,000 psi, a tensile strength of 219,000 psi and an elongation of 7.4 percent.

Center crack fracture toughness specimens, 4 in. wide by 18 in. long by 0.103 in. thick, were machined from this material. The plane strain fracture toughness, K_{Ic}, was determined by pop-in methods using an electrical displacement gage. The fracture toughness, K_c, of the material was determined using the same technique. These values are summarized in Table 1.

Irwin[11] has described a relative plastic zone size, β, equal to $K_c^2/2\pi\sigma_{ys}^2$. He has shown that β_c equal to 2π will arrest a through-crack whose length is equal to twice the wall thickness (2t crack). Calculation of β from the average K_c value gave a β_c value of 5.55.

These rocket motor bodies were filled with oil and hydrotested at -40 F by the Thiokol Chemical Company. After hydrotest, the rocket motors were filled with solid propellant and static fired at -40 F. These pressure vessels passed the required service test satisfactorily.

The second example of pressure vessels made from materials having intermediate fracture toughness is the development of a one-piece solid propellant rocket motor case by Lyon, Incorporated. The objective of this work sponsored by the U. S. Army Materials Research Agency is to develop a rocket motor case which is free of welds in the stressed area.

The geometric details of the pressure vessel are given in Figure 3. The manufacturing technique employed consisted of a hot cupping operation to form one end and to start the cylindrical portion. A series of cold drawing operations coupled with intermediate anneals were employed to form the cylindrical portion. The igniter boss was formed by a hot punching operation.

The material selected for this case was 300M steel (C 0.42 percent, Mn 0.87, P 0.007, S 0.008, Si 1.61, Ni 1.68, Cr 0.87, Mo 0.43, V 0.056, and Al 0.054). The pressure vessel was quenched and tempered at 600 F. The tensile properties developed are given in Table 2.

Fracture toughness specimens, 3 in. wide by 12 in. long, were also heat treated with the pressure vessel. The plane strain fracture toughness, K_{Ic}, was measured by the pop-in technique using the electrical displacement gage. The fracture toughness, K_c, of these samples was also determined using displacement measurements. These values are summarized in Table 3.

Table 1

Fracture Toughness of D6A Steel Heat Treated to 200,000 psi Yield Strength

W (in.)	B (in.)	Stress at "Pop-In" (psi)	a_o (in.)	K_{Ic} (psi $\sqrt{in.}$)	Stress at Failure (psi)	a (in.)	K_c (psi $\sqrt{in.}$)
4.00	0.107	45,200	0.538	60,700	81,800	0.760	135,000
4.00	0.105	56,600	0.507	73,400	83,500	0.955	161,500
4.00	0.108	48,000	0.526	63,600	80,700	0.930	153,000
4.00	0.107	49,000	0.540	66,000	77,800	0.918	146,000

Table 2

Tensile Values of 300M Steel

Direction	Yield Strength 0.20% offset (psi)	Tensile Strength (psi)	Elong. (%)
Longitudinal	232,200	283,500	7.0
Longitudinal	232,200	282,500	7.0
Transverse	236,100	285,500	8.0
Transverse	232,200	285,500	7.0

Table 3

Fracture Toughness of 300M Steel Samples
Heat Treated with Pressure Vessel

Direction	W (in.)	B (in.)	Stress at "Pop-In" (psi)	a_o (in.)	K_{Ic} (psi $\sqrt{in.}$)	Stress at Failure (psi)	a (in.)	K_c (psi $\sqrt{in.}$)
Longitudinal	3.00	0.079	76,000	0.402	88,000	87,200	1.022	147,300
Longitudinal	3.00	0.079	69,600	0.435	84,300	78,500	1.109	151,800
Transverse	3.00	0.081	69,100	0.426	82,800	82,200	0.680	130,800
Transverse	3.00	0.081	68,300	0.421	81,200	75,000	0.683	121,000

Calculation of the β values from the average K_c values gave a β_c of 5.27 in the longitudinal direction and 3.57 in the transverse direction.

The completed pressure vessel was placed in a test fixture for hydrotest. The vessel was then pressurized using sodium dichromate treated water. The following test cycle was planned:

1. Load to 560 psi in five 100 psi increments and one 60 psi increment.
2. Hold at 560 psi for three minutes.
3. Depressurize.
4. Repeat steps 1, 2 and 3.
5. Load initially in 100 psi increments to 500 psi and then in smaller increments until the yield stress is obtained. After yielding, load continuously until failure.

On the third cycle, a leak developed at the seal of the loading fixture at 962 psi internal pressure and the test had to be discontinued. Analysis of strain gage readings taken during these tests showed that a hoop stress of 243,000 psi was obtained at an internal pressure of 860 psi. This value of stress exceeded the uniaxial yield strength of 232,000 psi.

A new retaining ring which possessed greater resistance to radial expansion was fabricated. The pressure vessel was again placed on the test fixture. Failure occurred prematurely at 800 psi internal pressure which corresponded to a hoop stress of 232,000 psi. A photograph of the failed pressure vessel is shown in Figure 4.

The β_c values of the pressure vessels made from D6A and 300M steels are essentially the same, namely 5.55 for the D6A steel and 5.27 for the 300M steel. However, the pressure vessel made from D6A steel withstood a rather severe service test whereas the 300M steel pressure vessel failed below the biaxial yield strength. It is apparent that some differences exist between the two pressure vessels.

Irwin[12] has derived an expression for the stress intensity of a part-through crack in a uniformly stressed plate. His expression is given in equation 6:

$$K_{Ic}^2 = \frac{1.2\,\pi\sigma^2 a}{\Phi^2 - 0.212\,(\sigma/\sigma_{ys})^2} \qquad (6)$$

where $\Phi = \int_0^{\pi/2} [\sin^2\theta + (a/c)^2 \cos^2\theta]^{\frac{1}{2}}\, d\theta$

This equation may be used to explore what is likely to happen when a pressure vessel containing a surface crack is loaded. As the load increases, K will increase and will eventually reach a value at which the crack will start to increase in depth. At this point the crack growth is occurring under plane strain conditions, equivalent to the situation for a through-the-thickness crack in a very thick plate. The value of K for the start of crack growth will therefore be equal to the value of K_{Ic} for the material. If the value of K_c for the thickness in question is sufficiently greater than the value of K_{Ic}, slow crack growth will continue against increasing resistance requiring increasing load to maintain it. Slow crack growth may continue until the crack has penetrated through the wall and started to extend as a through-the-thickness crack.

If the ratio of K_c for the thickness in question to K_{Ic} is less than a certain value, onset of rapid fracture will occur before the crack has penetrated the wall. Equation 6 may be used to relate the stress and crack dimensions to K_{Ic}. The value of K_c does not affect the conditions for fracture.

Srawley[13] has shown that for stress levels approaching the yield stress and an a/c ratio greater than one-half, the K_c/K_{Ic} ratio must be greater than two for the K_c value to govern the fracture behavior.

Examination of the fracture toughness data in Table 1 for D6A shows the K_c/K_{Ic} ratio is equal to 2.26 and the fracture behavior is governed by K_c. The fracture toughness data for 300M in Table 3 show the K_c/K_{Ic} may vary from 1.63 to 1.87. Under these conditions, the fracture behavior is controlled by K_{Ic}.

The failed 300M pressure vessel was sectioned to remove the fracture surfaces. The entire fracture surface was found to be 100 percent shear except at a single initiation site. The appearance of the fracture origin is shown in Figure 5.

Examination of the fracture origin indicated that a pit approximately 0.006 to 0.007 in. deep on the inner surface had served as the stress concentration to initiate the fracture. Extending from this pit is a semicircular area of flat fracture with many bright facets which is characteristic of stress corrosion. Radiating from this semicircular area are fingers of flat fracture with bright facets, and between these fingers are roughened areas indicating slow crack extension. This entire area is considered as the plane strain defect at instability. The depth of a semicircular crack at instability was calculated from equation 6 using a K_{Ic} value of 82,000 psi $\sqrt{\text{in.}}$ and the hoop stress at failure. The calculated crack depth at instability was 0.074 in.

The actual crack depth as measured on the fracture surface is 0.074 in. which is in agreement with the calculated value.

It is important to note that the conditions for failure of this pressure vessel can be described in terms of stress and defect size by means of fracture mechanics and that these calculations have been verified by a fracture analysis of the pressure vessel after failure.

Pressure Vessels Fabricated from Materials of Limited Fracture Toughness.

A more critical situation is provided by a 20 in. diameter experimental pressure vessel made of 20 percent nickel maraging steel. The design chosen was a helical welded cylinder using 0.040 in. thick strip. A helix angle of 11 degrees was selected to obtain maximum weld efficiency and was based upon results obtained from uniaxial tests of welded coupons.

The experimental pressure vessel was fabricated by the Budd Company from cold rolled and aged, 20 percent nickel maraging steel strip (C 0.008 percent, Mn 0.008, P 0.004, S 0.005, Si 0.019, Cb 0.42, Ni 19.97, Ti 1.85, Al 0.47, B 0.001, Zr 0.018, Bal Fe). After the cold rolling operation, the strip was held at -100 F for 16 hours and aged at 675 F for 3 hours to develop the full mechanical properties. This treatment developed a yield strength of 307,000 psi and a tensile strength of 308,000 psi in the base metal.

The pressure vessel was tested hydrostatically using a non-corrosive hydraulic oil as the pressurizing medium. The vessel failed prematurely at a gage pressure of 770 psi. This gave a calculated value for the hoop stress of 192,000 psi or a hoop stress to yield strength ratio of 0.62. A photograph of the failed pressure vessel is shown in Figure 6.

Three-inch wide by 12 in. long center crack fracture toughness specimens were cut from the failed case in both the longitudinal and transverse direction. The plane strain fracture toughness, K_{Ic}, of these specimens was measured by means of a pop-in method using displacement measurements. The fracture toughness, K_c, of the material was measured using the same technique. These results are summarized in Table 4.

Using an average K_c value from these specimens, calculation of the β value gave a β_c equal to 2.54 in the longitudinal direction and β_c equal to 0.61 in the transverse direction. The K_c/K_{Ic} ratio for this material is 1.33 which indicates that the K_{Ic} value governs the fracture behavior.

Table 4

Fracture Toughness of 20 Percent Nickel Maraging Steel

Direction	W (in.)	B (in.)	Stress at "Pop-In" (psi)	a_o (in.)	K_{Ic} (psi $\sqrt{in.}$)	Stress at Failure (psi)	a (in.)	K_c (psi $\sqrt{in.}$)
Longitudinal	3.00	0.061	61,000	0.414	71,900	63,100	0.624	95,600
Longitudinal	3.00	0.061	60,000	0.411	70,400	67,000	0.640	103,300
Transverse	3.00	0.061	44,700	0.425	50,600	44,700	0.455	55,700
Transverse	3.00	0.061	32,900	0.424	37,400	33,000	0.458	41,200

The burst vessel was examined to determine the origin of failure. The failure was 100 percent shear except for the origin. The origin of fracture appeared to a series of surface defects oriented in a line normal to the rolling direction of the strip and on the outer surface of the case.

One of these pits was deep enough to initiate a small plane strain fracture origin as shown in Figure 7. Examination of the plane strain fracture origin showed that it was approximately eleven times as long as it was deep. Under these conditions equation 6 reduces to:

$$K_{Ic}^2 = 1.2\ \pi\sigma^2 a \qquad (7)$$

Since the crack is oriented perpendicular to the longitudinal direction of the sheet, the longitudinal value of K_{Ic} will be used to calculate the depth of the defect.

An average value of 71,700 psi $\sqrt{\text{in.}}$ for K_{Ic} and a hoop stress of 192,000 psi were used to calculate the crack depth at instability. This calculation gave a crack depth of 0.036 in. at instability as compared to a measured depth of 0.030.

It will be noted that the actual defect size is somewhat smaller than the calculated value. However, this is to be expected since the defect exceeds half the wall thickness so that the crack border is near the inner surface of the wall. The data presented here illustrate the stress elevating effect of local reduced wall stiffness.

Studies of Scale Models of Solid Propellant Rocket Motors.

After completion of this preliminary program, completed cases manufactured by the Budd Company and ARDE Portland, Incorporated were available for test. The cases supplied by the Budd Company were fabricated from 20 percent cold rolled 0.040 in. thick 18 NiCoMo maraging steel strip. The case itself was produced by spiral wrapping and welding. The maraging steel used for these cases exhibited a yield strength of 277,000 psi after aging at 990 F followed by aging at 770 F after welding. The design of this case is shown in Figure 8.

The cases supplied by ARDE Portland were fabricated from 301 stainless steel preforms. The preforms were stretched 14.2 percent or 15.8 percent at -320 F to form the case. After stretching, the cases were aged at 800 F for 20 hours. This treatment resulted in a yield strength of 264,000 psi for the cases stretched 14.2 percent, and a yield strength of 280,000 psi for the cases stretched 15.8 percent. The design of these cases is shown in Figure 9.

The tensile properties of the 301 stainless steel and the 250 grade maraging steel are given in Table 5. Room temperature and -65 F values are included in this table.

The rocket motor cases were hydrotested using oil as the pressurizing medium at room temperature and at -65 F. These results are summarized in Table 6. The data show a reasonable biaxial elevation of the burst stress and that these cases are acceptable from this viewpoint. However, it should be borne in mind that these tests were performed on custom made cases which would be relatively free of defects when compared with commercially manufactured ones.

It was desired to evaluate these cases under conditions more closely simulating production. A committee was organized by Dr. Peter Kosting of the U. S. Army Materiel Command, to design a set of experiments to accomplish this objective. Based on the results of the previous experience in analyzing service failures, it was decided to employ the fracture mechanics approach. Part-through cracks were to be used since they would more closely simulate actual defects. The defect size would be calculated using the plane strain fracture toughness, K_{Ic}, of the material. It also was decided that the failure stress would be equal to or greater than the yield strength.

Fracture Toughness Studies of Maraging Steel.

Considerable data have been published concerning the plane strain fracture toughness of the 250 and 300 grades of maraging steel and the values vary from 40,000 psi $\sqrt{in.}$ to greater than 100,000 psi $\sqrt{in.}$ Analyses of these data show that most of these values were determined by the pop-in method as described by Boyle, Sullivan and Krafft[16], and the experiments were performed using a wide range of plate thicknesses. In an attempt to resolve further the relatively large discrepancies observed in these data, the values of K_{Ic} were plotted as a function of the plate thickness. The curve is shown in Figure 10. The data indicate that the higher values of fracture toughness obtained were influenced by plasticity during pop-in and that reliable plane strain results could be obtained only with thick (0.20 in. or thicker) specimens.

Recently, Brown and Srawley[18] made a comprehensive study of the specimen size requirements for determining plane strain fracture toughness. They concluded that the minimum thickness of the specimen for accurate K_{Ic} measurements should be $2.5\ (K_{Ic}/\sigma_{ys})^2$. The same dimension was determined for the crack length. Applying these criteria to a steel having a yield strength of 270,000 psi and a K_{Ic} of 70,000 psi $\sqrt{in.}$ gave a minimum thickness of 0.167 in.

Table 5

Tensile Properties of Cryogenically Stretched Formed 301 Stainless Steel and Cold Rolled and Aged 250 Grade Maraging Steel Sheet Used for Rocket Motor Cases*

Material	Test Temp. (°F)	Direction	Yield Strength 0.20% Offset (psi)	Tensile Strength (psi)	Elong. (%)
301 SS Cryogenically Formed	R.T.	Long.	225,200	249,000	4.0
		Trans.	223,900	245,100	5.5
	-65	Long.	--	268,500	3.5
		Trans.	--	275,500	5.2
250 Maraging Steel	R.T.	Long.	277,000	287,500	2.8
		Long.	--	304,200	2.2
		Trans.	--	327,600	1.8

*Data from Thiokol Chemical Company[14,15].

Table 6

Hydrostatic Test Results for Solid Propellant Rocket Motors

Case	Test Temp. (°F)	Burst Pressure (psig)	PD/2t (psi)	Biaxial Elevation (%)
ARDE-Portland 301 SS				
No 1	-65	2750	310,500	13.8
No 2	- 65	2660	300,100	9.1
No 5	- 65	2900	342,800	17.0
Budd Co. Maraging Steel				
No 1	R.T.	1175	293,800	9.2
No 2	-65	1305	326,200	7.2

According to data in Figure 10, it was concluded that a minimum specimen thickness of 0.20 to 0.25 in. would be necessary to obtain valid plane strain fracture toughness values. The material used in this study was CEVM 300 grade maraging steel rolled to 1/4 in. thick plate. Four-inch wide strips were cut from the plate and solution annealed for one hour at 1600 F. These strips were cold rolled 20 percent by the Homer Research Laboratories of the Bethlehem Steel Company.

Strip-type tensile specimens and center cracked fracture toughness specimens were used. The specimens were aged at 990 F and 770 F for three hours at each temperature.

The plane strain fracture toughness was determined using the pop-in technique. The load-deflection curves were determined using a mechanical compliance gage similar to that described by Boyle[19]. The pop-in load was selected as the load which caused the first inflection in the load-deflection curve. The tests at -65 F were conducted by placing the entire test assembly in a cold box which was maintained at the test temperature. This equipment is shown in Figure 11. The specimens were held at temperature for one-half hour prior to testing. The results of the tensile tests are given in Table 7.

These tensile values are quite uniform but do not equal the room temperature yield strength of 279,000 psi developed in the Budd Company material. Approximately a 6 percent increase in tensile values was realized by lowering the testing temperature to -65 F.

The fracture toughness properties of this material are given in Table 8. Detailed analysis of the data shows that the values of plane strain fracture toughness are not greatly affected by the variables of fatigue cracking or method of detecting pop-in. Also, it will be observed that the lowering of the testing temperature to -65 F had a very slight effect on the plane strain fracture toughness.

These values of K_{Ic} for maraging steel appear to be lower than those reported by other investigators. These data were plotted as a function of yield strength in Figure 12. Examination of this figure shows a normal inverse first order dependency of K_{Ic} to yield strength. Since yield strength is an important factor that influences the plane strain fracture toughness, the plane strain fracture toughness of conventionally treated (1500 F, AC, aged 900 F, 3 hours) 300 grade maraging steel was determined at -65 F. The fracture toughness values of this material are given in Table 9. Since the yield strength of this material more closely approximates the yield strength of the rocket case manufactured by the Budd Company, a value for K_{Ic} of 40,000 psi $\sqrt{\text{in.}}$ was selected to compute the size of defect.

Table 7

Tensile Values for Cold Rolled and Aged 300 Grade Maraging Steel

Test Temp. (°F)	Specimen No.	Yield Strength 0.20% Offset (psi)	Tensile Strength (psi)	Elong. (%) 2 in.
R.T.	1	266,000	276,000	7.5
R.T.	2	266,000	273,000	6.5
R.T.	3	266,000	273,000	7.5
R.T.	4	269,000	276,000	6.5
- 65	1	284,000	291,000	6.0
- 65	2	285,000	290,000	6.0

Table 8

Fracture Toughness Properties of Cold Rolled and Aged 300 Grade Maraging Steel

Test Temp. (°F)	Specimen No.	Type Crack	Gage Type	Pop-In Load (lbs.)	Pop-In Stress (psi)	a_o (in.)	K_{Ic} (psi $\sqrt{in.}$)
R.T.	1	Wing	Mechanical	30,000	43,400	0.605	62,500
R.T.	2	Wing	Mechanical	29,000	42,600	0.637	63,000
R.T.	3	Wing	Mechanical	31,500	44,700	0.635	65,700
						Average	63,700
R.T.	4	Tension	Mechanical				62,600
R.T.	5	Tension	Mechanical				60,000
						Average	61,300
R.T.	6	Wing	Potential	51,200	49,300	0.532	65,400
R.T.	7	Wing	Potential	50,200	48,700	0.525	64,600
						Average	65,000
R.T.	8	Tension	Potential	55,800	51,800	0.417	60,600
R.T.	9	Tension	Potential	56,100	52,000	0.419	61,000
R.T.	10	Tension	Potential	55,800	52,700	0.405	60,300
						Average	60,600
-65	4	Wing	Mechanical	27,500	40,400	0.604	58,200
-65	5	Wing	Mechanical	28,500	41,900	0.597	59,500
-65	6	Wing	Mechanical	29,400	43,000	0.596	61,600
-65	7	Wing	Mechanical	26,300	38,600	0.605	55,600
						Average	58,700

Table 9

Plane Strain Fracture Toughness of
Conventionally Treated 300 Grade Maraging Steel at -65 F

Specimen No.	Pop-In Load (lbs.)	Pop-In Stress (psi)	a (in.)	K_{Ic} (psi $\sqrt{in.}$)
8	23,300	30,200	0.516	40,200
9	20,800	26,700	0.555	37,600
10	22,200	28,500	0.605	42,200
			Average	40,000

Fracture Toughness Studies of Cryogenically Formed 301 Stainless Steel.

Two lots of cryogenically formed 301 stainless steel were tested by Nelson and Burns[20]. One lot developed a yield strength of 220,000 psi and the other lot developed a yield strength of 265,-280,000 psi.

The plane strain fracture toughness of the 220,000 psi yield strength material was determined using the single-edge notched specimen. The slow notched bend specimen was used to determine the plane strain fracture toughness of the higher yield strength material. These data are summarized in Table 10.

Application of the criterion, a and B equal to or greater than 2.5 $(K_{Ic}/\sigma_{ys})^2$, indicates the specimens were too small for an accurate K_{Ic} measurement. This indicates that shear lips would develop during pop-in.

Development of Crack Geometry.

Since machined notches are generally not sufficiently sharp to simulate natural cracks, it is the best accepted practice to extend these notches by fatigue. In a fracture mechanics analysis, the development of a specified crack geometry is of importance. Consequently, the crack geometry specified must be stable during fatigue. The semi-circular crack is the most stable during fatigue since the K value is uniform along the crack front.

Solution of equation 6, using a K_{Ic} value of 40,000 psi $\sqrt{in.}$ and a failure stress equal to the yield strength, gave a crack radius of 0.009 in. and a crack length of 0.018 in. However, since such small defects are extremely difficult to detect and measure, it was decided to introduce a crack having a depth (or radius) of 0.015 in. and a length of 0.030 in. This defect represents a somewhat more severe test condition than the calculated one.

To calculate the crack geometry for the cryogenically stretch formed 301 stainless steel cases, equation 6 was solved using the K_{Ic} values for the higher strength materials reported in Table 10, and yield strength instability gave crack depth values 0.070 in. for a K_{Ic} of 96,500 psi $\sqrt{in.}$ and 0.057 in. for a K_{Ic} of 87,100 psi $\sqrt{in.}$ It is readily apparent that these defect sizes are not practical since they exceed the motor case wall thickness.

At this point it becomes necessary to develop a more realistic crack size for these rocket motor cases. As has been shown by Carman, Armiento and Markus[21], a crack depth greater than one-half the wall

Table 10

Plane Strain Fracture Toughness of
Cryogenically Formed 301 Stainless Steel
(Nelson and Burns[20])

Yield Strength 0.20% Offset (psi)	B (in.)	Specimen Type	Direction	Avg. K_{Ic} (psi $\sqrt{in.}$)	$\frac{K_{Ic}}{\sigma_{ys}}$
220,000	0.125	Single-Edge Notch	Long.	106,200	1.87
265,-280,000	0.125	Slow Notched Bend	Long.	96,500	1.00
265,-280,000	0.125	Slow Notched Bend	Trans.	87,100	0.84

thickness is not amenable to fracture mechanics analysis. Therefore, consideration of any minimum defect size had to be directed toward defects which were less than one-half the wall thickness in depth.

Since the mechanical properties of the higher strength cryogenically formed 301 stainless steel case very closely corresponded to those of the maraging steel case, it was felt that the same defect would be introduced into both cases. The lower strength cryogenically formed 301 stainless steel case had higher fracture toughness values, and it was decided to introduce the maximum size of flaw which would be amenable to fracture mechanics analysis. The size of this flaw was calculated to be 0.025 in. deep by 0.050 in. long.

Generation of the Defect.

It has been shown that notch sharpness can have a pronounced effect on the fracture properties of these high strength materials and that a natural crack is required to reproduce the effect of a natural defect. The previously described semi-circular crack geometry was introduced into the case wall by electro-discharge machining. It was decided to machine in a starter notch approximately half the crack dimensions required and grow this notch to its final crack dimensions by fatigue.

Initial attempts[22] were made to grow the notch to the final dimensions in the cryogenically stretch formed case by hydraulically fatiguing the entire case. However, this method was not successful due to cracking in the aft flange. It was necessary to develop a special fixture to fatigue the notch.

A test fixture was designed whereby a pressurizing medium was applied locally in the area of the starter notch to accomplish the fatigue crack growth. A sketch showing the basic parts of the fixture is presented in Figure 13.

The fixture consists of two segmented rings - one ring to fit the inside of the case and the other to fit the outside of the case. A dished-out area in the inside ring is aligned with the starter notch. A pressure seal (O-ring), concentric with the dished-out area, prevents loss of the pressurizing medium. The segmented ring was expanded into place (against the inside of the case) with shims. Pressure inlet and discharge ports were provided in the dished-out area through the back side of the ring. A hole was machined through the outside ring, which was then clamped around the cylindrical section of the case with the hole aligned with the starter notch. The outer ring was to prevent radial displacement of the case wall under pressurization except at the location of the starter notch.

The first evidence of fatigue crack growth was noted after approximately 28,800 cycles (0 to 750 psi gage). An additional 7,300 cycles (0 to 750 psi gage) were required to grow the crack to a length of 0.050 in.

In view of the success achieved in growing a fatigue crack in the ARDE Portland stainless steel case by the application of a local cyclic pressure, it was decided to use the same technique for growing a crack in the maraging steel case made by the Budd Company. This fixture was essentially a larger version of the previous one. The peak cyclic pressure varied between 475 and 500 psi gage and a cyclic rate of two cycles per second was used. A total of 22,000 cycles was necessary to generate this crack.

Hydrostatic Testing.

The primary objective of this investigation was to determine if the specially introduced flaws in these rocket motor cases would degrade their strength properties. It was decided to hydrostatically test these cases at -65 F. It was anticipated that the biaxial yield and tensile strengths would be obtained. The early attempts to extend the notch by fatigue in the ARDE Portland case resulted in a fatigue crack developing from a threaded hole in the aft flange and propagating into the dome. An attempt was made to arrest the crack by drilling a hole through the aft dome wall at the crack tip. The hole was plugged with a bolt. In order to prevent leakage through the cracked aft flange of the case, the aft section of the case was sealed with a liner material.

After the case was filled with oil, the system was cooled to -65 F. The case was subjected to four pressure cycles. Peak pressure was approximately 200 psi gage on the first two cycles and approximately 500 psi gage on the third cycle. On the fourth pressure cycle, the case pressure rise rate was approximately 500 psi gage per minute and the case burst at a pressure of 1785 psi gage. The failure initiated in the aft dome at the hole, which was drilled to arrest the fatigue crack and propagated to the aft skirt-to-cylinder junction. The area of the case containing the introduced defect was not affected by this fracture.

The pressure-strain relationships in the full-scale hydrostatic test were similar to those obtained in the localized area during fatigue crack growth. In view of this fact, it was decided to burst the cylindrical section containing the fatigue cracked notch by local pressurization. The fatigue cracked area and the fixture were cooled to -65 F and the section was pressurized with oil. A 0.2 percent offset in hoop strain was observed slightly under 3000 psi gage which calculated to a hoop stress of 332,000 psi.

Examination of the failed section showed that the defect had the recommended semi-circular and the desired dimensions (0.050 in. x 0.035 in. deep). Except for a small flat area adjacent to the crack, the fracture surface was full shear. The hoop stress at which yielding was observed showed the case could tolerate this size of defect without a loss in performance.

The Budd case (maraging steel) was suspended from a portable frame and placed inside the temperature conditioning box. Final connections for the strain gages, pressure transducers, and thermocouples were made. Pressurization oil, cooled to -75 F, was poured into the case through a hole in the aft plate and the carbon dioxide cooling system was connected. The oil filled case was allowed to stand in the -65 F environment for approximately two hours to assure a uniform temperature of the case and the oil.

When temperature stabilization was assured, the strain gages and pressure transducers were calibrated. One gage-set cycle was performed during which all gages operated satisfactorily. After the gage-set cycle, the case was pressurized to burst. Yielding, as defined by 0.2 percent offset in hoop strain, was observed at a pressure of 1335 psi gage. The case burst at a pressure of 1350 psi gage. These values resulted in a biaxial yield strength of 327,000 psi and a biaxial strength of 330,900 psi.

Examination of the fracture surface of the case showed that the crack had developed the recommended semi-circular geometry as shown in Figure 14. Measurements taken gave a crack length of 0.030 in. and a crack depth of 0.014 in. The indications of yielding from the strain gage data and the high burst strength show that this rocket motor case can tolerate this size of defect without a loss in performance. The hydrostatic test data obtained for these cases are summarized in Table 11.

Prevention of Failure by Premature Fracture.

In the example of pressure vessels fabricated from very high strength materials, it has been shown that a leak-before- burst criterion is the most realistic approach. In analyzing this class of materials for which fracture toughness values are available, theoretical calculations and the experimental data presented show that $\beta_c = 2\pi$ or $\beta_{Ic} = 1.5$ are needed to arrest a 2t crack. If pressure vessels are fabricated from materials having lower values of fracture toughness, great care must be taken to avoid small defects in both fabrication processes and material.

Table 11

Hydrostatic Test Data at -65 F for 301 Stainless Steel and Maraging Steel Rocket Motor Cases

Case Material	Case No.	Condition	Tensile Yield Strength at Room Temperature (psi)	Biaxial (Hoop) Yield Strength at -65 F (psi)	Biaxial (Hoop) Tensile Strength at -65 F (psi)
301 Stainless Steel	1	Smooth	264,000	279,400	310,500
	2	Smooth	264,000	272,100	300,100
	5	Smooth	280,000	334,500	342,800
	3	Precracked	280,000	332,200	352,100
Maraging Steel	3	Smooth	288,000	--	318,900
	2	Precracked	288,000	327,000	330,900

Irwin[23] has extended this idea of crack arrest to lower strength-higher toughness materials such as HY-80, A302B, and A212B. Although the V-notch Charpy impact test is commonly used to determine the Fracture Appearance Transition Temperature (FATT), the geometrical configuration of the specimens does not lend itself to analysis. Consequently, reference will be made to the simpler Nil Ductility Test (NDT) as discussed by Pellini and Puzak[24]. In the original concept, the Nil Ductility Temperature separated the temperature region in which a flat break occurred from the higher temperature region in which noticeable plastic bending accompanied separation.

In the interests of caution, toughness requirements are commonly studied on the basis of rapid rather than slow application of the service load. The fracture appearance transition temperature usually exceeds the NDT by about 60 F. Consistency with both of these observations requires that the dynamic K_{Ic} value is proportional to the yield strength about as follows:

$$\text{at FATT } K_{Id} = 0.95 \sqrt{\text{in.}}\ \sigma_{yd} \qquad (8)$$

where σ_{yd} may be estimated by a method proposed by Bennett and Sinclair[25].

From some exploratory calculations using properties characteristic of HY-80, A302B and A212B steels, it is found that a one-inch wall thickness satisfies a leak-before-break criterion at a temperature between NDT + 60 F and NDT + 120 F, even if the service load is as high as the static yield strength. Normally, the design of a pressure vessel does not require a gross average tensile stress in the cylindrical portion of the wall higher than about one-third of the yield strength. At such stress levels, the leak-before-break criterion is approximately satisfied at NDT + 120 F for wall thicknesses as thick as five inches. Table 12 shows the stresses corresponding to leak-before-break, σ_{LB}, for HY-80 steel.

CONCLUSIONS AND GENERAL DISCUSSION

Important practical situations are illustrated by the behavior of pressure vessels fabricated from D6A and 300M steels. The performance of these pressure vessels demonstrates the importance of the K_c/K_{Ic} ratio. For deep-short cracks, if this ratio exceeds two, the $\beta_c = 2\pi$ fracture arrest criterion applies and the fracture is governed by the K_c value. This situation is illustrated by the service performance of the D6A pressure vessel.

Table 12

Fracture Toughness and Design Properties of HY-80 Steel[23]

σ_{ys} (70 F) = 82,000 psi
NDT = -150 F

	B (in.)	β_{Ic}	σ/σ_{yd}	σ_{LB} (psi)	Yield and Design Stresses
at -90 F σ_{yd} = 122,000 psi K_{Id} = 116,000 psi $\sqrt{in.}$	1	0.912	0.693	84,000	(σ_{ys} (static) =
	2.5	0.364	0.358	44,000	(94,000 psi
	5	0.182	0.243	30,000	($\frac{94}{3}$ = 31,000 psi
at -30 F σ_{yd} = 113,000 psi K_{Id} = 126,000 psi $\sqrt{in.}$	1	1.25	0.880	99,000	(σ_{ys} (static) =
	2.5	0.50	0.440	50,000	(88,000 psi
	5	0.25	0.289	33,000	($\frac{88}{3}$ = 29,000 psi

On the other hand, if the K_c/K_{Ic} ratio is less than two, fracture arrest of a through-the-thickness crack is not possible, and the fracture behavior is governed by the value of the plane strain fracture toughness. This situation is illustrated by the performance of the 300M and 20 percent nickel maraging steel pressure vessels.

Fracture mechanics permits calculation of the size of defect and stress level for failure. These conditions have been verified by subsequent failure analysis and tests of specially notched and pre-cracked rocket motor cases. Close agreement between calculated and experimentally measured flaw sizes and failure stress was obtained for all these examples.

Techniques for using fracture mechanics in design to prevent premature failure are discussed.

ACKNOWLEDGEMENT

The author wishes to thank Dr. G. R. Irwin of the U. S. Naval Research Laboratory for his many helpful suggestions during the preparation of this paper, and Mr. J. I. Bluhm of the U. S. Army Materials Research Agency for his assistance in developing the experiments with the precracked rocket motor cases.

GLOSSARY

psi = stress, pounds per square inch

B = specimen thickness, inches

T = surface tension

a = half-crack length of internal crack or crack depth of surface crack

$\epsilon\epsilon RR$ = elastic energy release rate

W = work function per unit area

A = unit area

$\mathcal{G}$ = elastic energy release rate

σ = gross section stress

E = Youngs Modulus

K = stress intensity factor

r = distance ahead of crack tip

θ = angular coordinate measured from the crack plane

σ_x, σ_y, σ_z = rectangular components of tensile stress

τ_{xy}, τ_{xz}, τ_{yz} = rectangular components of shear stress

μ, ν, ω = displacements

γ = Poissons ratio

σ_{ys} = 0.2% offset yield strength

β = relative plastic zone size

Φ = an elliptic integral

c = half of the crack length of a surface crack

FATT = fracture appearance transition temperature

NDT = nil ductility transition temperature

σ_{yd} = dynamic yield strength

K_{Id} = dynamic plane strain fracture toughness

σ_{LB} = leak before burst stress

G = shear modulus

Subscripts:

I = first or opening mode of fraction

c = critical value of a parameter

o = initial value

REFERENCES

1. G. R. Irwin, "Relation of Crack Toughness Measurements to Practical Applications", Welding J. Res. Suppl. (Nov. 1962).

2. A. A. Griffith, "The Phenomena of Rupture and Flow in Solids", Philosophical Trans. Royal Soc. of London (1920).

3. G. R. Irwin, "Fracture Dynamics", Fracturing of Metals, ASM (1948).

4. E. Orowan, "Fundamentals of Brittle Behavior in Metals", Fatigue and Fracture of Metals (MIT Symposium, June 1950), John Wiley & Sons, Inc., New York (1952).

5. C. E. Inglis, "Stress in a Plate Due to the Presence of Cracks and Sharp Corners", Proc. of the Inst. of Naval Architects (March 1913).

6. G. R. Irwin and J. A. Kies, "Fracture Theory as Applied to High Strength Steels for Pressure Vessels", Golden Gate Metals Conference, San Francisco, Calif. (1960).

7. G. R. Irwin, "Analysis of Stresses and Strains Near the End of a Crack Traversing a Plate", Trans. ASME, J. Appl. Mechanics (1957).

8. G. R. Irwin, "Fracture Mechanics", Structural Mechanics, Pergamon Press, New York (1960).

9. H. M. Westergaard, "Bearing Pressures and Cracks", Trans. ASME, J. Appl. Mechanics (1939).

10. F. A. McClintock and G. R. Irwin, "Plasticity Aspects of Fracture Mechanics", Fracture Toughness Testing and Its Applications, ASTM STP No. 381 (April 1965).

11. G. R. Irwin, "Fracture Testing of High Strength Sheet Materials Under Conditions Appropriate for Stress Analysis", Report 5486, U. S. Naval Res. Lab. (July 1960).

12. G. R. Irwin, "Crack Extension Force for a Part-Through Crack in a Plate", J. Appl. Mechanics, V. 29, Trans. ASME, V. 84, Series E (1962).

13. J. E. Srawley, "The Slow Growth and Rapid Propagation of Cracks", U. S. Naval Res. Lab., Report No. 5617 (May 1961).

14. D. L. Daigle, "Evaluation of Three ARDE Portland Cryogenic Stretched Formed Subscale Rocket Motor Cases", Thiokol Chemical Corp., Huntsville Div., Report No. 21-65 (April 1965).

15. Final Technical Report, "Manufacture and Hydrotest of Three 20 In. Diameter Maraging Steel Pressure Vessels", Control No. A-5180, The Budd Company (May 16, 1963 to October 16, 1964).

16. R. W. Boyle, A. M. Sullivan and J. M. Krafft, "Determination of Plane Strain Fracture Toughness with Sharply Notched Sheets", Welding Journal, V. 41, No. 9, Research Suppl. 428-s to 432-s (1962).

17. A. W. Brisbane, J. W. Hawn and R. T. Ault, "Fracture Toughness and Delayed Failure Behavior of 18 Percent Nickel Maraging Steel", Fourth Maraging Steel Project Review, Technical Documentary Report No. ML-TDR-64-225, V. 1 (July 1964).

18. W. F. Brown Jr. and J. E. Srawley, "Current Status of Plane Strain Fracture Toughness", NASA TMX 52209 (June 1966).

19. R. W. Boyle, "A Method for Determining Crack Growth in Notched Sheet Specimens", Materials Research and Standards 646 (Aug. 1962).

20. Thiokol Quarterly Interim Report No. 33-65, Thiokol Chemical Corp., Huntsville Div., Huntsville, Ala. (May 1965).

21. C. M. Carman, D. F. Armiento and H. Markus, "Fracture Toughness and Pressure Vessel Performance", Trans. ASME, J. Eng. for Power, V. 86, Series A, No. 4 (Oct. 1964).

22. D. L. Daigle and J. M. Nelson, "Evaluation of Three AMRA Program Rocket Motor Cases", Thiokol Chemical Corp., Huntsville Div., Report No. 16-66 (July 1966).

23. G. R. Irwin, "The Leading Edges of Fracture Mechanics", Thurston Lecture, ASME Meeting, New York (Nov. 1966).

24. "Tentative Method for NDT of Ferritic Steels", ASTM Designation E208-63T (April 1963).

25. P. E. Bennett and G. M. Sinclair, "Parameter Representation of Low Temperature Yield Behavior of Body Centered Cubic Transition Metals", ASME Paper 65-Met-11 (1965).

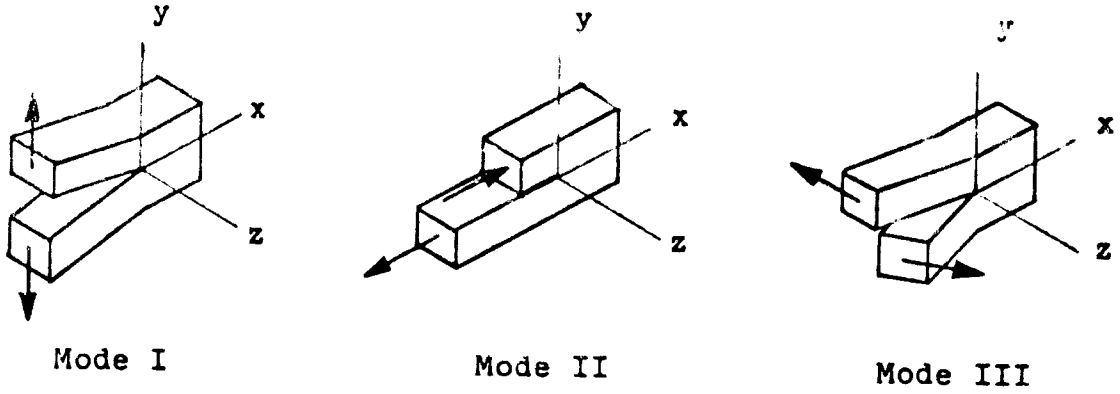

Figure 1. The Basic Modes of Crack Surface Displacements.

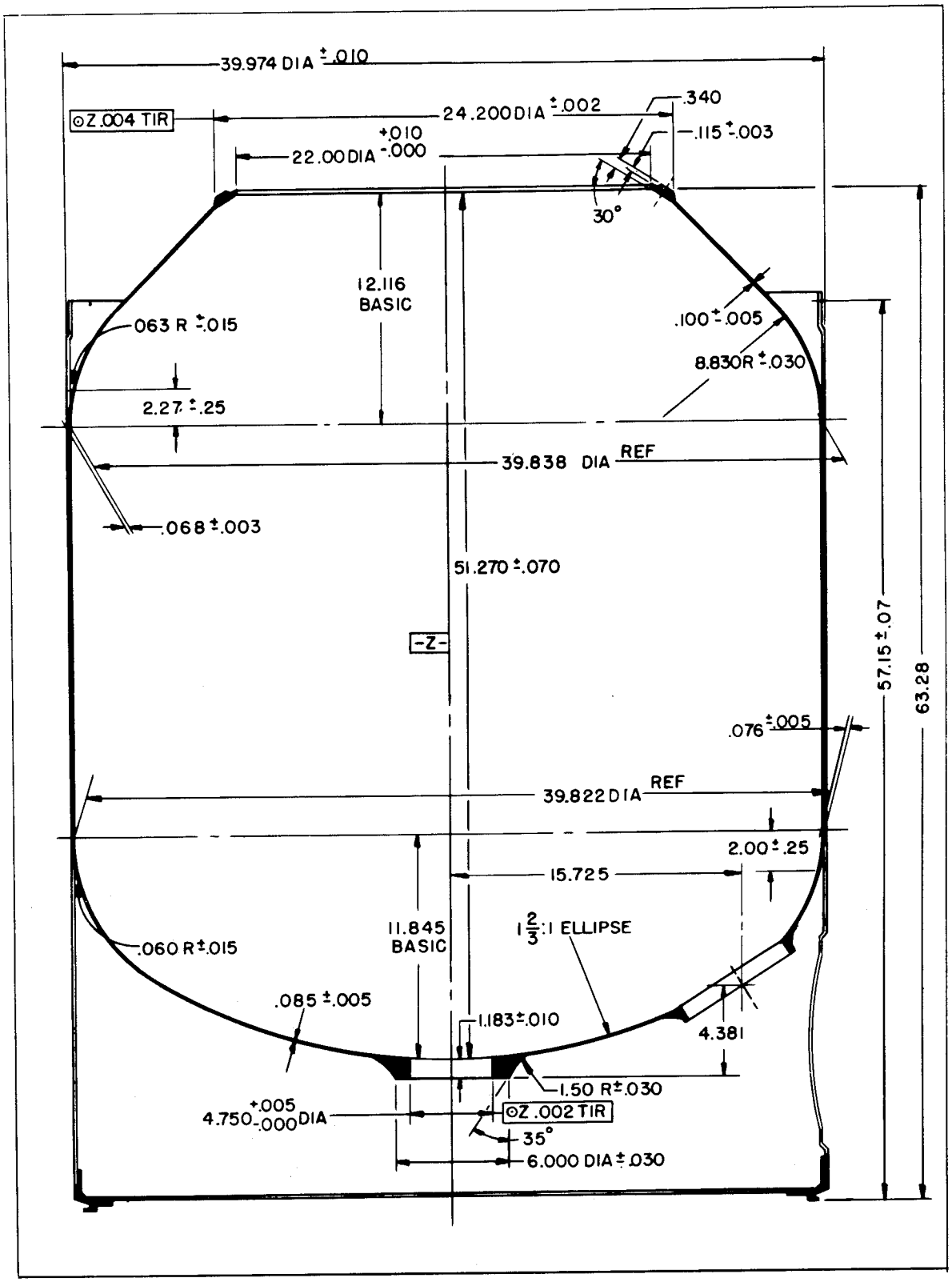

Figure 2. Drawing of Full Scale 40 Inch Diameter Rocket Motor Case.

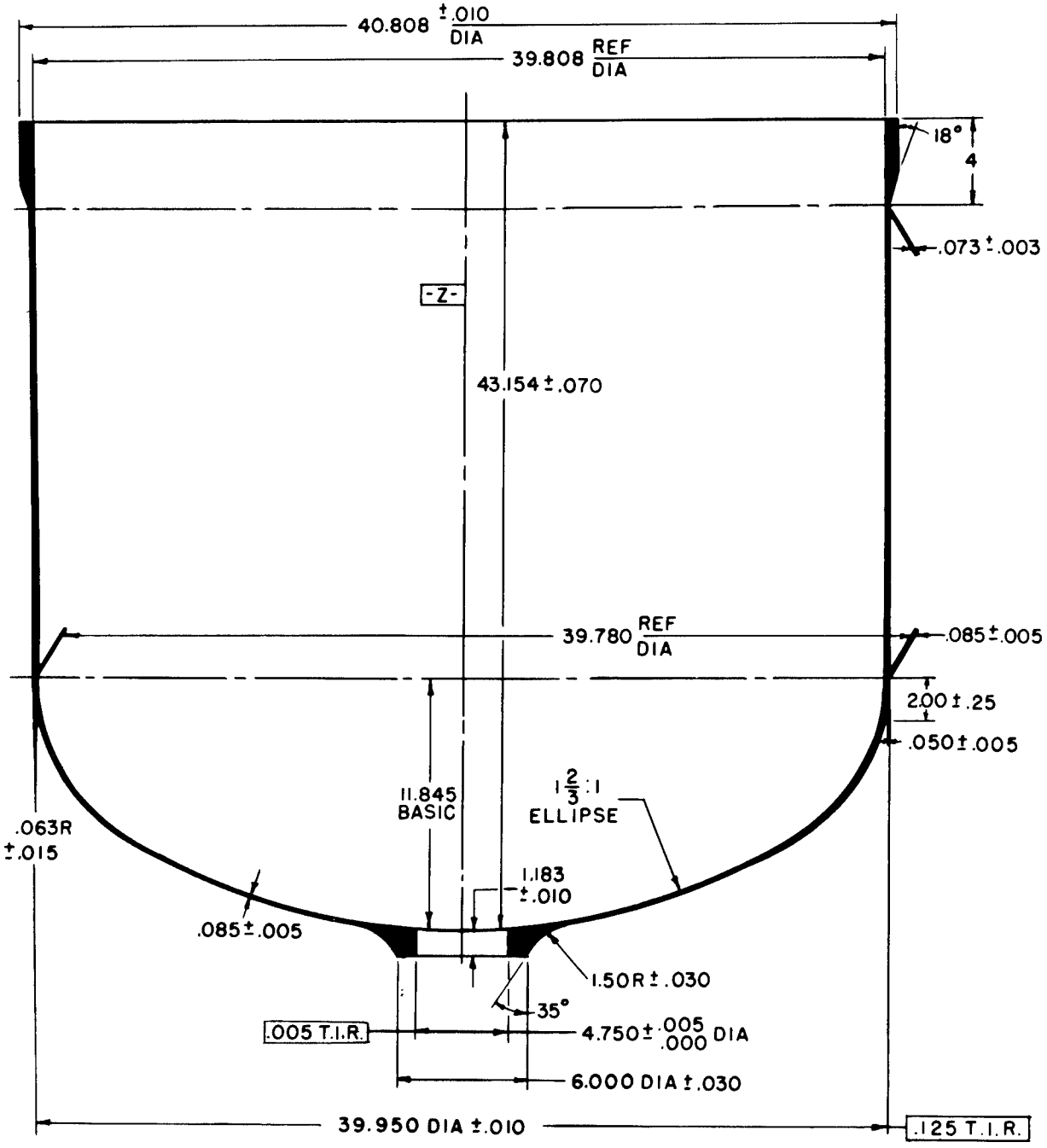

Figure 3. Drawing of 40 Inch Diameter Model Pressure Vessel.

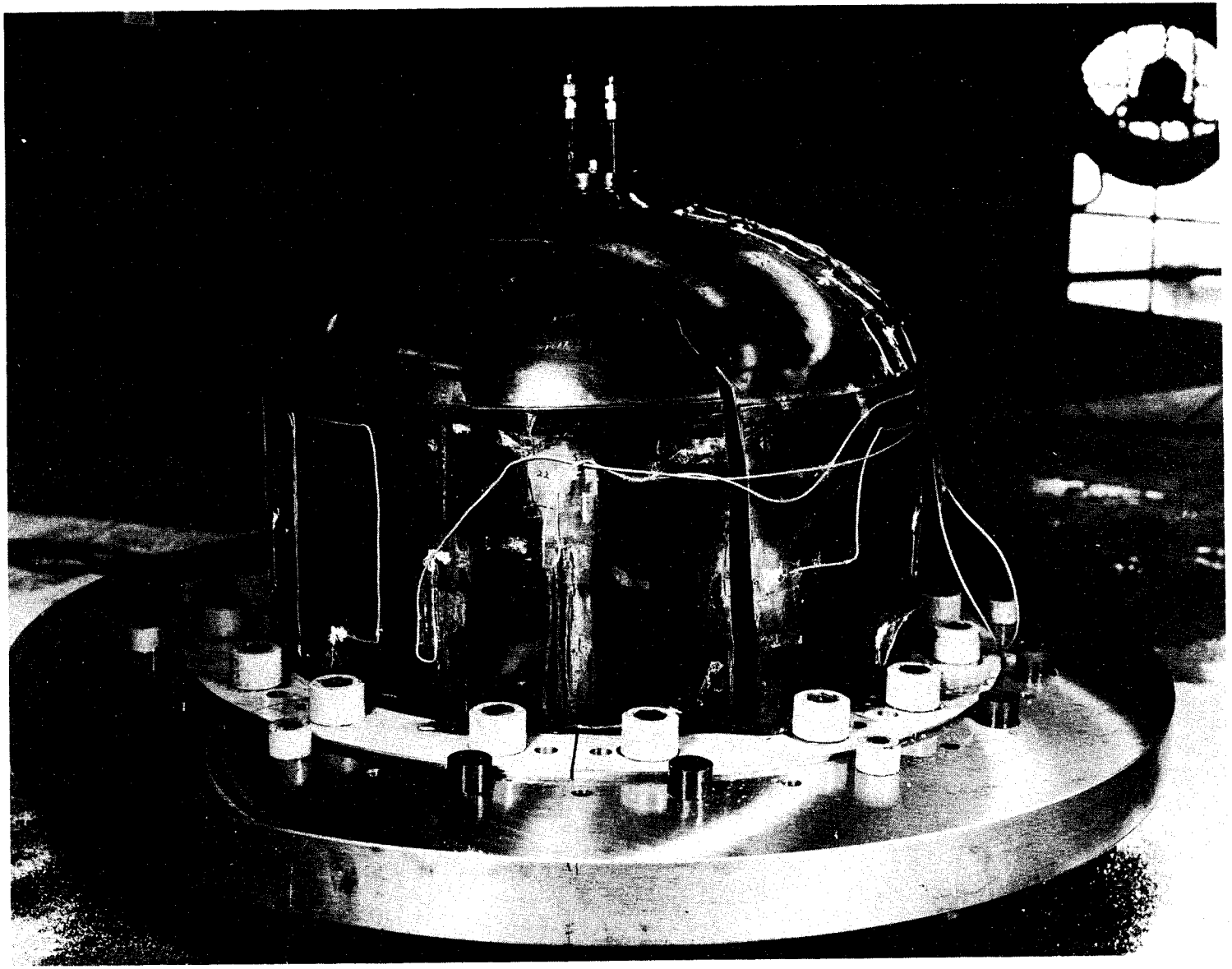

Figure 4. Photograph Showing Failure of 40 Inch Diameter Model Pressure Vessel.

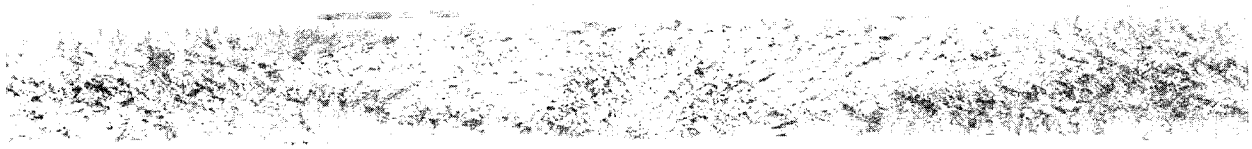

Low Magnification - 8X

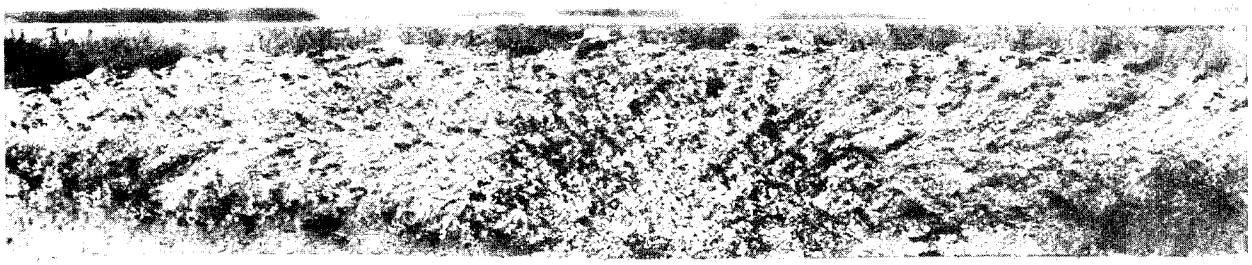

High Magnification - 15½X

Figure 5. Photograph Showing Origin of Failure in 40 Inch Diameter Model Pressure Vessel Made From 300M Steel.

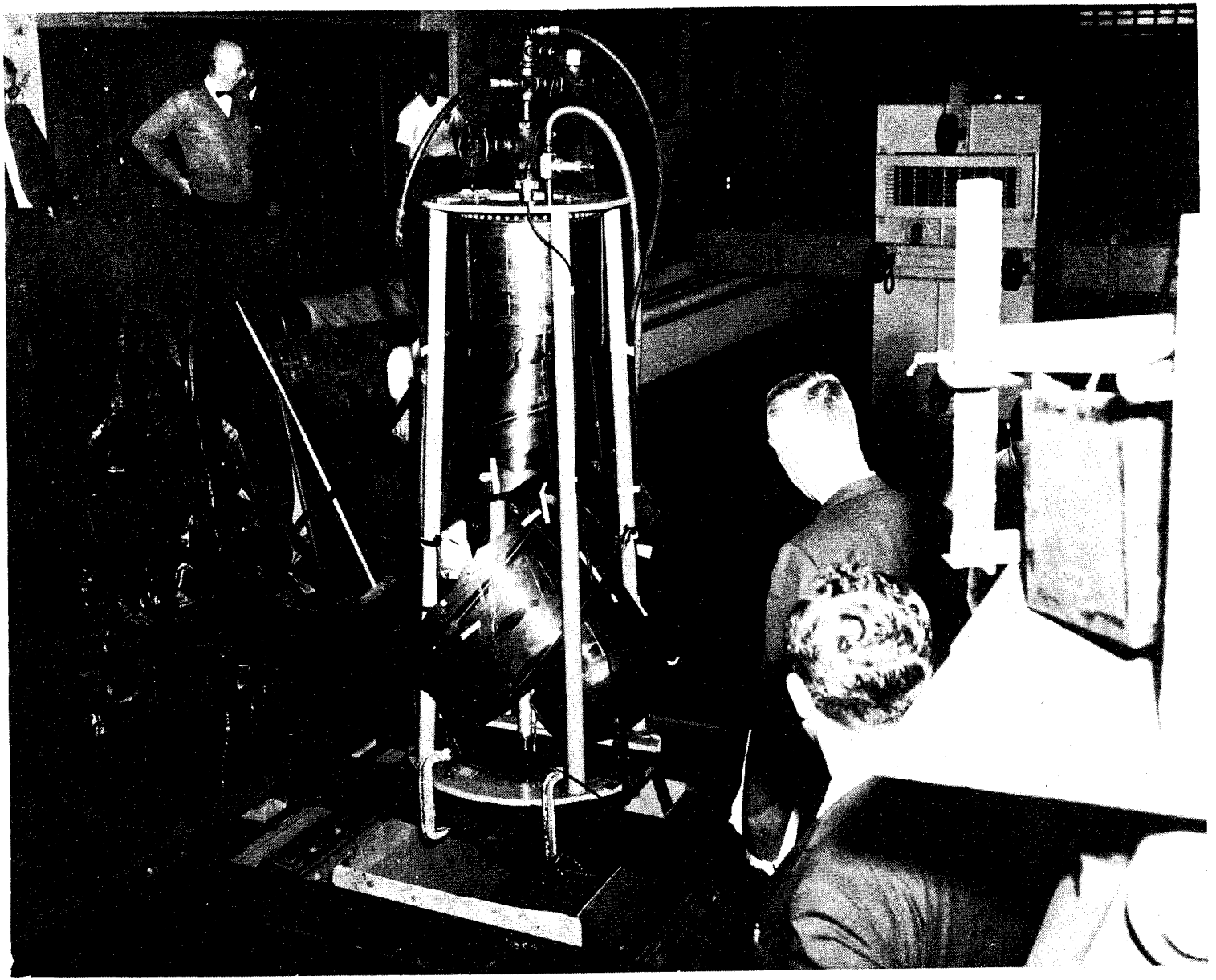

Figure 6. Photograph Showing Failure of Experimental 20 Inch Diameter Pressure Vessel Made From 20 Percent Nickel Maraging Steel.

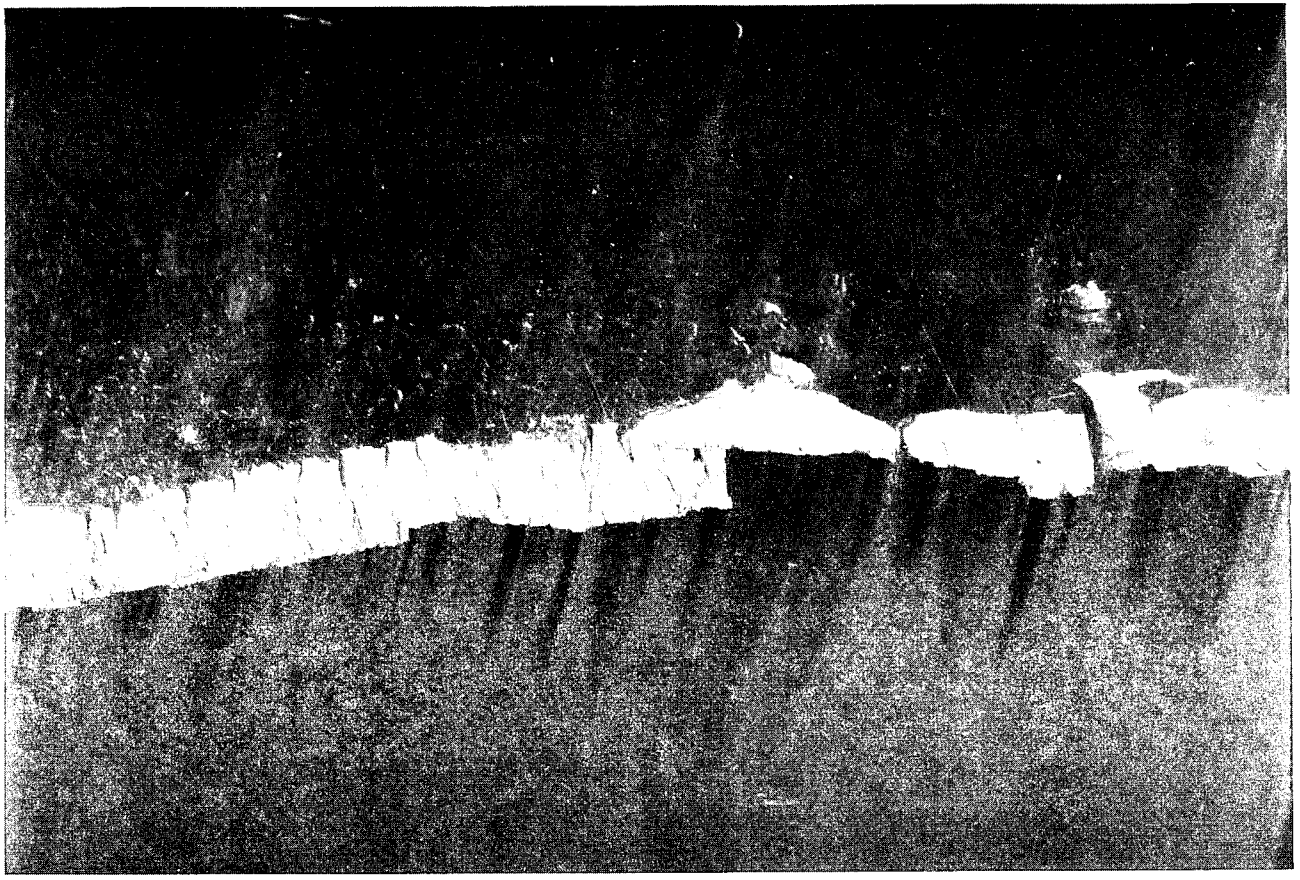

Figure 7. Photograph of Origin of Failure of Experimental 20 Inch Diameter Pressure Vessel.

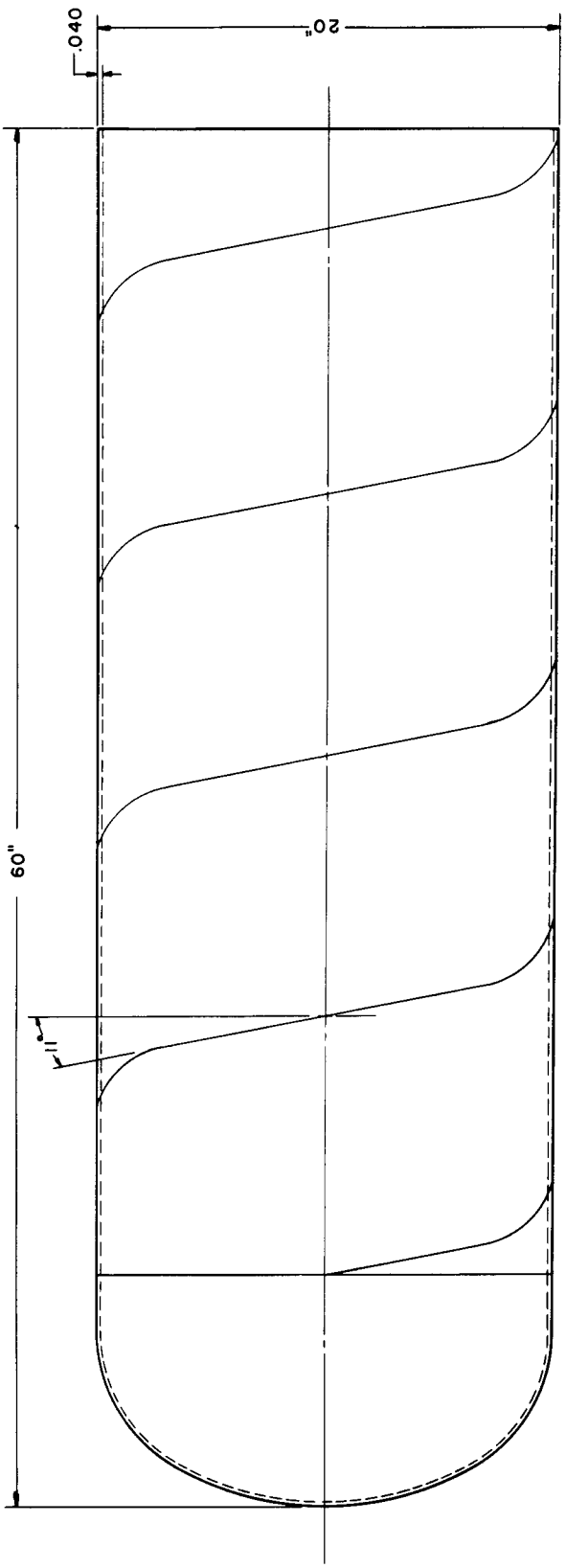

Figure 8. Design of 20 Inch Diameter Rocket Motor Case Fabricated by the Budd Company.

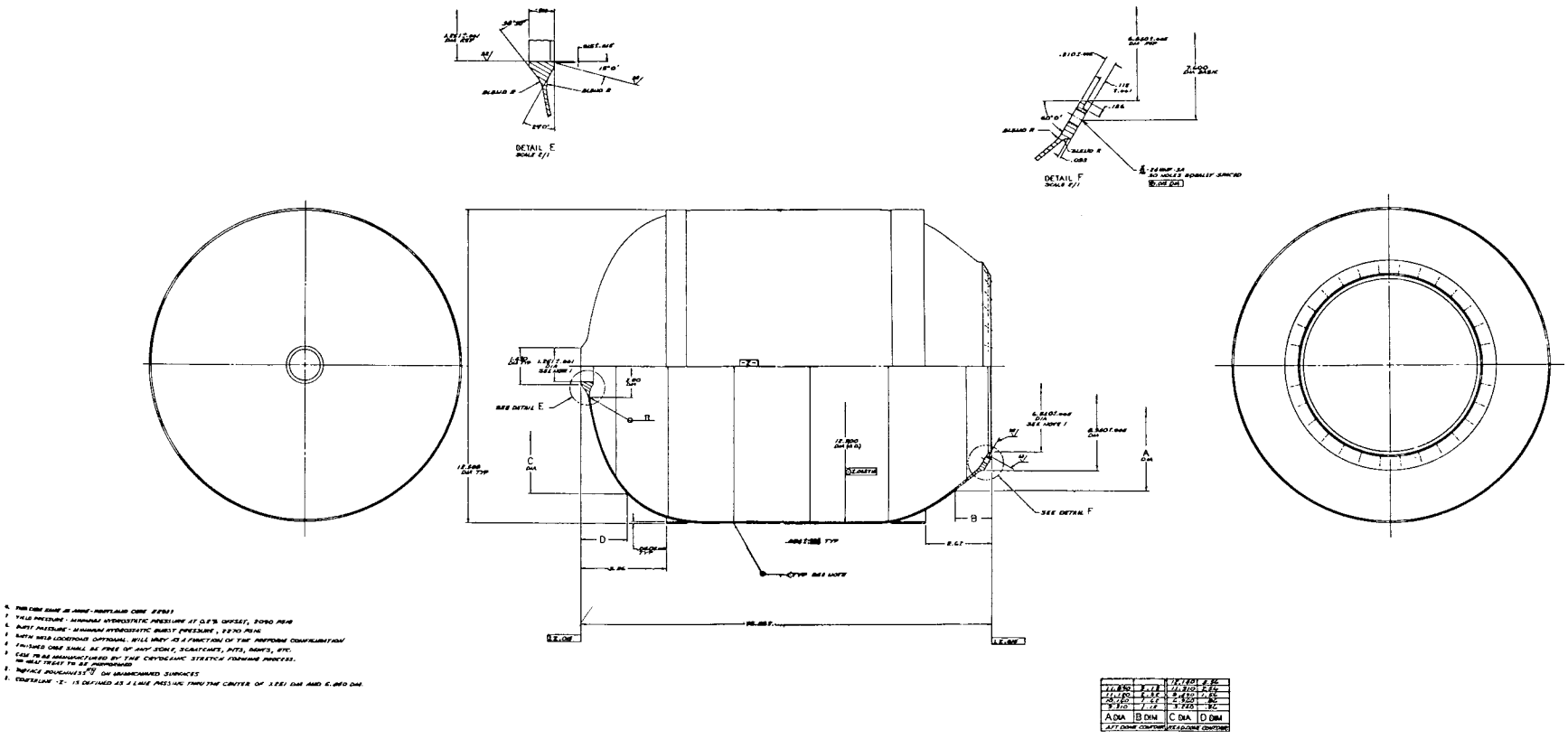

Figure 9. Design of 12 1/2 Inch Diameter Rocket Motor Case Fabricated by ARDE - Portland.

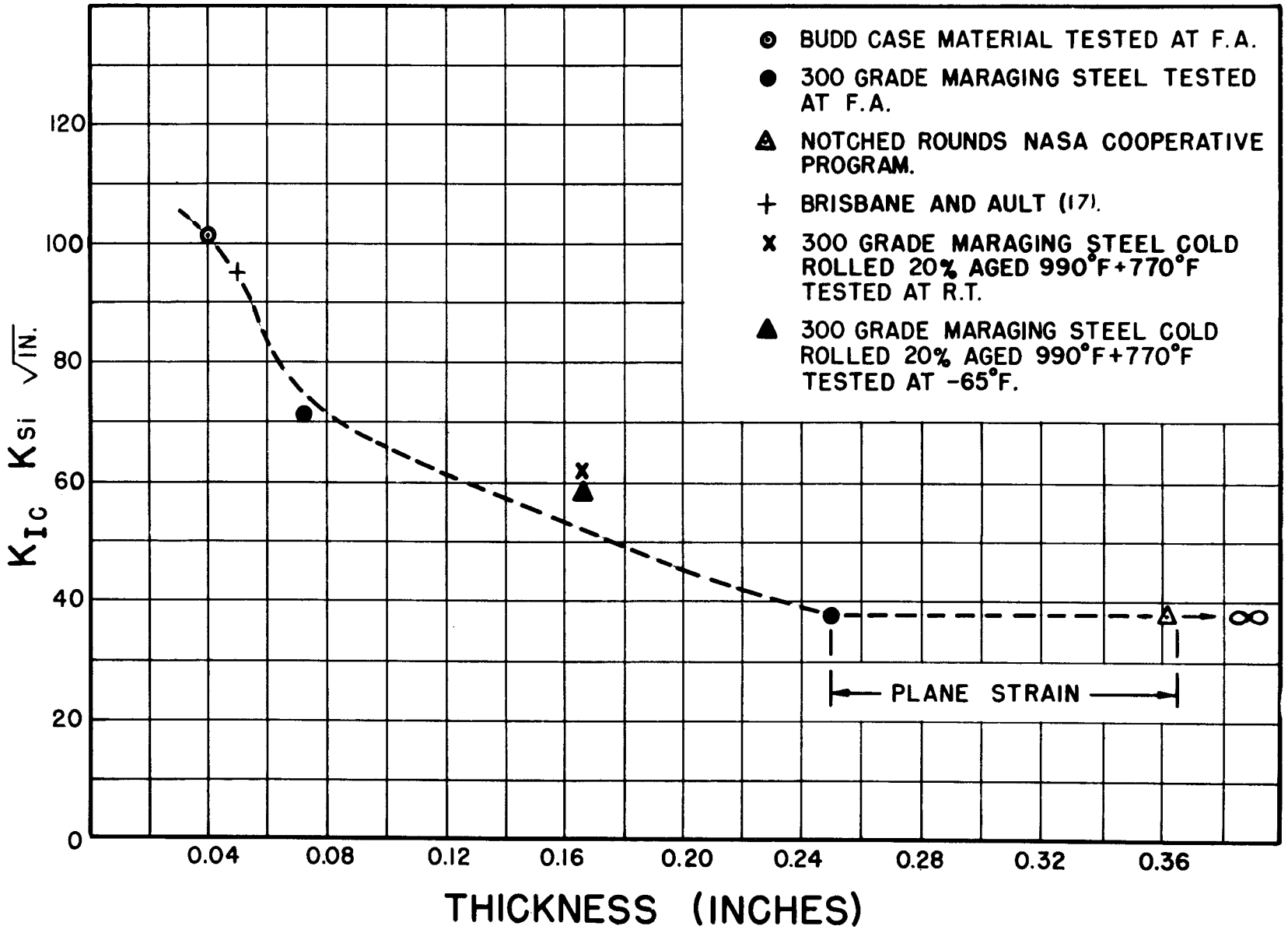

Figure 10. Pop-In Values of Plane Strain Fracture Toughness as a Function of Plate Thickness for 300 Grade Maraging Steel.

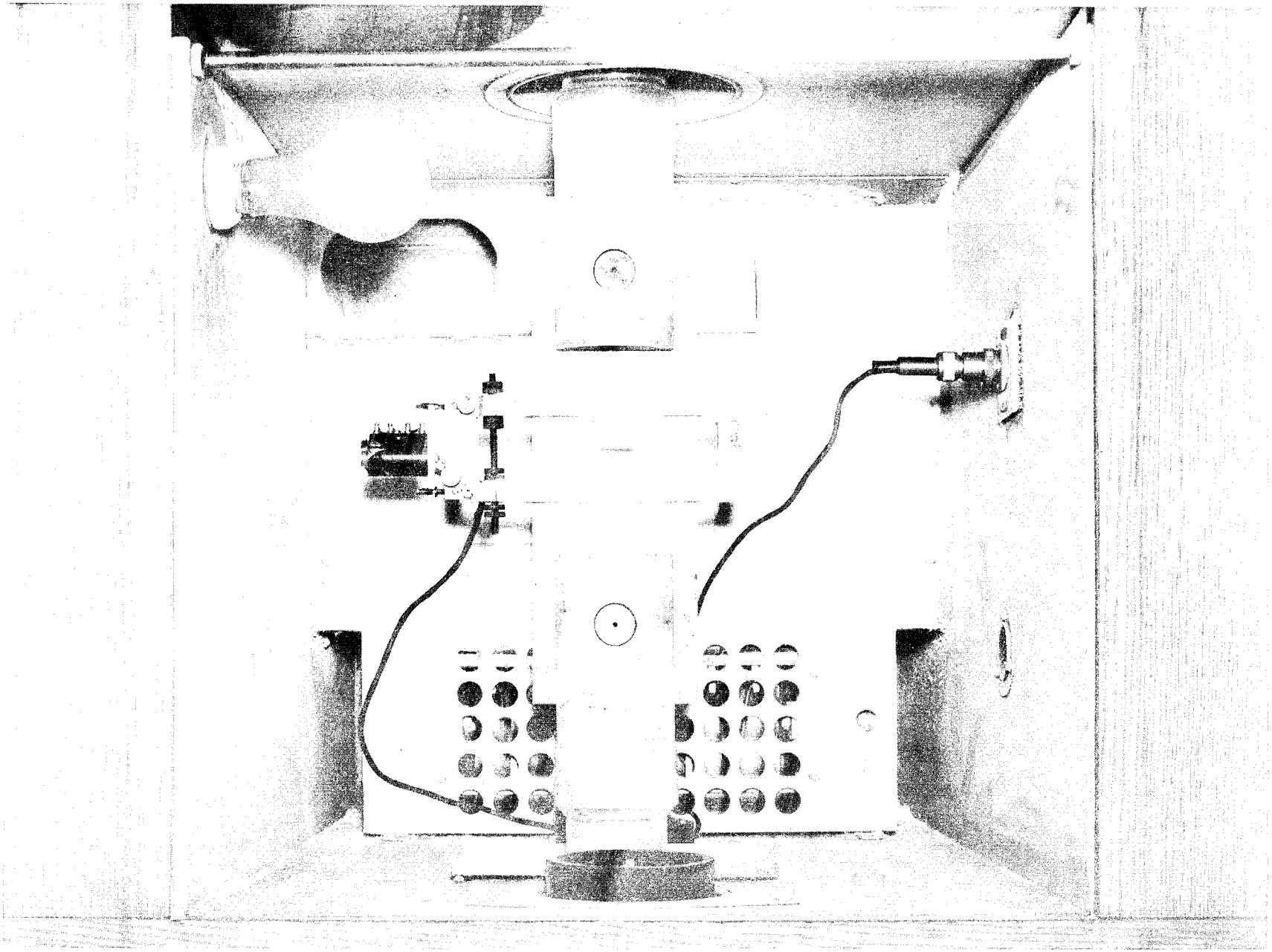

Figure 11. Photograph of Low Temperature Testing Equipment.

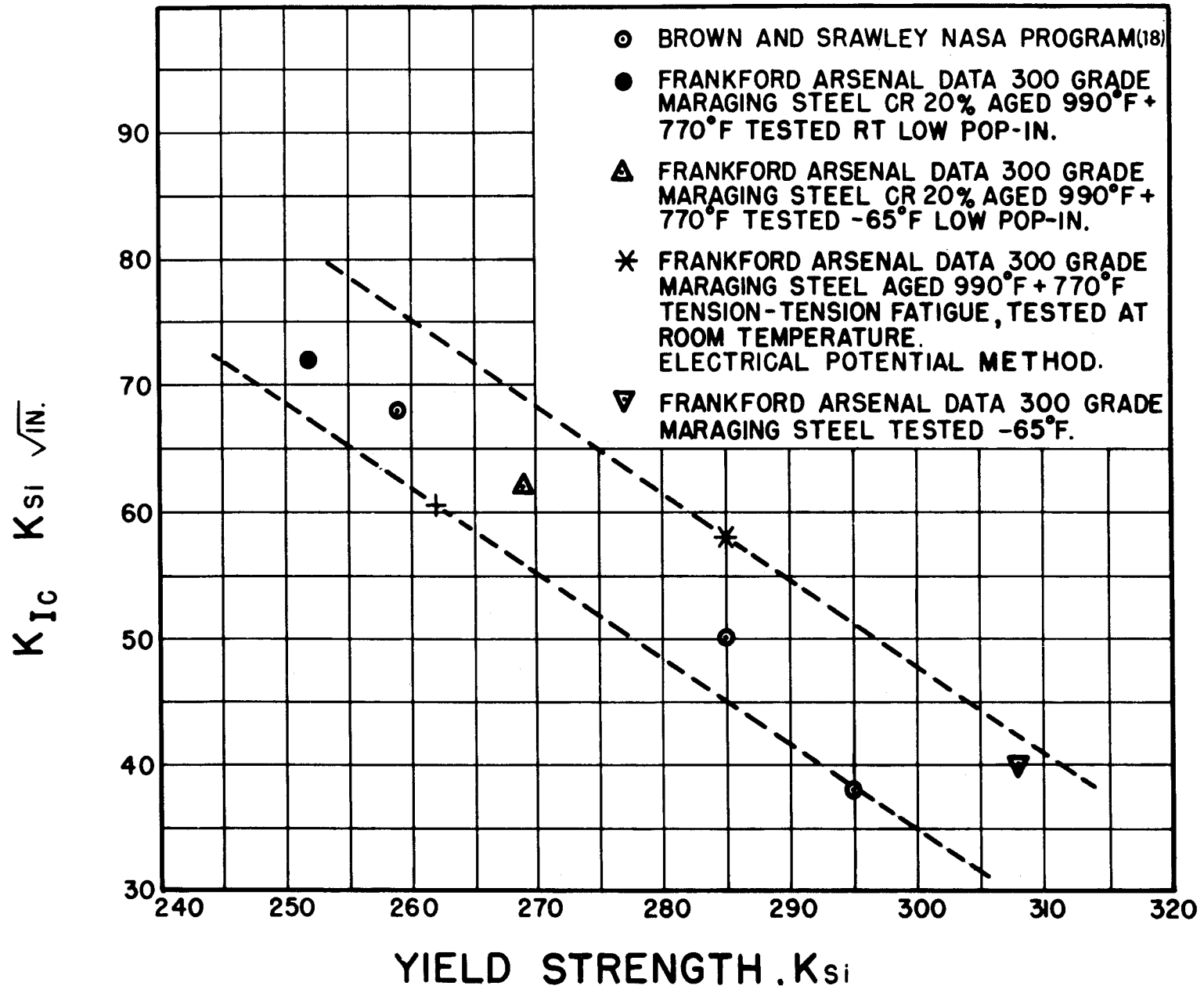

Figure 12. Plane Strain Fracture Toughness Values Versus Yield Strength for Maraging Steel.

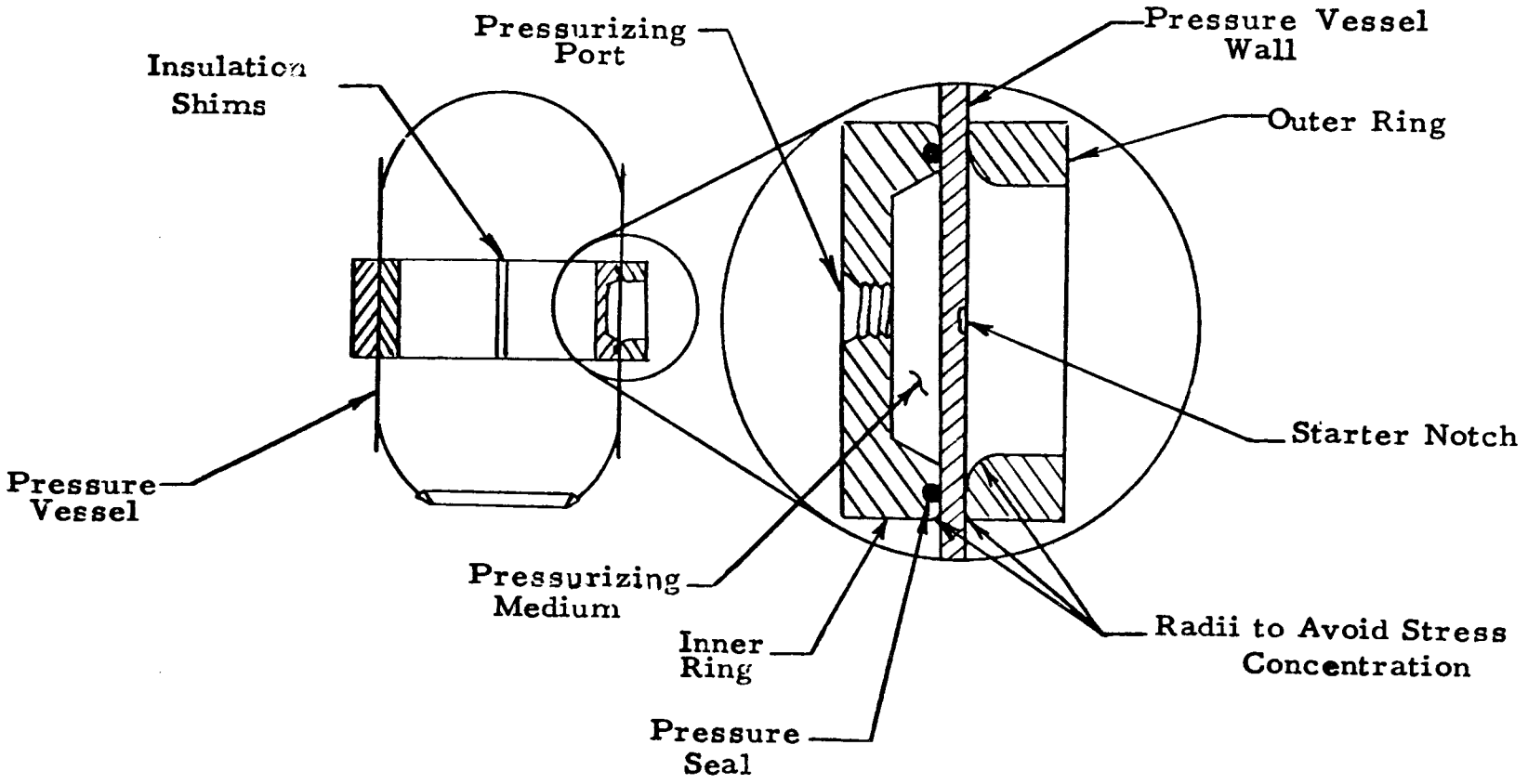

Figure 13. Sketch of Pressure Cycling Test Fixture.

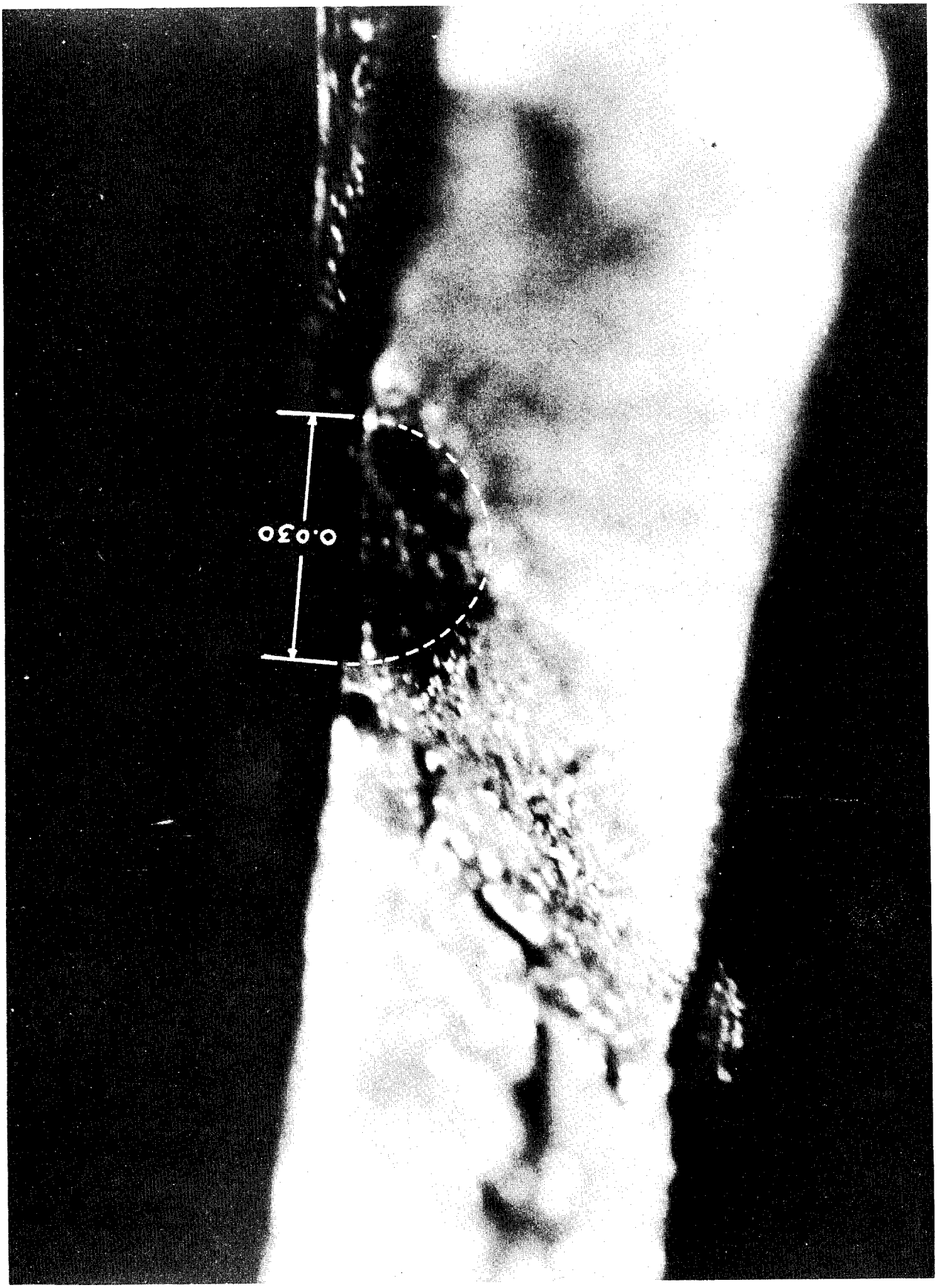

Figure 14. Fracture Origin in Budd Company Rocket Motor Case.

A SYSTEM APPROACH TO THE NONDESTRUCTIVE TESTING OF COMPOSITE MATERIALS

George Martin

North American Aviation, Inc.

Los Angeles, California

INTRODUCTION

The terms "quality control", "nondestructive testing", and "defect detection" have become almost synonymous. The classic picture of the nondestructive testing (NDT) expert is that of the coin tapper looking for flaws, which the shop blames on the material, and the metallurgist on the shop. Fortunately, this classic picture is slowly fading. NDT is now being seen, albeit still rather dimly, as a method of predicting system performance prior to the system mission. This new concept received a great impetus when the aerospace industry changed from a mass production approach to a job shop operation.

The purpose of this paper is to analyze NDT procedures, fundamentally, in terms of the mechanical properties of materials to which they can be directly related, with special reference to the problems of composite materials and structures. To cover this field, a multidisciplinary approach is required. Data and methods used by electrical engineers, mechanical engineers, metallurgists and physicists must be considered. Common terms which may have differing meaning in several disciplines must therefore be defined.

Mechanical properties are the properties which characterize the response of a material, structure or system to a mechanical load. They can be divided into three groups as follows:

1. The actual strength of the material, structure or system. This is defined as the load level at which a physical separation takes place, which catastrophically reduces the load-carrying ability. This limitation is important, because we know that physical separation in a material or structure can occur to quite an appreciable extent without significantly affecting the load-carrying ability. An example is fracture toughness, where a crack must grow to a critical size before it becomes embarrassing.

2. The stress level at which a deformation occurs, which renders the system ineffective. This may be the yield point in a simple specimen; it may also be an excessive amount of creep or any other arbitrary factor selected by the designer. For instance, many high temperature structures are designed to a 0.1 percent creep limit, i.e., the designer expects that amount of deformation during service and allows for it in the design.

3. The deformation of the system up to the stress level indicated by group 2. Almost exclusively, the stress/strain relation in that region are assumed to be linear and reversible, i.e., perfectly elastic. This group of properties is therefore referred to as the elastic properties of the material, structure or system.

It is important to note that groups 1 and 3 are the most important. This seems to be due to a fundamental reason and a practical consideration. The fundamental reason is the experimentally demonstrated fact that the stress difference (but not the strain difference) separating the level at which complete failure occurs and the level at which significant deformation occurs generally do not differ greatly. The practical reason is that beyond the point of significant deformation the stress/strain relations become very complex and can only rarely be expressed analytically.

So far, we have not restricted ourselves to any limitations as to complexity of the system. The foregoing observations are as applicable to a complex heterogenous and discontinuous structure, such as a wing, as they are to a homogenous and continuous material. These considerations are illustrated in figure 1 in the form of a stress/strain diagram. Such diagrams can be plotted for any desired spatial point in our system under given service conditions, such as vibrations, temperature, etc. The purpose of the diagram is to show that there is no necessary relationship between the service response and the maximum load. Estimates of system performance therefore face two distinct problems: (1) to estimate the maximum load-carrying capacity, and (2) to estimate the service moduli.

Two approaches to NDT of systems are now possible. In one we can inspect the constituent materials and determine their compliance with a preset reliability level, and then check their joints with a similar level of reliability. In a system or structure where the total performance is the sum of the performance of each definable member, such an approach is justified, provided we can determine both maximum load-carrying ability and moduli of each member. However, as structural systems tend to become systems where the component materials interact, such as in a filamentary composite, this approach is no longer justified and the system must be evaluated as a whole.

The term "composite" also needs definition. Here, it will be used to describe a structure consisting of several phases arranged in geometrically definable patterns. Two types can be distinguished: the continuous type and another type which, for want of a better definition, we shall call the discontinuous type. These definitions relate to the appearance of one of the phases in a cross section of the system. Both types may be two or three-dimensional composites such as cross-plyed fiber-reinforced composite. The term "phase" refers only to materials with properties of the same order; for instance, the phase consisting of the air or a foam filling between the ribs or struts of a two-dimensional composite need not be considered, unless it alters the properties of the composite. The types of composites are illustrated in figure 9.

Basically, therefore, the search for NDT approaches requires the determination of two distinct mechanical properties. The first is the maximum load-carrying ability which we shall call the strength; the other is the determination of the deformation moduli, which generally reduces to a determination of the elastic constants. Before we can study the problem in composites, it is useful to scan the state-of-the-art of solutions to the determination of these two groups of properties in simple, that is, homogenous isotropic and continuous materials. The term homogenous is used here on the engineering scale and does not eliminate materials comprising several metallurgical phases or containing microscopic inclusions or defects.

NONDESTRUCTIVE DETERMINATION OF THE STRENGTH OF SIMPLE MATERIALS

Two basic approaches are used to determine nondestructively the strength of isotropic materials. The first is the empirical approach in which we relate the strength to a signal obtained by the measurement of a variety of physical properties and, from empirically determined calibration curves, determine the strength of the sample. For instance, stresses or metallurgical transformations can be related to the electric resistance of many commercial alloys. Direct resistance measurement or eddy current methods can therefore in many cases be calibrated to indicate deviations of the sample from a standard and, in some cases, also be used to give quantitative information. Such methods are generally simple, but calibrations have to be carefully standardized and results cannot generally be extrapolated beyond the limits of the standards. Another variant of this approach is the utilization of empirical relationships which may occur between the strength of a material and its modulus. As figure 1 shows, modulus measurements cannot be extrapolated to the strength value unless an empirical test shows that the modulus is in some way related to strength for a particular material.

The other approach is based on the assumption that a material without defects has a known strength which is proportionately decreased by defects in the material. This approach is capable of considerable refinement. Simple examples of this approach are radiography, which detects defects caused by density changes, or the use of microwaves in plastics, which are attenuated to a varying degree by porosity. Theoretically, once the assumption underlying this approach has been demonstrated for a given material, extrapolations can be carried out. In its ultimate refinement, this approach could be used to determine the strength of a material from measurement of its actual atomic or molecular structure. The theoretical strength of a perfect metallic lattice is about E/11. Point defects, line defects, precipitates, solute atoms and inclusions detract from this perfection and reduce the strength of metals and alloys to a level approximately three orders of magnitude lower than the theoretical strength. The total load-carrying ability of a material is therefore its theoretical load-carrying ability, were it a perfect lattice, less the loads required to overcome all the stresses and resistances introduced by its many lattice, microscopic and macroscopic defects. Of course, it is unlikely that a rigid analysis of all the various factors will ever be evolved because of their many interactions. However, it has been shown that the losses due to various defects can be related to the damping of an energy impulse. Furthermore, specific losses cause damping at specific impulse frequencies. In recent years, our understanding of the defect/damping loss relationships has made tremendous strides and now offers one of the most potent tools for the nondestructive determination of actual strength.

Damping is quantitatively described by a loss factor, η, given by

$$\eta = W_D/2\pi W_o \qquad (1)$$

i.e., the energy dissipated per cycle/total energy input. W_D can be related to a specific damping coefficient, D, by

$$W_D = \int_0^V D dV \tag{2}$$

In isotropic materials the specific damping coefficient is a function of the material response in terms of its intrinsic properties, temperature, frequency and stress response. Thus

$$W_D = \int_0^{\sigma d} D\frac{dV}{d\sigma}\, d\sigma \tag{3}$$

for the general case where the stresses throughout the structure are not uniform. This integral may be rewritten by introducing a coefficient D_d, the damping coefficient at the maximum stress σ_d in the structure, as follows:

$$W_D = W_d V_o \alpha \tag{4}$$

where α is a damping energy integral

$$\alpha = \int_0^1 \left(\frac{D}{D_d}\right) \frac{d(V/V_o)}{d(\sigma/\sigma_o)}\, d(\sigma/\sigma_d) \tag{5}$$

This integral can be solved analytically for simple cases and by graphical or computer methods for many other cases, provided the damping function

$$D = f(\sigma) \tag{6}$$

is known.

The total strain energy W_o is given by

$$W_o = \int_0^{V_o}\int_0^{\varepsilon_{max}} \sigma d\varepsilon dV \tag{7}$$

within the elastic range, $E = \sigma/\varepsilon$, and

$$W_o = \int_0^V \frac{1}{2}\frac{\sigma^2}{E}\, dV$$

which can be rewritten

$$W_o = \frac{1}{2} \frac{\sigma_d^2}{E} V_o \beta \tag{8}$$

where σ_d is the maximum stress and β is a stress distribution integral given by

$$\int_o^1 (\sigma/\sigma_d)^2 \frac{d(V/V_o)}{d(\sigma/\sigma_d)} d(\sigma/\sigma_d) \tag{9}$$

The values for the damping energy integral and the stress function integral for various loading conditions are given in Table I. Actual structures in isotropic materials may now be analyzed if appropriate assumptions are made for the damping function $D = f(\sigma)$ and the modulus function $M = f(\sigma)$. Note also that the values of the damping energy integral and the stress function integral are unity only for the case where a uniform stress distribution exists throughout the structure, such as in a simple tensile or compressively loaded member. The damping function is frequently expressed as

$$D = T\sigma^n \tag{10}$$

and values for the integral α as a function of n are included in Table I.

For the elastic case, equation 8 becomes

$$W_o = \frac{1}{2} (\sigma_d^2/E) V_o \beta \tag{11}$$

and substituting this equation and equation 4 into equation 1, the loss factor η is given by

$$\eta = (E/\pi)(D_d/\sigma_d^2)(\alpha/\beta) \tag{12}$$

The factor α/β is unity only for the case where the damping function exponential n is equal to 2 for any loading condition or for the case of the simple tensile or compressively stressed member. This observation is important because many damping experiments are performed, for instance, on vibrating beams, where this factor is not unity, but has been neglected. The error which can be introduced by ignoring the stress distribution in structures which are not loaded in simple tension or compression is indicated from the size of the factor shown in figure 3, plotted against the exponent "n". This exponent is known to vary to about 30, especially at higher stresses. The loss factor n is also frequently denoted by $\tan \delta$ or by ϕ where $\tan \delta$ is the loss angle, and for small values of δ equal to the phase angle ϕ by which the strain lags behind the stress in sinusoidal loading.

An analytic expressions descriptive of the stress/strain relationship other than elastic can be assumed, and inserted in equation 7, and further solutions for the loss factor can be derived. For simplicity, let us assume the

simplest loading case of tensile or compressive loading, which removes the integral of strain variation over the volume and α and β become unity. Equation 7 therefore becomes

$$\int_0^{\varepsilon_d} \sigma d\varepsilon = \sigma_d \varepsilon_d - \int_0^{\varepsilon_d} \varepsilon d\sigma \tag{13}$$

For elastoplastic materials, the relationship

$$\sigma = K\varepsilon^m \tag{14}$$

is frequently used. Equation 13 can therefore be integrated to

$$W_o = \left[\frac{\sigma_f^{(1+m)/m}}{K^{1/m}} - \frac{m}{1+m} \frac{\sigma^{(1+m)/m}}{K^{1/m}} \right] V_o \tag{15}$$

The total work to failure at stress σ_f is

$$W_f = \left[\frac{\sigma_f^{(1+m)m}}{K^{1/m}} \right] \left[\frac{1}{1+m} \right] \tag{16}$$

Combining this with equations 1 and 4

$$\eta = D_d / W_f \tag{17}$$

Further solutions depend now on the relation between D and σ. If we assume equation 6 to hold to failure

$$\eta = T\sigma_f^2 \Bigg/ \left\{ \left[\frac{\sigma_f^{(1+m)m}}{K^{1/m}} \right] \left[\frac{1}{1+m} \right] \right\}$$

which becomes

$$\eta = L\sigma_f^{\ell} \tag{18}$$

where

$$L = T/K^{1/m}\, m \times 2\pi \text{ and } \ell = n + (1+m)m$$

The value of such a relationship lies in the fact that η can be determined from a number of comparatively simple experiments, under the assumptions made here. Again, these assumptions were:

1. A uniform distribution of stress and strain throughout the structure

2. A simple time independent exponential relationship between stress and strain and between the specific damping coefficient and stress

If the exponential relationships cannot be assumed, but actual stress/strain curves and specific damping coefficient/stress curves are available for the material, a solution for equation 1 can still be obtained by graphical or computer methods. If the stress distribution throughout the specimen is not uniform, then an integration factor taking care of this variation must be introduced in the relationship through a strain distribution integral γ analogous to the integrals α and β.

Our problem becomes somewhat more complex if time dependent stress/strain and damping coefficient/stress relationships occur. This is the case with visco-elastic materials, which include metals at elevated temperature and most organics. The approximate behavior of such materials is described by a model called a linear visco-elastic body, which can be simulated by the spring and dashpot arrangement shown in figure 4 and whose behavior is given by the mathematical relationship:

$$\sigma + \tau_\varepsilon \dot{\sigma} = M_r(\varepsilon + \tau_\sigma \dot{\varepsilon}) \tag{19}$$

The modulus M_r is called the relaxed or steady-state modulus, the factors τ_ε and τ_σ are the relaxation times for stresses at constant strain and for strain at constant stress, respectively.

Such a system may be loaded by a continuous and constant load or strain, such as a creep load, or it may be loaded by repetitive load impulses. In the latter case the ratio of peak load to strain in phase with the load is called the dynamic or unrelaxed modulus M_u. M_u and M_r are proportional to the ratio of σ_o and τ_ε. Under conditions of periodic loading

$$\sigma(t) = \sigma_o \exp(i\,\omega t) \text{ and } \varepsilon(t) = \varepsilon_o \exp i\,\omega t \tag{20}$$

and equation 19 therefore becomes

$$(1 + i\,\omega\tau_\varepsilon)\sigma_o = M_R(1 + i\omega\,\tau_\sigma)\varepsilon_o \tag{21}$$

or in terms of a complex modulus M^*

$$M^* = \frac{1 + i\omega\,\tau_\sigma}{1 + i\omega\,\tau_\varepsilon} M_R \tag{22}$$

The real component of this modulus is the ratio of stress to strain in phase with the stress, M_ω, given by

$$M_\omega = \frac{1 - \omega \tau_\varepsilon^2}{1 + \omega^2 \tau_\sigma \tau_\varepsilon} M_u \tag{23}$$

For values of $\omega \tau_\sigma \tau_\varepsilon << |M_\omega$ tends to be equal to M_r, while for values of $\omega \tau_\sigma \tau_\varepsilon >> |M_\omega$ tends toward M_u. The loss factor η can be related to this frequency modulus by

$$\eta_\omega = - \frac{\pi}{2} \frac{d \ln M_\omega}{d \ln \omega} \tag{24}$$

The concept of strength in such materials is more difficult to define, because it is no longer a material variable, but also depends on the loading rate. For instance, in the model in figure 4, a very rapid loading rate would eliminate the dashpot effect, unless its viscosity coefficient is very low, while a very slow loading rate would make the strength of the system virtually dependent on the strength of the spring with spring constant K_2. Material properties could thus be deduced from the comparison of the relative system response at two frequencies varying significantly in terms of the viscosity and spring constants. Once the fact of the nonconstancy of strength is realized, evaluation of the damping characteristics of such systems can be used to obtain much valuable information on material quality and properties.

Of particular importance to material evaluation are damping peaks at specific frequencies, which can be related to physical phenomena within the material. The loss factor can be related to the relaxation times and frequency by the equation

$$\eta = \frac{\omega(\tau_e + \tau_\sigma)}{1 + \omega^2 \tau_e \tau_\sigma} \tag{25}$$

This equation has a peak for values of $\omega^2 \tau_e \tau_\sigma = 1$ and a frequency versus loss factor graph indicates a number of characteristic peaks associated with specific phenomena. Such a spectrum is shown in figure 5. A great deal of work has been done in recent years on the analysis of such spectra and the study of their significance. However, many of these studies have been directly related to solid-state physics phenomena, which as yet cannot be fully exploited for applications in NDT. The problem is the determination of the relationship between stress and relation times for various frequencies. As the stress level increases, not only the peaks of the relaxation spectrum shift, but also the position of the several peaks and new peaks that appear. This is indicative of various deformation mechanisms at different stress levels for a given material. A complete physical and analytical understanding of these mechanisms, at this time, seems rather remote. However, the general approach and a qualitative understanding of the relation of the factors and moduli involved is a very promising approach to NDT. Very useful results have been obtained

by measurement of damping of magneto-elastic, ultrasonic and comparatively low frequency (sonic) vibrations to establish test methods for fatigue limits and strength levels. Damping resonance peaks, not only of mechanical vibrations but including ultrasonic vibrations, and also of electromagnetic vibrations and interactions, have also been used successfully for NDT inspection purposes.

One of the basic assumptions underlying the treatments in this section has been the isotropy of the material. This implies that the phenomena discussed are volume or mass phenomena independent of any surface properties. However, many mechanical properties are closely related to surface effects and manifest themselves, in their early stages at least, by surface perturbations. An analysis of the vibratory phenomena of a surface, covering electromagnetic as well as mechanical vibrations, would therefore be very useful for the development of NDT methods for such surface sensitive properties. However, as far as can be ascertained, no such analysis is yet available, though numerous experiments with surface vibrations, such as high frequency current effects and ultrasonic surface waves, have shown promise.

The philosophy underlying this discussion on strength determination resolved itself into a negative approach, the measurement of losses detracting from the theoretical or maximum strength. Consideration must be given to the positive approach of direct methods of measurement of measuring cohesive properties nondestructively. This problem must be attacked on at least two scales: the atomic scale and the metallurgical or microscopic scale. As yet, no actual methods seem to be available. One can, however, speculate on possible approaches. Present destructive test methods depend on the measurement of cohesion between lattice sites, i.e., the positively charged force centers. In metal, at least, these are electrically counterbalanced by the complex distribution of electron levels. Perturbations in this electron distribution carry through to the microscopic scale of approach. Phenomena associated with these electron levels are studied through a number of effects, such as Hall effects, electron resonance and nuclear magnetic resonance. A tentative start has been made in the evaluation of such effects for NDT purposes. It has been shown, for instance, that both the nuclear magnetic resonance and the Moessbauer effect are stress dependent.

ELASTIC PROPERTIES OF SIMPLE MATERIALS AND NDT

The determination of elastic properties of materials for nondestructive purposes has several applications. First, a knowledge of elastic properties as such is required for material evaluation. Secondly, elastic properties can be used as a basis for empirical extrapolation of strength data. Finally, a knowledge of elastic properties is essential for the determination of stresses within the elastic range, such as the wide field of measurement of residual stress. Three principal methods are available for the nondestructive determination of elastic properties: X-ray diffraction, deflection measurement and mechanical vibration analysis.

The use of X-ray diffraction depends on the measurements of the lattice parameter response to small known strains. However, in polycrystalline materials the measured values do not agree too well with elastic properties obtained by other tests. This is due to the elastic anisotropy of the crystallites of the polycrystals and the selective properties of an X-ray beam, which tends to pick out crystallites with certain orientations only. Correction factors can be developed, but these factors are available for a limited number of alloys only. A further disadvantage of the X-ray method is that only surface layers can be examined; a bulk examination requires successive surface removal and is a very tedious method.

Deflection measurement methods are simply bend, torsion, tensile or compression tests carried out with relatively low forces. The practical problem is generally that of measurement of very small strains. However, a more fundamental problem exists in these tests and that is the restraint placed on the structure by whatever method is used to transmit the load. For instance, in the testing of a sheet, grips are used to hold opposite edges to apply tension. These grips also constrain the contraction of the sheet and strain measurements near the edges would therefore give erroneous results, as far as the true elastic properties of the sheet material are concerned. The same problem applies in bending, where the clamping affects the deflection quite profoundly. If the deflection under a given load is used to measure the elastic constants, considerable variations can occur. For instance, in a simple beam the maximum deflection for the freely supported beam, centrally loaded, is four times that of the same beam under the same central load, but with the ends clamped rigidly. For plates the variation is even greater.

If a load is applied to a structure and subsequently suddenly released, the deformed structure will not return to its original shape immediately, but will vibrate with a frequency called the natural frequency of the structure. If a force pulse is applied to the bar at that frequency, the vibrational amplitude will tend to increase. A resonance condition between the pulse and the structure is established and this frequency is also called the resonant frequency. For any point on a vibrating structure, the transverse inertia force of the element mass is equal to the restoring force component in the transverse direction. In the simplest case, that of a slender bar of length ℓ under tension T, with mass w/g, whose stiffness can be ignored, this balance can be expressed as

$$\frac{W}{g}\frac{\delta^2 y}{\delta x^2} = T\frac{\delta^2 y}{\delta x^2} \tag{26}$$

$$\frac{\delta^2 y}{\delta t^2} = a^2\frac{\delta^2 y}{\delta x^2} \tag{27}$$

where $a^2 = T\,g/w$

In the case of a bar with stiffness E, that value replaces T for the equation of motion (21). From these equations, the frequency equation for the bar can be derived, which is

$$\sin\frac{\omega_c \ell}{a} = 0 \tag{28}$$

where ω_c is the natural frequency.

$$\omega_c = n\pi\sqrt{Tg}/\ell\sqrt{w} = n\pi\sqrt{Eg}/\ell\sqrt{\rho} \tag{29}$$

for the case of an ideal bar with no stiffness or a bar with stiffness E. The latter case makes the assumption that the material of the bar is not restrained laterally but can expand and contract as the pressure wave travels along it. This condition applies only if the diameter d of the bar is of the order as the wavelength of the pulse. As this wavelength λ approaches the value of $\lambda = 2d$, the lateral contractions are important and the value of E must be replaced by the shear modulus G. The integer n determines the modes of vibrations which are referred to as the first, second, etc, harmonic. Now, $\ell\pi\omega_c$ is a velocity, and is the velocity of travel of a compression wave along the length of the bar. This velocity can be measured by a number of experimental arrangements and from it the elastic constants can be determined. The simple equation (29) applies only to a slender rod. For bulk solids the Poisson ratio ν must be considered. In this case the speed of the compression wave U_p

$$U_p = \sqrt{E(1-\nu)/\rho(1+\nu)(1-2\nu)} \tag{30}$$

Another example is the case of a cantilever beam fixed at one end; the natural frequency of transverse vibrations is given by

$$\omega_x = [(2n-1)\pi/2\ell]\sqrt{Eg/\rho} \tag{31}$$

Solutions are available for a number of other simple systems.

We thus have two vibrational methods of measuring the elastic constants. The first is to measure the velocity of wave propagation, as discussed above. The second method is the determination of the natural frequency by pulsing the system with a varying frequency pulse and noting by means of displacement gages or accelerometers, etc, the frequency at which maximum amplitudes indicative of resonance conditions occur. Either method can be used comparatively, i.e., comparing a structure under test and a standard, or as an absolute

method. In either case a number of specific errors must be guarded against. First, the clamping device must be standardized for comparative methods or accurately known for absolute methods. Secondly, dimensional uniformity and isotropy of physical properties must exist and, third, the choice of test frequencies must be such that restraint conditions and damping effects can be ignored. Finally, the question as to which harmonic is tuned in may be a very real problem in many tests.

The above examples consider only the longitudinal wave propagation relationships. In addition to the longitudinal wave, lateral or shear waves are set up in a vibrating member which can contract and expand freely or with limited restraint. Further wave modes are originated whenever these longitudinal or shear waves encounter a free surface or interface. Such wave modes are the Rayleigh waves, which extend to a depth about equal to a wavelength into the material from the surface, and Lamb waves, which are true surface waves. The application of a torsional loading initially sets up shear waves, which in turn may be converted to longitudinal waves within the bulk of the material, and to surface waves. Such wave interactions may become very complex, but have been used in some cases for the evaluation of elastic properties.

PROPERTY DETERMINATION OF CONTINUOUS COMPOSITES

A continuous composite has beer defined as a continuous matrix containing continuous filaments, as shown in figure 2, or lamellar plates of another material. Specific examples would be glass fiber or glass cloth reinforced plastic, boron fiber reinforced metal matrices, laminated sheets consisting of metal, wood laminae, etc. Qualitatively, several factors are involved in the material response to a load: first, the mechanical properties of the constituent materials, such as the fiber and matrix; second, the relative proportions of the constituent materials; third, the interface properties and, fourth, the geometric factors, both as to distribution of the constituent materials and the overall geometry of the part and, finally, the mode of loading. These factors are to some extend interdependent. For instance, geometric constraints may change the effective properties of the constituent materials. From a materials evaluation and research point of view, a complete analysis of each of these factors is desirable. However, from the designer's or system engineer's point of view, we are only interested in deviations from an expected norm. These deviations may be in elastic properties or strength and, not only their magnitude, but also their geometric extent has to be determined.

A number of relations have been established for elastic constants and stress/strain relationships in filamentary composites. These generally consider the material to be perfectly elastic and have not yet been related to natural frequency equations. However, a noteworthy observation relates to the measurement of deflections by the use of strain gages. In an orthotropic body the use of simple strain gages fixed along the principal axis is not enough. Strain gage rosettes of either delta or Y shape must be used to obtain adequate data for the calculation of the principal strains.

If we consider the composite as an orthotropic material, with properties differing along each Cartesian coordinate, a number of solutions for such problems are available. Most of these solutions make the assumption of uniform properties along each coordinate and linearly elastic properties. Under these conditions the equation of motion of an orthotropic plate of thickness h, freely supported, is given by

$$D_1 \frac{\delta^4 w}{\delta x^4} + 2D_3 \frac{\delta^4 w}{\delta x^2 \delta y^2} + D_2 \frac{\delta^4 w}{\delta y^2} = -\rho h \frac{\delta^4 w}{\delta t^2} \qquad (32)$$

where

$$D_1 = E_x h^3/12(1 - \nu_{xy}\nu_{yx})$$

$$D_2 = E_y h^3/12(1 - \nu_{xy}\nu_{yx})$$

$$D_3 = G_{xy} h^3/(6 + h^3/24(1 - \nu_{xy}\nu_{yx})(\nu_{yx}E_x + \nu_{xy}E_y)$$

where w is the deflection.

Only four of the five elastic constants are independent; Maxwell's reciprocal theorem can be used to show that the plate's transverse strain due to unit longitudinal stress must be equal to the longitudinal strain due to unit transverse stress, i.e.,

$$\nu_{xy} = (E_x/E_y)\nu_{yx} \tag{33}$$

The natural frequency of the orthotropic plate of dimensions a x b can then be calculated and is

$$\omega_{m,n} = \frac{\pi^2}{\rho h} D_1 \left(\frac{m}{a}\right)^4 + \left[2D_3 \left(\frac{m}{a}\right)^2 \left(\frac{n}{b}\right)^2 + D_2 \left(\frac{n}{b}\right)^4\right]^{1/2} \tag{34}$$

There are four independent elastic constants in the equation, which can be determined from four values of m and n. The above equations apply to a freely supported plate. Edge clamping conditions become quite critical. They can be expressed as a factor for the natural frequency, but the size of this factor may be quite appreciable. For instance, for a thin isotropic plate, the factors for some edge clamping conditions are below:

NATURAL FREQUENCY CLAMPING CORRECTION FACTORS
FOR THIN SQUARE PLATES

	1st Mode	6th Mode
All Edges Free	20	60
One Edge Clamped	3	54
Two Opposite Edges Clamped	20	80
All Edges Clamped	33	150

Resonance analysis can therefore be used to determine elastic properties and deviations from elastic properties due to material defects in composite structures. However, absolute measurements are complicated by the fact that deviations from a standard will change the nodal patterns and therefore also change the effects of clamping conditions. A very good example of the utilization of this analysis is the use by Rolls Royce (Reference 1) of a computer programed analysis of a number of nodal points and frequencies of complete engine shrouds. As a result of this program, Rolls Royce are able to determine not only the reliability of elastic properties of the structure, but also any dimensional variations.

In the testing of filamentary composites, deviations from elastic properties are most likely to be due to either degradation of either the matrix or the fiber material, changes in the volume percentage of fibers or changes in the fiber direction. Figure 6 shows the dependence of a composite modulus and Poisson ratio on fiber direction. Evidently quite small deviations result in large changes, initially, in the mechanical properties. The problem of deciding whether an observed change in modulus is due to material degradation or change in fiber direction can be resolved by additonal testing, such as standard radiography, for fiber alignment. It has been shown (Reference 2) that fiber alignment can be shown quite well by radiography even in multilayer structures.

CONCLUSIONS

The classical methods of nondestructive testing, i.e., the inspection for gross defects of the component materials of a system, are no longer adequate for the inspection of composite systems, where there is extensive interaction of the properties of the component materials. Under these conditions the composite must be tested as a system. From the point of view of system reliability, too, such an approach, rather than a search for gross defects, which must by empirical means be correlated with system performance, is desirable. The mechanical properties to be determined are either elastic moduli or strength properties. Any relation between these two groups is coincidental and must be established empirically. Vibrational analysis and methods based on the examination of the response of the composite system to pulsed vibrations appear to be the most promising approach at present. Elastic properties can be related to resonant frequency phenomena, and many relations between the attenuation of such pulses and strength parameters have been established. The application of this approach is limited by the mathematical complexity of the analytical approach to all but the simplest systems. However, differential methods could be used to establish compliance of a test system with a system standard. Experimentally, a wide variety of pulse exciting and response sensing elements is available. Limited use has also, so far, been made of the many analogs present between vibrational response and the behavior of an alternating current or the possible use of analog computer could be used as system standard in comparative tests, with a digital computer in a feedback loop analyzing the variations between test part and "standard". It is suggested that the increased use of composite materials not only in the aerospace industry, but in industry generally, should now provide the incentive for an extended study and application effort on field of vibrational analysis as a nondestructive testing tool.

Another direct approach to the measurements of elastic constants is the measurement of wave propagation velocity, particularly ultrasonic velocity measurements. Figure 1 shows the acoustic velocity for a number of composites and composite matrix and fiber materials. The diagram compares experimentally determined data with the results of the longitudinal velocity calculated from the elastic constants. The acoustic velocity in alloys was calculated by means of the equation

$$v = \sqrt{Eg(1 - \nu)/\rho(1 + \nu)(1 - 2\nu)} \tag{35}$$

The estimation acoustic velocity in the composites examined assumed a composite consisting of a plate of matrix bonded transversely to the direction of wave propagation to a plate of filament material. Under these conditions the velocity is

$$v = v_m v_f/(v_m f_f + v_f f_m) \tag{36}$$

where the subscripts f and m refer to the fiber and matrix respectively and f is the appropriate volume fraction. The results show good agreement between experiment and estimate in composites. Deviations are probably due to the uncertainty in the values of the elastic constants of the materials in the composite.

The determination of strength presents quite a different problem from the determination of elastic properties. The strength of a filamentary composite up to a certain critical fiber volume is a function of the ultimate strength of the matrix material and its volume percentage only. With such composites the measurement of bulk properties, i.e., measurements assuming the composite to be an orthotropic solid, would give erroneous results. In such materials a strength correlation could only be established by measuring the fiber volume and then determine any parameter related to the matrix strength. For instance, the theory of damping measurements could be applied by measurement of the attenuation of a surface wave in the isotropic matrix material surface layers. Composites in which the content exceeds the critical volume can, theoretically, be considered as orthotropic solids. Attenuation measurements using ultrasonic waves are currently being conducted but results are not yet known.

The strength properties of filamentary composites depend on the degree of adhesion between fibers and matrix. It has been shown by direct radiographic observation of markers spaced between fibers and matrix that, up to the failure of the composites tested, no differential strains, longitudinally to the fiber axis, occurred between fiber and matrices. Because the elastic moduli of fiber and matrix differed, a load transfer between fiber and matrix must have occurred during loading, which is limited either by the strength of the composite component materials or by the shear strength of the interface bond. The experimental determination of this shear strength allowing the transfer of loads from the matrix to the fibers is a problem, which so far has been solved neither destructively nor nondestructively. A possible approach is through the measurement of the width of the diffusion affected zone width (analogous to the heat affected zone concept in welding), and empirical correlations of that width with shear strength. In the case of a single bond line, as obtained in solid-state (diffusion bonded) materials, a correlation

appears to exist between that zone width and the tensile strength. This is shown for two systems in figure 8. Microscopic measurements on boron/titanium interface diffusion zones have shown this zone to be about 2 microns thick. This is of the same order and, if a relationship between this thickness and shear strength can be established, methods suitable for the measurement of interface bond strength can be utilized. The problem of this interface will be discussed later for the case of the flat laminate interface. No solutions are available for the case of a cylindrical laminate interface, as would be the case in filamentary composites. However, the approach appears entirely feasible.

As far as the nondestructive determination of composite strength is concerned, we are still very much in the old position of having to inspect for defects rather than for properties. The state-of-the-art of defect inspection in composites has been reported elsewhere (Reference 2). It was concluded that standard techniques of radiography and pulse-echo C-scans can be used to define single fiber breaks and matrix disbonds in a number of applicable composite systems. The two principal problem areas for which no ready solutions were available were the problems of interface bond strength and residual stress measurement of the fiber embedded in the composite. For laminated composites, models are available for perfectly elastic materials and elastic material with visco-elastic interfaces. The latter is of particular importance, because they give a possible approach to strength determination as well as determination of elastic constants. Furthermore, the problems of discontinuous composites can, in some cases, be reduced to that of the laminate with a visco-elastic interface.

Kerwin (Reference 4) has analyzed the problem of a visco-elastic layer sandwiched between two elastic plates and reduced the solution to two parameters, one geometrical and another one a shear parameter related to moduli and frequencies. His work is mainly aimed at the calculation of optimum damping effects from such layers and damping patches, but could be adapted to the analysis of the interaction of adhesive properties and system damping. Experimentally, damping in even very thin interface layers has been demonstrated on solid-state bonded titanium alloy blocks. The blocks, 2 inches thick with a single bond, were examined by pulse echo methods using 2-1/2 to 10 MHz frequency pulses. The echo from the bond line showed up clearly and indicated an attenuation which changed with varying bond strength. Results are shown in figure 9. Apart from demonstrating a damping factor/strength relationship, the example quoted also shows the very fine limit of sensitivity which such methods can achieve.

The types of composites considered here are principally the sandwich-type of structure, which can be presented by two-dimensional models, and the honeycomb structure. Other structures, for instance a structure with a dimpled sheet welded between flat facing sheets, are of course used, but not on a wide enough scale to warrant extensive mathematical analysis. Structures consisting of such composites may vibrate in two different ways. First, the panel may vibrate as whole and, secondly, the facing sheet elements between the honeycomb cells or connecting struts may vibrate. The first way of vibration is closely related to the shear properties of the core while the adhesive or joint properties between core and facing sheets play a relatively small part. In the second way of vibration, these joint properties become very important.

Considering a honeycomb panel as a plate, its natural frequency of vibration is given by Wallace (Reference 5)

$$\omega_c = \frac{M_p}{\rho}\pi^4\left[\frac{1}{a^2} + \frac{1}{b^2}\right]^2 \left[1 + \frac{M_p\pi^2}{t_c G_c}\left(\frac{1}{a^2} + \frac{1}{b^2}\right)\right] \tag{37}$$

where a and b are the breadth and width of the panel, G_c the core shear modulus, t_f the facing sheet thickness, t_c the core thickness, ρ the panel mass/unit area and M_p the panel modulus given by

$$M_p = \frac{t_f(t_c + t_f)^2 E}{2(1 - \nu)^2} \tag{38}$$

Equation 35 will be sensitive to changes in E and ν of the facing sheet and to the panel geometry. Damping due to the facing sheets, core and adhesive losses is ignored. More complex analysis of the stress/strain relationships in honeycomb beams exist, such as those given by Avery (Reference 6), Pretlove (Reference 7), and Mead and Froud (Reference 8), Thompson and Clary (Reference 9), and Fang, Forray and Benedicto (Reference 10). Some of these consider the damping due to visco-elastic bonds. In either case relationships have or can be established between the natural frequency and modes, and the elastic constants. However, the complexity of these relationships removes them from the scope of this paper. Of particular interest is a relationship established by Avery (Reference 6) between the damping of the structure, in his case a beam, and the loss coefficients of the facing sheet and adhesive. After some simplification, he obtained for the damping ratio

$$\text{Ratio} = \frac{\eta_a E_a t_a}{2E_f t_f} + \frac{\eta_f}{2} \tag{39}$$

where the subscripts a and f refer to the adhesive and facing sheet, m and t are the thicknesses, and E the elastic moduli. η_a and η_f are the loss factors of the adhesive and facing sheets.

The vibrational properties of a sandwich panel, as a structure, can therefore be utilized to test for the elastic and visco-elastic constants of the component materials. However, the practical problem of vibrating and measuring the response of an entire structure makes this approach rather cumbersome for general NDT purposes. This leaves the possibility of exploring the properties of the honeycomb through analysis of the response of individual elements. Of particular interest is the bond strength of the adhesive of the facing sheets to the core. In order to demonstrate the relationship between damping coefficient and bond strength, resonance peaks were measured in simple lap joint specimens bonded with adhesive degraded to various strength levels lower than the maximum (Reference 11). From these peaks the loss factor can be determined by measuring the frequency bandwidth at half peak amplitude and dividing by the peak frequency. The results are plotted in figure 10. A clearly visco-elastic response is indicated, from which, for instance, an indication of the relaxation time as given in Equation 23 can be obtained. Assuming an average relaxation time $\tau = (\tau_\varepsilon \tau_\sigma)^{1/2}$ this average time for the material tested is about 8.45 microseconds for the 1000 psi material and 3.50 microseconds for the 4000 psi material.

In order to apply the approach to honeycomb structures, a number of concepts must be defined and clarified, an experimental procedure must be developed, and a theoretical approach must be organized. The concept of bond strength, for instance, depends both on the test method and the number of cells tested. In order to determine the effect of the number of cells on flatwise tensile bond strength, specimens were prepared using 4-3/4-inch honeycomb composites in forms containing one, two, three, four, five or more honeycomb cells. The results of these tests are shown in figure 11. A single cell exhibited a greater strength than any multicellular test specimen. However, for multicellular test specimens, the apparent strength increases with the number of cells tested. A correction factor can be applied to multicellular structures to allow for the fact that several cells share the same cell walls. For cluster arrangements, as tested here, the correction factor is approximately

$$\text{factor} = \frac{11 + 4(n - 2)}{6n} \qquad (40)$$

where n is the number of cells greater than two. For a dual cell structure, the correction factor is 11/12. The corrected curve indicates that for cell numbering up to about 10, the strength is approximately constant. The greater strength for the unit cell is probably due to the additional core web bond area. A test probe can, therefore, be designed to cover an area of about 10 cells and yet still give an indication of cell strength down to a dual cell structure.

So far, only one side of the honeycomb has been considered. The next step is to determine vibrational resonance properties of a true honeycomb structure with facing sheets connected to both sides of a rigid core. Finally, consideration must be given to the fact that these walls are not rigid, and that there is interaction between the structure vibrations and the vibrations of the air contained in each cell. In fact, essentially each cell can be compared to a drum. The various stages of this theoretical approach are shown in figure 12. The modulus E* for the bond denotes a complex visco-elastic modulus.

A suitable transducer to excite panel vibrations and measure the vibration amplitude of the response must be capable of ranging over a wide frequency band, should minimize noise and coupling problems, and be suitable for field inspection applications. Two systems appeared to be the most promising: the first is a driver displacement oriented system (hereafter referred to as the DOT transducer system) where an electromagnetic driver is combined with a displacement measurement unit in a single system. An alternate system makes direct use of the damping mechanism and includes an oscillating system at approximately 30 KHz wherein the adhesive bond damping becomes part of the oscillator circuit Q.

A series of Saturn 4-3/4-inch thick honeycomb composites with various degraded adhesive bond strengths were tested with the DOT system. Correlation of the measured responses and corresponding flatwise tensile test data is given in figure 12 for specimens with 0.040-inch thick facing sheets. A significant difference is noted in the responses with qualitative agreement with the expected behavior, i.e., the lower strength bond gives a greater response. The repeatability shown in figure 11 is better than the differences between destructive test data from specimens taken from honeycomb composites.

Experimental data obtained so far have shown a semiquantitative agreement of test data and predicted response. There are a number of observations which cannot be completely explained. Two points in particular require elucidation. The flatwise tensile test used to determine bond strength covers about 20 cells. It has been assumed that the bond strength for each cell is the same. However, the tensile test can report only an average strength for all the cells in the sample. Likewise, a probe measures the total response from the number of cells it covers. No information is available on the relative variations of bond strength from cell to cell, which might affect the average tensile test or probe results differently. Another point noted was the apparent lack of frequency shift with bond strength. This may be associated with the restraint conditions imposed on the honeycomb sheet by the DOT transducer during preliminary tests.

ACKNOWLEDGEMENTS

The author gratefully acknowledges the many helpful comments and supplemental data provided by his colleagues Mr. J. F. Moore, Dr. D. O. Thompson, Dr. S. Tsang, and Dr. L. Lackman.

LIST OF SYMBOLS USED

a	dimension
b	dimension
D	specific damping energy, i.e., area within stress/strain hysterisis loop, in lb/cu.in.
E	Young's Modulus
f	volume fraction
g	acceleration due to gravity
G	shear modulus
h	thickness
l	constant, length
L	constant
m	exponential, harmonic number
M	Modulus
n	exponential, harmonic modulus
t	time, thickness
T	constant, tension
w	mass/unit length, deflection
W_d	total damping energy expended by system/cycle
W_o	total strain energy in system damping

α damping energy integral

β stress distribution integral

γ strain distribution integral

ε strain

η loss factor (for small phase angles $\phi = \tan \delta$)

ν Poisson ratio

ρ density

σ stress

τ relaxation time

ω angular frequency

REFERENCES

1. T. K. Draper, "The Application of Prestiffness Method of Solution to a Flat Plate to Find Frequencies and Nodal Patterns", Rolls Royce Ltd, Stress Report ASR 2668, September 1963.

2. G. Martin and T. F. Moore, "Research and Development of Nondestructive Testing Techniques for Composites".

3. G. Martin and S. Tsang, "A Study of the Failure Behavior of Filamentary Reinforced Metal Matrices", Annual Meeting Soc. Engineering Science, 1965.

4. E. M. Kervin, "Macromechanics of Damping in Composite Structures", Symposium on Internal Friction, Damping and Cyclic Plasticity, 1964, ASTM S.T.P. 37, 1965.

5. C. E. Wallace, "Stress Response and Fatigue Life of Acoustically Excited Honeycomb Panels", NAA Report NA-64-413, 1964.

6. C. P. Avery, "An Investigation of Longitudinal Shear Distribution and Damping in a Visco-Elastic Adhesive Lap Joint", WADD-TR-60-687, November 1960.

7. A. J. Pretlove, "Bond Stress in a Randomly Vibrating Sandwich", J. Sound Vibr. V.2, 1965, p 1.

8. D. T. Mead and C. R. Frond, "The Damping of Aluminum Honeycomb Sandwich Beams", ASD-TDR-62-1096, January 1963.

9. W. M. Thompson and R. R. Clarry, "An Investigation of the Natural Frequencies and Mode Shapes of Double Conical Sandwich Disks", NASA TN-D 1940, 1963.

10. T. C. Fang, M. D. Forray, R. L. Bendicto, "Deflections and Stresses in a Clamped Rectangular Sandwich Beam", J. Aerospace Sc 1962, November p. 1368.

11. T. F. Moore and G. Martin, "Development of Nondestructive Testing Techniques for Honeycomb Heat Shields", NAA Report NA-66-912, 1966.

Reference has also been made to:

C. Zewer, "Elasticity and an Elasticity of Metals", University of Chicago Press, 1948

L. S. Iscobson and R. S. Ayre, "Engineering Vibration", McGraw-Hill, 1958

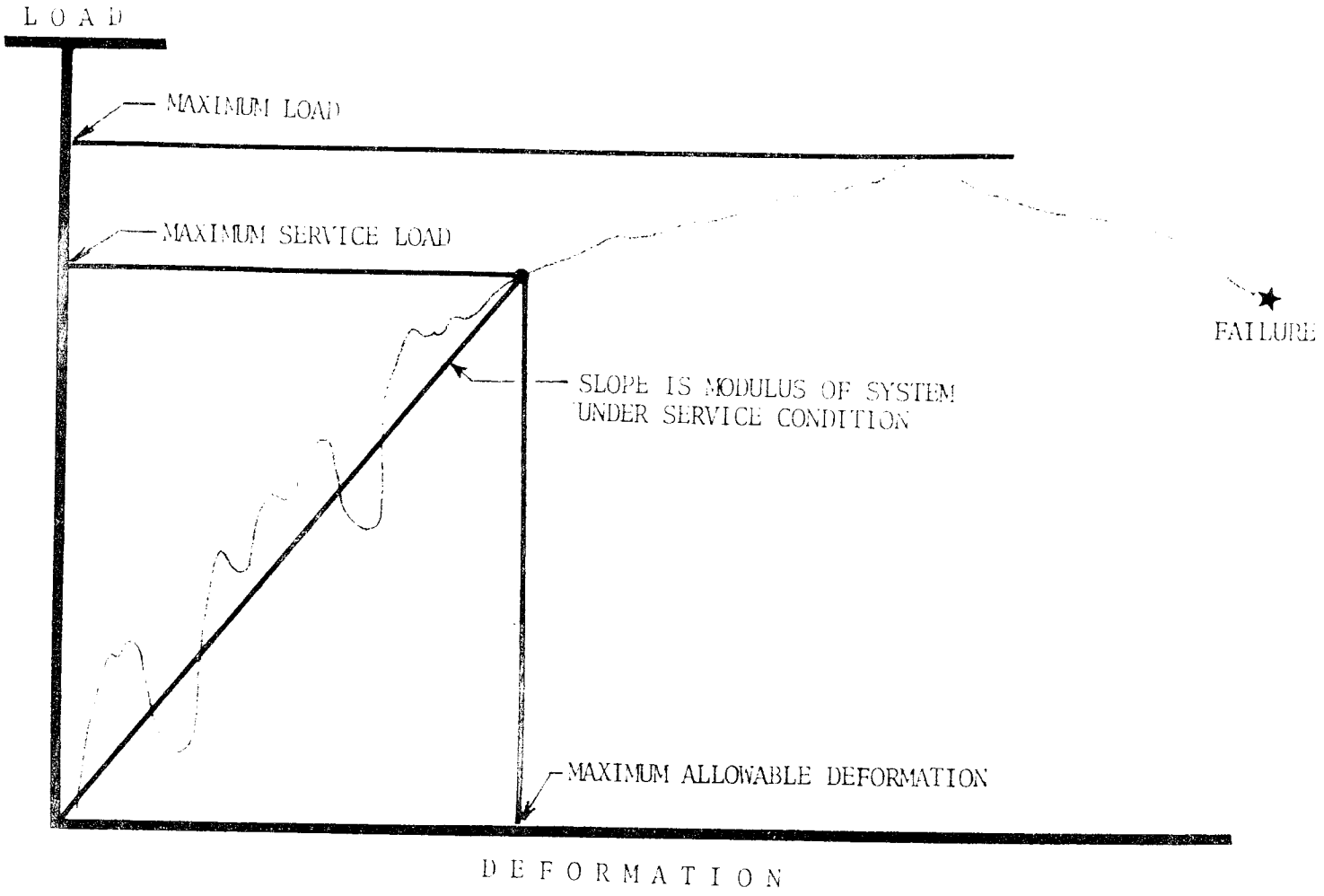

Figure 1. Load-Deformation Diagram of a System

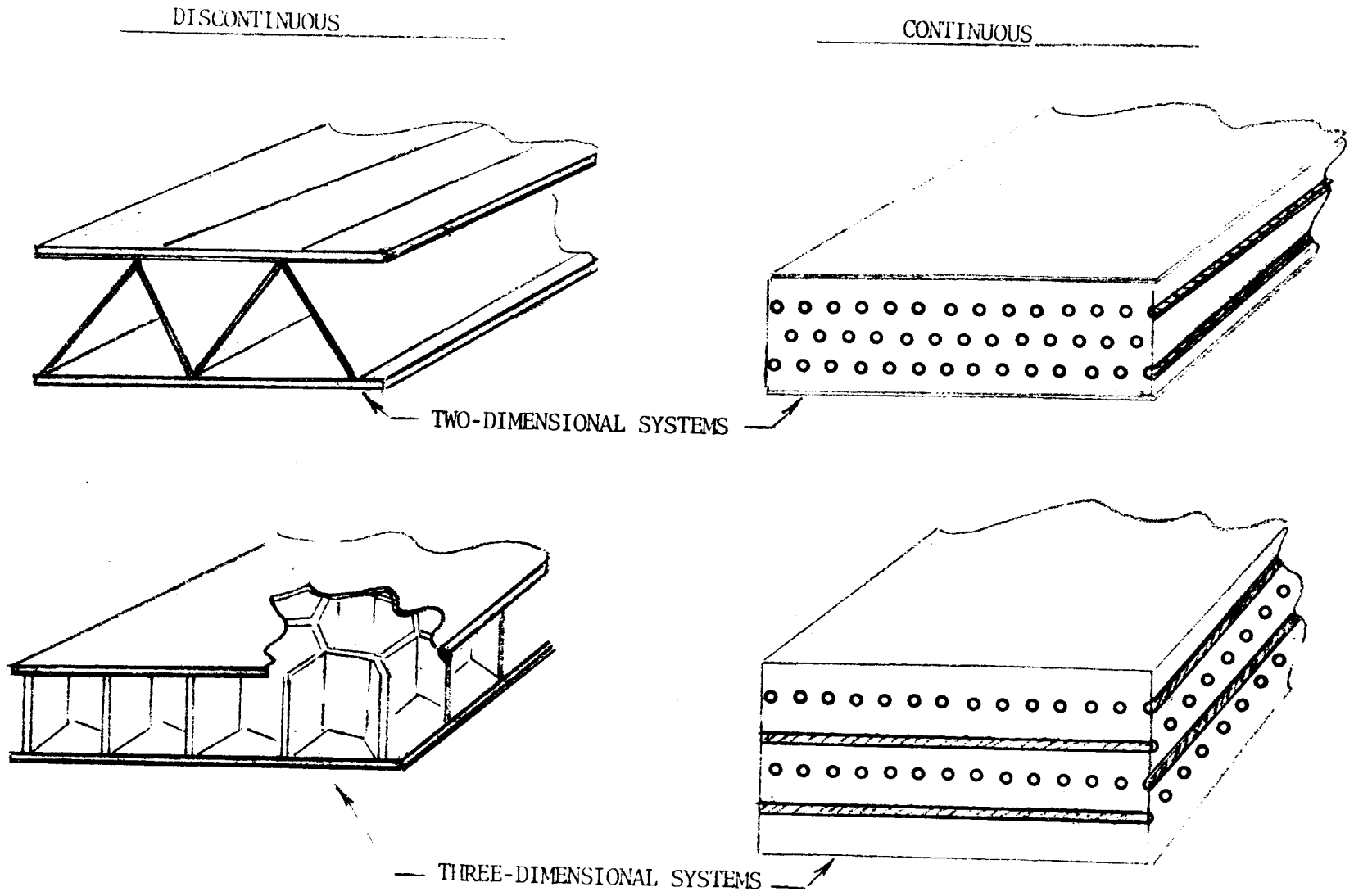

Figure 2. Composite Systems

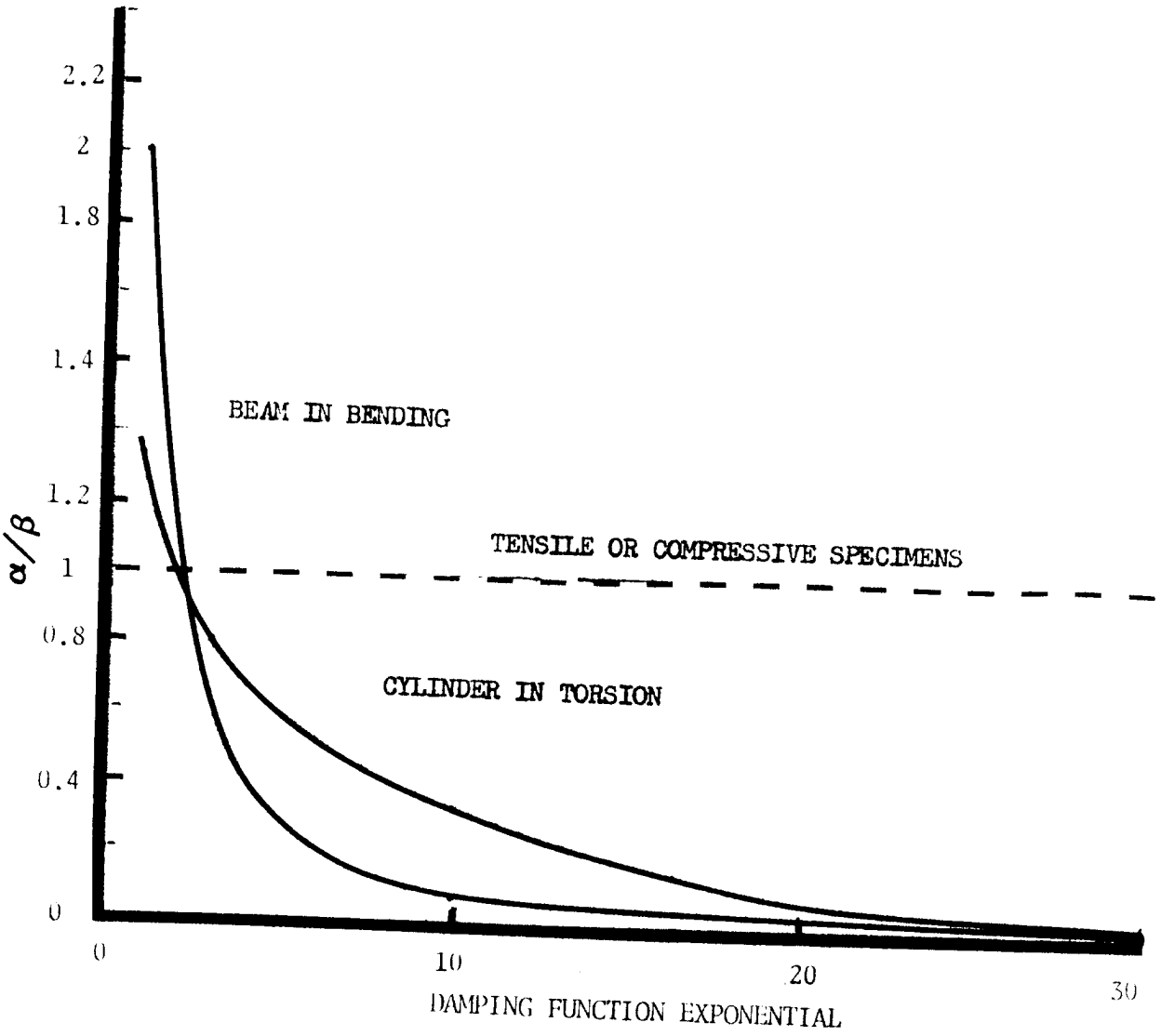

Figure 5. Values of the Internal Correction Factors as a Function of the Damping Function Exponential

(B. T. Lazan and L. E. Goodman, "Material and Interface Damping", Shock-Vibration Handbook, McGraw-Hill, 1961)

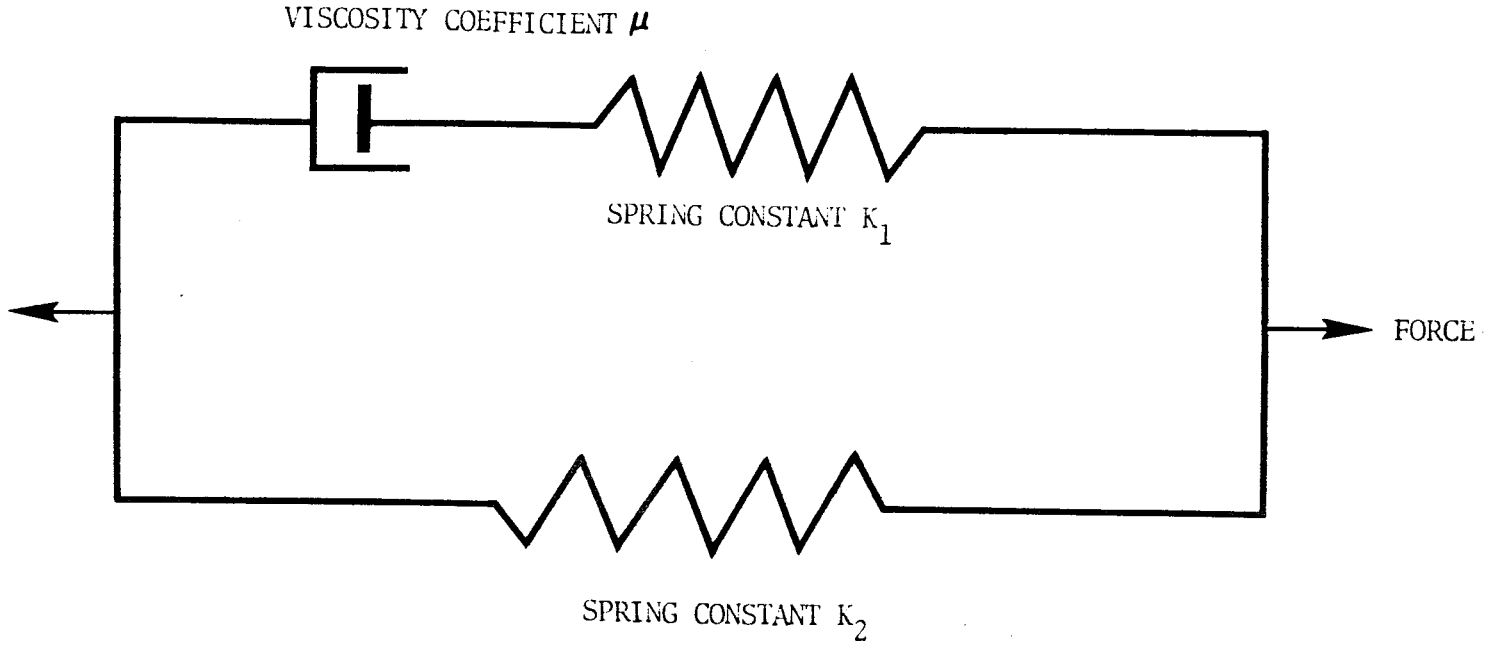

Figure 4. Model for a Linear Visco-Elastic Solid

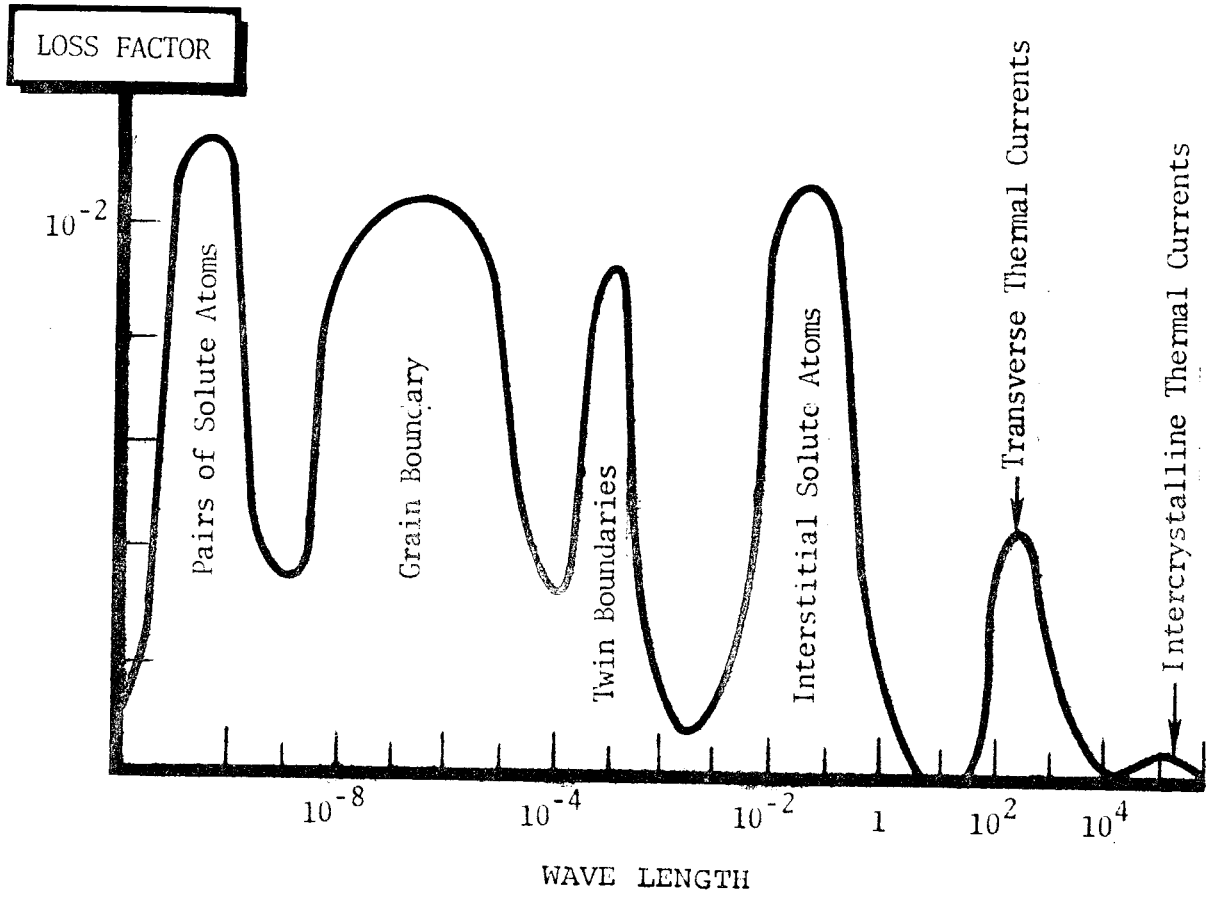

Figure 5. Schematic Frequency Spectrum Response

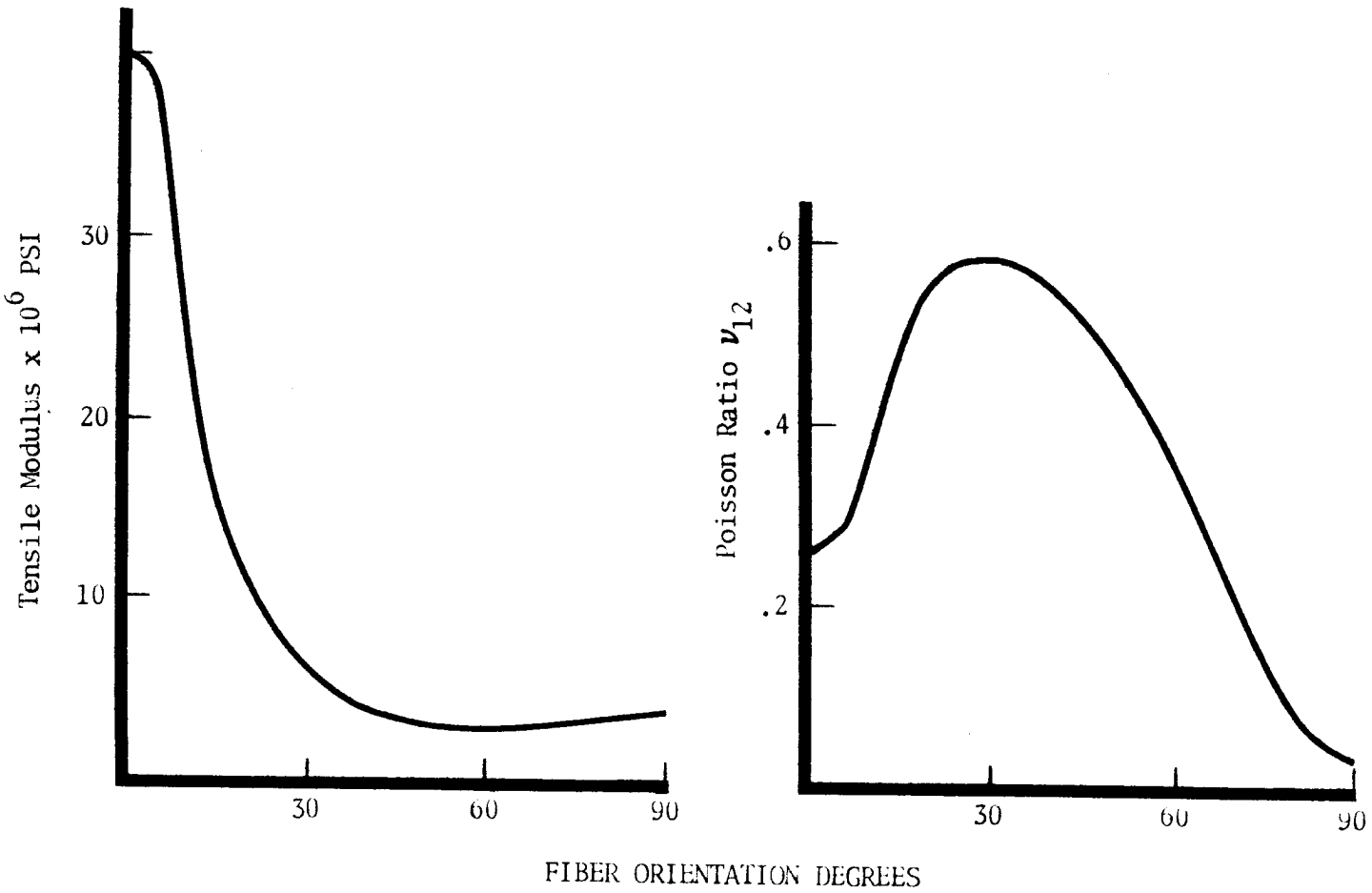

Figure 6. Directional Elastic Properties of Boron-Epoxy Filamentary Composite (Reference SWTSAI, "Mechanics of Composite Materials", AFML-TR-66-149)

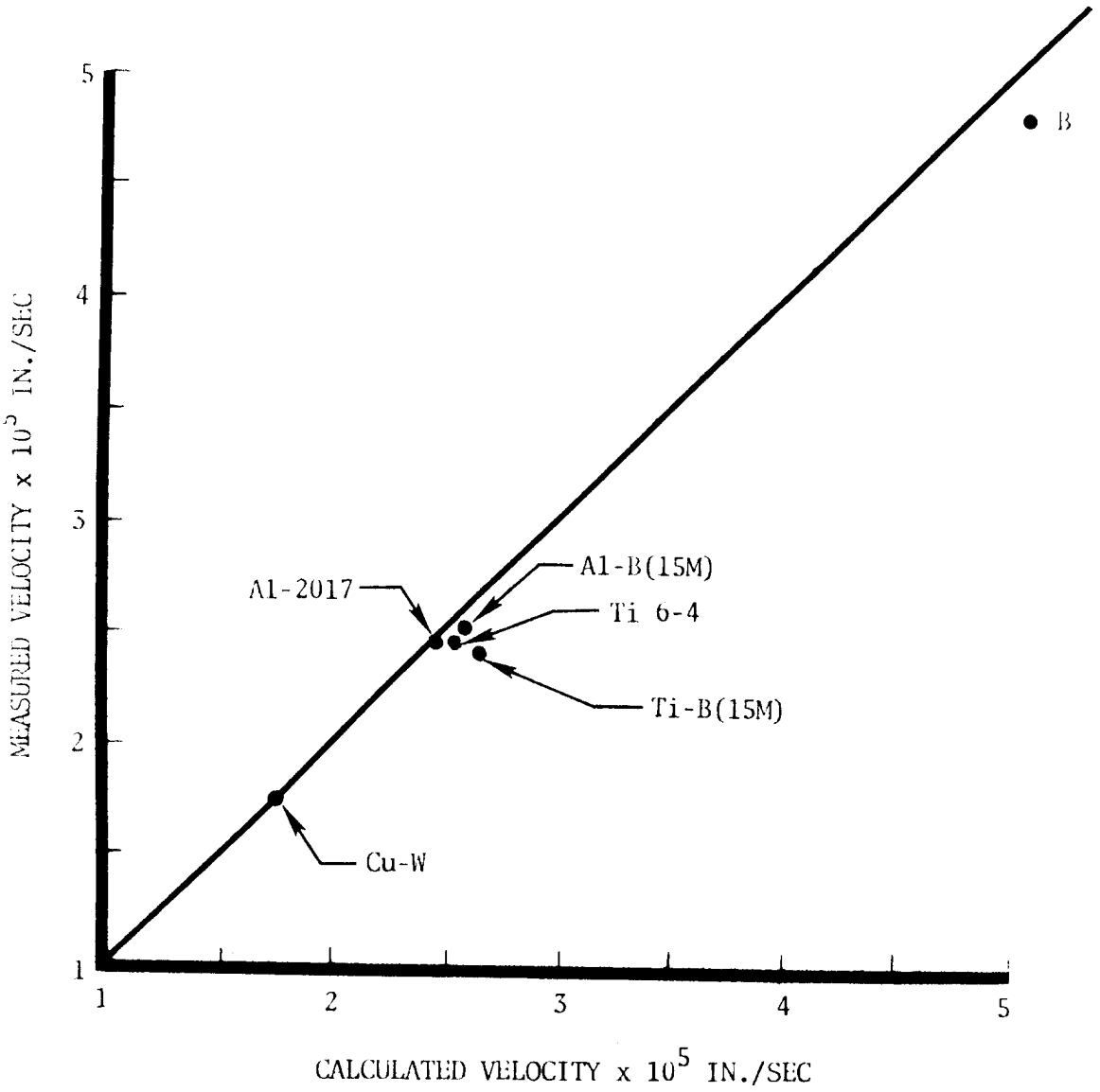

Figure 7. Theroetically and Experimentally Determined Acoustic Velocity of Filamentary Composites

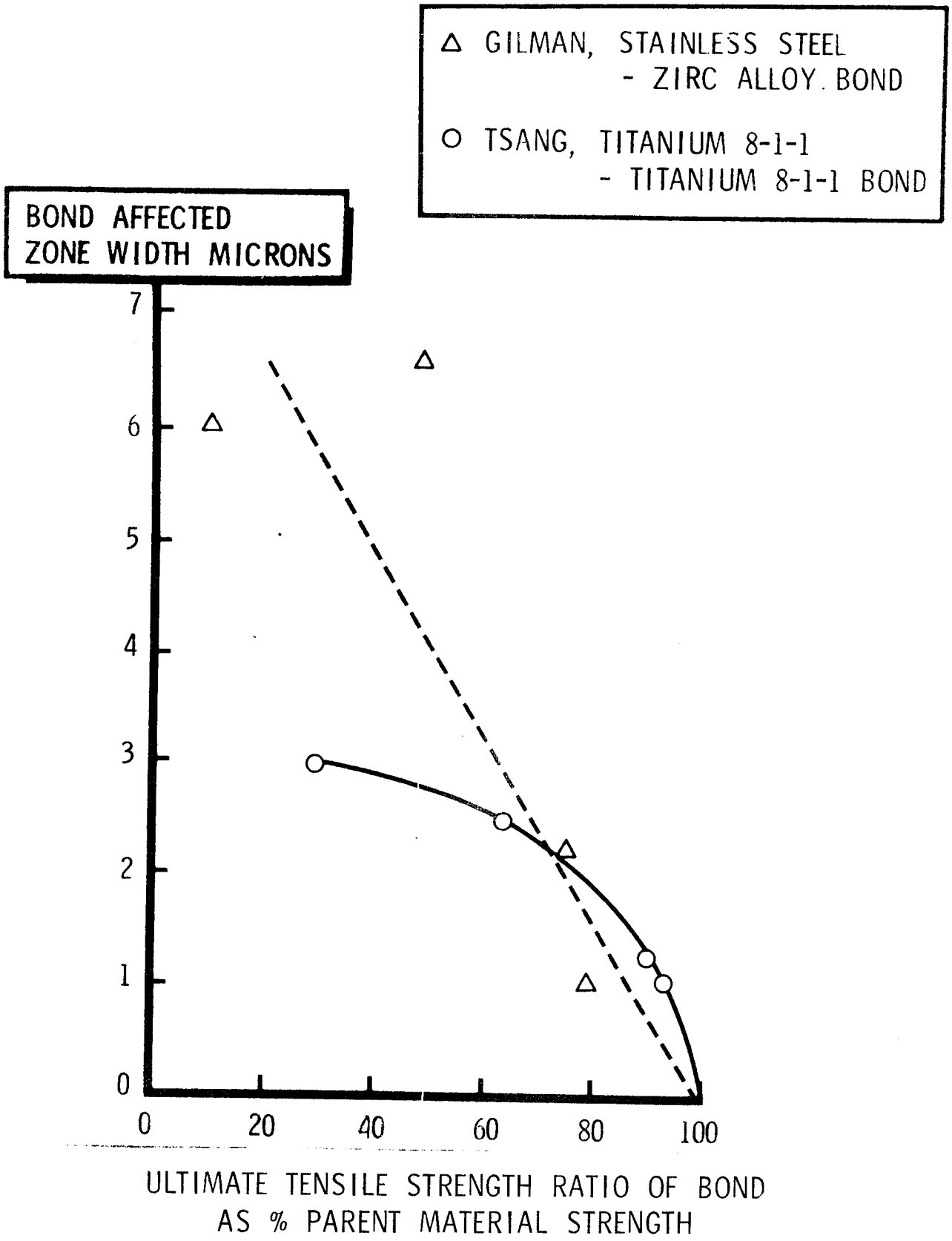

Figure 8. Relative Bond Strength and Width of Diffusion Affected Zone

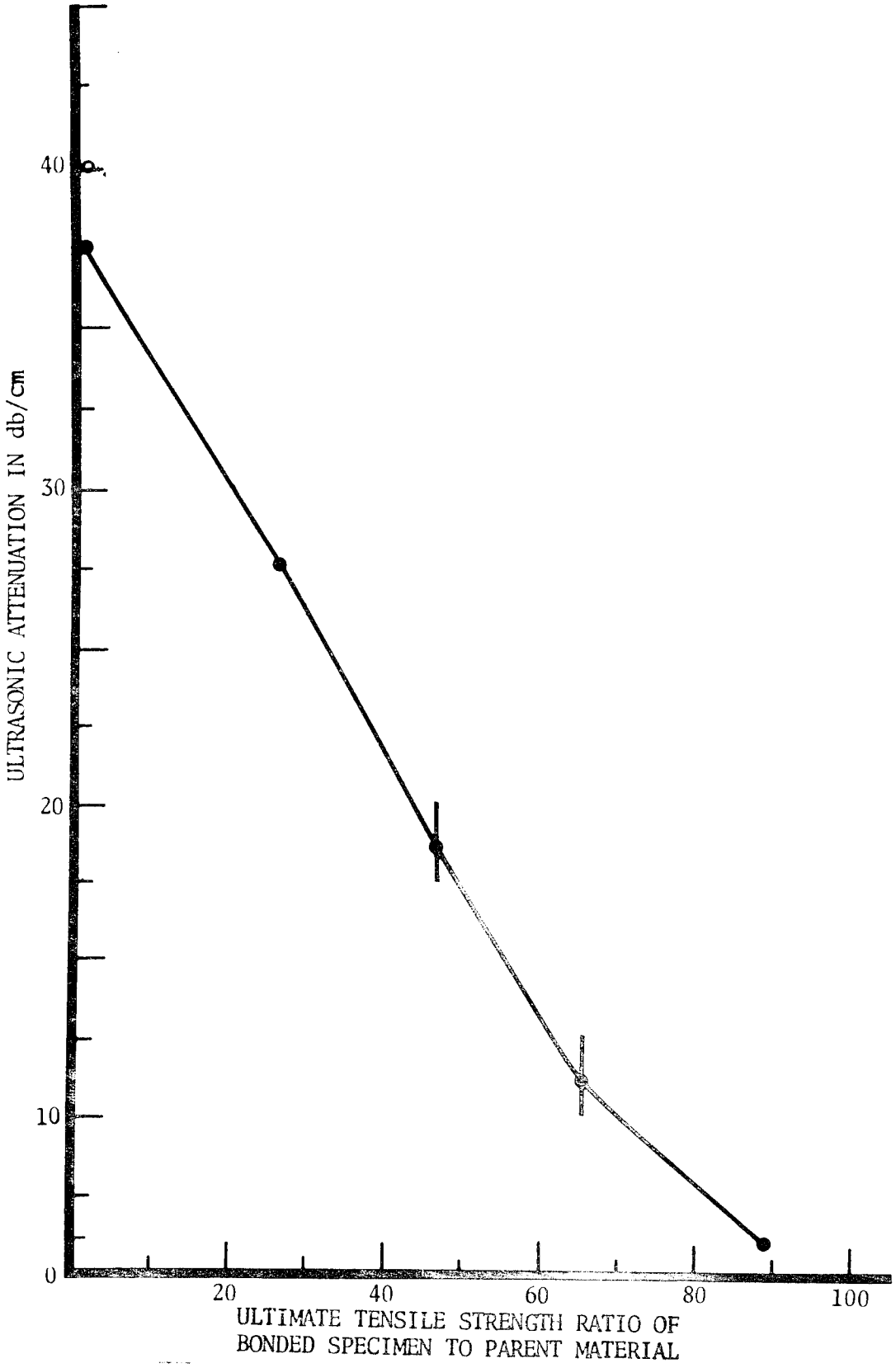

Figure 9. Relationship Between Ultrasonic Attenuation and Ultimate Tensile Strength of Diffusion Bonded Titanium

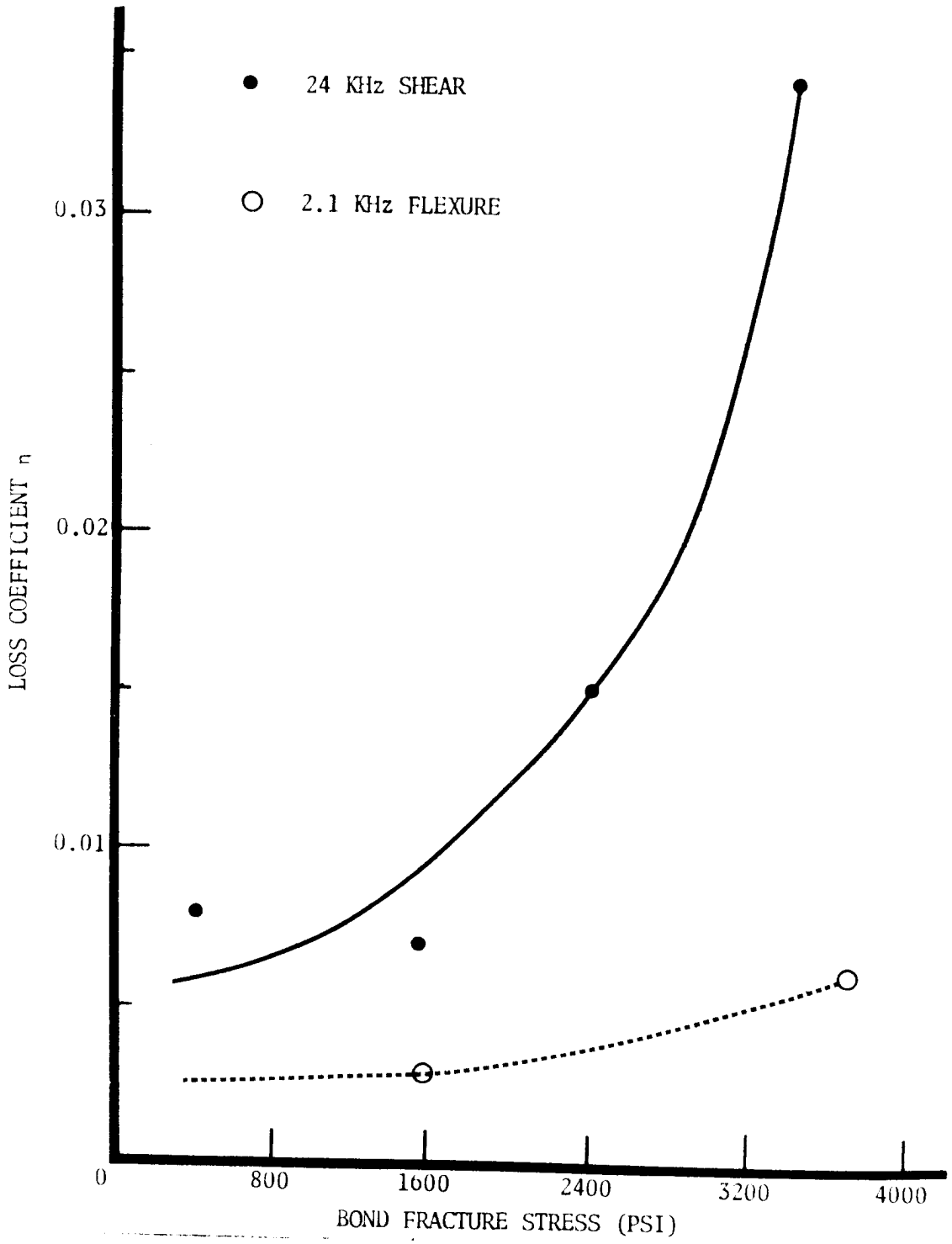

Figure 10. Relationship Between Adhesive Bond Shear Strength and the Loss Coefficient

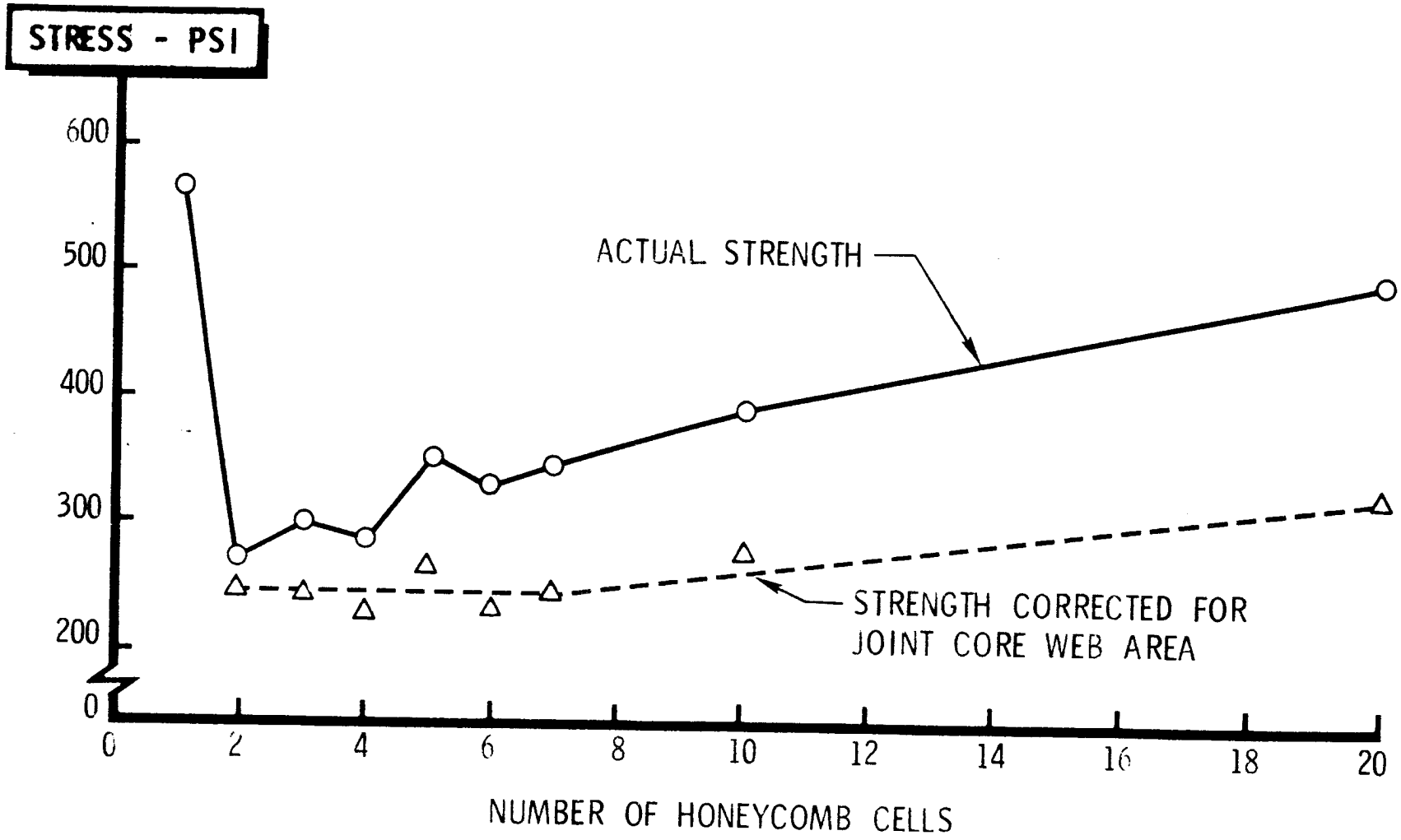

Figure 11. Graph Showing Strength Contribution of Individual Honeycomb Cells

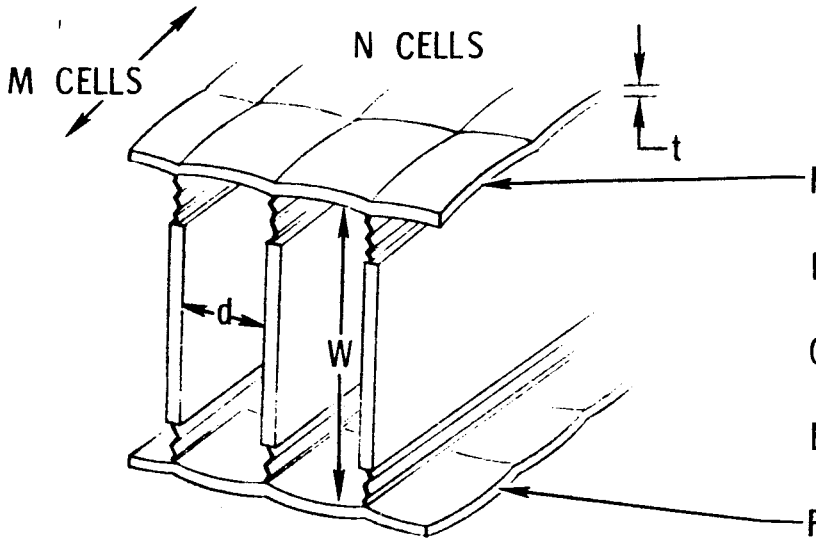

PROPERTIES AND DIMENSIONS

FACING SHEET	E_F	σ_F	t_1
BOND	E^*_{B1}	σ_{B1}	
CELL WALLS	E_W	σ_W	
BOND	E^*_{B2}	σ_{B2}	
FACING SHEET	E_F	σ_F	t_2

MODELS FOR THEORETICAL ANALYSIS

DIMENSIONS / MODEL	ONE	TWO		THREE OR DRUM MODEL				
	I	II	III	IV	V	VI	VII	VIII
M	0	1	∞	1	1	∞	∞	∞
N	∞	∞	∞	1	∞	∞	∞	∞
BOND	$E^*_{B'}$ B	$E^*_{B'}$ B	$E^*_{B'}$ B	$E^*_{B1} = E^*_{B2}$ $\sigma_{B1} = \sigma_{B2}$	$E^*_{B1} = E^*_{B2}$ $\sigma_{B1} = \sigma_{B2}$	$E^*_{B1} = E^*_{B2}$ $\sigma_{B1} = \sigma_{B2}$	$E^*_{B1} = E^*_{B2}$ $\sigma_{B1} = \sigma_{B2}$	$E^*_{B1} = E^*_{B2}$ $\sigma_{B1} = \sigma_{B2}$
CELL WALL	—	—	—	RIGID	RIGID	RIGID	RIGID	E_W, σ_W
FACING SHEET	—	—	—	$t_1 = t_2$	$t_1 = t_2$	$t_1 = t_2$	$t_1 = t_2$	$t_1 = t_2$

Figure 12. Schematic Diagram and Analysis Modes for Honeycomb Vibration Study

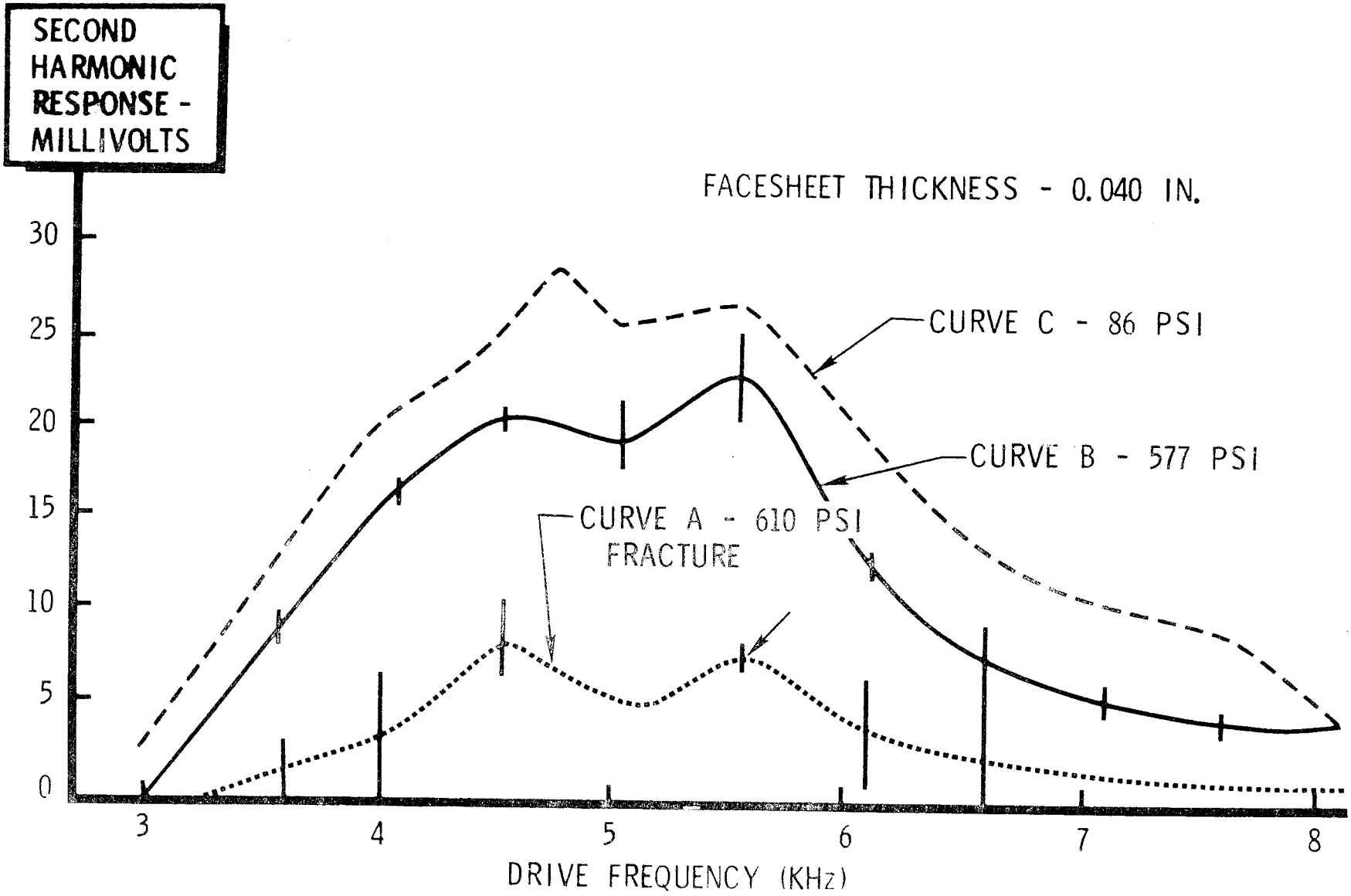

Figure 13. Vibration AC Response of 4-3/4 Inch (0.040 Inch Face Sheet) Honeycomb

LOW VOLTAGE AND NEUTRON RADIOGRAPHY TECHNIQUES FOR EVALUATING BORON FILAMENT METAL MATRIX COMPOSITES

J. A. Holloway and W. F. Stuhrke
U.S. Air Force Materials Laboratory
Wright-Patterson Air Force Base, Ohio

and

H. Berger
Argonne National Laboratory
Chicago, Illinois

Introduction

Glass filament-polymeric matrix composites have become familiar materials in recent years for lightweight structural applications. The recent development of a variety of new filaments has stimulated considerable interest and activity in the development of metal matrix composites. Metal matrices offer excellent potential for extending the capabilities of this class of materials beyond those available. Possible advantages to be gained are resistance to severe environmental conditions such as elevated temperatures, chemical attack, or erosion. Further advantages may be derived by utilizing the greater strengths of metal matrices to enhance transverse properties or to improve resistance to shear loading conditions and stress concentrations. Should this development be realized, these materials will be used in very high, critical load-bearing structures and components in future Air Force systems.

From the research and development programs being conducted in this area, certain detrimental conditions occurring within the filament and matrix materials have been realized which affect mechanical properties. One of these detrimental conditions is the interaction between the filament and matrix material which may take place during fabrication or under adverse temperature conditions. The subject investigation is directed toward establishing the feasibility of low voltage and neutron radiography for detecting the interaction. A simple specimen configuration was employed consisting of single layer boron filaments embedded in an electrodeposited nickel matrix.

METAL MATRIX COMPOSITES - THE NICKEL BORON SYSTEM

Background

The primary mechanism for attaining strength in these materials is the transfer of load from the matrix to the filament; thus the filaments should have a high tensile strength. For effective load transfer the filaments should

also have a high elastic modulus relative to that of the matrix. Table I contains a list of filamentary materials together with their associated properties. As presently fabricated, boron filament has a tensile strength of 5.5×10^5 psi, and an elastic modulus of 5.5×10^7 psi. It can be seen that other reinforcement materials are available which have tensile strengths $\geq 10^6$ psi. In addition all of these materials have a density below 0.2 lb/in^3.

The filaments and matrix should be effectively coupled or bonded to one another if efficient load transfer is to be realized. There are a number of techniques for incorporating the filaments into the metal matrix, all of which involve some degree of thermal environment. These techniques include (1) liquid metal infiltration (casting), (2) powder metallurgy, (3) electro- or vapor deposition, (4) diffusion bonding (solid-state welding), and (5) directional solidification of eutectic structures. The technique of diffusion bonding has received the widest application. This involves bringing a sandwich of foils and filaments to a relatively high temperature and subsequently pressing for a period of time. For the aluminum-boron system, this is representatively 490^o to 510^oC at 2000 to 10,000 psi for one to two hours. Under these conditions there is potential for interaction between the filament and matrix. It is this interaction which degrades the mechanical properties of the composite.

In order to establish the feasibility of the low voltage and neutron radiographic techniques for detecting the degree of filament/matrix interaction, boron reinforced nickel was chosen as the composite system to be used during the investigation. This choice was dictated by the available information on the system. A well-documented interaction occurs with time at temperature, and a fabrication technique, electroforming, is available which produces a specimen with no interaction since the fabrication is accomplished at room temperature.

Filament Fabrication

Increased interest in metal matrix composites is primarily due to the development of boron filament. This filamentary material is manufactured by vapor deposition of boron onto a resitively heated substrate. The substrate usually employed is tungsten wire with a diameter of about 1.2×10^{-3} cm; the average boron filament diameter is about 1×10^{-2} cm. As shown in Table I, the filament has a modulus of 5.5×10^7 psi and a strength range from 4.0 to 5.0×10^5 psi. It has an "amorphous crystalline" structure which, because of its highly strained condition, contributes to the strength.

Composite Fabrication and Mechanical Properties

The specimens employed for this investigation were prepared by the General Technologies Corporation (Contract No. AF 33(615)-3155) from 1×10^{-2} cm diameter boron filaments and electrodeposited nickel. The nickel was deposited on a stainless steel mandrel and the boron wound onto the nickel

surface during the deposition. The nickel was further deposited until the boron filaments were completely encapsulated. The fabrication method (Reference 1) produces boron/nickel specimens with no interaction between the filament and the matrix as shown in Figure 1. The photomicrograph of a section of the specimen shows the tungsten core in the center of the boron filaments which are embedded in the surrounding nickel matrix. The flat surface is a result of the deposition of the nickel on the surface of the stainless steel mandrel. Further nickel deposition produces the hills and valleys on the other surface of the specimen. The composite thickness varies from approximately 0.028 cm directly over the single layer filaments to approximately 0.023 cm in the area between adjacent filaments. The growth of the nickel during the electroplating process introduces a number of internal interfaces where the growth fronts merge. This can be seen in the Figure. These occur away from the filament and should have no effect on the reaction kinetics, at least not in the early stages of heat treatment. The interface between the boron and the nickel, however, is mechanical in nature. The boron surface is replicated in the nickel, but there is no bonding. This results in the need for some outside force to cause the intimate contact necessary for interaction to occur. This is provided under stress by the difference in Poisson's ratio of the two materials. In other cases the release of residual stresses in the as-deposited matrix provides the necessary force. This unfortunately often leads to unbalanced interactions. This is illustrated later by the photomicrographs of the samples heat-treated at various temperatures.

The single layer boron filament/nickel matrix sample was cut into five sections, one of which is shown in Figure 2. One of the five sections was reserved as a standard. The remaining sections were heat-treated in an argon atmosphere for one hour at 600°, 700°, 800°, and 900°C. The interdiffusion of the boron and nickel with the subsequent formation of an intermetallic boride which grows in annular rings outward from the filament as the temperature increases can be seen from Figures 3 through 6. The boron is progressively depleted and fairly rapidly saturated with nickel. As previously discussed, the release of residual stresses during heat treatment often leads to uneven interactions. A further complicating factor is the difference in thermal expansion between the boron and the nickel. This leads to a greater expansion of the nickel with temperature relative to the boron, further reducing the possible area of intimate contact and interaction between the boron and nickel. The uneven reaction growing as a result of the heat treatment can be seen in the figures. Many filaments have reaction zones which only extend around portions of the filament circumference, even in the sample heat-treated at 900°C as shown in Figure 6. A number of investigations (References 1 and 2) have considered the interactions occurring in boron filament/nickel matrix composites. This interaction has been observed metallographically after a heat treatment as low as 500°C for one hour. At the higher temperatures as many as five borides have been distinguished.

Stuhrke and Alexander (Reference 3) recently discussed in detail the influence of boron/nickel interactions on composite mechanical properties. Table II taken from this paper presents data showing the effect of time-temperature exposure on mechanical properties. An increase in strength and more significantly composite performance at 300°C after a one hour heat treatment has been observed but not satisfactorily explained. This may be due to the development of a slight surface interaction which accomplishes more effective bonding and load transfer. It may also be due to the reduction of residual stress, which permits more efficient accommodation of the matrix stresses. A very significant decrease in strength occurs as the time at temperature increases.

A fracture surface of one of the tensile test samples is shown in Figure 7. The degree of filament pullout at the fracture surface indicates that the as-deposited boron/nickel interface is very weak in shear. In those areas where the filaments are evenly spaced, little pullout occurred. In those places where the filaments were very close together, large "pipe organ" pullout was observed. This most likely is due to the presence of voids in the matrix caused by insufficient flow of the nickel plating solution into these areas. In addition, the points at which filaments touch become points of weakness leading to premature failure by brittle fracture of the fibers. Consequently, the sensitivity of the low voltage and neutron radiographic techniques for measuring filament spacing is also discussed.

NONDESTRUCTIVE TESTING TECHNIQUE DEVELOPMENT

General Discussion

It can be seen that composite strength is seriously degraded by the interaction occurring in the nickel/boron system during exposure to high temperatures. This indicates the need for nondestructive testing techniques which can be used to detect this condition, not only during the developmental stages but also during structural fabrication and throughout the service life of the material.

Other property variables and discontinuities may affect composite strength as significantly as the interaction between the filament and the matrix. These include cracks in the asprocessed filament; residual stresses in both the filament and matrix materials; lack of filament/matrix bond; lack of matrix/matrix bond; broken, misaligned, or unevenly spaced filaments, matrix porosity and inclusions. North American Aviation/LAD is presently evaluating nondestructive testing techniques for detecting these discontinuities (Reference 4). Broken and misaligned filaments in multilayer boron/titanium composites are reported to be detectable with radiography. Filament to matrix volume ratios varied from 8 to 21%. In addition, areas of lack of matrix/matrix bond as small as 1.6 cm^2 have been detected with pulse echo ultrasonics. As previously

stated, this investigation is primarily concerned with establishing the feasibility of low voltage and neutron radiography for detecting the boron/nickel interaction. The detection of broken and misaligned filaments is possible with both techniques.

Selection of low voltage radiography as one of the techniques to be evaluated during the investigation was made after a consideration of the basic X-ray absorption process. The X-ray attenuation of low atomic numbered materials is small. However, changes in the density of the nickel matrix associated with the formation of the boride intermetallic during heat treatment should be detectable. Sample thickness of only 0.025 cm dictates the use of relatively low energy radiation. Neutron radiography was considered applicable because of the high attenuation cross section of boron for thermal neutrons.

Low Voltage Radiography

The X-ray equipment used to radiograph the boron/nickel samples is shown in Figure 8. It is assembled in a manner similar to that reported by McClung (Reference 5). The X-ray tube is rated at 50 KVCP and 10 ma, and has an effective focal spot of 0.5 mm. The absorption of the X-ray tube window is equivalent to 0.5 mm beryllium. The tube is located on top of a chamber which is constructed so that a film cassette containing the sample can be inserted into the chamber 36 inches from the focal spot of the tube, and the cassette top removed without exposing the film to light. With all openings closed the chamber can also be evacuated. The X-ray absorption by the cassette top and the air between the source and the specimen is eliminated in this manner, decreasing exposure time and improving image contrast.

In order to evaluate technique sensitivity to changes in nickel thickness, a nickel step wedge was constructed with the steps ranging in thickness from 5×10^{-3} cm to 7×10^{-2} cm. A single boron filament was placed on each step of the wedge. All of the nickel/boron samples including the nickel step wedge were radiographed at 35 KVCP and 10 ma. Using Kodak fine grain positive film, the exposure time was 20 minutes. The samples were placed on top of the film within the cassette and the cassette top removed during the exposure. The resulting radiograph is reproduced in Figure 9. Only five of the eight steps of the nickel wedge are detectable radiographically. The image of the tungsten core within the filament appears on several steps of the wedge.

Neutron Radiography

Radiographic examination of composite materials containing boron or other low atomic number materials presents problems because of the low X-ray attenuation of such materials. Fortunately, in the case of boron filament composite materials, the boron can be imaged with neutron radiographic techniques (Reference 6). In this case, the high thermal neutron attenuation of boron can provide an excellent radiographic image of this material, even when it is contained in a matrix.

Examples of neutron radiographs of boron filaments in titanium and aluminum matrices are shown in Figures 10 and 11. The excellent contrast of the boron in the relatively neutron transparent matrix allows one to easily observe radiographically such anamolies as filament breaks, uneven spacing, and nonuniform distribution. Such discrepancies can also be observed in multi-layers of the composite, although it becomes difficult to obtain very reliable radiographic inspection of samples containing more than four layers. This of course depends upon the fiber-to-matrix volume ratio. In Figure 11 the confusing images caused by the overlapping layers make interpretation difficult.

The radiographs shown in Figure 10 and 11 were obtained with the Juggernaut reactor at Argonne National Laboratory, a facility which has been described (Reference 7) from a neutron radiographic point of view. The detection method for these radiographs and the one employed to radiograph the nickel/boron samples (and nickel step wedge) was the high resolution technique employing a 1.2×10^{-3} cm thick gadolinium back screen and single emulsion Kodak Type R X-ray film. The gadolinium screen technique has previously been shown to be a method capable of a high contrast resolution of 10 microns or better (Reference 8). With the particular film mentioned above, total exposures required for good radiographic film density were in the order of 5×10^9 thermal neutrons/cm^2. The neutron radiograph of the nickel/boron samples and the nickel step wedge are shown in Figure 12.

MICRODENSITOMETRIC ANALYSIS

General Description

The low voltage and neutron radiographs were scanned using the microdensitometer shown in Figure 13. Basically microdensitometry is a method for obtaining and recording very fine photographic detail by comparing the density on the film with some secondary standard. Some instruments used for this purpose employ two light sources. The Joyce Loebl instrument uses a double light beam from a single light source. This improves trace reproducibility by eliminating changes in light intensity caused by line voltage variations and lamp aging. One light beam passes through the film to be traced; the film image is magnified by an objective lens (up to 90X), collimated by an adjustable aperture, and focused on the photomultiplier tube after passing through a chopper. The aperture width may be adjusted so that the effective width of the light beam at the plane of the film is as small as two microns. The height of the aperture can also be adjusted up to 24 mm providing integration of the film grain, which improves the signal-to-noise ratio. The other beam passes through a variable density wedge, through the chopper, to the photomultiplier tube. The difference in light intensities of the two beams produces a voltage which is used to drive the recording pen. A combination of variable density wedges and filters is available for obtaining density profiles up to 6.0 density units. The recording

table and the film table are coupled mechanically by a lever or "ratio arm." Various ratios are available for expanding the recording with respect to the film image by a factor of up to 1000:1.

The most important instrument parameters which were maintained constant for all traces are:

1. Ratio arm 100.1
2. Variable density wedge ..... 2.0 density units
3. Aperture width ..... 200 microns
4. Aperture height 1.0mm

Actual film density was determined by scanning a variable density film step wedge used for calibrating the Ansco densitometer. A graph was then constructed relating pen deflection to the density on each step of the film wedge.

Microdensitometry -- Low Voltage Radiographs

Typical microdensitometer traces of a section of each sample and the nickel step wedge as imaged by low voltage radiography are shown in Figures 14, 15, and 16. Since a decrease in X-ray absorption produces an increase in film density and trace height, the relatively high film density recorded on the far right of the traces corresponds to the thin nickel section adjacent to the composite. The increase in nickel thickness near the edge of the composite produces a rapid decrease in film density until the first boron filament is reached. Then a rapid increase in film density occurs terminating in a peak broken by a sharp dip in density corresponding to the tungsten core. The large fluctuations are related to the relatively low and high X-ray attenuation of the boron and tungsten core respectively. A slight increase in film density occurs between individual filaments which represents the decrease in nickel matrix thickness as a result of the electrodeposition process previously discussed.

The diffusion of boron into the matrix is recorded as a change in boron filament width and height as the temperature of the heat treatment increases. Since the interaction produces an intermetallic compound whose density lies somewhere between boron and nickel, less radiation is absorbed in those areas where the diffusion zone is growing between adjacent filaments. This is reflected as an increase in film density corresponding to the actual thickness of the diffusion zone produced by the heat treatment. Diffusion zone thickness is defined here as the amount of intermetallic compound in a plane parallel to the X-ray beam. If the reaction zone is growing toward the top or the bottom of the sample, more radiation will be absorbed because the intermetallic is denser than the boron it replaces. This produces a decrease in film density immediately adjacent to the image of the tungsten core, again proportional to the diffusion zone thickness. The uneven densities recorded adjacent to the tungsten core and in the areas between adjacent filaments are indicative of the uneven diffusion occurring around portions of individual filaments seen on the photomicrographs.

The low voltage technique used to radiograph these samples is insensitive to boron. This can be seen from the trace of the nickel step wedge film image containing individual boron filaments on each step as shown in Figure 16. Only the image of the tungsten core appears on the trace. The technique is sensitive however to the intermetallic compound being formed and to the changes in the density of the nickel caused by intermetallic formation. An estimate of sensitivity was obtained by comparing changes in film density associated with the filaments of the sample heat-treated at 600°C with that of the standard sample. Traces chosen for comparison were correlated with the reaction zone as it appears on the photomicrograph of the 600°C sample. Filaments were selected where the reaction zone had formed between adjacent filaments. A diffusion zone thickness of approximately 1×10^{-2} cm produces a change in trace height of 1.0cm. This is equivalent to a change in film density of 6×10^{-2} units. Generally a change in film density of 1×10^{-2} is considered detectable.

In addition, the microdensitometer scan of the low voltage radiograph reveals uneven filament spacing. For example the scan of the film image of the standard sample (Figure 14) shows that the spacing between the first, second, and third filaments is about the same, increasing between the third and fourth. The distance between the fourth and fifth filament is even greater. Less nickel is deposited in this area during the electroplating process, and the slight decrease in nickel thickness produces the increase in film density.

Comparing spacing between the first and second filaments (7.5×10^{-3}cm) with that between the fourth and fifth filaments (1.2×10^{-2}cm), an increase in filament spacing of 3×10^{-3}cm produces an increase in film density of 5×10^{-2} units, corresponding to a decrease in nickel thickness of 2.5×10^{-3}cm determined from the photomicrograph of the standard sample.

Microdensitometry -- Neutron Radiographs

Typical traces of a section of the neutron radiographic image of each boron/nickel sample are shown in Figures 17 and 18, including the traces of filament images on the 5×10^{-3}cm and 7×10^{-2}cm steps of the nickel wedge. Like the traces from the low voltage radiographs, the relatively high film density on the far right corresponds to the thin nickel section adjacent to the composite. However the "dip" which is recorded is not produced by the increase in nickel thickness at the edge of the composite, but by the boron content of the filament. This is to be expected because of the high attenuation cross section of boron for thermal neutrons compared to nickel.

The "peak" in film density occurs at a point midway between each filament. An examination of the traces of the standard sample indicates that an increase in peak density is associated with an increase in filament spacing. For example the increase in spacing between the fourth and fifth filaments previously noted produces an increase in film density of 0.6 unit over that recorded between the third and fourth filaments. In this case however, the peak trace height does not

appear to be influenced by changes in matrix thickness, but is only a function of the spacing between the boron filaments. Using the scan of the low voltage radiograph of this sample, a change in filament spacing of 22% produces a density change of 30% for this particular radiograph.

Unexpected variations in the traces of these samples occurred. The average change in film density associated with each filament in the standard sample is lower than expected when compared to the traces of the sample heat-treated at 600°C. Results indicate that film density changes from 2.5×10^{-2} to 8×10^{-2} units occur for a given change in heat treatment. This variation in density is probably caused by uneven diffusion as noted on the low voltage radiographs and photomicrographs. Tests with other samples containing boron indicate that concentrations as low as 500 ppm are detectable with the neutron radiographic technique.

Figure 18 shows the trace of the neutron image of the sample heat-treated at 900°C as well as the trace of individual filaments imaged on two steps of the nickel wedge. The relative insensitivity of the neutron technique to changes in nickel matrix thickness can be seen from the figure. The nickel step wedge thickness varies from 5×10^{-3} to 7×10^{-2}cm, yet the associated change in film density over this thickness range is only 0.2 unit. The tungsten core does not appear on any of the traces. In addition the trace of the individual filaments is almost twice the actual filament diameter. The diameter, as imaged, remains relatively the same even though the boron filament located on the step wedge is displaced by a factor of 15:1 from the film. If this effect is caused by geometry it is not noticeable over these distances. The possible effect of the screen-film combination has not been determined at this time. One possible explanation is that the boron filament acts as a heat sink to the thermal neutrons (Reference 9). If this is so, the image of the filament should be a function of the neutron energy. This aspect is presently being investigated.

Discussion of Results

The low voltage radiographic technique evaluated during this investigation is sensitive to changes in the density of the nickel matrix caused by the formation of a boron/nickel intermetallic during heat treatment. Using the criterion that 0.01 density unit is detectable radiographically, a 16 micron change in intermetallic thickness can be recorded using microdensitometric analysis of the film image. Diffusion of boron into the nickel matrix is detectable under sample heat-treat conditions of 600°C for one hour. Microdensitometric analysis of the film image also accurately records filament spacing. The effect of uneven filament spacing on the amount of nickel deposited between the filaments during the electroplating process can be determined with this technique. An increase in filament spacing of 0.003cm produces an increase in film density of 0.05 unit, corresponding to a decrease in nickel thickness of 0.0025cm as shown on the photomicrographs of the standard sample.

Obviously the low voltage radiographic and microdensitometric techniques are more applicable for characterizing the reaction zone as a function of heat treatment in single layer metal matrix materials. With multilayered samples, visualization of the diffusion zone in a particular layer would be much more difficult. Laminography (Reference 10) may be useful for overcoming this difficiency, but this technique has not been investigated for this application.

The neutron radiographic technique is, as expected, much more sensitive to the boron filament material than the matrix surrounding the filaments. A change in nickel matrix thickness from 5×10^{-3}cm to 7×10^{-2}cm only changes the film density by 0.2 unit. An examination of the traces of the film image of the sample which was not heat-treated indicates that the peak density recorded between the filaments is a function of the filament spacing. A change in filament spacing of 22% was recorded as a 30% change in film density. Unexplained variations in the average film density of the standard and the one heat-treated at 900°C occurred. However, based upon an analysis of the density profile of the film image of the samples heat-treated at 600° and 700°C, a change in film density of 2.5×10^{-2} to 8×10^{-2} should be detectable for each change in heat treatment employed during this investigation. Tests with other samples containing boron indicate that concentrations as low as 500 ppm are detectable with the neutron radiographic technique.

One of the unexpected variables is the large diameter of the boron filament imaged by the neutron radiographic technique. The diameter of the filament as recorded by the microdensitometer is twice the actual diameter of the filament. The spacing of the filament from the film does not influence image diameter, at least over the distances employed during this investigation. The effect of the film-screen combination is being considered, as well as the possibility that the boron acts as a heat sink for the thermal neutrons.

Inspection of boron filament quality on a production-type operation could be accomplished with much lower total exposures by using faster film techniques. A scintillator method (Reference 11), for example, requiring a total exposure of only about 10^5 thermal neutron/cm^2, could be used and has been shown (Reference 8) to be capable of resolving at least 5×10^{-3}cm.

A suitable neutron source might present a problem in a production inspection operation since nuclear reactor sources have been most widely used for neutron radiography. Reactor sources are preferred because of the high intensity neutron beams available (10^6 to 10^8 neutrons/cm^2-sec). Reasonably inexpensive, commercially available reactors can be considered for such work. However, radioactive (Reference 12) and small accelerator sources (Reference 6 and 13) are also feasible and recent work in this area looks promising. Such sources seem capable of supplying thermal neutron beam intensities in the 10^4 to 10^6 neutron/cm^2-sec range.

Conclusions

The feasibility of low voltage radiography and neutron radiography coupled with microdensitometry has been established for detecting the interaction of boron and nickel nondestructively under conditions of heat treatment as low as 600°C for one hour.

The low voltage radiographic technique has been shown to be very sensitive to the change in the density of the nickel matrix caused by the formation of the boride intermetallic. Because of the large thermal neutron absorption cross section of boron, the neutron radiographic technique is much more sensitive to the boron concentration in the intermetallic compound than to changes in density or thickness of the nickel matrix or tungsten core.

Both techniques should be applicable for inspecting boron and boron compound filaments embedded in other matrix materials. The low voltage radiographic technique should be sensitive to matrix density changes caused by the interaction of other filament materials. It is hoped that the data presented will be useful together with other NDT techniques for completely characterizing filament reinforced metal matrix composites, and that with further technique development will contribute to the evaluation of these materials in multilayer configurations.

REFERENCES

1. Alexander, J. A., Research on Boron Reinforced Metal Matrix Composites, AFML-TR-67-101, Air Force Materials Laboratory, Wright-Patterson Air Force Base, Ohio, June 1967.

2. Schneidmiller, R. F., White, J. E., "A Compatibility Study of SiC, and B Fibers in Be, Fe, Co, and Ni Matrices," Presented at the 10th National SAMPE Symposium and Published in Volume 10 of Advanced Fibrous Reinforced Composites, Western Periodicals Co., Hollywood, California. November 1966.

3. Stuhrke, W. F., Alexander, J. A., "The Effect of Boron-Nickel Properties on Mechanical Properties" Presented at ASTM Meeting, Chicago, Illinois, 2 November 1966.

4. Martin, G., Moore, J. F., Research and Development of Nondestructive Testing Techniques for Composites, AFML-TR-66-270, Air Force Materials Laboratory, Wright-Patterson Air Force Base, Ohio, February 1967, USAF Contract No. AF 33(615)-2865, North American Aviation Corp., Los Angeles Division.

5. McClung, R. W., "Techniques for Low Voltage Radiography," ORNL 3252, Oakridge National Laboratory, Oakridge, Tenn., March 1962.

6. Berger, H., Neutron Radiography, Elsevier Publishing Co., Amsterdam, 1965.

7. Berger, H., "Characteristics of a Thermal Neutron Beam for Neutron Radiography," Int. J. Applied Radiation and Isotopes, 15, 407-414 (1964).

8. Berger, H., "Resolution Study of Photographic Thermal Neutron Image Detectors," J. Applied Physics, 34, 914-918 (1963).

9. Glasstone, S., The Elements of Nuclear Reactor Theory, D. Van Nostrand Co., Inc., 1952, page 91.

10. Blanche, J. F., "Nondestructive Testing Techniques for Multilayer Printed Circuit Boards," Proceedings of the Second Technology Status and Trends Symposium, NASA, Huntsville, Alabama, October 26-27, 1966.

11. Wang, S. P., Shull, C. G., and Phillips, W. C., "Photography of Neutron Diffraction Patterns," Rev. Sci. Instr., 33, 126 (1962).

12. Cutforth, D. C., Argonne National Laboratory, Idaho, personal communication, 1966. See also, Cutforth, D. C., "On Optimizing an Sb-Be Source for Neutron Radiographic Applications," to be presented at the 27th National Conference for the Society of Nondestructive Testing, Cleveland, Ohio, October 1967.

13. Barton, J. P., University of Grenoble, Grenoble, France, personal communication with H. Berger 1966.

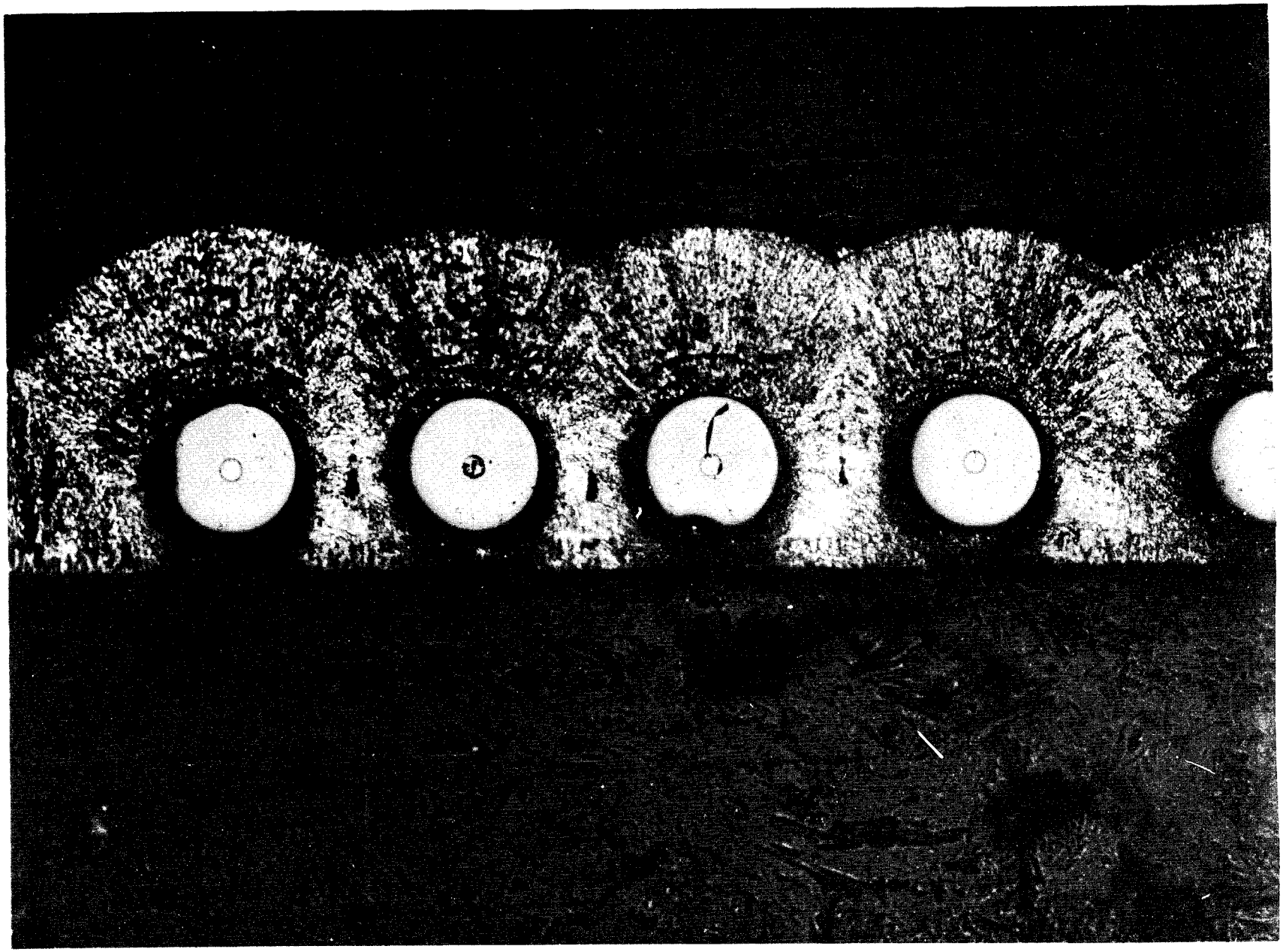

Figure 1. Section of the Boron/Nickel Composite Prior to Heat Treatment (100X)

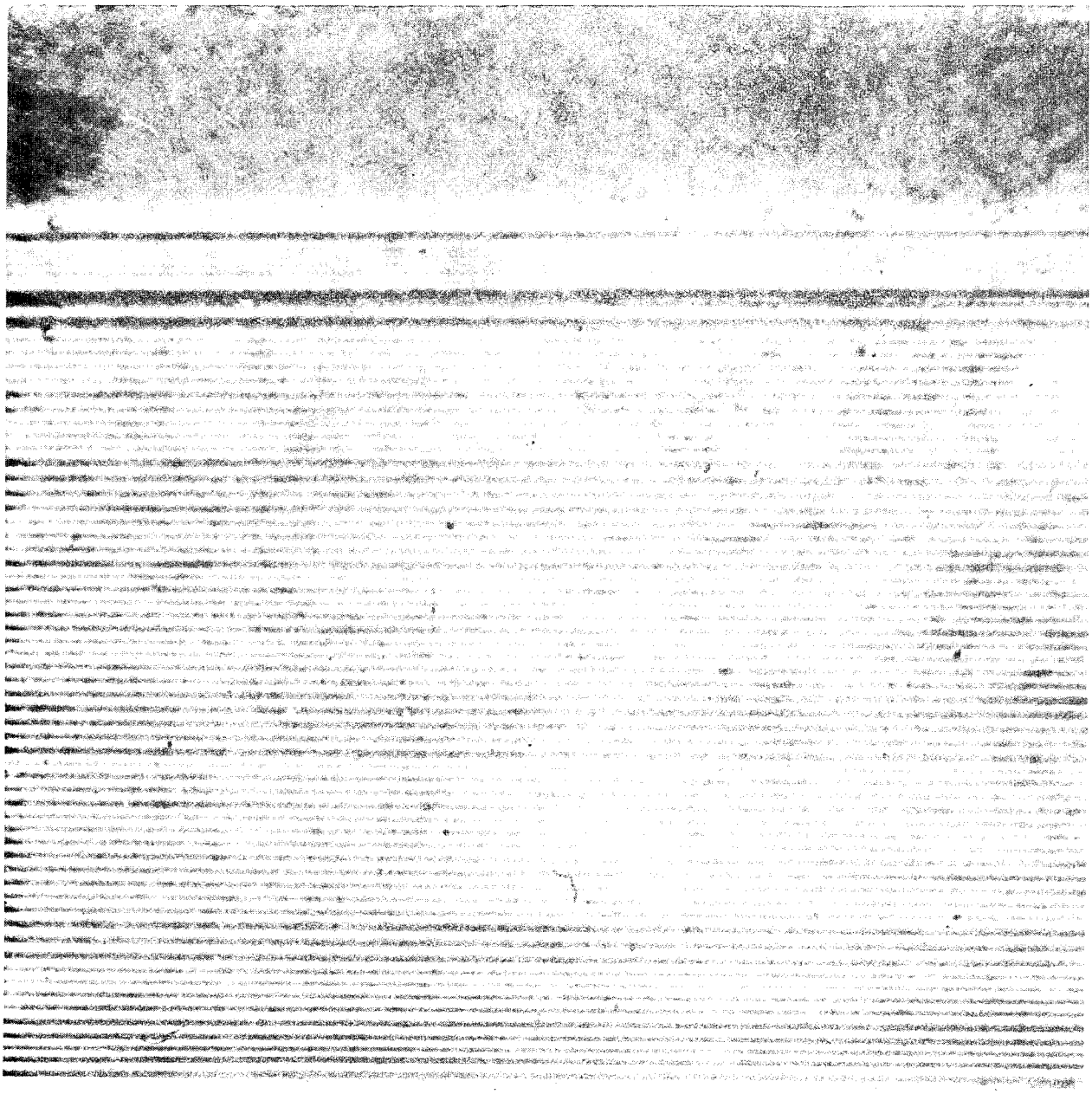

Figure 2. Section of the Boron/Nickel Composite (100X)

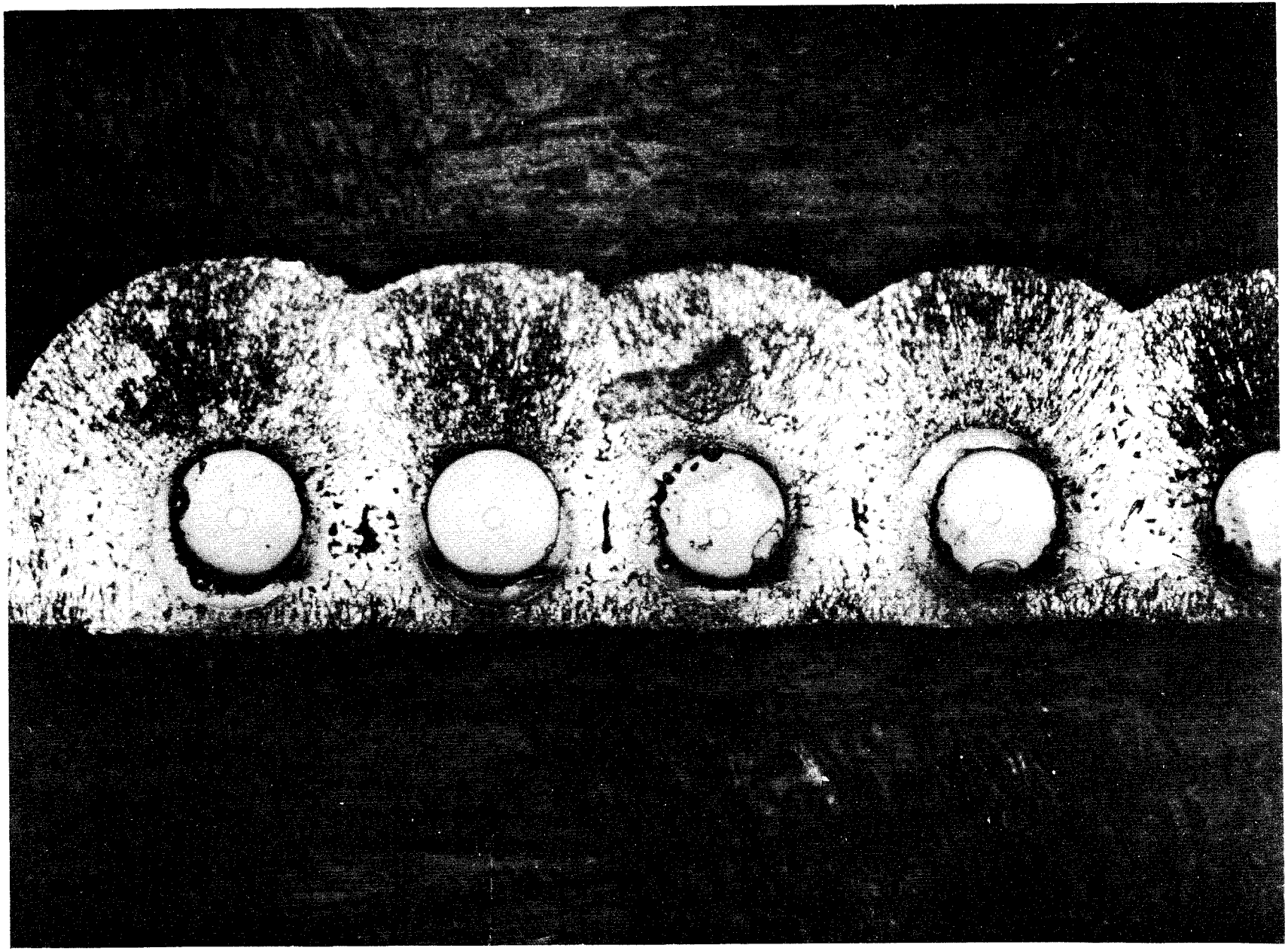

Figure 3. Section of the Boron/Nickel Sample Heat-Treated at 600°C (100X)

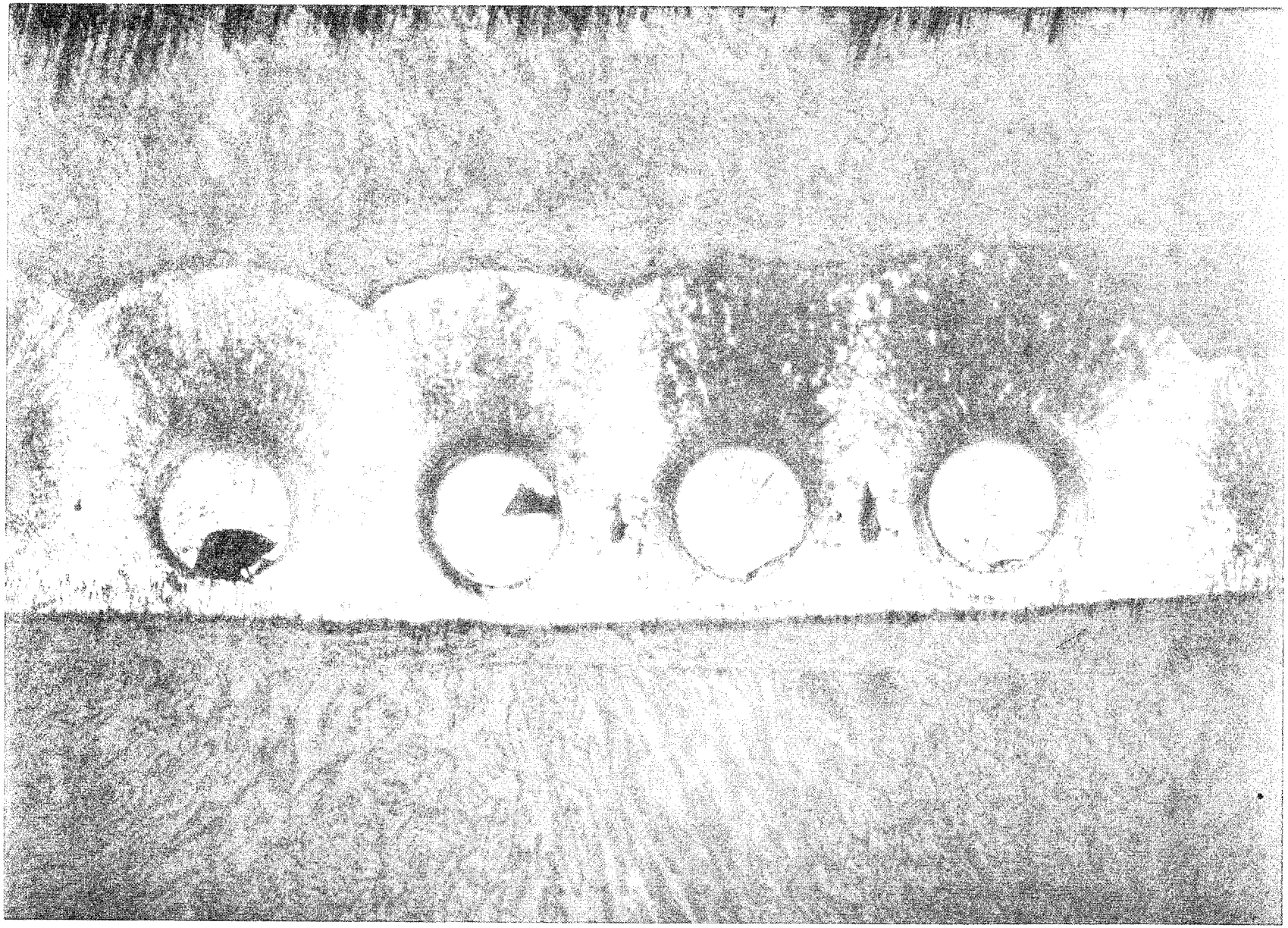

Figure 4. Section of the Boron/Nickel Sample Heat-Treated at 700°C (100X)

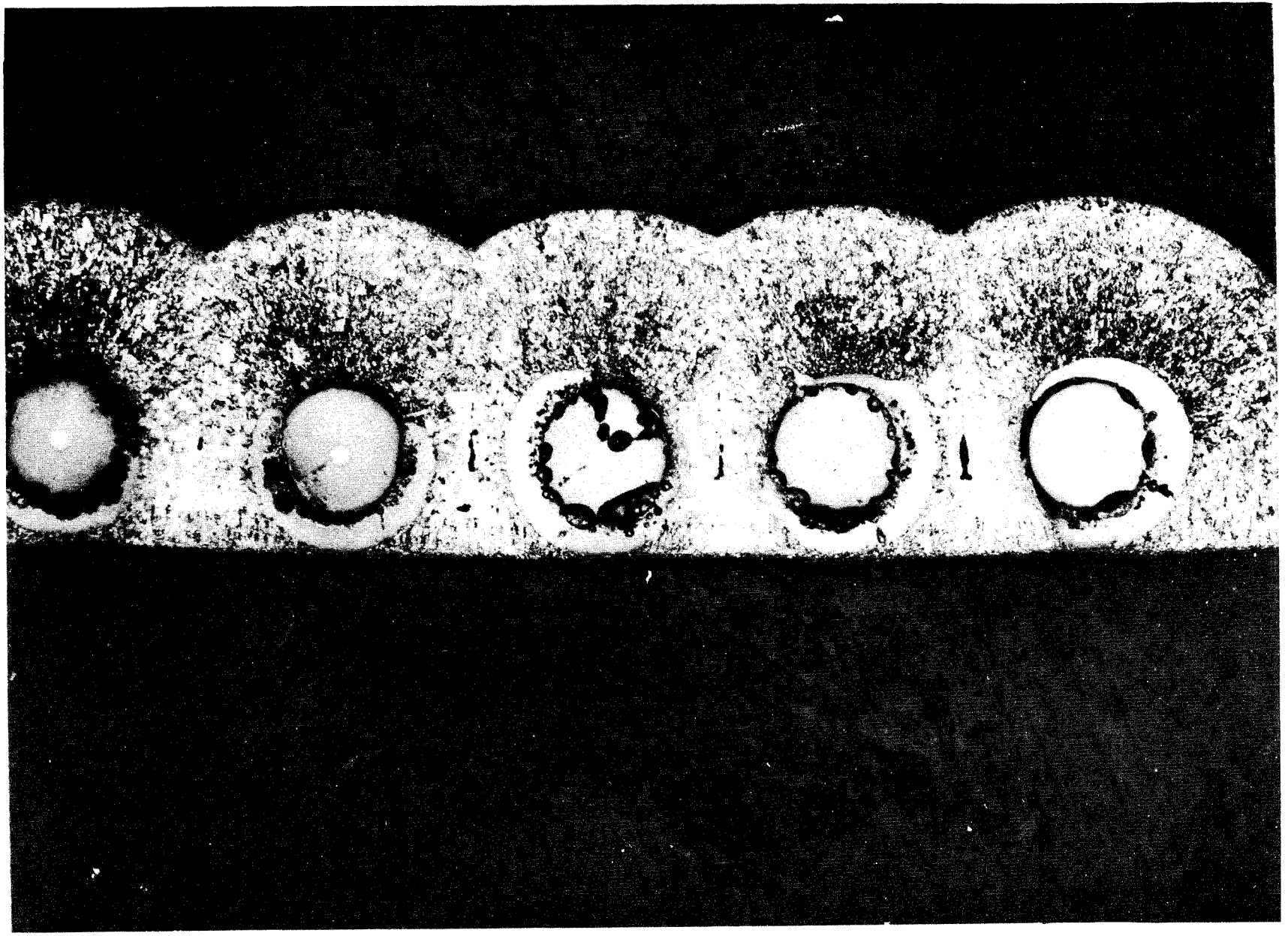

Figure 5. Section of the Boron/Nickel Sample Heat-Treated at 800°C

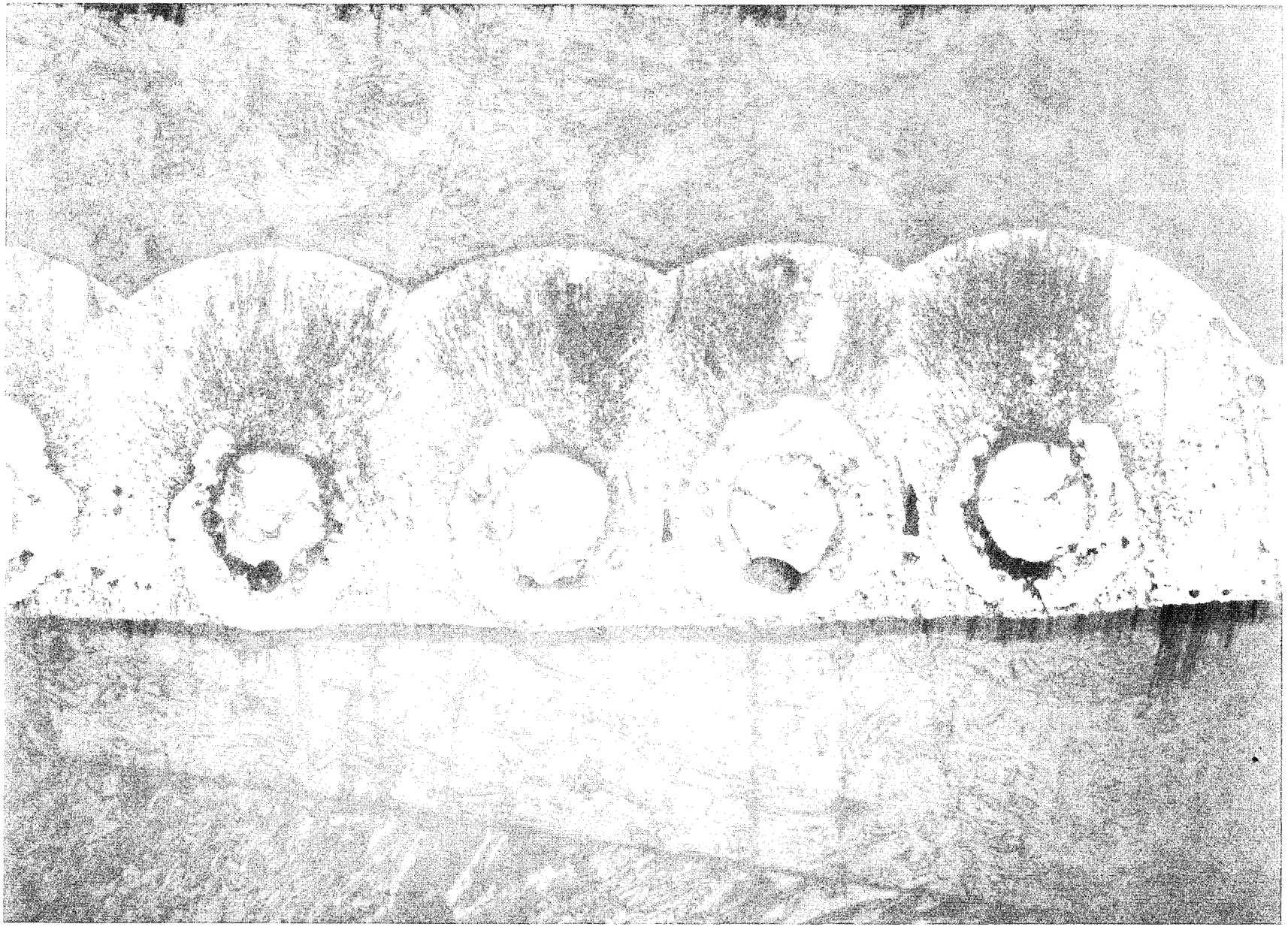

Figure 6. Section of the Boron/Nickel Sample Heat-Treated at 900°C (100X)

Figure 7. Fracture Surface of a Boron/Nickel Sample After Tensile Test (100X)

Figure 8. Low Voltage X-Ray Equipment

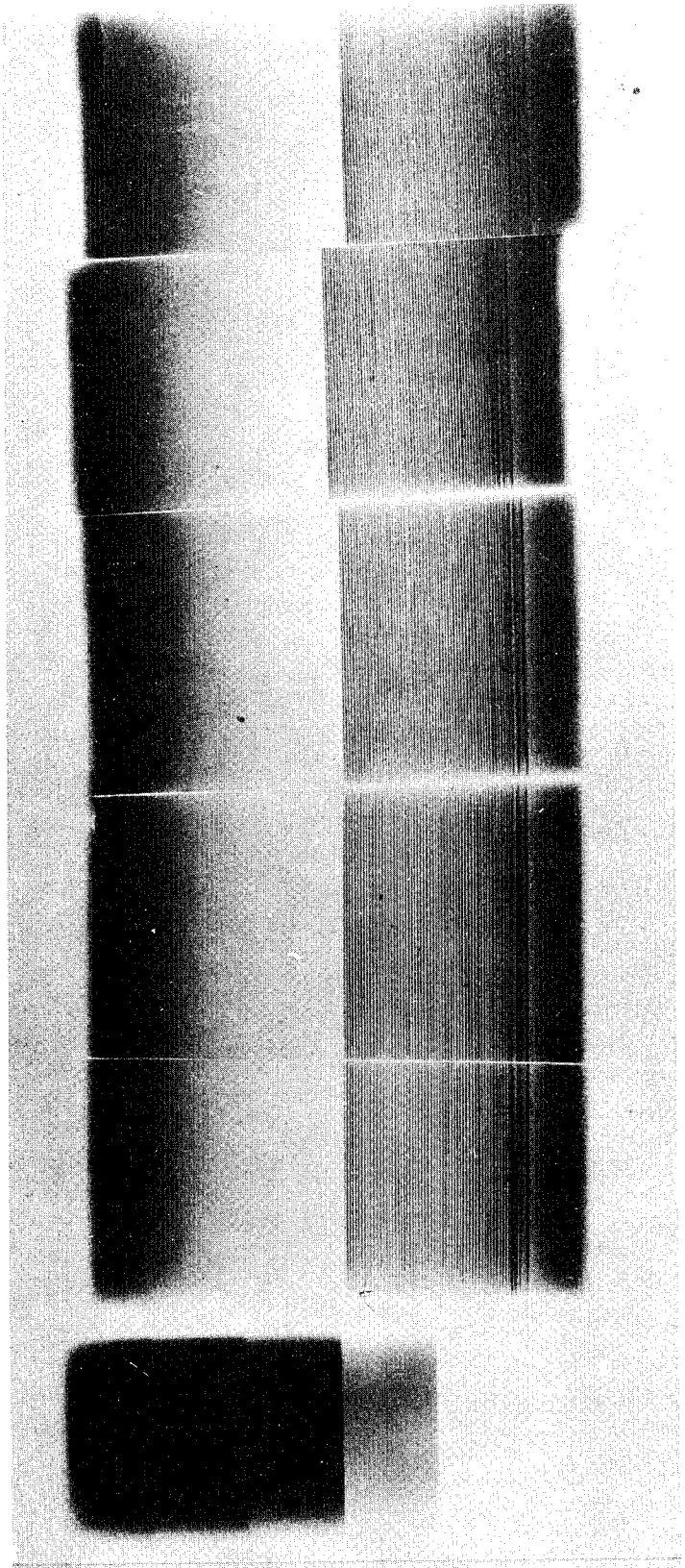

Figure 9. Low Voltage Radiograph of the Boron/Nickel Samples and the Nickel Step Wedge (100X)

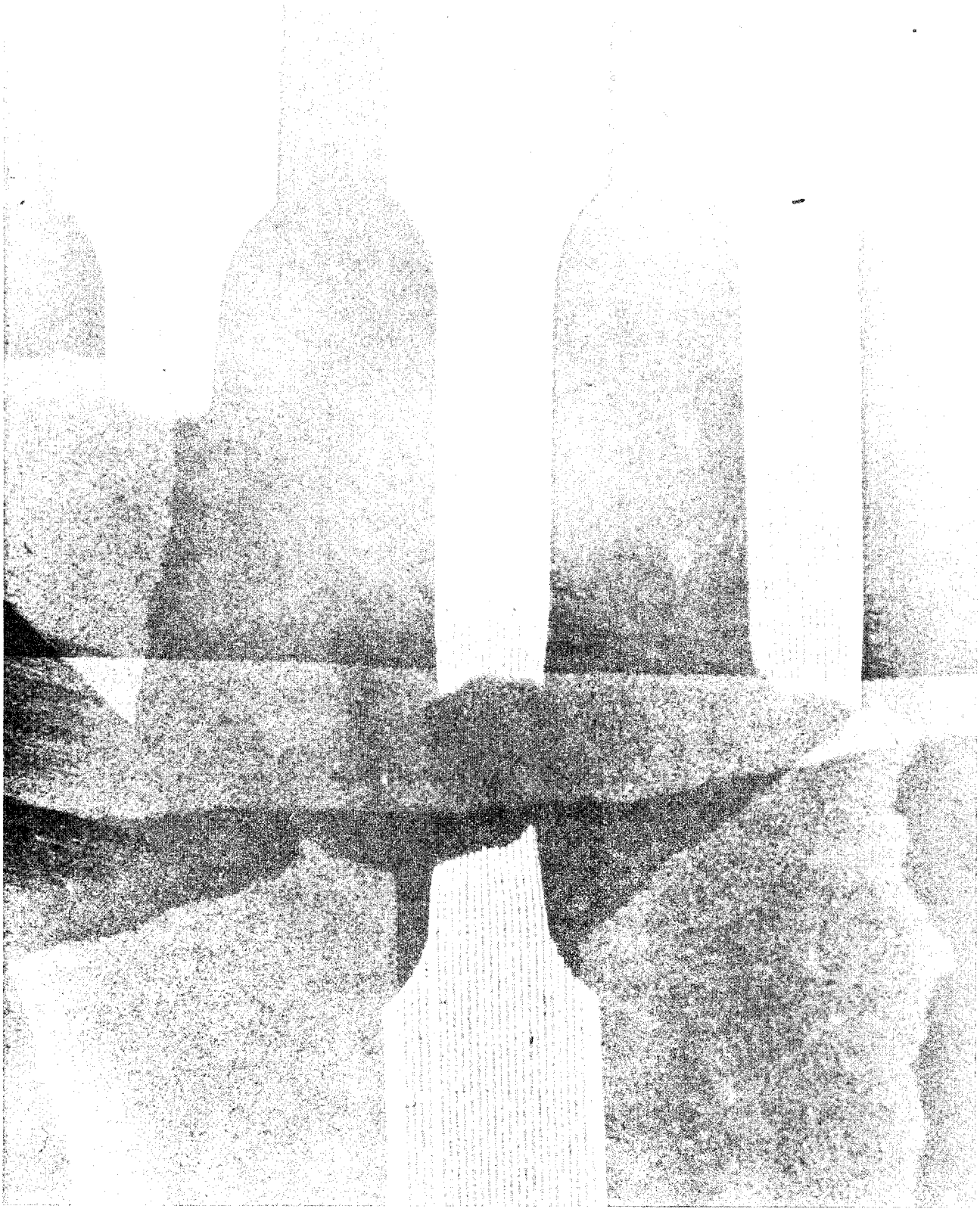

Figure 10. Neutron Radiograph of Boron/Titanium Composite (100X)

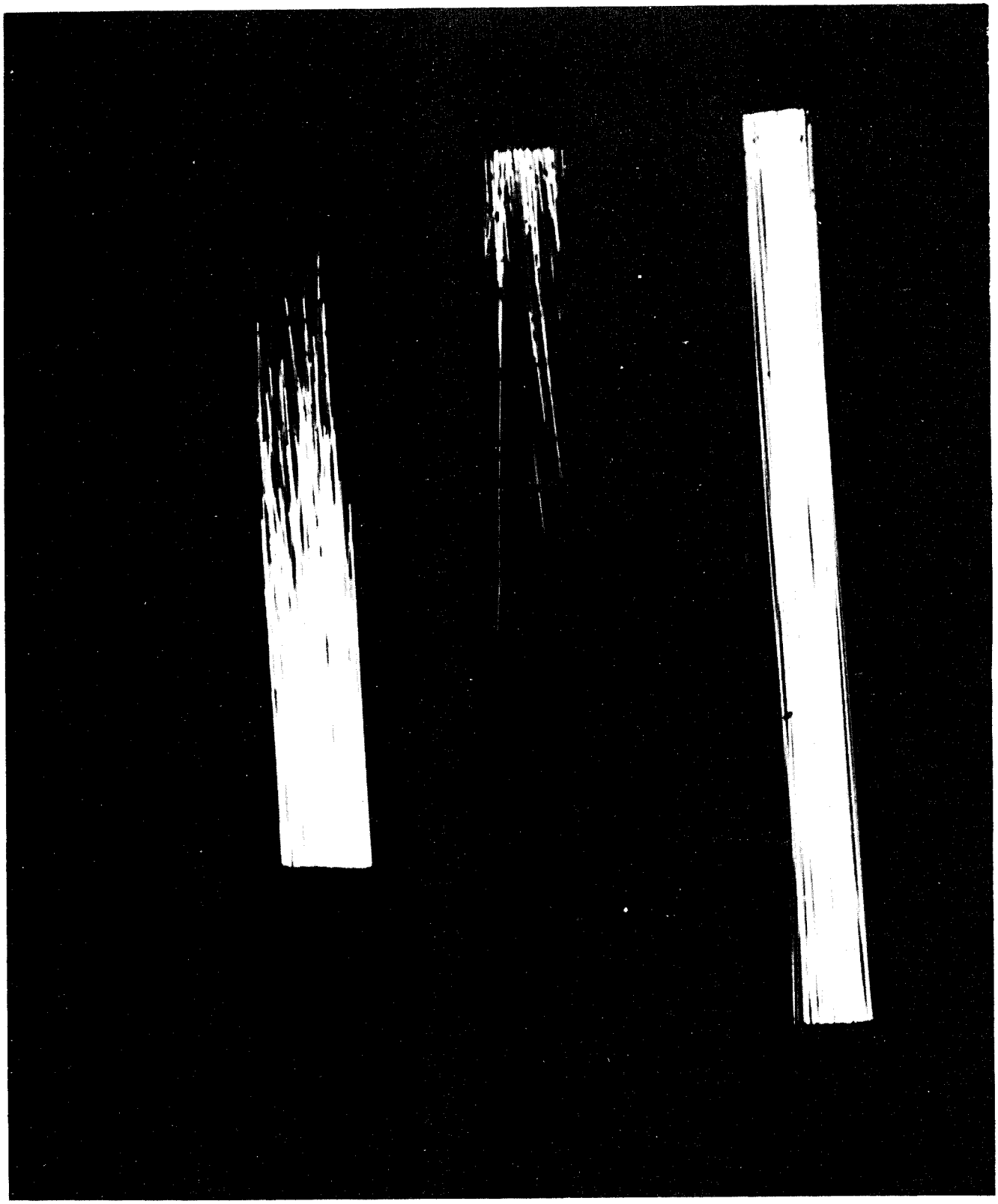

Figure 11. Neutron Radiograph of Boron/Aluminum Composite (100X)

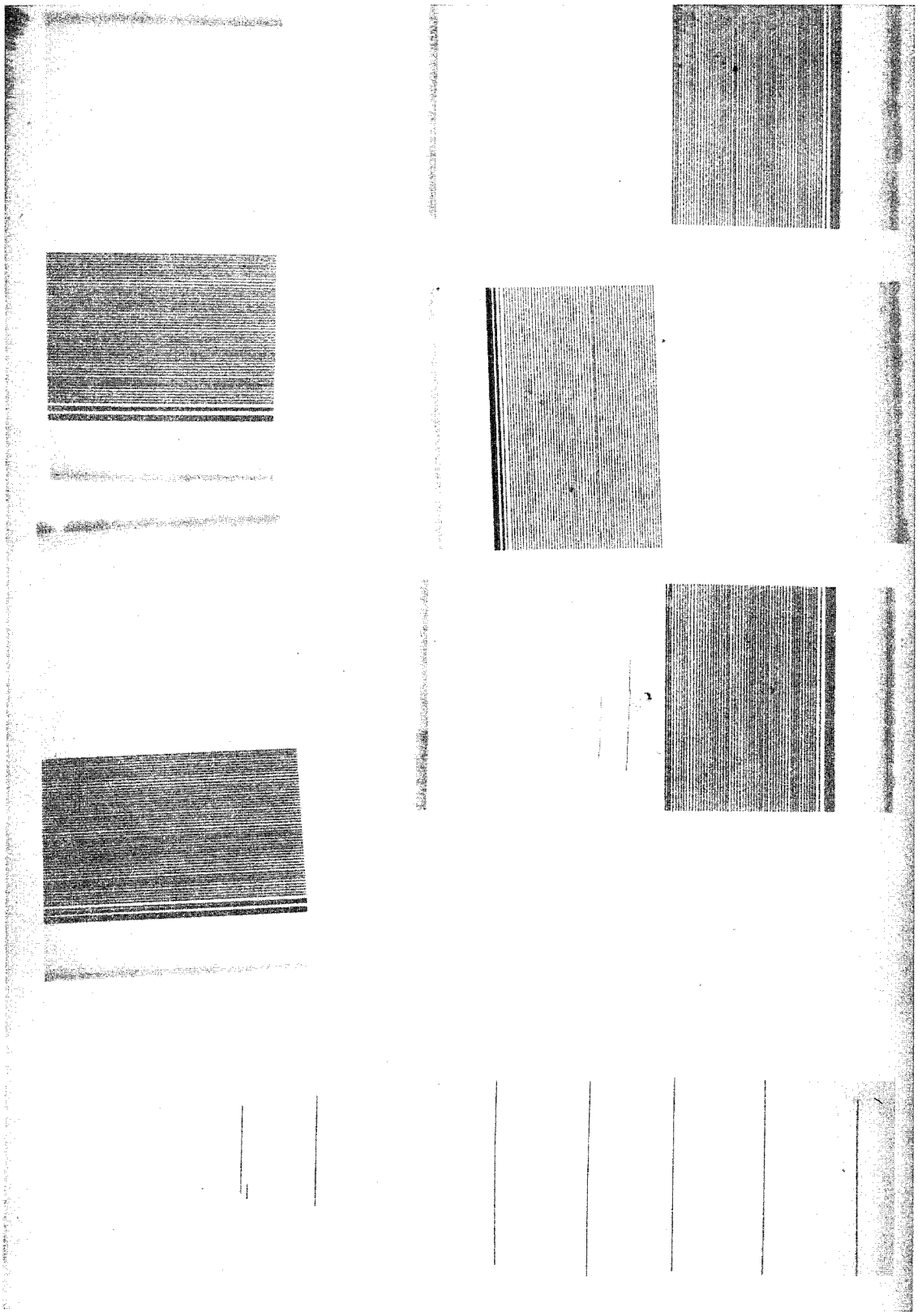

Figure 12. Neutron Radiograph of the Boron/Nickel Samples and the **Nickle Step Wedge (100X)**

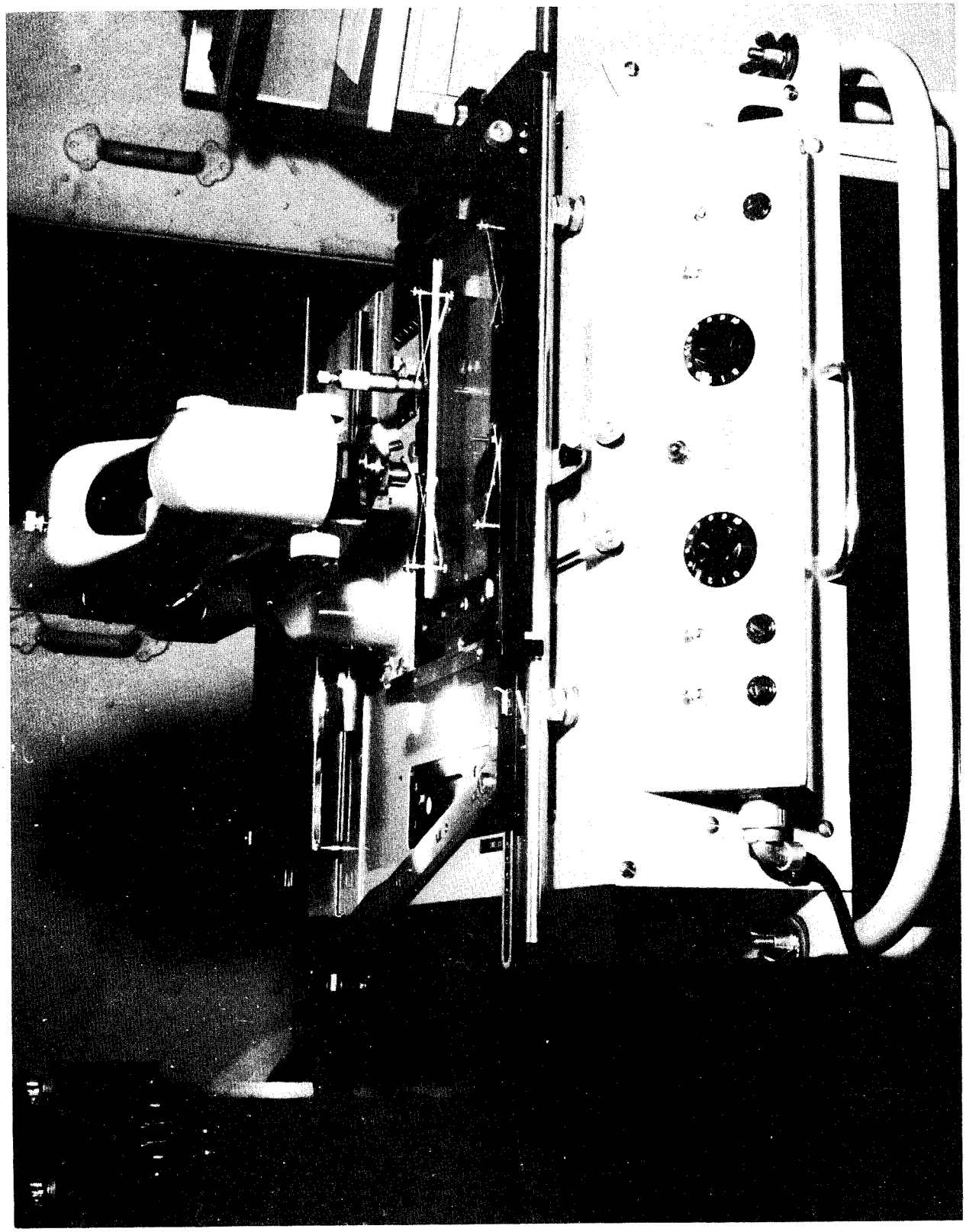

Figure 13. Joyce Loebl Microdensitometer

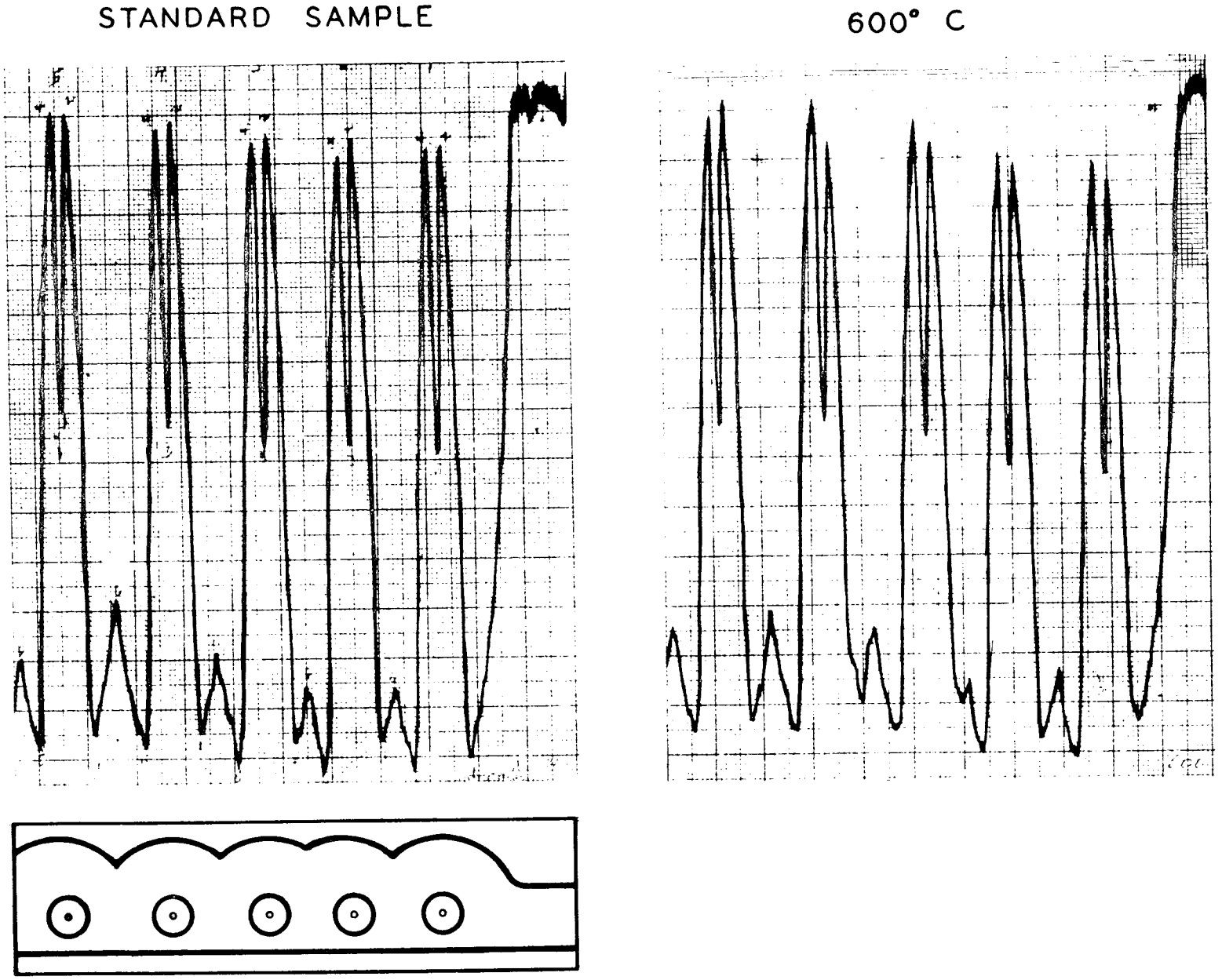

Figure 14. Traces of Low Voltage Radiographic Image of the Standard Sample and 600°C Heat-Treat Sample

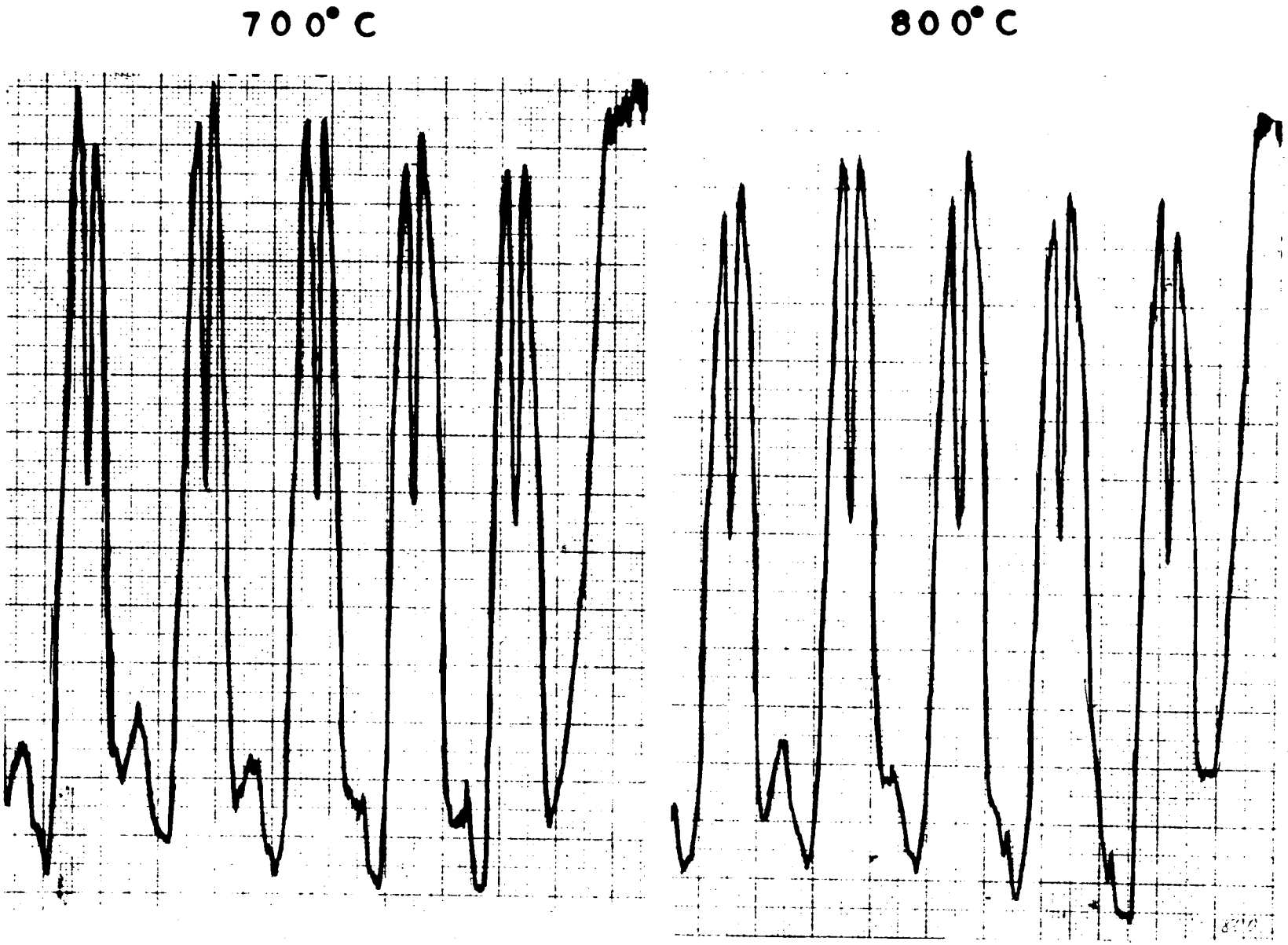

Figure 15. Traces of the Low Voltage Radiographic Image of the 700°C and 800°C Heat-Treat Samples

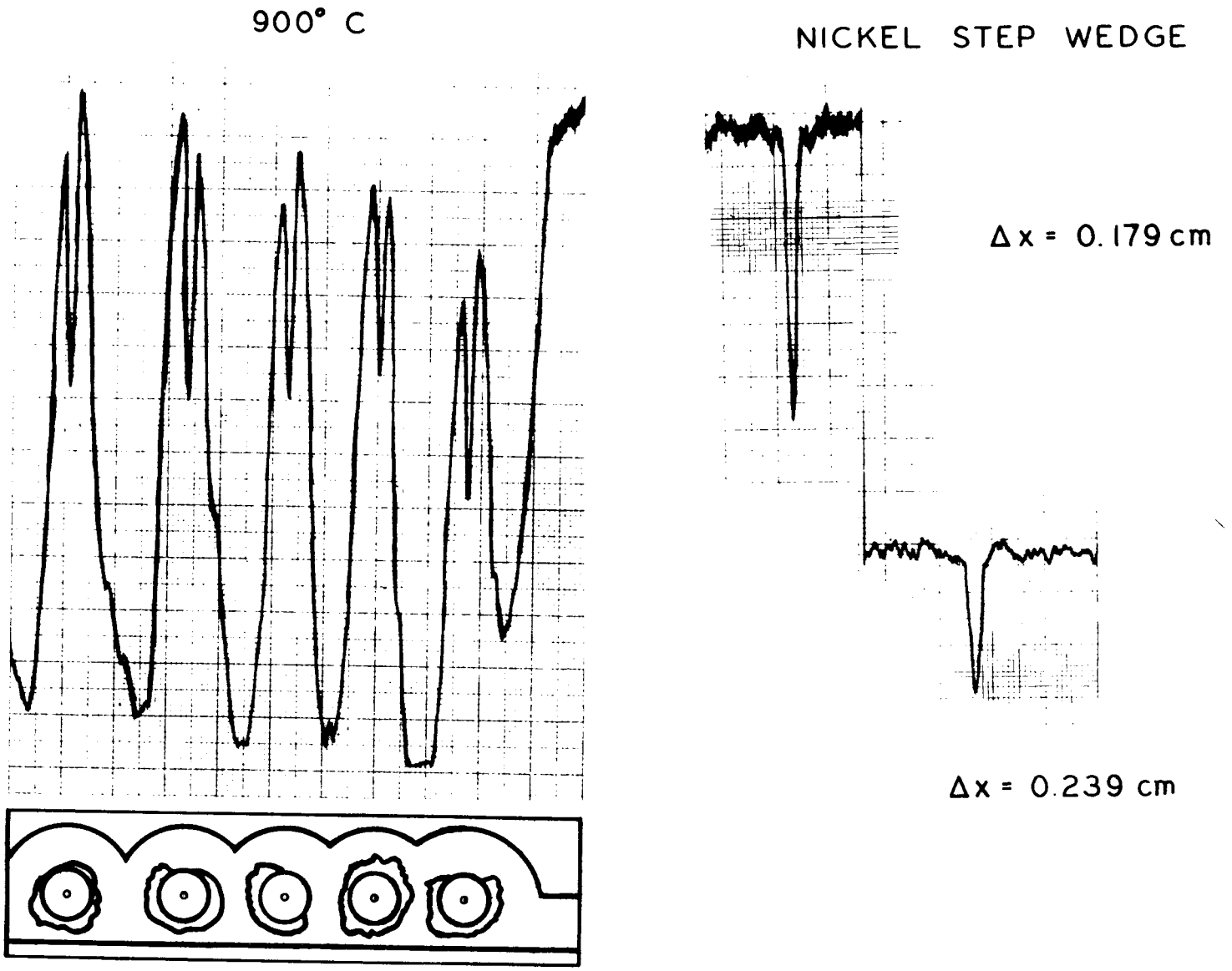

Figure 16. Traces of the Low Voltage Radiographic Image of the 900°C Heat-Treat Sample and Nickel Step Wedge

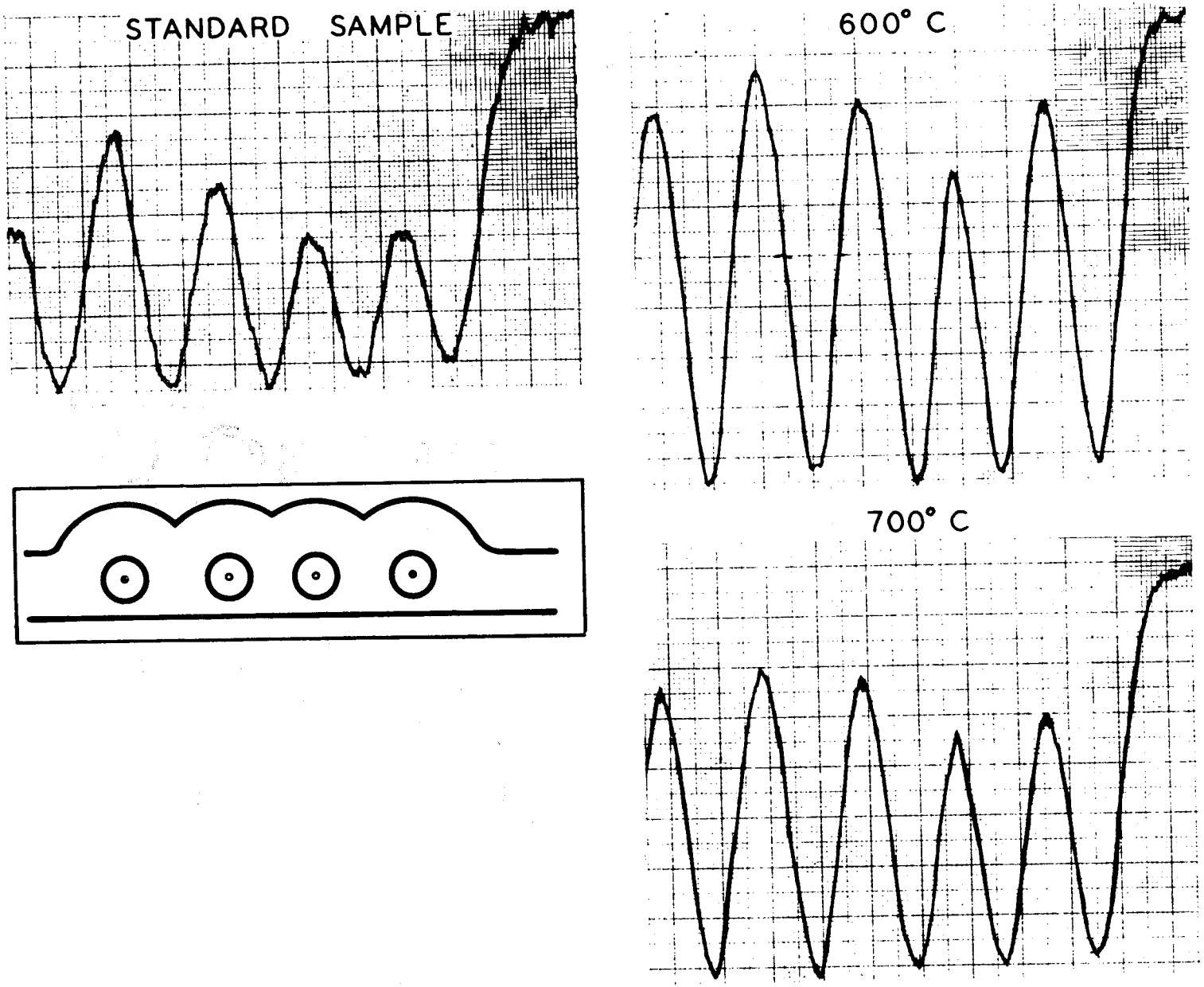

Figure 17. Traces of the Neutron Radiographic Image of the Standard Sample and the 600°C and 700°C Heat-Treat Samples

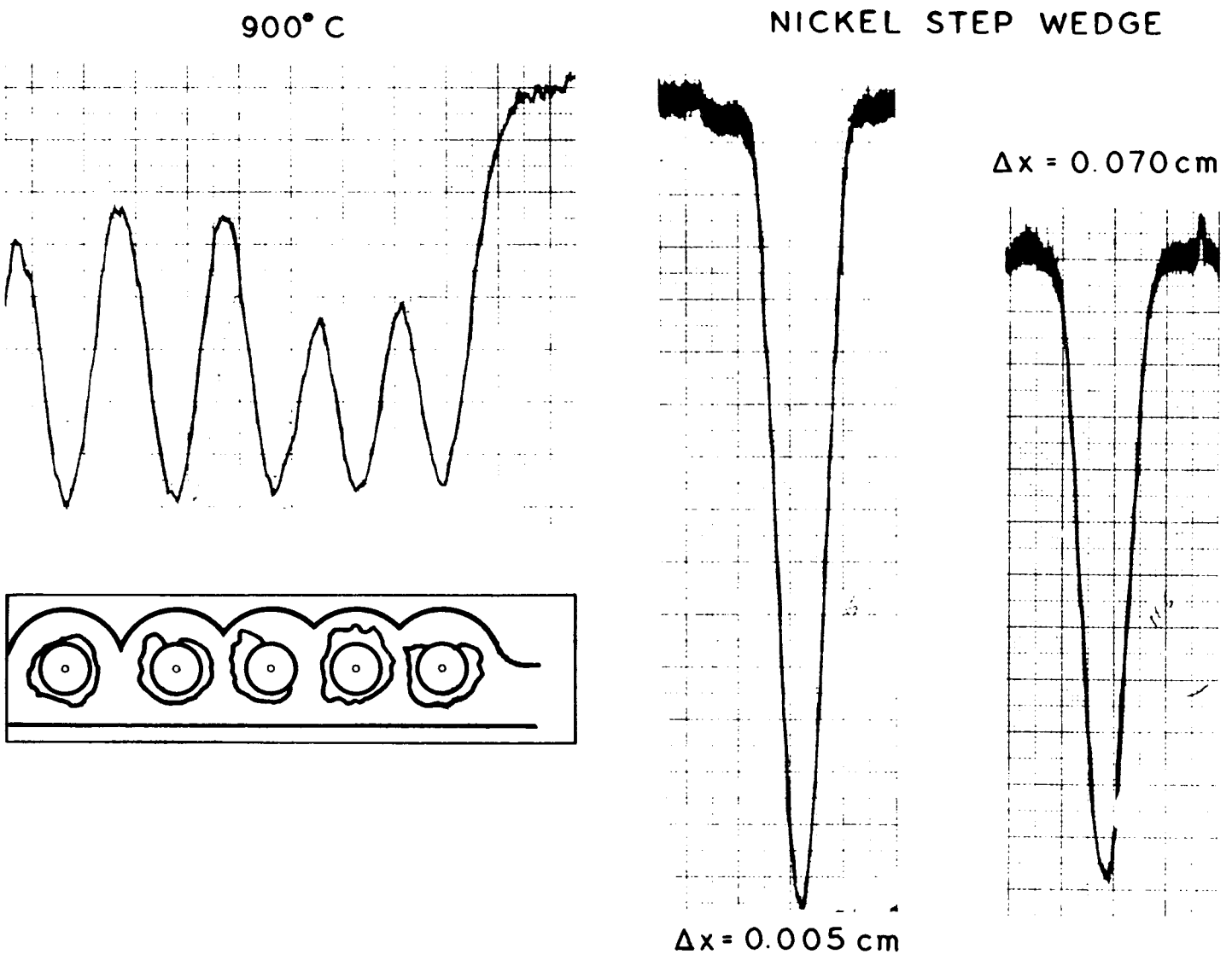

Figure 18. Traces of the Neutron Radiographic Image of the 900°C Heat-Treat Sample and Nickel Step Wedge

DESIGNING NONDESTRUCTIVE TESTS TO DEFINE MATERIAL CHARACTERISTICS

R. S. Sharpe

Nondestructive Testing Centre, A. E. R. E., Harwell, U. K.

Any attempt to correlate materials characteristics with systems performance presupposes that adequate and appropriate data about the magnitude and variability of the characteristics are available; in a form and with a mode of presentation that will allow a quantitative form of correlation to be made. It is generally misleading to try to correlate material characteristics with performance after service or after failure. This is because structural degradation during service, at failure, or during the prelude to failure may well modify the defects which were initially present in the material.

Most of the available N.D.T. techniques have limitations when it comes to accurately sizing or identifying a defect, particularly in the case of internal defects where any form of direct visual observation cannot be used. Thus, before a satisfactory programme of correlation can be mounted, considerable attention must be paid to the design of the pre-service testing.

Much effort over the years has gone into improving the sensitivity of non-destructive tests (Fig.1). In fact it is partly because of the extreme sensitivity now available that the need to provide correlations with systems performances arises. Only in this way can realistic standards of acceptance now be set. As a point of distinction we can define any variation from perfection as a 'defect'. A 'defect' becomes a 'flaw' at the point where its size or variability has an effect on systems performance (Fig.2).

What is now urgently required is more attention paid to designing tests to provide the maximum possible data on the variability of materials characteristics of which the classical 'defect' of the nondestructive tester (the crack or similar material discontinuity) is only one in a wide range of significant characteristics (Fig.3).

In reactor technology, where it is particularly difficult to simulate the service environment artificially, it is a common, and natural, philosophy to over-inspect until the experience of systems performance can be used to set realistic 'flaw' levels. This is, in fact, an area where it is very appropriate that emphasis should be put on the characterisation and recording of defects when designing pre-service tests. Only by doing so is the right kind of data made available for detecting correlations when the trends of reactor performance are analysed.

A considerable amount of effort has been put into this aspect of testing in the Nondestructive Testing Centre at Harwell. Although the applications have been specifically related to nuclear components the ideas and techniques are of much wider interest and very relevant to the context of this conference.

The programme of work has been particularly associated with the stainless steel cans used to contain the ceramic fuel in the latest design of British air-cooled nuclear power reactors. The materials characteristics of the cladding that may vary - and hence may influence systems performance and fuel element endurance - are dimensions, surface profile and grain size, in addition to the more generally recognised type of flaw introduced during fabrication (Fig.4).

Considering flaws first, these can be sensitively detected by ultrasonic techniques. However, whilst ultrasonic techniques can accurately locate a suitably orientated defect, information about the true size and nature of the defect is less readily inferred from the usual form of test display. Facsimile recording largely overcomes this limitation and provides a considerable amount of additional information from which the characteristics of the defect can be more precisely deduced[1]. This form of recording inevitably sets a limitation to the speed of inspection but when the tests are being specifically designed for correlating with systems performance, inspection speed is of secondary importance. By making use of this technique to characterise defects, Cobb and Brown[2] have been able to study their significance under conditions of hydrostatic loading, in tests specifically designed to predict the influence of defects of a particular type on systems performance. Their work has shown that photoelastic coatings can be used very effectively to observe the redistribution of surface stresses around surface cracks, although the coatings can only be used at room temperature and only applied to out-of-pile tests. While tests of this type obviously lead to a clearer overall appreciation of defect behaviour, any form of extrapolation to a different environment, a different temperature or a different deformation mechanism immediately introduces difficulty and uncertainty.

The advantages of facsimile recording for pre-service tests have been very considerably extended by incorporating contoured plotting of test data. Hodgkinson[3] has developed a signal processing unit compatible with a modularised system of N.D.T. circuitry currently being designed at Harwell. This accepts an analogue signal and provides a variably stepped output which can be fed to a facsimile recorder, where it manifests itself as six distinct and predetermined shades (Fig.5). Wells and Davey[4] have developed a complementary circuit which provides a discretely contoured, although somewhat less flexible, form of display from a digitised signal, such as is available from a scaler output (Fig.6).

Both systems have considerable potential in nondestructive testing and there is now a considerable fund of experience building up on the application of this type of quantitative recording to monitoring materials variables in fuel element canning.

As an example we can consider monitoring the bore of the tubing. This can now be done with a capacitance gauge developed by Cotterell[5] which floats axially in the tube on an air-bearing. This forms the basis of a fast inspection technique and produces a continuous output compatible with the contoured recording system already described. Since the air bearing accurately locates the gauge head axially, either radius or diameter measurements can be monitored continuously (Fig.7). Since an identical form of record canbe made subsequently on the same tube, patterns of local deformation produced by a controlled mechanical test, or developed during service, can obviously now be studied in considerable detail. The possibility of using this technique on tubing before and after use in a corrosive environment is also currently being studied by Britton[6]. Again, the philosophy is that if the bore variations can be compared point-by-point on sequential records a very detailed assessment of the progress of the corrosion will become possible.

Another potential 'defect' in the fuel can is wall thickness and this again lends itself to a similar form of data presentation. A high speed ultrasonic resonance technique, based on experimental work of Aveyard[7] has been developed by Wells and Davey[8] and its principle of operation analysed in detail by Aldridge[9]. The resonant frequency is automatically followed, without the need for a wide frequency sweep, as the immersed tube is rotated past either a single probe (pulsed operation) or a double probe (continuous wave operation). The resonant frequency is presented directly on a digital recorder or, again, fed as a digitised input into a contoured facsimile recorder (Fig.8). The direct result of a test of this type is that virtually none of the test data is wasted and the presentation allows the maximum use to be made of the data in any analysis of systems performance related to this particular variable. Davey has shown that digitised data of the type obtained from ultrasonic micrometry can also be presented in the form of a histogram (Fig.9). This naturally produces an averaging effect although in some circumstances, it will adequately emphasise significant features in the distribution of the data. A similar type of presentation can be applied to a flying spot profilometer developed by Wells and Davey[10]. This has been designed to convert the profile of a fuel can into an electrical signal by servo locking the scanning light spot of a cathode ray screen onto the surface of the can. In this way, any particular aspect of the profile can then be converted into a digitised signal and fed to some form of data analyser.

On the purely materials aspect of the fuel can, work is currently in hand to develop an ultrasonic technique to monitor variations in grain size distribution within the wall of the tubing. Because of the high level of elastic anisotropy in stainless steel, ultrasonic energy is subject to considerable scatter when the dimensions of the grains are of the same order as the wavelength of the ultrasound. Following earlier work on uranium[11], it has now been shown that the scatter can be displayed on a facsimile recorder (Fig.10) or statistically analysed in terms of amplitude variation[12].

A common feature of all these techniques is the emphasis on assimilating a considerable amount of detailed data, recording in a way that lends itself to easy interpretation and subsequent analysis when the results of systems performance can be collated. Until this type of test becomes more widely adopted a lot of testing will continue to be abortive and completely unsuited to any form of quantitative correlation on which realistic specifications must be based.

The most probable direction of further development is to combine a large number of tests on all possible variables using multiple test heads and combining the results with computerised storage of data. The subsequent performance results, and where possible the results of an identical post service test, can then subsequently be incorporated into a full programme of detailed data analysis. The work on fuel element tubing is currently being orientated in this direction at Harwell.

The whole question of correlating 'defects' with systems performance is one of the aspects of materials testing that will be receiving more attention in Britain now that a Centre for Research and Development in nondestructive testing has recently been set up at Harwell[13]. Financed from government funds the Centre will have a continuing programme of research on the fundamental and underlying problems of this type. In addition it will carry out sponsored work for industry and provide a detailed information and technical advisory service.

ACKNOWLEDGEMENTS

In preparing this paper I have drawn freely on the experimental results and experiences of my colleagues working in the Harwell N.D.T. Centre which have formed the main substance of this paper.

REFERENCES

1. R. S. Sharpe and S. Aveyard, "The inspection of thin walled stainless steel reactor grade tubing", J. Iron Steel Inst., 201, 1963, pp.856-862.

2. E. Brown and H.R.W. Cobb, "The effects of defects in thin walled 18/8 stainless steel tubing", Nuclear Energy, 1966, pp.253-261 and Straid, 2 (4), October 1966, pp.15-25.

3. W. L. Hodgkinson, "A quantised system of facsimile recording", Atomic Energy Research Estab. Rep., AERE-R 4688, 1964.

4. F. H. Wells, lecture at Inst. Phys. and Phys. Soc. meeting on "Factors limiting the speed of ultrasonic testing", London, December, 1966.

5. K. Cotterell, "Capacitance bore gauge for tubing", to be published.

6. C. F. Britton, Harwell, private communication.

7. S. Aveyard and R. S. Sharpe, "Applications of ultrasonic pulse interference", Proc. 4th Int. Conf. on Non-Destructive Testing, London, 1963, pp.150-154.

8. F. H. Wells, C. N. Davey and C. Sharpe, "Automation of tube thickness measurements using ultrasonics", Proc. Symp. Non-Destructive Testing in Nuclear Technology, Bucharest, May, 1965, vol.I, pp.321-329.

9. E. E. Aldridge, "A numerical study of the mode of working of the ultrasonic micrometer used in thickness measurements of stainless steel tubing", Atomic Energy Research Estab. Report, AERE-M 1742, 1966.

10. F. H. Wells and C. N. Davey, Harwell (to be published).

11. R. S. Sharpe and S. Aveyard, "The visualization of an ultrasonic extinction network in coarse-grained uranium", Applied Materials Research, 2, 1962, 170-176.

12. E. E. Aldridge, Harwell (to be published).

13. R. S. Sharpe, "Diagnostics for the engineer", New Scientist, 33, 1967, pp.258-260.

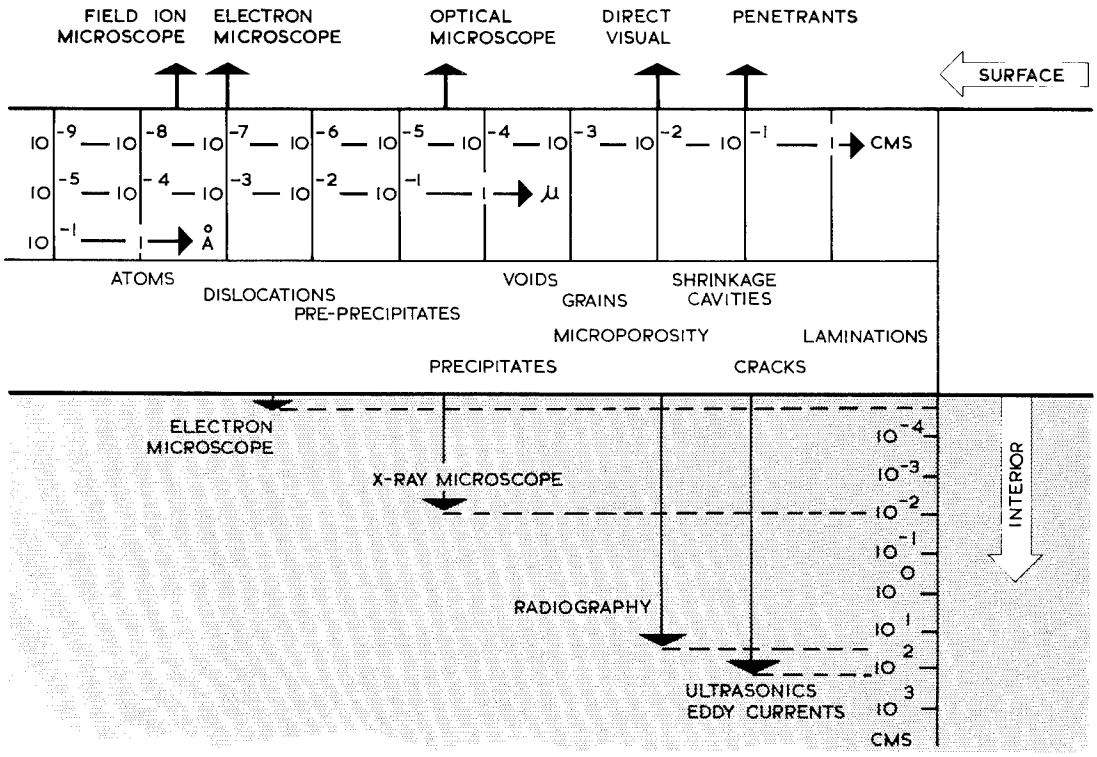

Fig. 1 The Sensitivity of Nondestructive Testing Techniques.

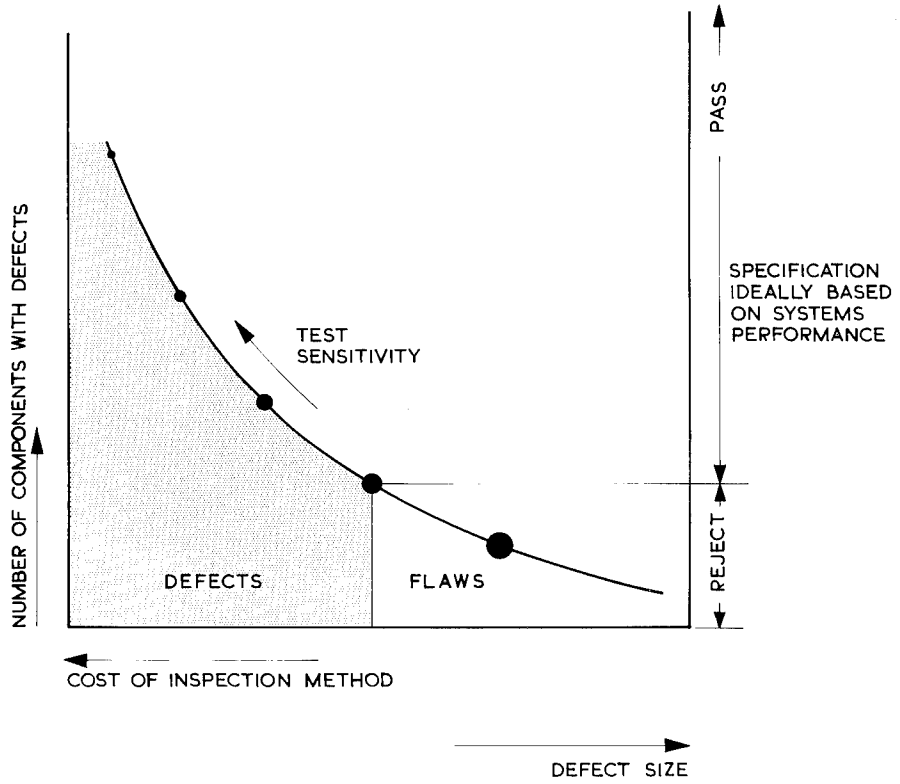

Fig. 2 The Significance Level Separating Flaws and Defects.

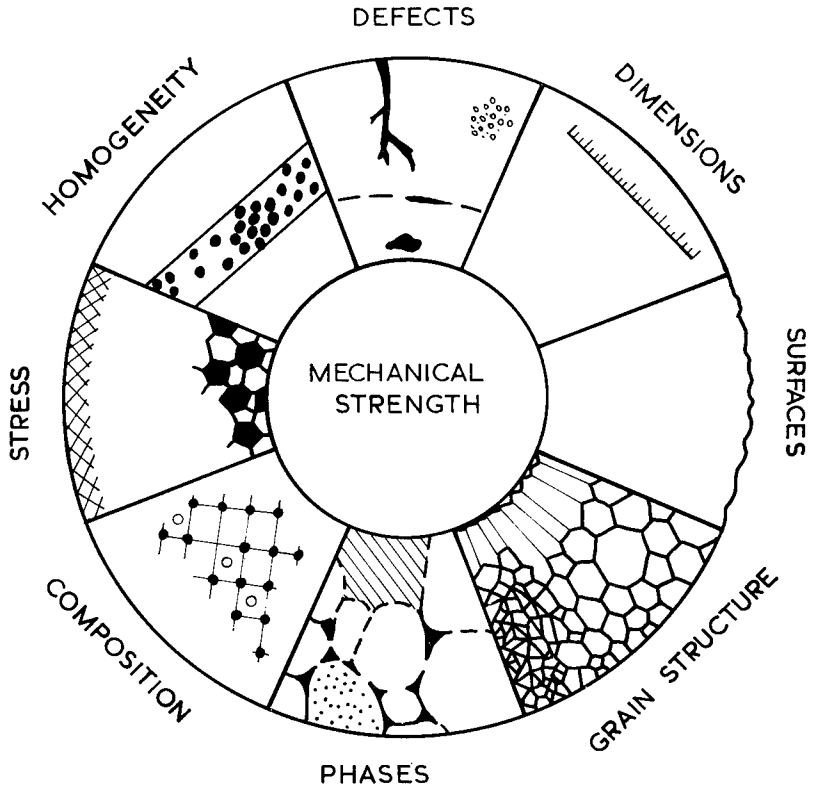

Fig. 3 The Structural Characteristics Whose Control Collectively Constitutes Nondestructive Testing.

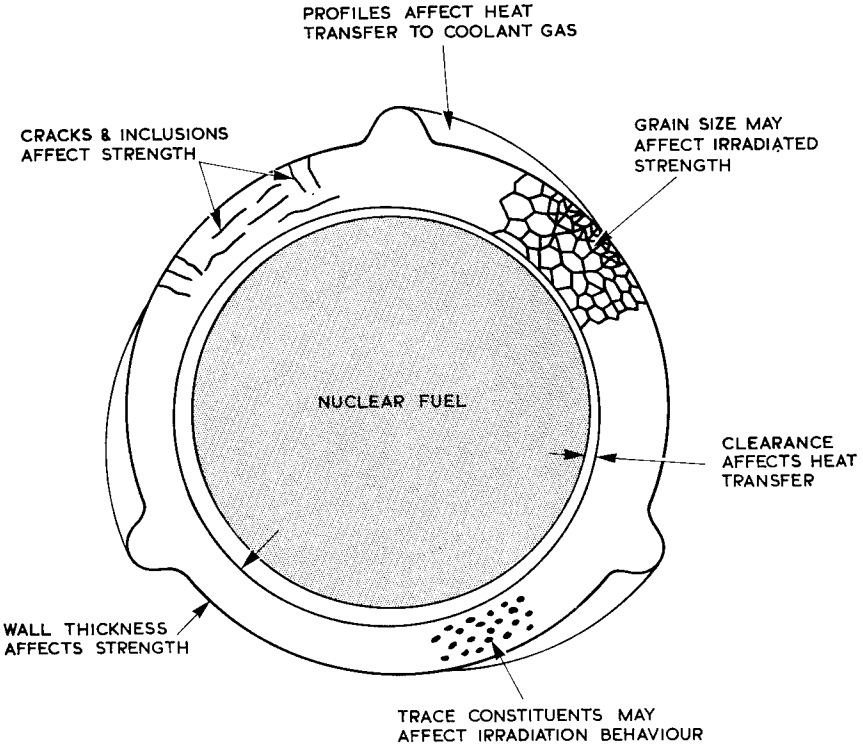

Fig. 4 Some of the Characteristics of Fuel Element Design that Need to be Controlled Nondestructively.

Fig. 5 Quantised Form of Recording Eddy Current Signals.

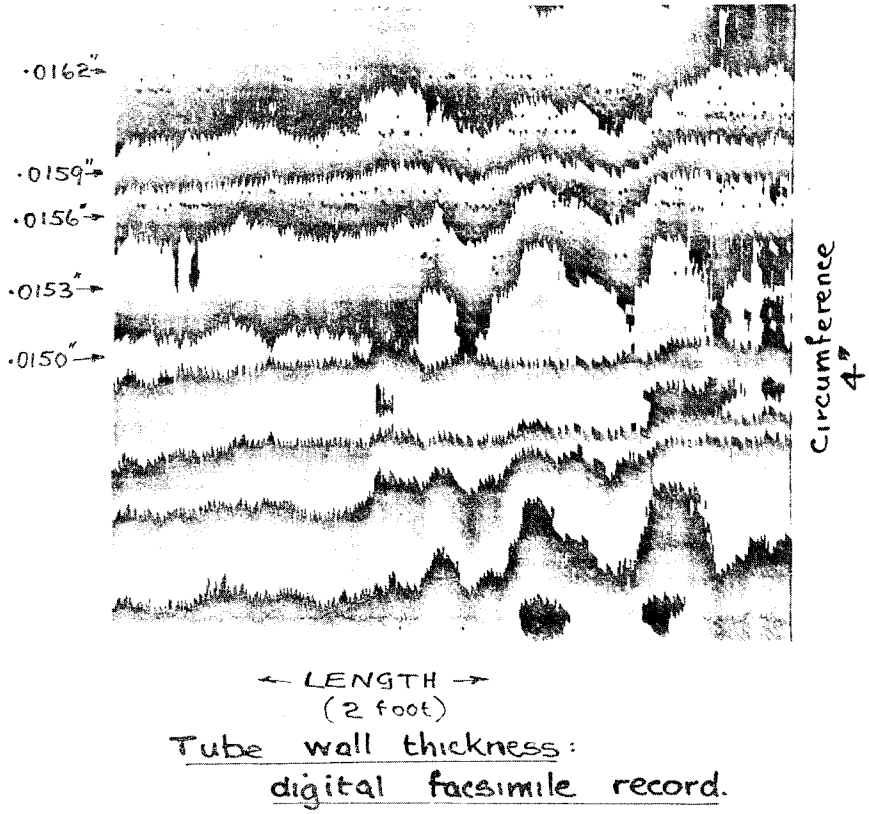

Fig. 6 Quantised Digital Display From Ultrasonic Resonance Technique.

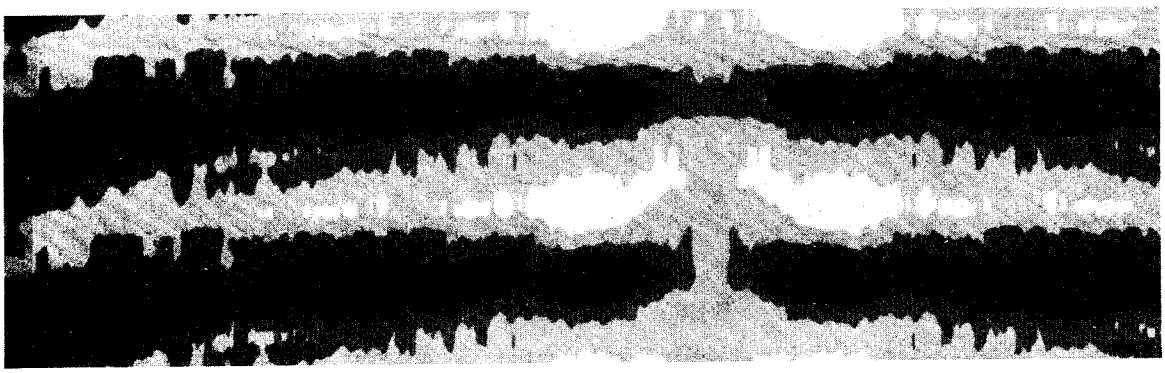

Fig. 7 Quantised Display of Tube Bore Measurements From a Capacitance Gauge Head.

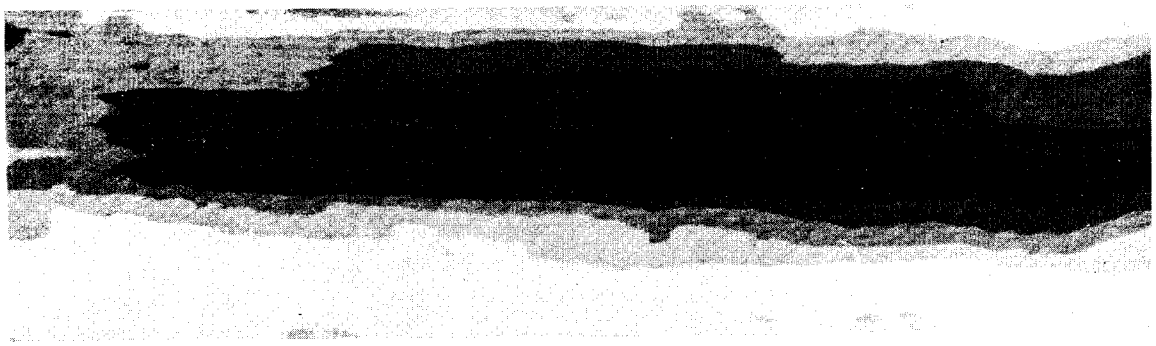

Fig. 8 Quantised Analogue Display of Tube Wall Thickness From Ultrasonic Resonance Technique.

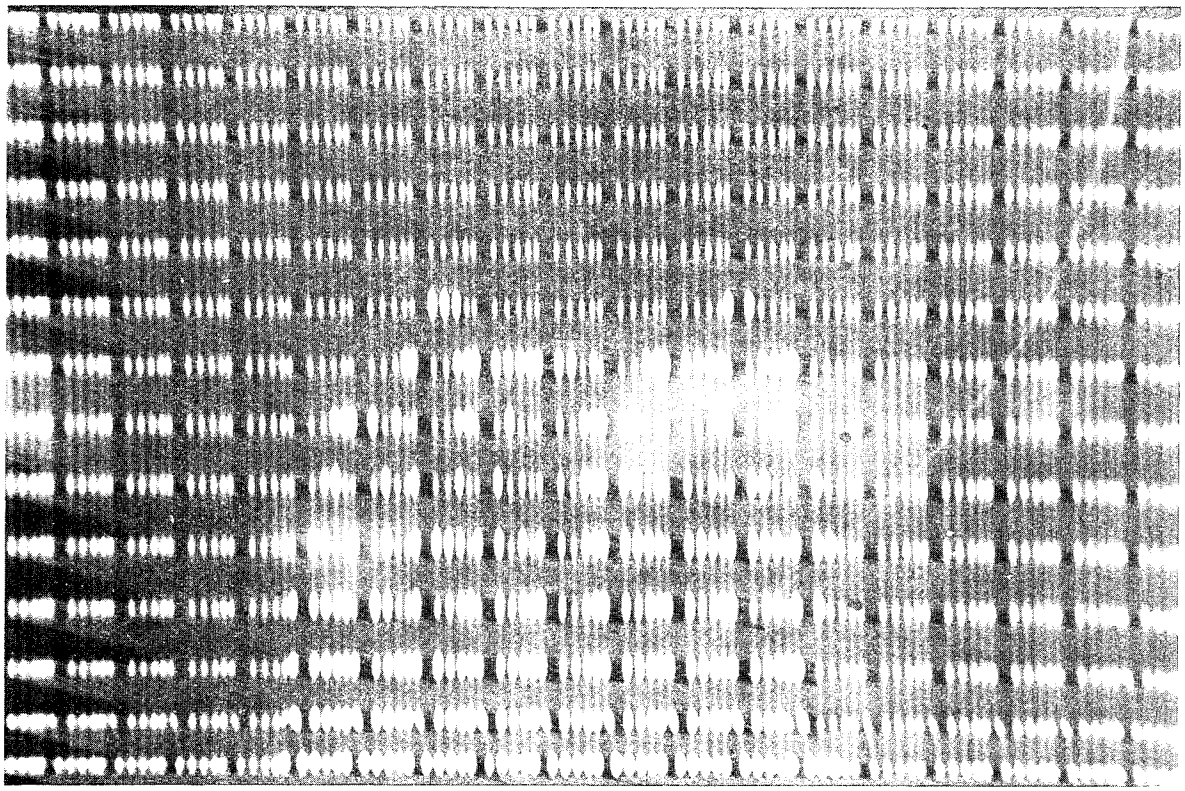

Fig. 9 Histogram Presentation of Tube Wall Thickness Variability.

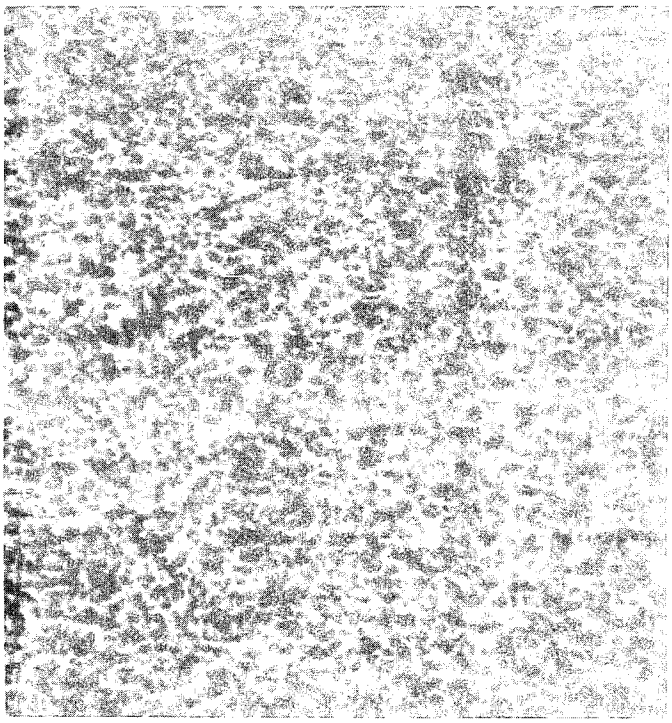

Fig. 10 Facsimile Record of Amplitude of Ultrasound Scattered From Grain Structure of Stainless Steel Tube.

DETECTION OF CONCEALED CRACKS BENEATH FASTENERS BY ACOUSTIC MEANS

R. M. Schroeer

Arvin Systems, Inc.

Dayton, Ohio

Crack detection requirements and crack detection techniques are probably the most discussed topics in nondestructive testing literature and at nondestructive testing symposia. The reason for this fact is twofold: a general need for a detection technique exists and a practical solution which provides a reliable technique to be acceptable by production and maintenance personnel is still missing.

The wide variety of types of cracks, size, location, material, etc. has certainly contributed to the many techniques which have been proposed, studies and applied on a laboratory basis. It can be expected that there will not be only one universal solution.

Little attention has been paid to the development of easily-read defect indicating instrumentation. However, if we do not develop systems which eliminate the oscilloscope as test indicator, we will not have a practical solution which brings the quality control to the production line and to the maintenance shop.

The importance of an early detection of cracks cannot be overemphasized. They influence significantly the mechanical strength of a body and the performance of a system.

The most widely used techniques for crack detection are: x-ray, ultrasonic, and eddy-current. Their limitations are well known. The continuing research efforts to create better and more reliable systems is the best proof of these limitations.

In many cases, the detection of cracks in the surface or very close to the surface of a specimen is possible. Ultrasonic, eddy-current, and magnetic field methods can be applied, but extreme care in their application and interpretation of results limit their application to highly trained and experienced personnel.

The detection of cracks deep in the specimen, without reaching the surface, is much more difficult. This type of defect became very critical in high performance airplanes where cracks are generated by high frequency vibrations. These cracks are hidden under fastener heads, they do not extend to the surface, and they are nearly undetectible with present day methods.

Figure 1 shows two locations of cracks under a rivet fastener. Cracks may develop either at the lower edge of the upper plate or at the neck of the rivet hole.

The only technique which may be applied to detect these cracks is the ultrasonic technique. Anyone who is familiar with ultrasonic testing is immediately aware of the difficulties. The ultrasonic energy cannot be injected perpendicular to the specimen's surface, but under a carefully selected angle. Therefore, the reflected energy must be picked up at a spot different from the input. The transducer must be carefully guided around the fastener head because the angular location of the crack is unknown. The coupling layer must always be preserved and the operator has to understand and interpret the numerous traces and signals on the oscilloscope screen. As in many other cases of application of ultrasonic testing, this method must be called impractical, to say the least.

The method which will now be discussed is based on the application of sonic energy in the form of a short pulse and the evaluation of the damping of the vibrations generated by the applied mechanical (sonic) pulse or pulses. This means that the cracks themselves are not detected but their influence on the behavior of material in the vicinity of the crack, in our special case around the fastener, is used as an indication for the presence of a crack.

The short pulse applied to the fastener head can be generated either as a single mechanical shock or as repetitive shocks, but it is important that the pulse excites a large number of frequencies. The vibrations in response to these shocks are detected by an accelerometer and the signals are then processed as explained later.

The theory of the effect of a crack on time-to-damp may be summarized as follows:

1. A finite crack reduces markedly the radial stiffness of the hole.

2. The interplate friction forces acting to damp the normal modes of the assembly are reduced accordingly.

3. The reduced hole stiffness facilitates the "worming" of the fastener head deeper into the conical hole when the assembly is subjected to vibrations at high frequencies.

4. The resulting shortening of the fastener greatly relieves the axial tension in the fastener and the compression of the plates in their thickness direction.

5. As a result, the accelerometer signal from a tap on the fastener has a definite longer time-to-damp when a crack is present.

A mathematical analysis of the radial deformation of the hole without and with crack results in the two equations (Figure 2):

$$D = \frac{(1+\nu) \cdot p \cdot R_H}{E}$$

$$D' \cong \frac{(1+\nu) \cdot p \cdot R_H}{E} \left[1 + (1-\nu)\frac{d}{R_H}\right]$$

where D = the displacement at the edge of the hole without crack
D' = the displacement at the edge of the hole with crack
R_H = radius of the undeformed hole
p = radial pressure
E = Young's modulus
ν = Poisson's ratio
d = crack depth

The equation for D' reduces to that for D when the crack depth d goes to zero (no crack).

Comparing these two equations it will be noted that a crack increases the hole radial growth due to a wall pressure. For example, if d is 20 per cent of R_H (a crack depth equal to 10 per cent of the hole diameter), then the hole growth due to wall pressure is increased approximately 14 per cent by the presence of the crack. That is, a hole having a diameter of 0.25 inch would be 14 per cent more compliant radially if it had a crack only 0.025 inch deep.

A tap on a fastener head, or its vicinity, will excite to some degree most of the normal modes of a plate assembly. Exceptions would be those modes having a mode line passing through the fastener which is tapped, but there are few such modes for a given fastener.

If an accelerometer is placed on the plate assembly near the fastener which is tapped, it will sense nearly all of the normal modes which are excited and a signal from the accelerometer has a rich spectrum of normal mode frequencies.

Modes of extremely high frequency do not receive much energy from a tap on a fastener, so their amplitudes are relatively small in the accelerometer signal and they die out in a very short time. Modes of low frequency do not involve much relative slip of the plates and in a plate assembly such as an aircraft wing the mode lines tend to be close to the fasteners. But, there is an intermediate range of frequencies in which one would expect to see the most pronounced effect of a crack on the time-to-damp of the accelerometer signal. Even within the intermediate range of frequencies the various frequencies may respond differently, depending on the design characteristic of the fasteners and their surroundings. For a connection between a thin skin and a heavy beam, the frequency displaying the most drastic influence from a crack is different from that frequency which is most characteristic for a thin skin and light beam combination.

The following Figures 3 and 4 illustrate this influence on the frequency spectrum. Figure 3 shows the characteristic part of the frequency spectrum for a fastener connection of two 1/8 inch plates without and with crack, having the important frequency range around 11.0 KHz, and Figure 4 shows the characteristic frequency spectrum for a fastener connection of two 1/4 inch plates, with a much lower critical frequency of around 5.4 KHz. The entire frequency spectrum shows numerous other mode frequencies, which do not change in their amplitudes as a result of a crack.

If the total output signal of the accelerometer would be displayed on an oscilloscope, a trace would be observed which contains all frequencies excited by the shock pulse and detected by the accelerometer. Because only one or two frequencies out of the entire spectrum show a longer time-to-damp, the overall trace may not indicate a clear difference between no-crack and crack condition. Figure 5 shows an example. However, if we use a bandpass filter which suppresses those frequencies which do not change and display only the characteristic frequency, then we obtain a significant "crack effect." Figure 6 is an illustration of a filtered signal.

In many cases, this "crack effect," displayed on the oscilloscope, is very evident and after some experience one may be capable to judge immediately the trace for a crack or no-crack characteristic. But a more reliable indication is required, which not only shows the presence of cracks but also may provide a differentiation between various dimensions of cracks. This can be achieved by integrating the filter output by electronic means and indicating this integrated signal on an instrument. The longer the time-to-damp, the larger the area under the trace envelope and the larger the integrated signal. Figure 7 shows two examples for integration.

Figure 8 shows a schematic of the total system in its simplest form. It is self-explanatory. An interesting feature is the use of a tape recorder which stores the signals from the accelerometer for later evaluation, if an immediate "live" analysis cannot be performed. It is, of course, also possible to store the filtered signals as a permanent inspection record.

Although most of the experiments and tests were performed on samples with simulated cracks, extensive tests have been conducted on a wing of a damaged F104 airplane and other samples. Our test results on the wing have been correlated with Zyglo test results.

Conclusions

The technique of testing fasteners for hidden cracks by acoustic means using the "time-to-damp" as a criterion for the presence or absence of a crack has been proven as a feasible approach, which also promises to become a practical method. More research and development work is indicated to achieve the optimum performance. It seems to meet not only the requirement for detecting small cracks, it also offers the possibilities to provide a direct numerical readout of the test result.

Acknowledgements

The problem of detecting cracks hidden under fastener heads was initially brought to our attention by Mr. Walter Trapp, Chief, Strength and Dynamics Branch, Air Force Materials Laboratory, who encouraged us to study possibilities for a solution of this problem. The crack detection technique discussed in this paper was originated by Arvin Systems, Inc. as an in-house project. Since July 1, 1966 the program has been funded by the Air Force Materials Laboratory.

We are indebted to the following Air Force Materials Laboratory personnel for their continuous support and guidance: Mr. Richard Rowand, who initiated the contract; Mr. Harold Kamm, who serves as the Air Force Materials Laboratory Project Engineer; and Mr. J. A. Holloway, who prepared the test samples and helped with numerous discussions.

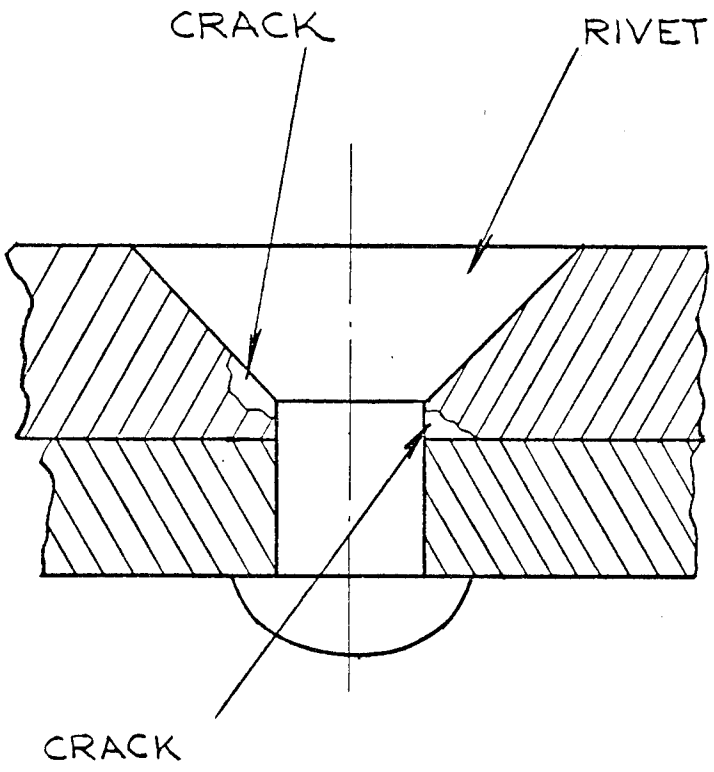

FIG. 1 CRACKS BENEATH RIVET

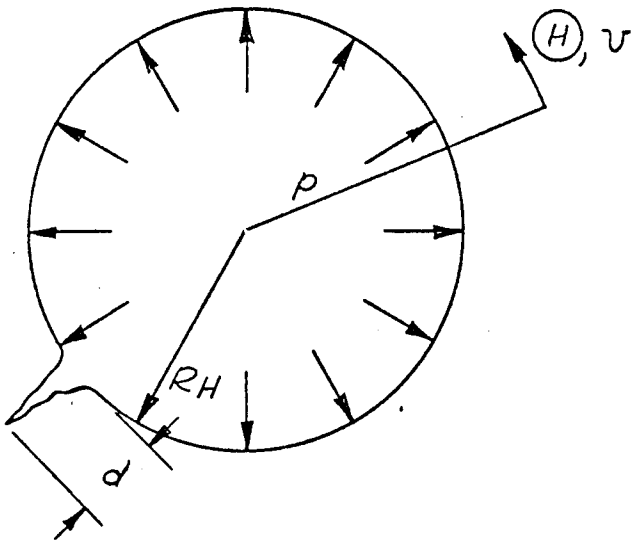

FIG. 2 FASTENER HOLE WITH CRACK

NO CRACK CONDITION:

$$D = \frac{(1+v)\cdot p \cdot R_H}{E}$$

CRACK CONDITION:

$$D' \cong \frac{(1+v)\cdot p \cdot R_H}{E}\left[1+(1-v)\frac{d}{R_H}\right]$$

D = DISPLACEMENT AT EDGE OF "NO CRACK" HOLE

D' = DISPLACEMENT AT EDGE OF "CRACK" HOLE

R_H = RADIUS OF UNDEFORMED HOLE

p = RADIAL PRESSURE

E = YOUNG'S MODULUS

v = POISSON'S RATIO

d = CRACK DEPTH

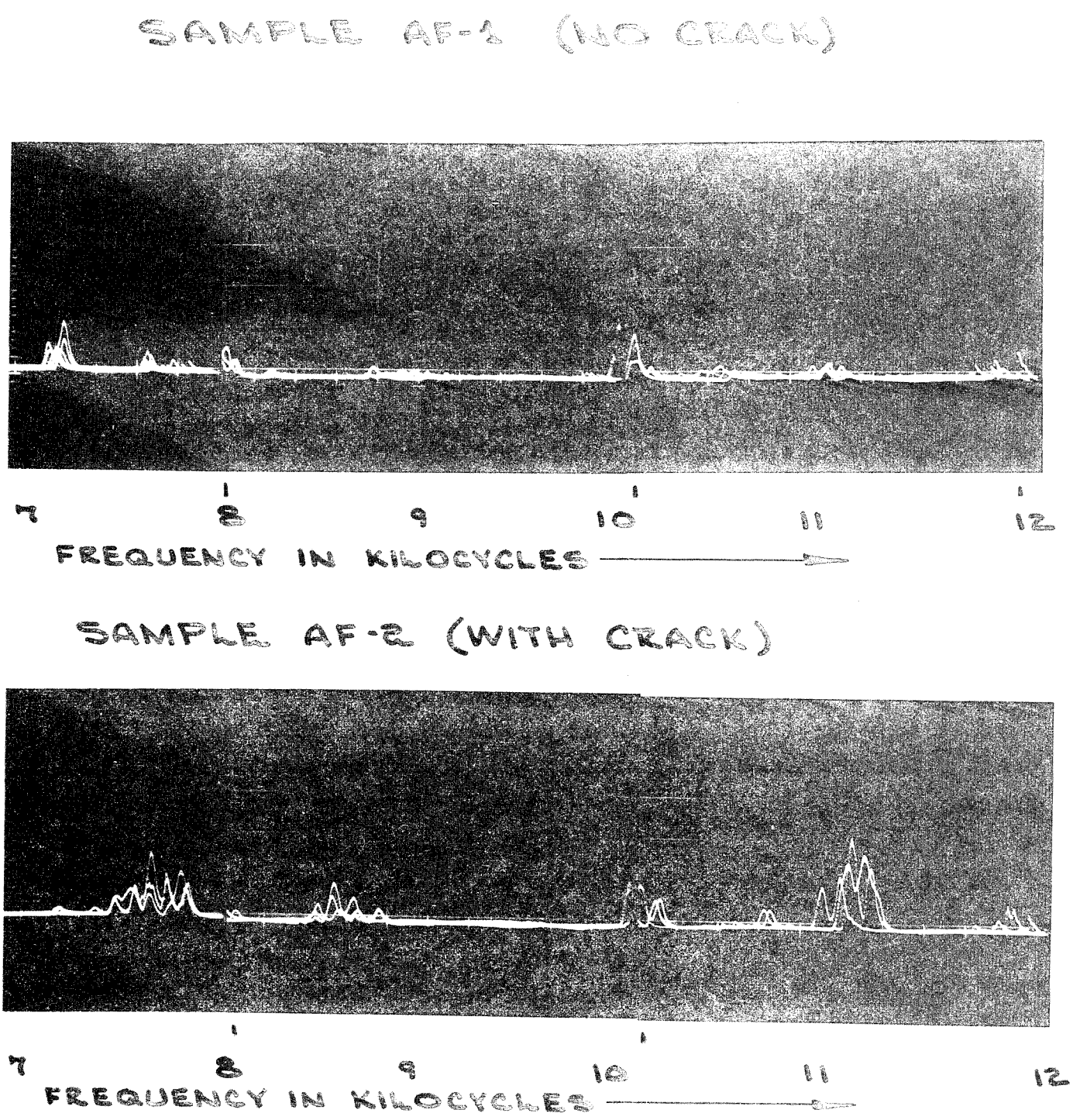

FIGURE 3. Critical frequency spectrum for 1/8 inch plates without and with crack

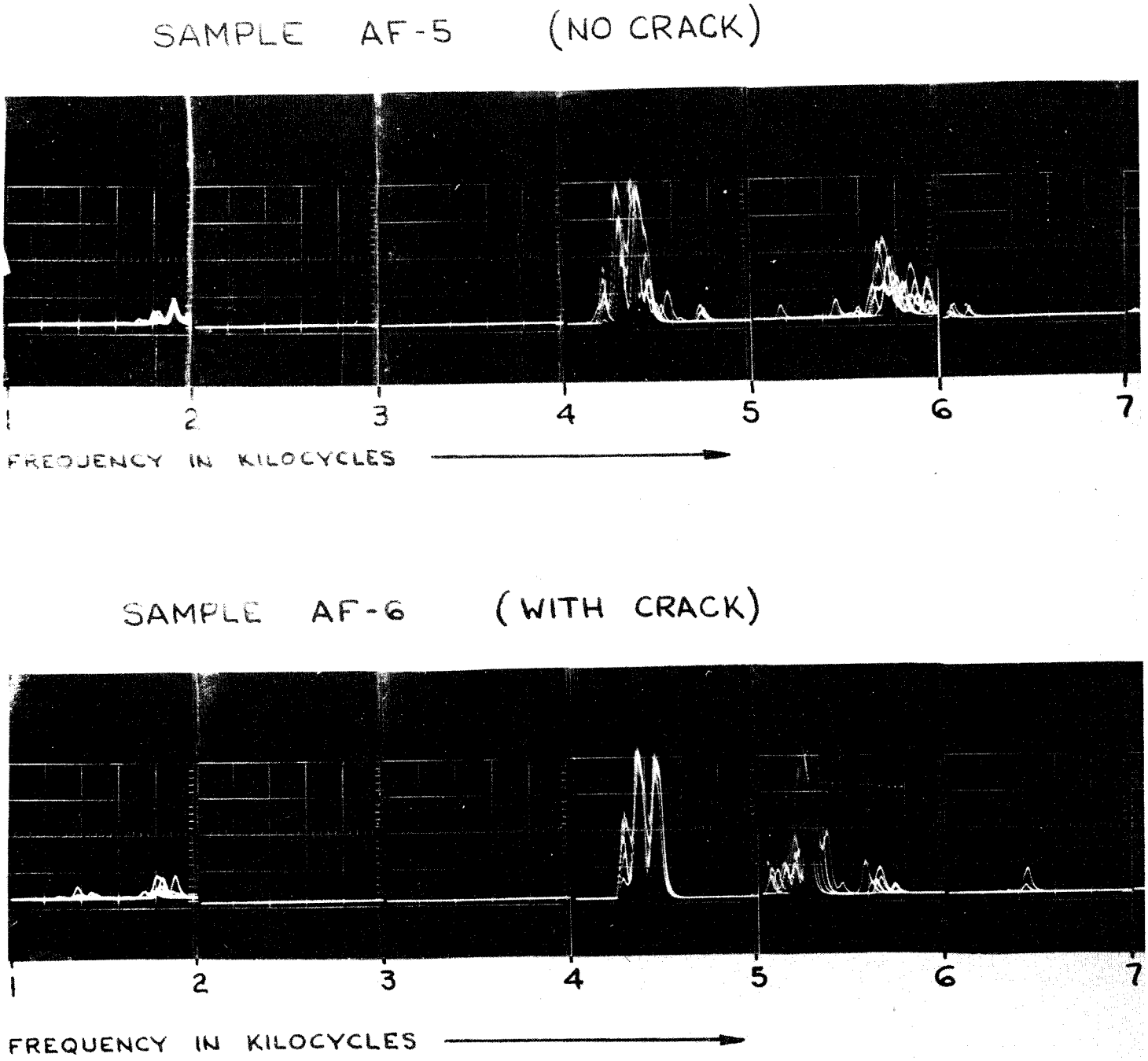

FIGURE 4. Critical frequency spectrum for 1/4 inch plates. without and with crack

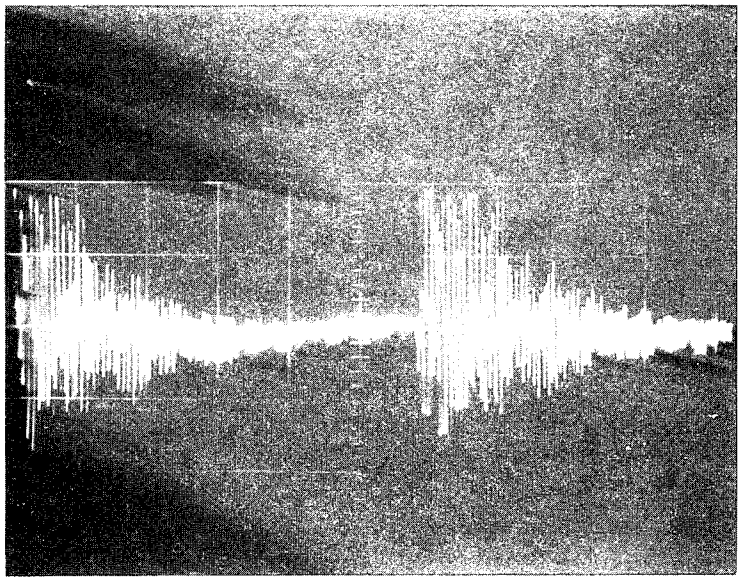

SAMPLE AF-1
HOLE #2 (NO CRACK)

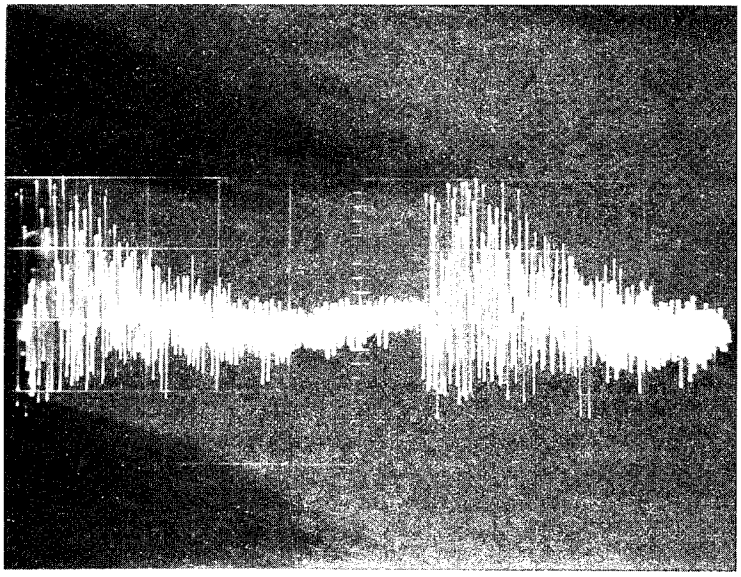

SAMPLE AF-2
HOLE #2 (WITH CRACK)

FIGURE 5. Unfiltered signal, no-crack and crack

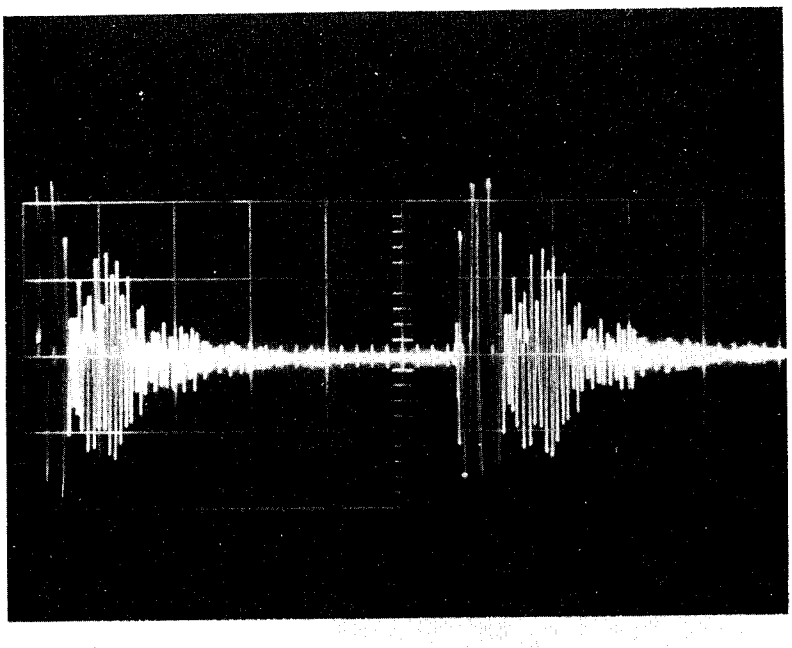

SAMPLE Nº AF-1
HOLE #2 (NO CRACK)

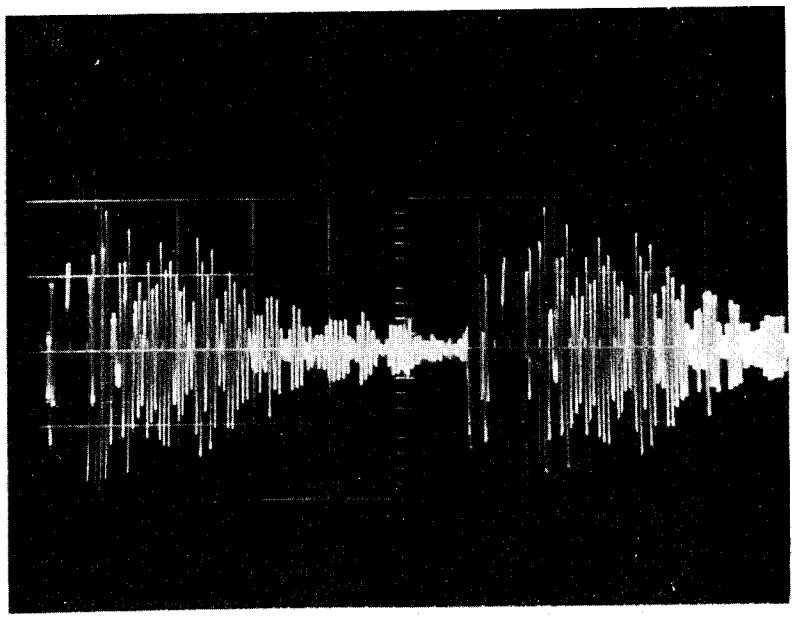

SAMPLE Nº AF-2
HOLE #2 (WITH CRACK)

FIGURE 6. Filtered signal, no-crack and crack

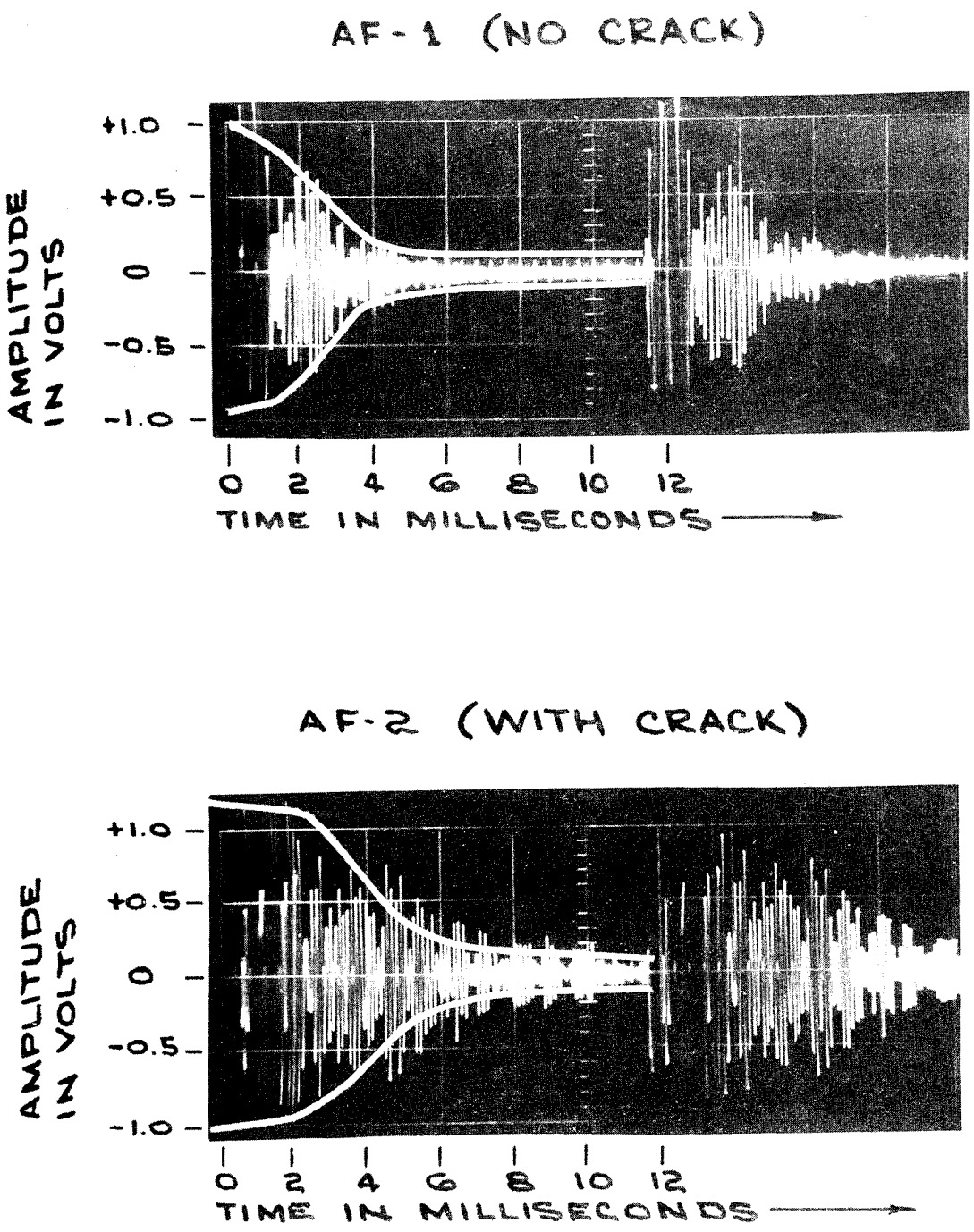

FIGURE 7. Area under trace-envelope to be integrated indicating presence of crack

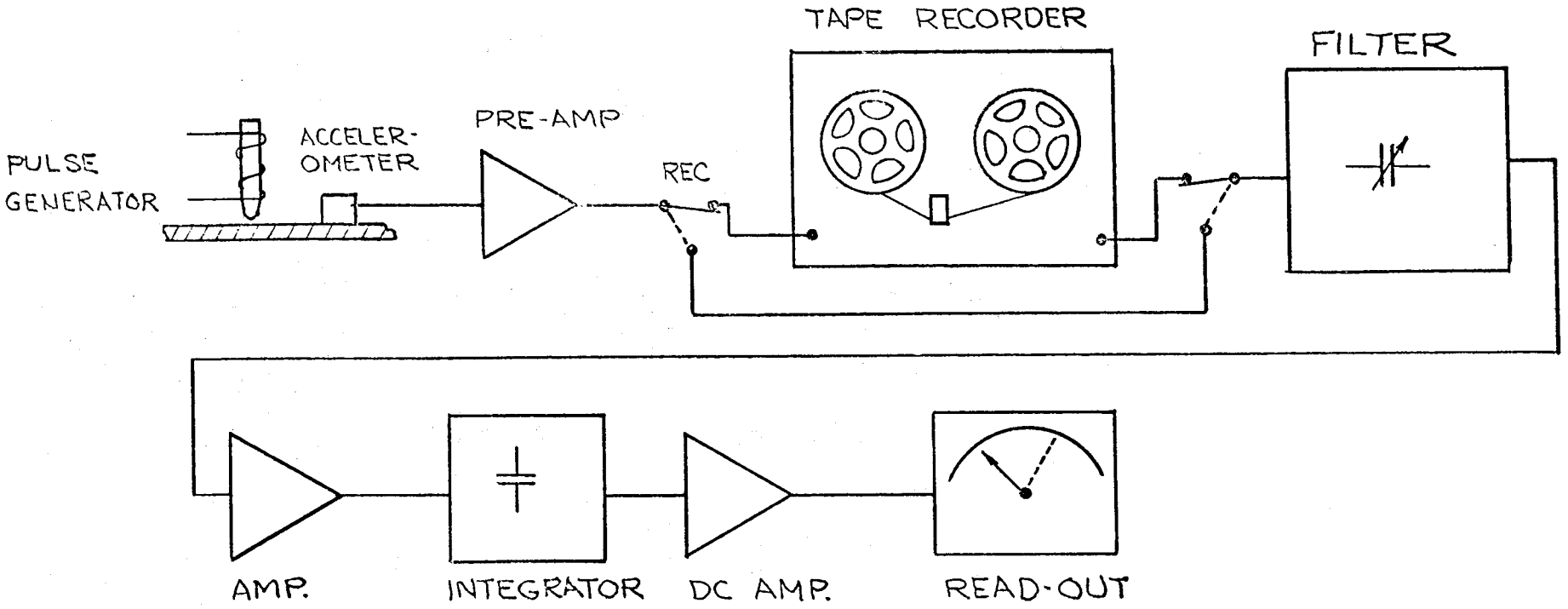

FIG. 8 SCHEMATIC OF CRACK DETECTION SYSTEM

CORRELATION BETWEEN FLAWS AND SERVICE PERFORMANCE

R. Halmshaw

R.A.R.D.E., Ministry of Defence, U.K.

Everyone involved in non-destructive flaw detection is, sooner or later, faced with answering the question, "Does it matter?", in relation to some flaw which has been detected during examination of a specimen.

In an ideal world the radiographer (or other N.D.T. expert) would be limited to answering the questions - "what is it?" or "where is it?" i.e. the identification, location and size of the flaw - but this is really no more than buck-passing - someone still has to answer the question, "does it matter?". In this same ideal world that would be the job of the designer, but often he is not available for consultation, and anyhow one cannot run a committee for every flaw which turns up on non-destructive testing. So, we are back to the radiographer, possibly together with an inspector representing the customer, and whether we like it or not, they have to settle this acceptance question.

It has been argued, rather naively, that tucked away in people's experience - radiographers, inspectors, designers, research workers - is all the information necessary to set up acceptance standards. After all, to take one example, higher pressure boilers have been fabricated and radiographed for about 30 years with no evidence of any great quantity of failures, so the standards of acceptance used must be reasonably satisfactory. Accordingly, various symposia have been organized - and this has happened in several countries, as well as internationally - to get the experts together to discuss and prepare acceptance standards. It was also thought to be a good idea to discuss failed structures - the causes of failure - as these should give information on the magnitude of the defects which caused failure.

Unfortunately this procedure has not worked well, and not much progress has been made. In general, the experts cannot tell you that a particular size of flaw is likely to cause failure, and that another (smaller) size of flaw is acceptable-not even if the Service conditions are known and can be specified. Secondly, it is amazing how few examples can be documented where failure can be said to be primarily due to a flaw which was, or could have been, found by NDT. Most failure investigations are regarded as commercial secrets between the producer and customer, and of those where information is available, the large majority are caused by design errors, use of wrong material, or inadequate control of Service conditions.

The number of examples where an internal flaw was responsible for failure is a very small proportion of the whole. I propose to come back to this subject, later.

WELDS

Earlier, I mentioned radiography of boiler-welds: this was not to decry other methods of NDT - merely that radiography is one of the older methods usually referred to as NDT, that butt-weld inspection is one of the more widely used applications of radiography, and that radiography produces a permanent record which can be referred to.

If one examines boiler-weld radiographs taken in the 1935-40 period two conclusions can be made:

(1) The quality of the radiography, i.e. the sensitivity, is greatly inferior to that of present-day radiographs.

(2) The level of acceptable flaws is much more rigorous now than 30 years ago. The standard of acceptance, even allowing for increased working pressures and temperatures, is not the same. (Fig. 1)

In particular the acceptable quantity of porosity was much less severe in 1937 than today.

It seems clear that acceptance is based more on a judgement of what is high-quality welding than on considerations that a particular flaw might lead to failure. Thus, as welding techniques have improved and welding electrodes have gotten better so that slag inclusions and porosity have become less prevalent, so the acceptance level has risen. Acceptance appears to be based on a dual standard.

(1) Cracks, lack of penetration are rejected because these are serious flaws which can lead to failures.

(2) Porosity and slag inclusions are rejected because they should not nowadays occur in any quantity in high-class welding - their presence indicates that the workmanship is not as good as it should be.

I should now like to look at the subject of flaws in welds from another point-of-view. How much is known about the significance of flaws from mechanical tests of welds into which flaws have been introduced?

In the U.K. most of this work has been done at B.W.R.A. and the authorities are undoubtedly Newman and his colleagues. (1) I should like to start by quoting from a paper by Newman and Gurney (2) on tests of 1/2" thick steel butt-welds:

"It has been shown, for example, that whereas quite severe defects may have little or no effect on the fatigue strength of circumferential butt-joints in pipe (e.g. in unbacked joints the strength is dominated by the stress concentration effect of the root area), the fatigue strength of machined butt-joints in plate depends critically on the presence or absence of defects.

In reality there is no anomaly between such results. Whether or not a given defect will influence fatigue strength will be determined by the inherent fatigue strength of the joint in which it occurs - 'inherent' here meaning 'in the absence of defects'. Welded joints give a wide range of inherent fatigue strengths. Taking unwelded mild steel plate strength as 100%, the strengths of typical fusion-welded joints in the same material can vary between 100% and 20% without the intervention of any influence from defects."

Nevertheless, Newman has found reasonable correlation between fatigue strength for long endurances (6×10^5 - 1×10^6 cycles) and length of slag inclusion seen radiographically, for inclusions of roughly the same thickness. When, however the work was extended to 1 1/2" thick steel welds no similar correlation was found; the authors think that this may have been due to the over-riding influence of hydrogen in the metal in the thicker welds. On the 1/2" welds a diagram can be drawn of permissible defect length for different classes of welded structure (Fig. 2) and it is suggested that in the absence of other evidence that this standard can be taken as suitable for 1/2" and thicker steel welds.

On 1/2" welds, Newman (3) has also found a correlation between reduction of fatigue strength and defect severity (measured as a percentage reduction of area) for lack of penetration, and this has also been confirmed by work in Belgium by Guyot and colleagues (4). It was noted that fatigue cracks could originate at the edge of the weld overfill or at the incomplete penetration, whichever was the greater stress-raiser.

The importance of surface notches, undercut and similar surface stress-raisers - defects which are not always regarded as important in non-destructive testing - needs to be emphasized. Newman makes the point that the most common source of failure in welding is the fillet weld working at too high a stress: a badly made fillet weld with a poor profile introduces points of stress concentration which can be of the order of 5-10 times the average stress.

The essence of the fatigue strength problem is the geometry of the construction. Weld profiles and design are usually far more important factors than internal defects.

To summarize: There are many factors which affect the ability of a welded joint to withstand Service conditions, and the presence of flaws such as pores and slag inclusions is only one of these factors. If the other factors can be controlled, the significance of welding flaws can be assessed, but alternatively the influence of other factors may completely swamp the effect of any small flaws.

As examples,

(1) Some welding techniques inevitably introduce hydrogen into welds. The hydrogen is dissolved in the liquid weld metal and diffuses on cooling. Martensite may form in the heat-affected zone due to rapid heating and cooling and if hydrogen diffuses into this area, it will make it extremely brittle so that cracks may occur. Such cracks, which do not necessarily reach the surface, are very difficult to detect with certainty with any N.D.T. method - some may be found, but some will be missed.

(2) Many welding techniques introduce filler metal, which is not of the same composition as the parent plate; also, adjacent to the weld, melting may destroy the properties of the original alloy. Again, therefore, weld strength can be seriously affected by factors other than flaws found by radiography or ultrasonic testing.

In weld inspection in general therefore, it would seem that the right approach to the problem of acceptance standards, assuming that fatigue strength is the criterion of serviceability, is to identify unacceptable stress concentration conditions. Therefore, a general list of unacceptable defects is not possible, particularly for a range of weld designs and finishes. More attention than is customary should also be paid to various things not usually considered as flaws - surface finish, surface defects, weld profile. So far as flaws are concerned, all that it seems possible to state is that in the present state of knowledge, all cracks and lack of penetration, when detected, should be regarded as unacceptable in any weld with pretensions to high quality.

CASTINGS

In castings the significance of casting flaws in relation to Service performance is even more difficult to assess than in welds. Probably less fundamental work has been done on castings than on welds, and the problem is inherently more difficult in that it is not easy to stress a complex casting in a manner which is representative of Service conditions. Again in most practical examples it is likely that other factors than internal flaws - surface condition, heat-treatment, wall thickness - will have a dominating influence on suitability for Service.

With small castings which are for high-duty use and which are to be made in some quantity, it ought to be possible to produce an acceptance standard based on tests to destruction of castings of each specific pattern, but in practice this appears to be done only very rarely. In the aircraft industry, few patterns of casting are used in sufficient quantity to justify extensive destructive testing, and even when this is done, it occurs only after a preliminary selection of "good" castings by the foundry. Thus it is extremely rare for destructive testing to be done on castings known to contain internal flaws. One of the few examples found was an investigation of the influence of different degrees of microporosity in light-alloy castings: the details are to some extent a commercial secret, but the general conclusion was that a moderate degree of microporosity could be tolerated.

In practice, the level of acceptance of a casting is set in terms of

(1) the degree of soundness which can be attained by the foundry on a large proportion of castings to the particular design, i.e. a percentage rejection rate;

and very rarely on

(2) advice from the designer on the significance of any flaws found by N.D.T., based on sectioning and destructive testing.

There seems to be very few cases where a casting is loaded under conditions which simulate Service conditions and then cycled to destruction. This is, of course a very expensive procedure - the cost of one test to failure on an aircraft wing main beam forging has been quoted as $50,000.

In the U.S.A. work has been done on tensile testing of standard test blocks of cast steel containing intentionally-introduced defects and curves of the type shown in Fig. 3 have been produced for a range of defect types and casting thickness.(5) I am open to be convinced that this type of test has much relevance to the strengths of complex castings, even of the same material, but at least it represents some available data on the significance of defects in castings, even if under relatively artificial conditions. This American work is intended to provide a physical basis for the sets of reference radiographs of castings which are becoming available through ASTM and other organizations.(6) If the reference radiographs are accepted as standards, the costly practice of static testing each new design of casting to establish standards could be eliminated. It is easy to deride this work, and the whole subject of reference radiographs, but on the other hand, the present state of affairs is entirely unsatisfactory.

The programme of work outlined by Mattek was for type 410 stainless-steel castings, heat treated to a particular value of U.T.S. and only U.T.S. and elongation were measured. It is still to be shown that the results are also applicable to other steels, other conditions, and other thicknesses.

STUDIES OF FAILURES

Troughton (7) has analyzed the main causes of failure in aircraft, based on a study of 52 case histories. He shows that 11 of these failures were due to the flight conditions being different from those assumed in the design: 18 were due to the test loadings not being representative of those arising in practice and 9 because the test specimens were not representative of the material actually used. Most of the other failures were due to faulty detail design and there was little evidence that faulty material had been the cause of any failures.

The author has been given access to a large number of failure reports and metallurgical investigations on aircraft castings in another aircraft company and it is remarkable how few, out of several hundred reports during the past twenty years, show any evidence of failure being attributable to casting flaws which could be detected by N.D.T. methods. It must be borne in mind, however, that by the time castings reach the aircraft constructor they have already had one screening by non-destructive examination. Grossly defective castings should not therefore get past this first screening.

A few specific case histories, summarized in Figs. 4, 5, 6, and 7 have some interest. All concern light alloy material.

Fig. 4 shows a photograph of fracture and a section through the defective area. The report states that "This component failed by overload because of a local casting defect which had the effect of reducing the effective cross-sectional area. Anodic penetration down cracks from the surface indicate that these cracks, (as well as the porosity) were present in the original casting."

Fig. 5 shows an elevator pulley bracket casting, where failure is reported to be due to "localized areas of porosity and dross inclusions at the locations of the fractures, which reduced the strength characteristics at that cross-section and caused failure at comparatively low loads".

Fig. 6 shows a cockpit canopy casting failure. The conclusions of the examination are mixed:

"At the region of failure the casting was not to drawing dimensions. At the position of fracture and corresponding to the reduced section caused by a bolt hole, there was a casting defect (inclusion). It is understood that the reduction of section due to the two causes is sufficient to account for the failure".

Radiographs taken elsewhere in this casting showed similar small inclusions, but the failure was caused by the association of casting flaw, bolt hole and abnormally thin section.

Fig. 7 shows a steering lever casting on which the conclusions are quite clear: "The cracking was due to a cold shut type of defect, which was aggravated by heat-treatment, and which should have been detected and rejected by the inspection department".

Todd (8) has analyzed failures in ships. Over 200 failures in a period of 5 years, covering both hulls and machinery of a fleet of cargo liners, none were due to flaws which would have been found by conventional non-destructive flaw detection. Most failures again, were due to errors in detail design or to the use of material of inferior quality - faulty heat-treatment, or use of the wrong grade of steel.

Two cases with which the author has been personally concerned are worth detailing. One concerned a fabricated A-bracket for a ship - the bearing and arms supporting the rear end of the propellor shaft. In a new design the arms were butt-welded on to stubs on a cast tube and gamma-radiography showed that the welds, which varied from 1"-4" in thickness, contained a moderate amount of dispersed slag inclusions. As the structure was a very heavy section and not severely stressed the makers and the radiologist were of the opinion that the welds were good enough: the customer was doubtful. It was found that the specification permitted a drop test to be requested and this was arranged. The bracket was dropped 10 ft. on to concrete in such a manner that one arm struck the ground first and the heavy bearing a moment later. One arm snapped off - about 3" away from the weld! I am far from clear what this proved - there were no significant casting defects on the line of fracture - but it initiated a wonderful argument as to who was going to pay for the broken bracket.

The other example concerned wrought armour plate, 6" thick, which was used for shell-proving and which had been producing erratic results. About 50 proving plates were examined ultrasonically and the quantity, size and distribution of non-metallic inclusions was found to vary over a very wide range, from virtually clear plate to what can only be described as "very dirty".

It seemed obvious that these inclusions could be the cause of the variations in performance and two clean and two very dirty plates were used on a firing trial. The results were entirely at variance with our hopes; both "clean" plates shattered prematurely. A metallurgical investigation was undertaken on the pieces and it was found that the "clean" plates were both in a brittle condition and also had very low Izod values.

A second trial where shell were fired at clean and dirty areas of the same plate also failed entirely to show any correlation between performance and defects, and it seems quite clear that factors other than inclusions of this magnitude and location control shell-stopping ability in armour. Although the correlation obtained was therefore negative, and it could be argued that non-destructive testing of armour-plate is a useless procedure, the work at least established some levels of defect severity which did not affect performance in the specific conditions used.

THE USES OF NON-DESTRUCTIVE TESTING

Much of the above discussion suggests that for flaw detection in metals, non-destructive inspection is an ineffective technique. Taken by itself, without knowledge of Service conditions, design factors and visual inspection it seems to me that it is quite limited in its usefulness. Of course, everyone knows of examples of N.D.T. revealing internal defects which no right-minded engineer would dream of allowing into service - see Fig. 8 - and one or two examples of this sort in complicated and important components can justify the cost of many months of routine N.D.T. inspection - but in the majority of cases of N.D.T. flaw detection, interpretation of the significance of the findings has to be done without adequate background information.

I read the recent Lester Honour lecture by Commander Smiley on "N.D.T. in the Polaris Programme", with great interest. There he states quite catergorically that a programme of correlation of motor defects with performance was undertaken such that at the end they can now be 99% certain in predicting the effect of any defect found, on performance. I have not seen the results of this work - I presume that the information is highly classified - but if it can be done on such a large, complicated and expensive item as a Polaris motor, it must be possible to do it on almost any structure. I should dearly like to know how many motors were test-fired to achieve this correlation and what percentage of the project-cost such tests represent. I find the implication that N.D.T. - radiography and ultrasound - provide adequate data to get a correlation with rocket motor performance rather intriguing. This has not been our experience on small solid-propellant motors - where a proportion of "rogue" results occur.

Finally, having suggested that the value of N.D.T. flaw detection may sometimes be questionable, I should like to briefly outline a few applications of N.D.T. which seem to me to be more justifiable.

First of all, radiography (and fluoroscopy). My own particular field includes much assembly inspection - checking the correctness of assembly of ordnance items - the presence of a spring or a ball, alignment of surfaces, gap widths, etc. Interpretation is not usually difficult, and skill and experience are necessary rather than judgement. An extension to this type of work is the use of radiography to measure internal spacings and gap widths. This is a relatively new and expanding application. Special fine-grain single emulsion film can be used where desirable, to improve accuracy of measurement: $\pm$ 0.001 is already achieved and better is probably possible.

Ultrasonic testing like radiography can be either flaw-detection or something quite different. A few methods which are already being used are:

(1) ultrasonic velocity measurements for the determination of mechanical properties of cast-iron

(2) ultrasonic attenuation measurements for the control of heat-treatment of steel castings

(3) thickness measurement

(4) bond-checking - still a little controversial!

(5) checking of metal grain size by attenuation measurements.

Other, relatively new applications can be mentioned:

(1) Sonic testing of modular cast-iron, for checking the degree of modularity and the measurement of U.T.S.

(2) Quality control of ball bearings, etc. using magnetic properties

(3) Tube thickness control with eddy currents

It is a feature of many of these applications that great care has to be taken to fix all the other parameters but the one to be measured. If this is not done, or cannot be done, the results obtained can be completely mis-interpreted. Nevertheless, the success which many of these applications have already had, suggests that the scope of N.D.T. is far from exhausted, whether or not we ever obtain realistic data on the significance of defects in castings and welds!

REFERENCES

1. R.P. Newman. Brit. J. N.D.T. 7. (4). 90-96 1965

2. R.P. Newman; T.R. Gurney. Brit. Welding J. 11 (7) 341-352 1964

3. R.P. Newman; M.G. Dawes. Brit. Welding J. 12 (3) 117-120 1965

4. F. Guyot, H. Louis, J. Martelee, W. Soete. I.I.W./11.5 Report V-366-66/OF, 1966

5. L.J. Mattek. Materials Res. & Standards. 633-637. 1962

6. ASTM. A.S.T.M. Reference Radiographs, E. 186.

7. A. Troughton. J. Royal Aeronautical Soc. (to be published, 1967)

8. B. Todd. W. of Scotland Iron & Steel Inst. Trans. 72, 42-62. 1964/65

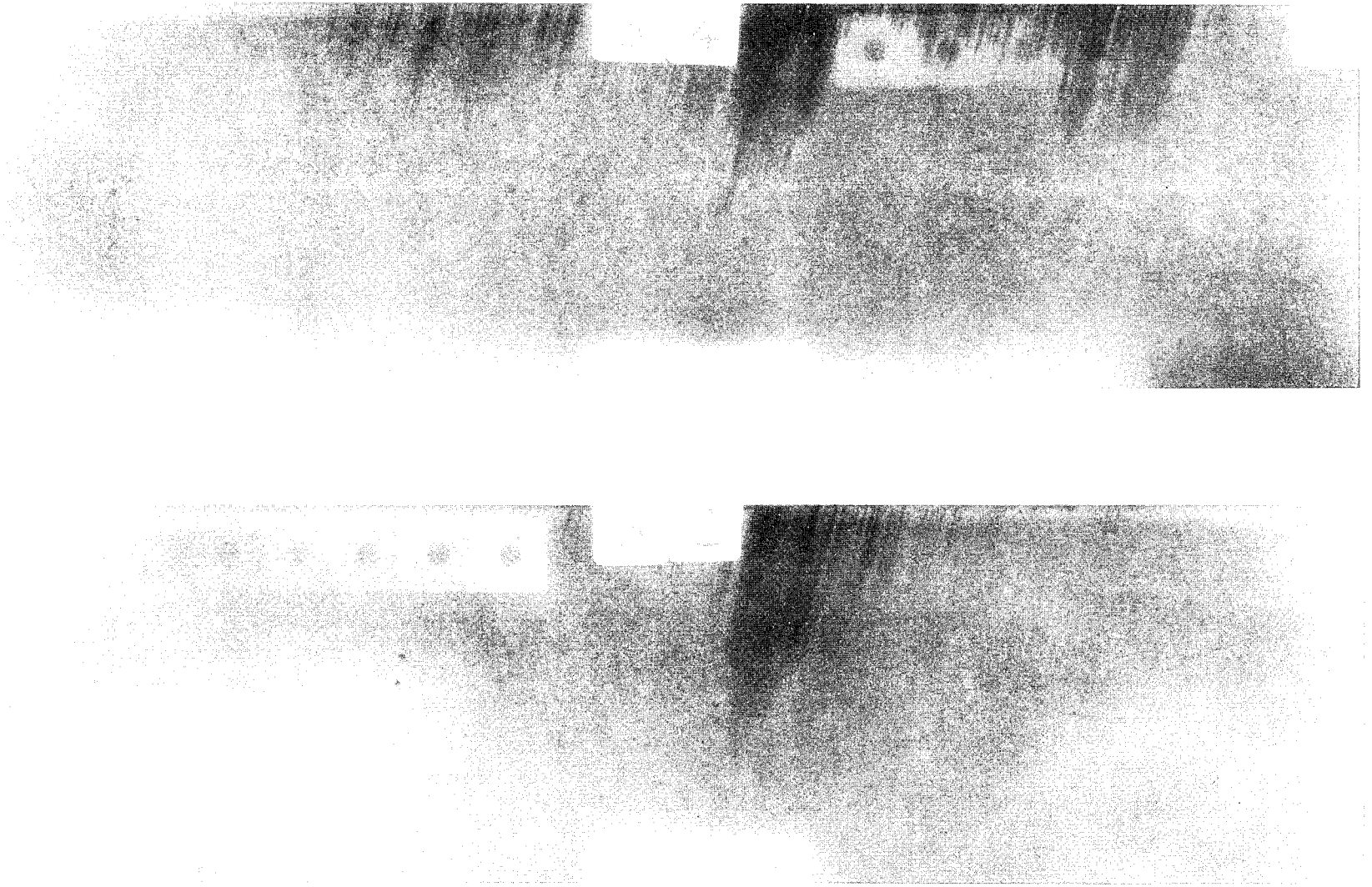

Figure 1. Two examples of boiler weld radiographs of 3/4" thick, showing defects regarded as acceptable.

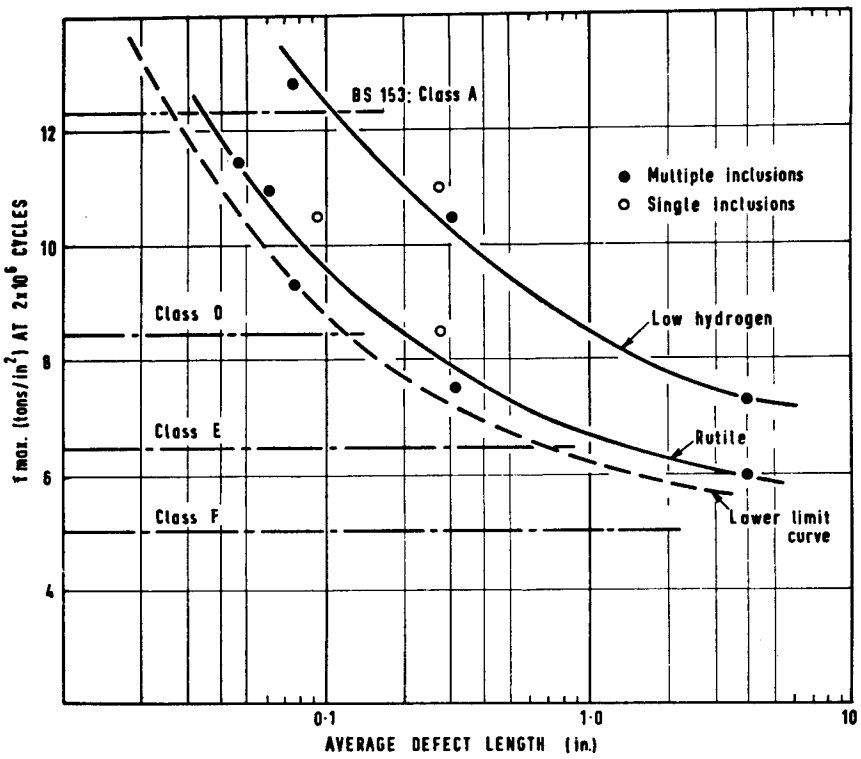

Figure 2. Relationship between inclusion length and fatigue strength - 1/2" thick steel butt-welds (Newman).

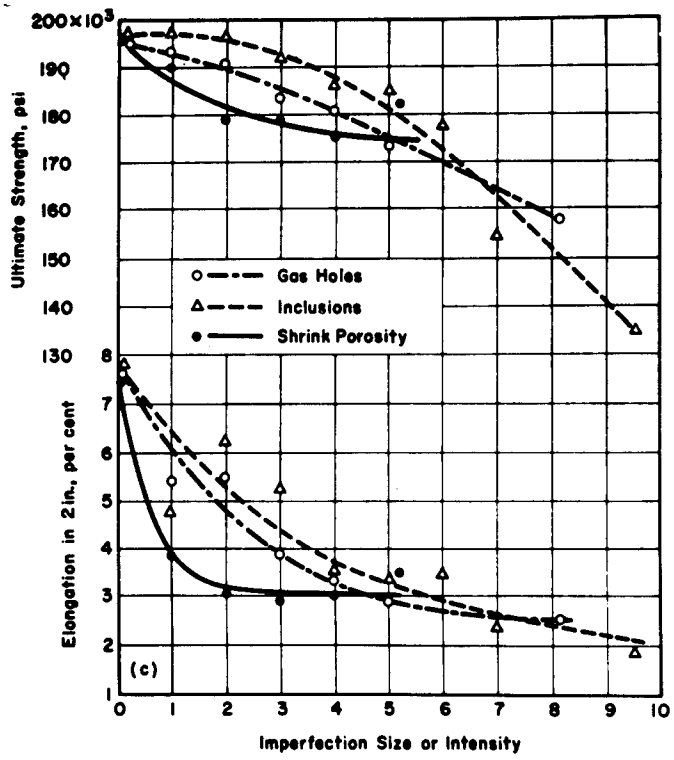

Figure 3. Correlation between defect size and ultimate tensile strength in type 410 cast stainless-steel 0.3" thick (Mattek).

Figure 4. Aircraft casing failure:

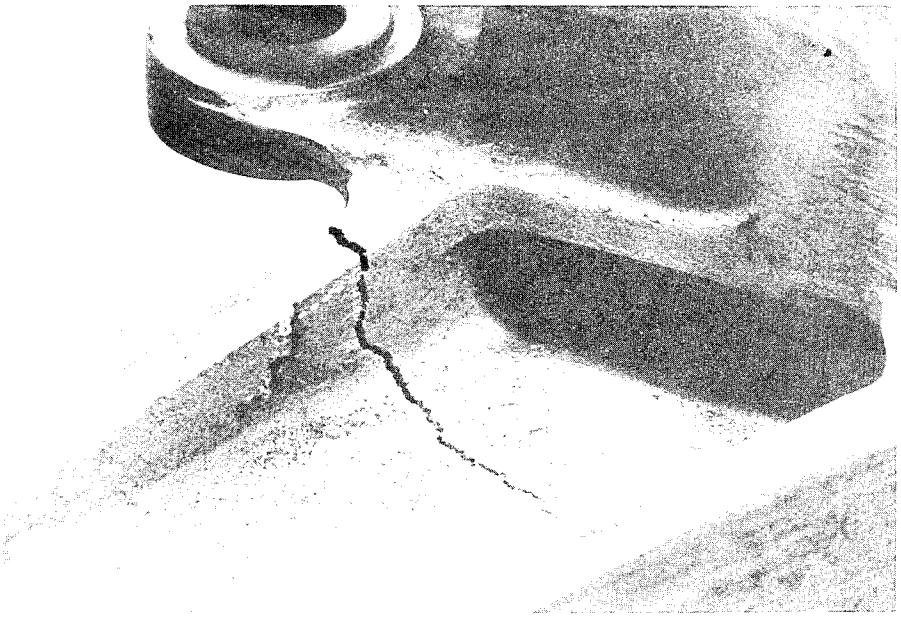

(a) Photograph of crack

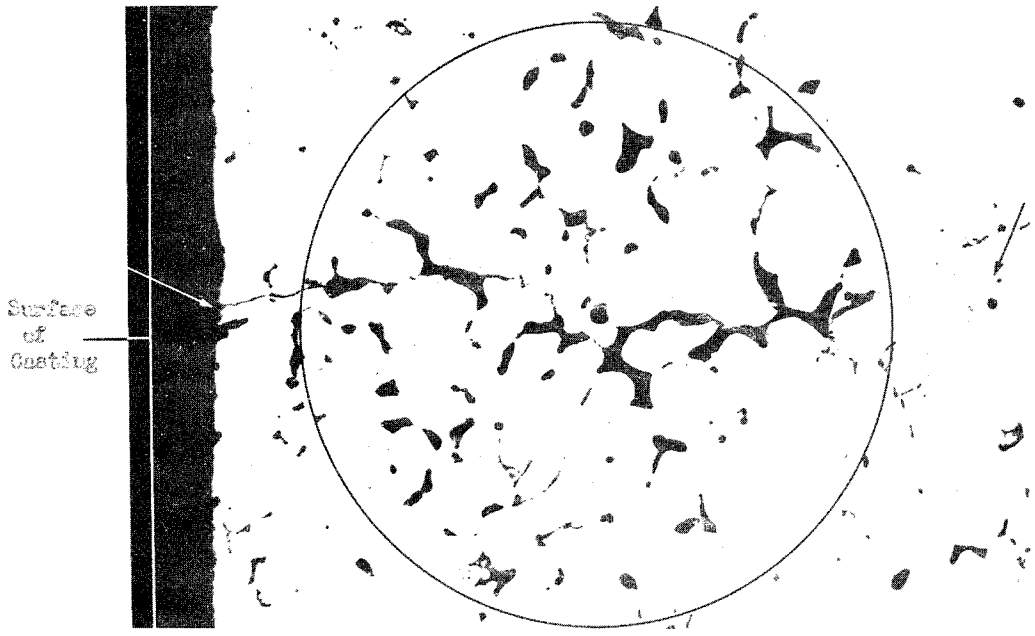

(b) Microphotograph of region of porosity near surface at region of failure (150x).

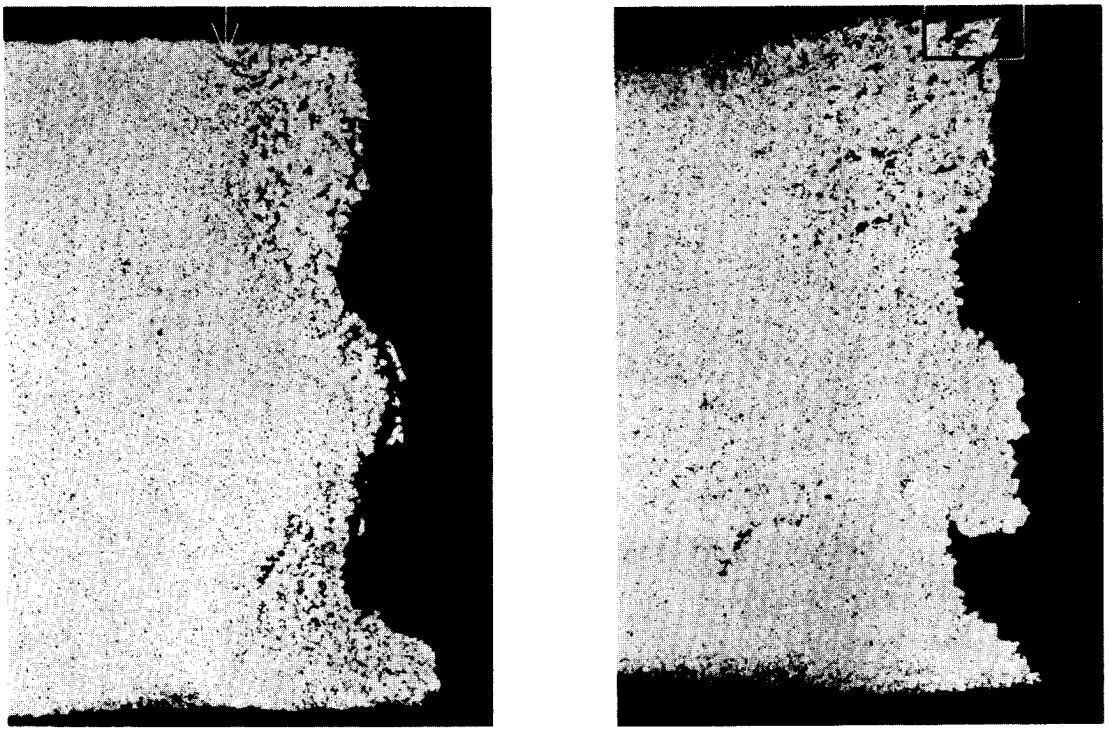

Figure 5. Cross-sections of fracture in pulley bracket casting showing localized areas of porosity close to fracture face (10x).

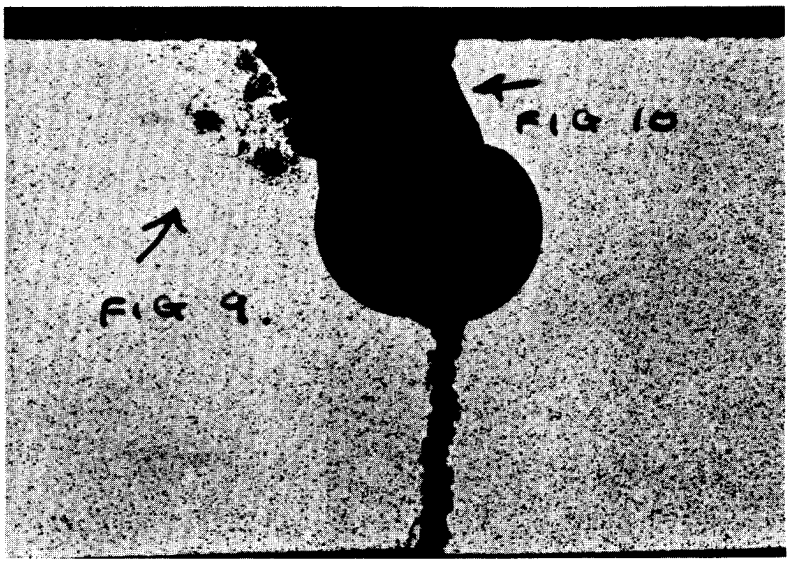

Figure 6. Macrograph of section through defective zone of cockpit canopy casting.

Figure 7. Defect in steering lever casting:

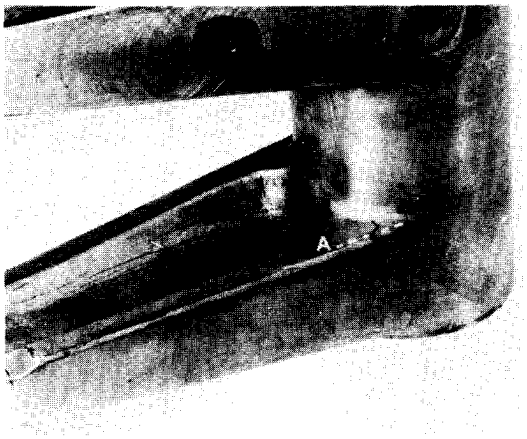

(a) Photograph of defect

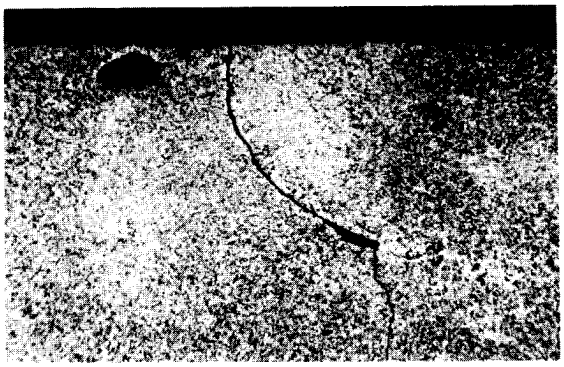

(b) Macrograph of section (19x)

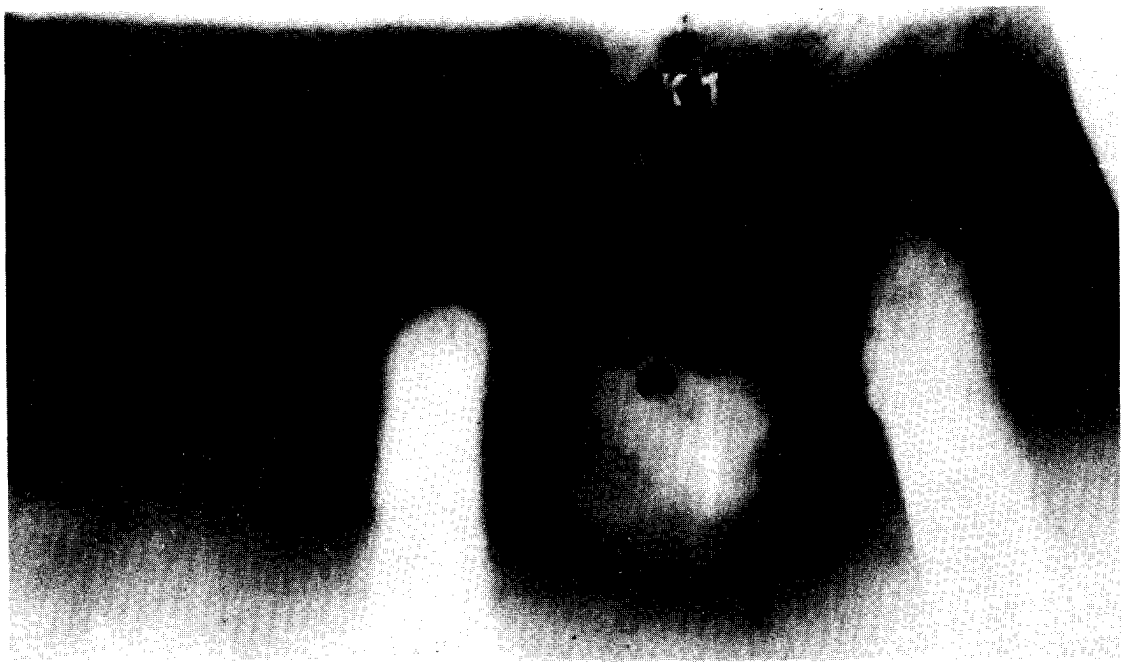

Figure 8. Radiograph of repaired area of casting, wall thickness 1". (An attempt had been made to remove shrinkage pipe by drilling holes and filling these with welding. Holes are not properly filled and weld has cracked extensively).

AN ENGINEERING BASIS FOR ESTABLISHING RADIOGRAPHIC ACCEPTANCE STANDARDS FOR POROSITY IN STEEL WELDMENTS

H. Greenberg
Westinghouse Research Laboratories
Pittsburgh, Pa.

Most design engineers and quality control personnel soon come to realize that very few, if any, weldments are completely free from porosity and inclusions. They then have the difficult task of establishing limits on the size, distribution, and total number of flaws that can be tolerated for a given application. In some cases, acceptance standards may be based on failure analyses either of production parts or specially designed and artificially flawed specimens tested in such a way as to simulate service conditions. The latter type of analysis can yield realistic estimates of critical flaw sizes responsible for initiating premature failures; but, unfortunately, only in a few applications have a sufficiently large number of parts been destroyed to establish valid limits.

What does a designer do when he has neither the time nor facilities to conduct a destructive test program? The usual procedure is to review all available specifications and select acceptance standards which have been successfully applied to other similar parts for a reasonable period of time. For steel weldments, the radiographic standards in the ASME Boiler Code, particularly Section VIII, the Unfired Pressure Vessel Code, have frequently served this purpose. In particularly critical applications such as nuclear pressure vessels, designers have felt that the standards should be somewhat more restrictive than those applied to ordinary boilers so they established a new set of radiographic standards, namely those in Nav Ships 250-1500-1. In other very highly stressed applications such as rocket motor cases, radiographic standards have been established as a result of a compromise between design engineers who insist on perfection and manufacturing personnel who are concerned with costs and delivery schedules.

Radiographic standards in the Unfired Pressure Vessel Code were first adopted by ASME in about 1931. All cracks and incomplete fusion were considered rejectable. Inclusions or cavities were acceptable if less than 1/3 T (thickness of plate)long and if separated by 2 T of solid metal. Acceptance levels for porosity were illustrated by prints of radiographs, four of which were included as part of the 1931 specification. Actual radiographs were substituted for the four prints in 1934 and these remained in use until 1951. Present day penetrameters were adopted for use in 1940. The radiographic acceptance standards for slag inclusions and porosity were made more restrictive for the first time in 1934, but then remained essentially the same until 1951 when they were tightened considerably. They were subsequently slightly revised in 1959 and finally were loosened as to size of pore but tightened to permit fewer pores in 1962. A compilation of the changes in the radiographic acceptance standards in the Unfired Pressure Vessel Code may be found in Figure 1. Sheets showing allowable porosity in

1/2" to 1 1/4" thick plate from the 1959 and 1962 Codes and a corresponding one from Nav Ships 250-1500-1 are included as Figures 2, 3, and 4, respectively. Maximum permissible pore sizes from the three specifications are:

	1959 Code		1962 Code		250-1500-1	
Sizes	Dia.	No. in 6"	Dia.	No. in 6"	Dia.	No. in 6"
Large	.075"	15	.090"	10	.065"	8
Medium	.045"	33	.060"	25	.050"	15
Fine	.035"	65	.035"	50	.040"	20
Assorted	-----	50	-----	40	-----	15

These standards do not appear to be based on critical flaw size concepts but instead reflect what should be obtainable with good welding practice by a conscientious experienced welder. Their unqualified use frequently results in unnecessary weld repairs which increase the cost and delay the delivery of critical parts. Furthermore, where automated TIG and MIG procedures are used for production welding, manual weld repairs, necessary because of the removal of tiny pores, may actually reduce the reliability of the product. This is so because of the inherent danger of making repairs in weld metal which may be hot short (e.g. Inconel), or else in a highly restrained condition with high residual stresses present in the vicinity of the weld repair.

Engineers and scientists now have a much better understanding of failure mechanisms and the minimum size of flaw that can initiate premature failure under given service conditions of stress, temperature, and environment. Radiographic acceptance standards should be based on these advanced concepts.

A number of factors must be taken into consideration when deciding upon the maximum size of flaws that can be tolerated in a given application, namely:

(1) mechanical properties, including fracture toughness, of the part
(2) applied stress level (including any residual stresses)
(3) cyclic nature of applied stress
(4) temperature
(5) environment
(6) degree of uncertainty in the above data
(7) potential consequences of failure.

An illustration of such factors for the 120" diameter rocket motor case is shown in Figure 5.

The first problem is to decide the most likely failure mode, e.g., fatigue, brittle fracture, ductile shear, creep-rupture, stress-corrosion, etc. From the data in Figure 5, it was concluded that, in this application, we need not concern ourselves with normal fatigue (because of the low number of cycles - one or two

hydrotests and a firing), creep-rupture (because of the low service temperature), or stress-corrosion (because of adequate protection by paint). Close control on minimum section thickness and the tensile test results obtained in qualification tests eliminated ductile shear from consideration, leaving brittle fracture as the failure mode of most concern. Brittle fracture could conceivably occur during hydrotest or in the actual firing; the latter could be considered a low cycle fatigue failure.

Fortunately, we now have a means of estimating critical flaw size for initiation of brittle fracture based on the fracture mechanics approach originally proposed by Griffith[1] and more recently modified by Irwin[2] and others.[3] The various tests for measuring toughness have been thoroughly covered elsewhere[4, 5] and will not be discussed here. Let it suffice to say that expressions have been developed for plane strain fracture toughness (G_{Ic}) and the plane strain critical stress intensity factor (K_{Ic}) from which the critical flaw size for initiation of brittle fracture can be determined.[4] For practical engineering purposes, the plane strain toughness values, being the most conservative estimates, may be considered as material constants applicable to all geometries and loading conditions in a manner somewhat analogous to yield strength.

The critical depth "a" of a semi-elliptical surface flaw is expressed as follows:[4]

$$a = \frac{K_{Ic}^2 \left[\phi^2 - 0.212 \left(\frac{\sigma_G}{\sigma_{ys}}\right)^2\right]}{1.21 \pi \sigma_G^2}$$

where K_{Ic} = plane strain fracture toughness, psi $\sqrt{\text{in.}}$
σ_G = applied stress normal to the flaw, psi
σ_{ys} = tensile yield strength, psi
ϕ^2 = an elliptical integral which is dependent upon the ratio of crack depth "a" to 1/2 crack length "ℓ".[6]

The critical sizes of internal elliptical flaws may be estimated in a similar fashion using:

$$a = \frac{K_{Ic}^2 \left[\phi^2 - 0.212 \left(\frac{\sigma_G}{\sigma_{ys}}\right)^2\right]}{\pi \sigma_G^2}$$

The only differences between the two expressions are that the total flaw depth for internal flaws is "2a" and the constant "1.21" is deleted from the denominator. From these two equations we can calculate critical flaw sizes

provided that we know the yield strength of the material, its fracture toughness K_{Ic}, and the applied stress. For the 120" rocket motor case design conditions, the yield strength is 190 ksi, K_{Ic} is 70 ksi $\sqrt{in.}$, and the hoop stress has been calculated to be 170 ksi. The critical sizes of both surface and internal cracks oriented normal to the hoop stress (the most severe condition) are shown in Figure 6. As may be seen from the data, flaw geometry is an important consideration. Long, shallow flaws are just as effective in triggering catastrophic failure as shorter, deeper flaws.

It must be emphasized that these critical flaw sizes were determined for very sharp cracks. They should, therefore, be applicable with a very large margin of safety to less dangerous flaws such as porosity and inclusions. In this paper, porosity, nonmetallic inclusions and tungsten particles are treated as though they are identical in nature and any possible effects of sharp edges, corners, or tails on these flaws are ignored since they cannot be more severe than the sharp cracks on which the calculations were made.

K_{Ic} values for D6ac steel welds were determined at Westinghouse on large edge-notched tensile specimens previously described by Wessel.[7] Although four such tests on fully heat treated weldments showed a range in K_{Ic} from 80 to 97 ksi $\sqrt{in.}$ for the TIG weld metal, a value of 70 ksi $\sqrt{in.}$ was used in the calculations leading to Figure 6 since this value was reported elsewhere[8] for D6ac weld metal. Actually, five measurements of K_{Ic} may be insufficient to establish its variability in welds, particularly porous ones. Porosity in welds may be due to excessive nitrogen in the shielding gas which could not only cause porosity but could result in a high concentration of iron nitrides in the adjacent weld metal which could seriously reduce its toughness and ductility in segregated areas. The safest approach, therefore, is to use the lowest measured value of K_{Ic} for the weld metal rather than the average value or that of the base metal. The K_{Ic} of the D6ac base metal was measured to be 110 ksi $\sqrt{in.}$ and that of the heat-affected zone was 97 ksi $\sqrt{in.}$

From the curves in Figure 6, it becomes evident that for the material in question, an internal crack less than 0.24" in diameter and a surface crack less than 0.20" in diameter cannot initiate a brittle fracture. In keeping with conservative practice, a safety factor should be applied to compensate for minor variations in manufacturing practice. If we substitute 200,000 psi, the ultimate strength of the material, for the 170,000 psi design stress originally used to calculate the critical flaw sizes shown in Figure 6, we get new values for the critical dimensions of both surface and internal flaws, shown graphically in Figure 7. These curves show that round disc-shaped internal cracks less than 0.17" in diameter are not large enough to trigger a brittle failure in this application even at an applied stress of 200,000 psi; however, a similar flaw present on the surface need only be 0.07" deep and .14" long. Keeping in mind that we are treating porosity as though it were a sharp crack, we must define the rejectable diameter of an individual pore as the critical length of the more severe surface flaw since radiography cannot distinguish a surface pore from an internal

one. For the application in question, the critical diameter of a single pore is therefore limited to 0.14". Figure 7 also shows that the critical length of an internal flaw does not increase appreciably until its depth is decreased to about 0.08". Continuing in this same vein, one can then interpret Figure 7 to indicate that even though an elliptical internal flaw 0.06" x 0.35" is sufficient to initiate a brittle failure, internal pores less than 0.06" deep cannot cause a brittle fracture regardless of length for the example and application cited. On the other hand, elongated surface flaws need only be .027" deep in order to initiate a brittle fracture.

Having established the maximum permissible size of a single pore, we can now concern ourselves with groupings of pores and/or inclusions in the form of clusters or aligned porosity. Peterson[9] has shown that two equal sized pores greater than one pore diameter (d) apart have negligible effect upon one another in uniaxially stressed (cylindrical) sections; this critical ligament is 1.5d for biaxial stresses (spherical dome) sections.* For the sake of uniformity and also to incorporate another safety factor into our acceptance standards, let us assume that pores within 3d of one another may interact to increase the stress level. Those greater than 3d apart need, therefore, only be considered as individual, randomly scattered porosity and should not be included in any groupings of clusters or aligned porosity.

As stated above for the 120" rocket motor case, a single pore 0.14" dia. should be considered rejectable. Two pores less than 0.14" dia. should likewise be rejected if they are sufficiently less than 3d apart to cause the stress intensity at the surface of one of the pores to increase to that of the critical 0.14" dia. pore. How close two small flaws must be to one another to equal the stress intensity of a single 0.14" dia. flaw can be calculated from Chart 8 in Peterson's paper[9] which is herein reproduced as Figure 8. The ordinate in Figure 8 is expressed in terms of a ratio of stresses rather than as a percent increase in stress as originally presented by Peterson. In these calculations, it is assumed that the ratio of stresses (the increased stress due to proximity of a second flaw divided by the stress due to a single flaw) varies inversely as the square root of flaw diameter. The critical proximities (ligaments) of pairs of various size flaws resulting from these calculations are presented in Figure 9. From this curve, which utilizes the same 2:1 safety factor originally used in establishing 3d as the critical ligament for large flaws, it is apparent that two 0.10" dia. pores less than 1d apart or two 0.060" dia. pores less than 1/2d apart are as critical a crack starter as a single 0.14" dia. pore.** Pores less than 0.060" dia.

---

*Tiffany[10] in a recent report of experiments conducted on D6ac steel specimens containing two co-planar elliptical surface flaws (artificial notches extended by fatigue) concluded "...there is very little interaction between co-planar flaws unless they are surprisingly close together." This is in agreement with the results of Peterson's analysis.

**Payne in a recent paper[11] came to a similar conclusion using a different theoretical approach supported by Tiffany's[10] experimental data.

can be ignored unless there are more than two within 1/2d of one another. If we consider three or more adjacent pores less than 0.060" dia. and within 1/2d of one another as being elliptical flaws encompassing all adjacent pores and the metal between them, we can establish realistic limits for clusters and aligned porosity based on the critical flaw sizes shown in Figure 7.

We now have all the data needed to develop a set of conservative standards for porosity in TIG welds in the 120" rocket motor case, namely:

(1) Single pores in excess of 0.14" diameter are rejectable.
(2) Two pores between 0.060" and 0.14" in diameter are rejectable if they are less than a critical ligament "L" apart. The critical ligaments are shown in Figure 9; if the pores are not of the same diameter, use the diameter of the smaller pore in determining the critical ligament.
(3) Aligned porosity, three or more pores less than 0.060" dia., all within 1/2d of one another, and whose extremities intersect a straight line, is rejectable if the total length of the grouping exceeds 0.20".
(4) A cluster of pores, all of which less than 0.060" dia. and within 1/2d of one another, are rejectable if the total area of the grouping cannot be encompassed by a circle 0.14" in diameter or an ellipse 0.06" x 0.20".

Assuming that the radiographs do not show a general condition of segregated porosity sufficient to significantly reduce the effective cross-sectional area of the part, these four statements are all that is required unless one wishes to include a workmanship requirement restricting the total number of pores in some given length of the weld, e.g., ten pores (with diameters larger than 0.060") per foot. The latter type of restriction should not, however, be a basis for rejection but rather should be used to alert welding personnel that remedial action is required to correct a welding process going out of control.

If similar sets of standards were developed for the steels and welding procedures permitted by the Boiler Code, the six pages of porosity charts in the Appendix could be eliminated. At this point, let us return to Figure 3 (one of the six pages) and examine the various charts critically, assuming for sake of illustration that they are being considered for application to the 120" rocket motor case. To begin with, the upper four charts appear to express merely a workmanship requirement and an extremely loose one at that. Two of the large pores (second chart) are actually within 1.5d of one another and should therefore be considered rejectable. There appears to be no justification for the 4T separation requirement for large pores, nor for the 2T separation between groups of aligned medium pores. On the other hand, the individual groupings of aligned medium pores (sixth chart) are too long and may exceed the critical length of an elliptical internal flaw.

As previously mentioned, pores have been treated as though they were disc-shaped sharp cracks rather than globular cavities. Radiography presents only a planar view of flaws, and the plane is not the one normal to the applied stress; furthermore, radiography is incapable of presenting the depth dimension of the flaw in the direction parallel to the beam of radiation other than by slight changes in film density. Since pores are essentially spherical, we can assume that the depth is approximately equal to the visible diameter on the radiograph; furthermore, it is conceivable that pores may have sharp edges or tails not visible on the radiograph so it may not be too great an error to treat the visible pore as though it were a sharp crack oriented in the worst possible direction. There is one other factor of safety not mentioned heretofore, namely, that radiographs reveal aligned porosity and clusters of pores as though they are all situated in the same plane. Actually, they may be located anywhere within the thickness of the weld and may therefore be much more than the critical ligament apart even though the radiograph shows them to be that close to one another.

Even though all radiographic standards unequivocally state that cracks and lack of fusion are rejectable, it has been shown[12, 13] that fine cracks clearly visible on the surface of the part or else detected by magnetic particle or dye penetrant tests are not always detectable radiographically even with the best of techniques. On the other hand, ultrasonic inspection, particularly with the use of angle beam search units, readily detects the presence of cracks and lack of fusion.[14, 15] Additional development work is required, particularly with respect to interpretation of results and establishment of standards for each specific configuration of welded joint before ultrasonic testing can be used to full advantage. For optimum results on critical assemblies, more than one nondestructive testing technique should be utilized because each of them has specific capabilities of flaw detection not enjoyed by the others.

This paper has been concerned only with radiographic standards for porosity and inclusions in welds subject to brittle fracture. Castings and wrought alloys can certainly be analyzed in a similar manner. In applications where fatigue is the anticipated failure mode, material properties would be weighted differently. The governing factor would be the rate of crack propagation until a critical flaw size is reached, at which point the remaining section would fail suddenly by either brittle fracture or shear depending on the temperature, stress, material properties, etc. The considerations involved in setting up standards for porosity in welds subject to fatigue and possibly complicated by a corrosive environment are beyond the scope of this paper. They can, however, be analyzed[10] and realistic radiographic standards for porosity can be developed for applications subject to fatigue conditions.

In summary, radiographic acceptance standards for porosity must be established specifically for a given application and should be based on critical flaw sizes for the anticipated failure mode. Modern concepts of fracture toughness and stress concentrating effects of holes in close proximity to one another should be utilized in developing the standards. For critical applications, radiographic inspection should be supplemented with ultrasonic, magnetic particle, and/or dye penetrant inspection techniques. Development work in the form of destructive testing of parts with deliverately introduced flaws should be strongly encouraged.

Acknowledgements

The writer wishes to acknowledge the support and encouragement of C. M. Miller, Manager of the Westinghouse Rocket Motor Case Department, Philadelphia, Pa. He is likewise indebted to his associates R. E. Peterson, E. T. Wessel, and F. E. Werner for many hours of fruitful discussion on this subject as well as many helpful suggestions following their critical review of the paper.

References

1. Griffith, A. A., "The Phenomena of Rupture and Flow in Solids," Royal Society Philosophical Transactions, Series A, v. 221 (1920) pp. 163-198.
2. Irwin, G. R., "Analysis of Stresses and Strains Near the End of a Crack," Journal Applied Mechanics, v. 24 (1957) p. 361.
3. Orowan, E., "Energy Criteria of Fracture," Welding Research Supplement, v. 20 (1955) p. 157s.
4. "Progress in Measuring Fracture Toughness and Using Fracture Mechanics - Fifth Report of a Special ASTM Committee," Materials Research and Standards, v. 4, No. 3, March 1964, p. 107.
5. Srawley, J. E. and Brown, W. F., Jr., "Fracture Toughness Testing," Paper presented at 67th Annual Meeting of ASTM, Chicago, Illinois, June 1964.
6. "The Slow Growth and Rapid Propagation of Cracks, Second Report of a Special ASTM Committee," ASTM Bulletin, May 1961, p. 389.
7. Wessel, E. T., "Brittle Fracture Strength of Metals," presented at ASTM 63rd Annual Meeting, Atlantic City, N. J., June 1960.
8. Informal Communication, S. M. Jacobs, UTC, June 16, 1964.
9. Peterson, R. E., "The Interaction Effect of Neighboring Holes or Cavities, with Particular Reference to Pressure Vessels and Rocket Cases," ASME Annual Meeting, 1964.
10. Tiffany, C. F. and Masters, J. N., "Applied Fracture Mechanics," Paper presented at the 67th Annual Meeting of ASTM, Chicago, Illinois, June 1964.
11. Payne, W. A., "Incorporation of Fracture Information in Specifications," Paper presented at the 67th Annual Meeting of ASTM, Chicago, Ill., June 1964.
12. Parker, F. C., "Are Standards or Codes Practical for Ultrasonic Examination of Metals and Weldments," Paper No. 56-A-185, ASME Annual Meeting, New York, N. Y., November 1956.
13. Hornung, R., "Experience in Flaw Detection by Means of Ultrasonics As Against Radiography," Brutcher Translation HB No. 5707, Stahl and Eisen, v. 83 (1963) pp. 298-304.
14. Renner, R. W., "Ultrasonic Inspection of Welds in Heavy Steel Plate," Westinghouse Research Labs Report 64-148-467-R1, March 4, 1964.
15. Renner, R. W. and Greenberg, H., "Correlation of Ultrasonic and Radiographic Inspection of a 3/8" Thick D6AC Welded Plate," Westinghouse Research Labs Report 63-848-467-R1, July 26, 1963.

	Date of Revision					
	1931 1932	1934 1935	1940 1943	1946 1949	1950	1951 1952 1956 1959(d) 1962(e)
Cracks	--	Unacceptable	Unacceptable	Unacceptable	Unacceptable	Unacceptable
Lack of Fusion or Incomplete Penetration	--	Unacceptable	Unacceptable	Unacceptable	Unacceptable	Unacceptable
Slag Inclusions Length	<1/3 T(a)	<1/3T; in addition, the summation of the lengths of small inclusions must be <T in a weld length of 12T	Same as 1934	<1/3T but not >3/4" regardless of thickness; in addition, the summation of the lengths of small inclusions must be <T in a weld length of 12T for aligned porosity; <1/4" are acceptable for any plate thickness	Same as 1946	<1/4" for T to 3/4"; <1/3T for T=3/4" to 2-1/4"; <3/4" for T over 2-1/4"; in addition, the summation of the lengths of small inclusions must be <T in a weld length of 12T
Proximity	>2 T	>6 L(b)	>6 L	>6 L	>6 L	>6 L
Avg. No.	<1/ft	--	--	--	--	--
Porosity	Compared to prints of four representative X-ray films	Compared to a standard set of radiographs supplied by the Boiler Code Committee	Same as 1934	Same as 1934	Same as 1934	Compared to porosity charts (in Mandatory Appendix) similar to Fig. 2
Sensitivity of Test	2%	2%	2%	2%	2%	2%
Penetrameter	None	Stepped strips with 3/16" dia. drilled holes	3 hole (2,3,4t)(c) but holes >1/16" dia.	3 hole (2,3,4t) but holes >1/16" dia.	3 hole (2,3,4t) but holes >1/16" dia.	3 hole (2,3,4t) but holes >1/16" dia.
Max. Allowable Working Stress in 55,000 psi T.S. Plate at Room Temperature	~11,000 psi	~11,000 psi	~11,000 psi	~11,000 psi	13,750 psi	13,750 psi

(a) T = thickness of plate or weldment
(b) L = length of longest individual inclusion or cavity
(c) t = thickness of penetrameter (2% of T)
(d) New porosity charts - Figure 2 (1 of 6)
(e) New porosity charts - Figure 3 (1 of 6)

Figure 1

Changes in Radiographic Acceptance Standards in the Unfired Pressure Vessel Code from 1931 - 1962

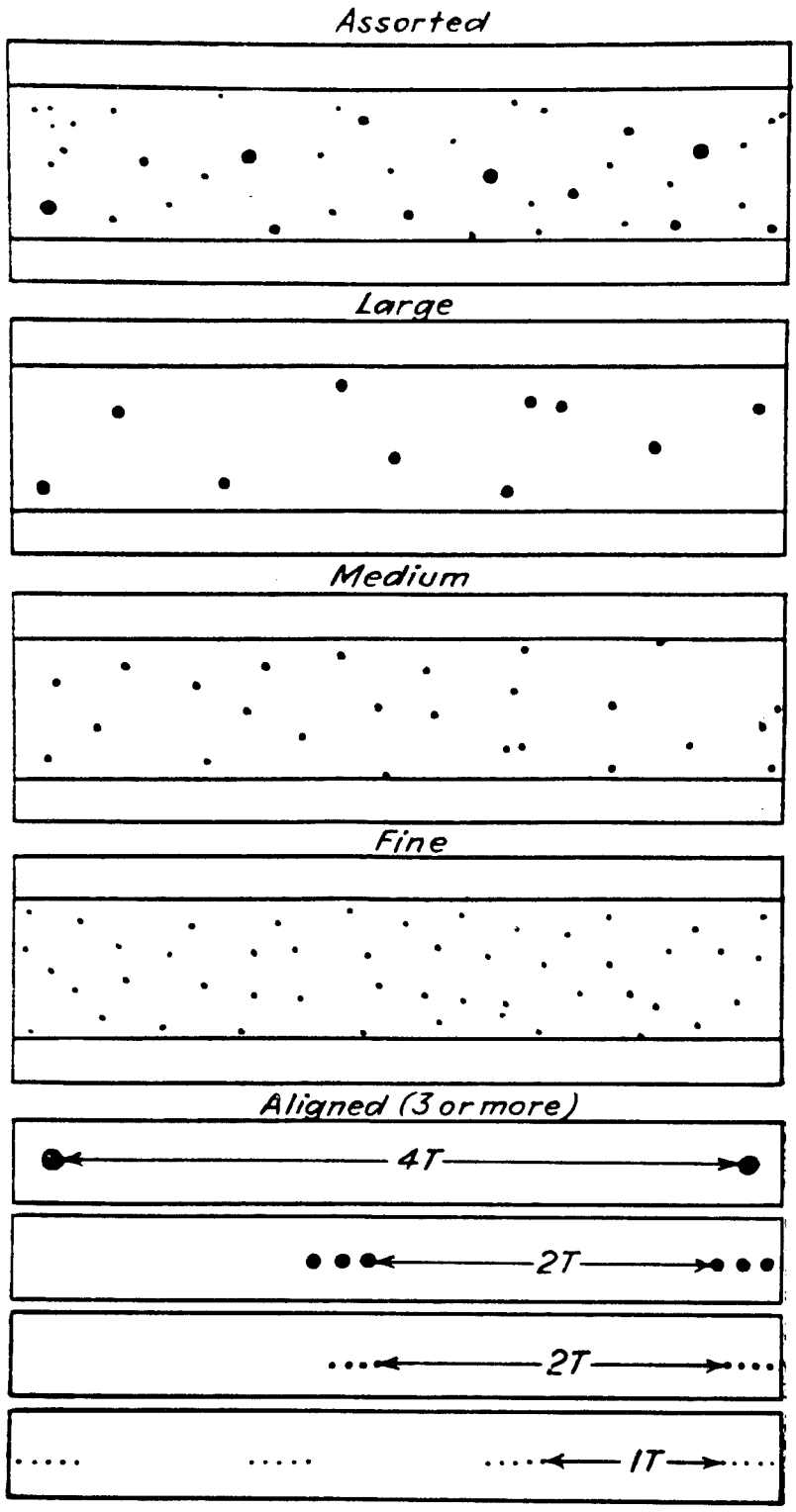

Figure 2

Porosity Standards for Welds 1/2" to 1-1/4" Thick

(Excerpted from the 1959 Edition of the Unfired Pressure Vessel Code)

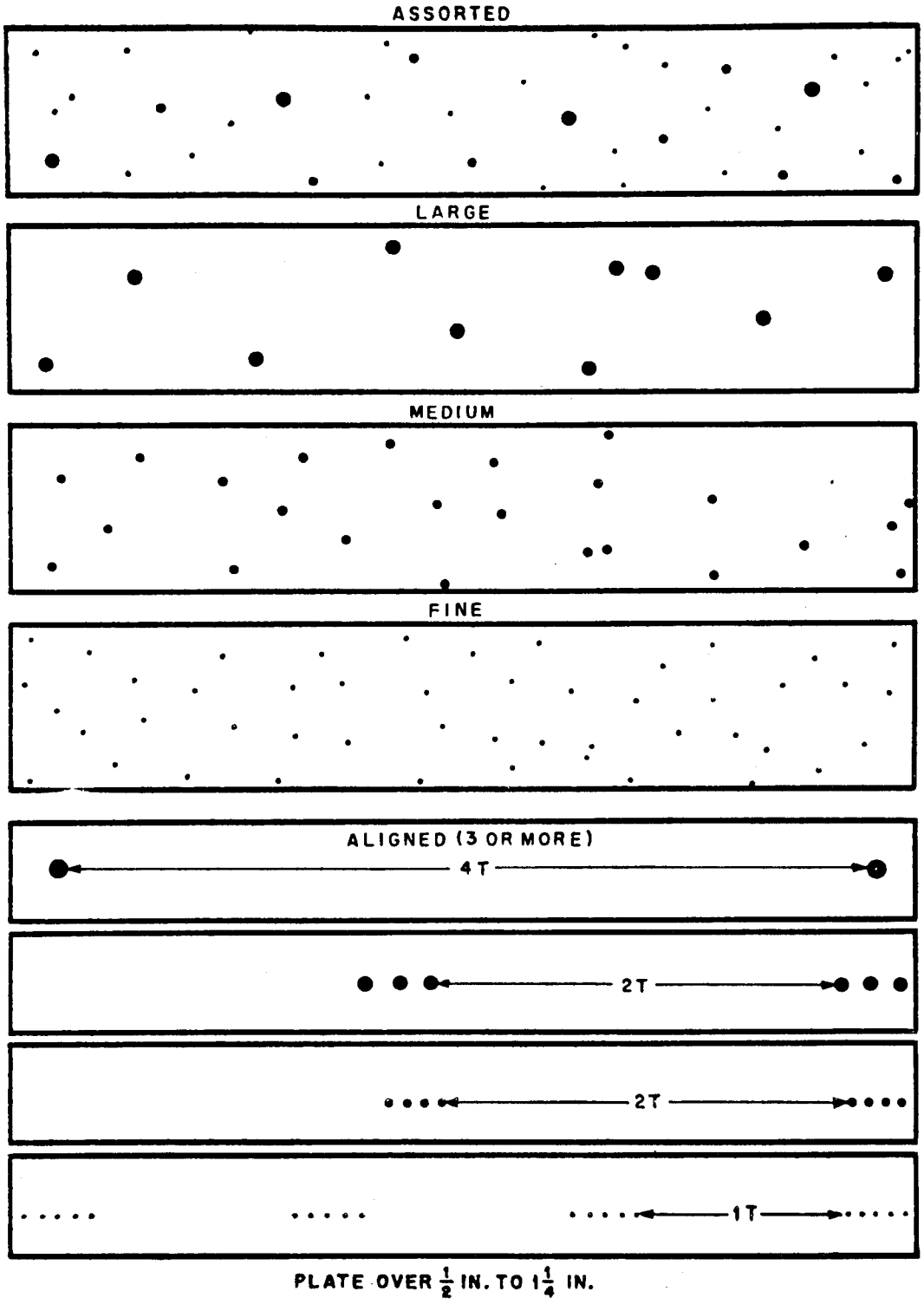

Figure 3

Porosity Standards for Welds 1/2" to 1-1/4" Thick

(Excerpted from the 1962 Edition of the Unfired Pressure Vessel Code)

WELDS OVER 1/2" TO AND INCLUDING 1" THICK (T= WELD THICKNESS)

ASSORTED-RANDOMLY DISPERSED

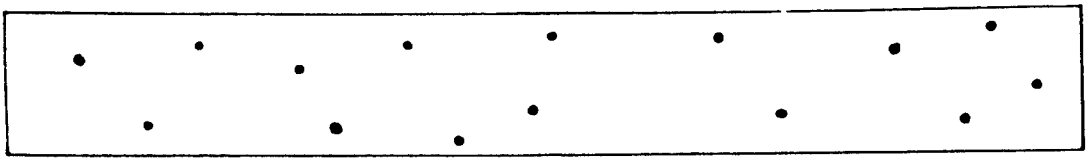

ALL SIZES TO 1/16" IN DIAMETER
MAXIMUM NUMBER OF INDICATIONS IN 6" = 15

CLUSTERS

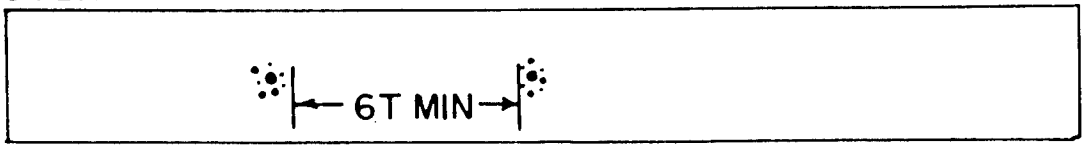

ALL SIZES TO 1/16" IN DIAMETER
MAXIMUM NUMBER OF IND. IN EACH CLUSTER = 8 (1 LARGE, 3 MED., 4 FINE)

LARGE-RANDOMLY DISPERSED

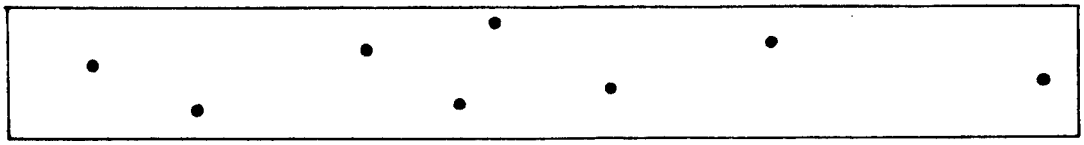

0.065" dia.

3/64" TO 1/16" MAXIMUM IN DIAMETER
MAXIMUM NUMBER OF INDICATIONS IN 6" = 8
MEDIUM-RANDOMLY DISPERSED

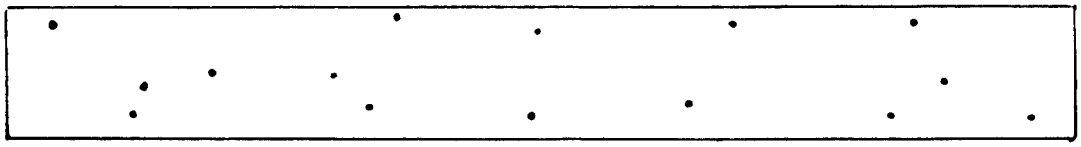

0.040" dia.

1/32" TO 3/64" IN DIAMETER
MAXIMUM NUMBER OF INDICATIONS IN 6" = 15
FINE-RANDOMLY DISPERSED

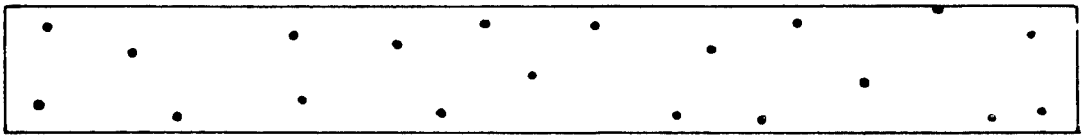

0.050" dia.

UP TO 1/32" IN DIAMETER
MAXIMUM NUMBER OF INDICATIONS IN 6" = 20
ALIGNED (3 IND. ARRANGED SUCH THAT THEY LIE ON A STRAIGHT LINE)

Figure 4

Porosity Standards for Welds 1/2" - 1" Thick

(Excerpted from Nav Ships 250-1500-1)

Application	- 120" dia. rocket motor case
Alloy	- 3/8" thick D6ac plate
Typical properties of D6ac welds	- 202,000 psi U.T.S. 190,000 psi Y.S. (0.2% offset) 11% Elong. (% in 2") 42% Reduction of Area 12 ft. lbs. Charpy V-notch at $75^{\circ}F$
Plane strain fracture toughness (K_{Ic})	- 70,000 psi $\sqrt{in.}$
Design stress level	- 170,000 psi hoop stress
Cyclic nature	- 2 to 5 cycles
Temperature	- 20° - 100° F
Environment	- Protected by paint
Degree of uncertainty	- $\pm$ 15% in strength level $\pm$ 10% in stress level
Potential consequence of failure	- Catastrophe with possible loss of life and certain loss of the total missile and mission

Figure 5

Considerations Involved in Determining Critical Flaw Size in the 120" Rocket Motor Case

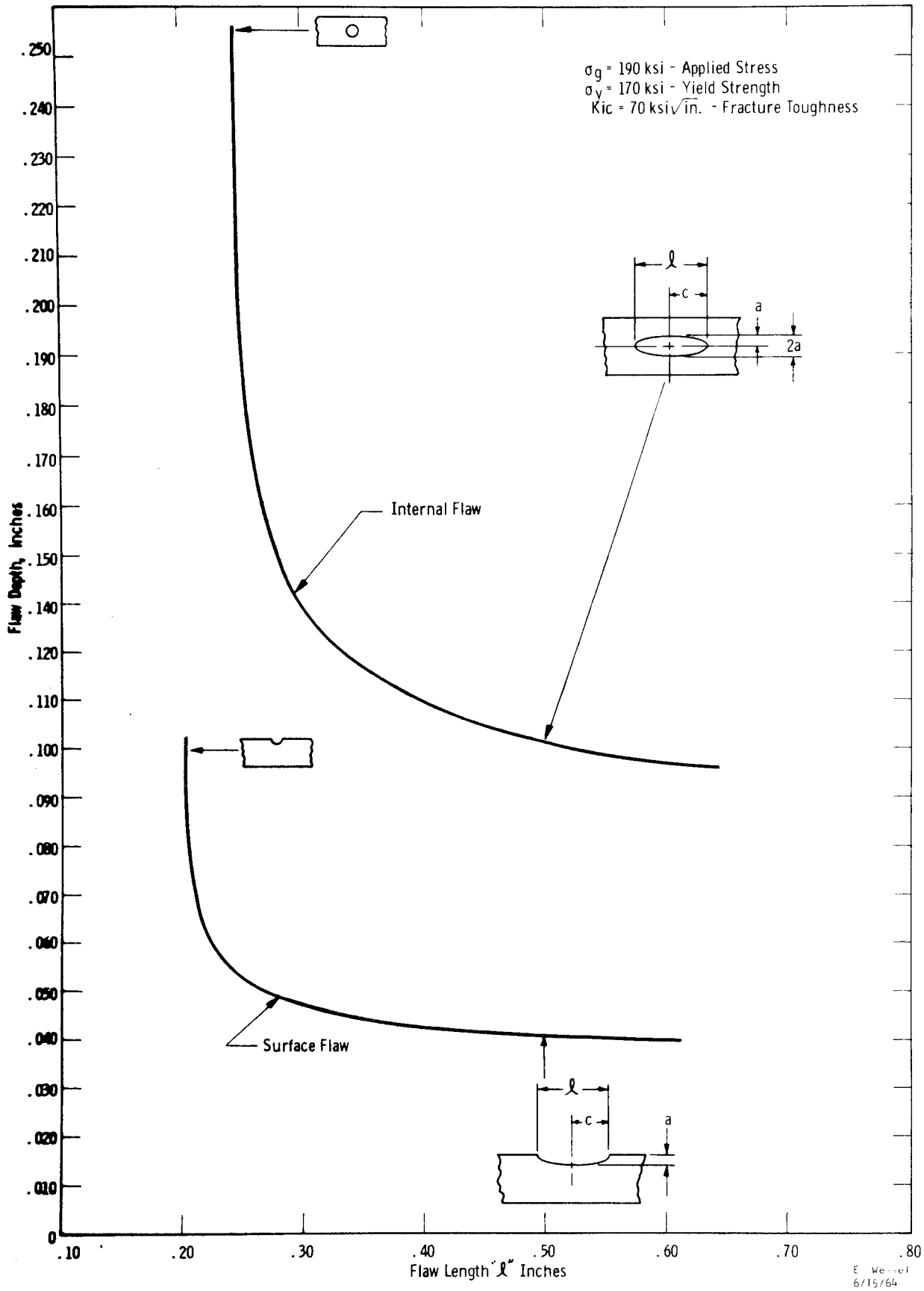

Fig. 6—Critical flaw sizes for D6 ac welds at an applied stress of 170, 000 psi

Curve 571131-A

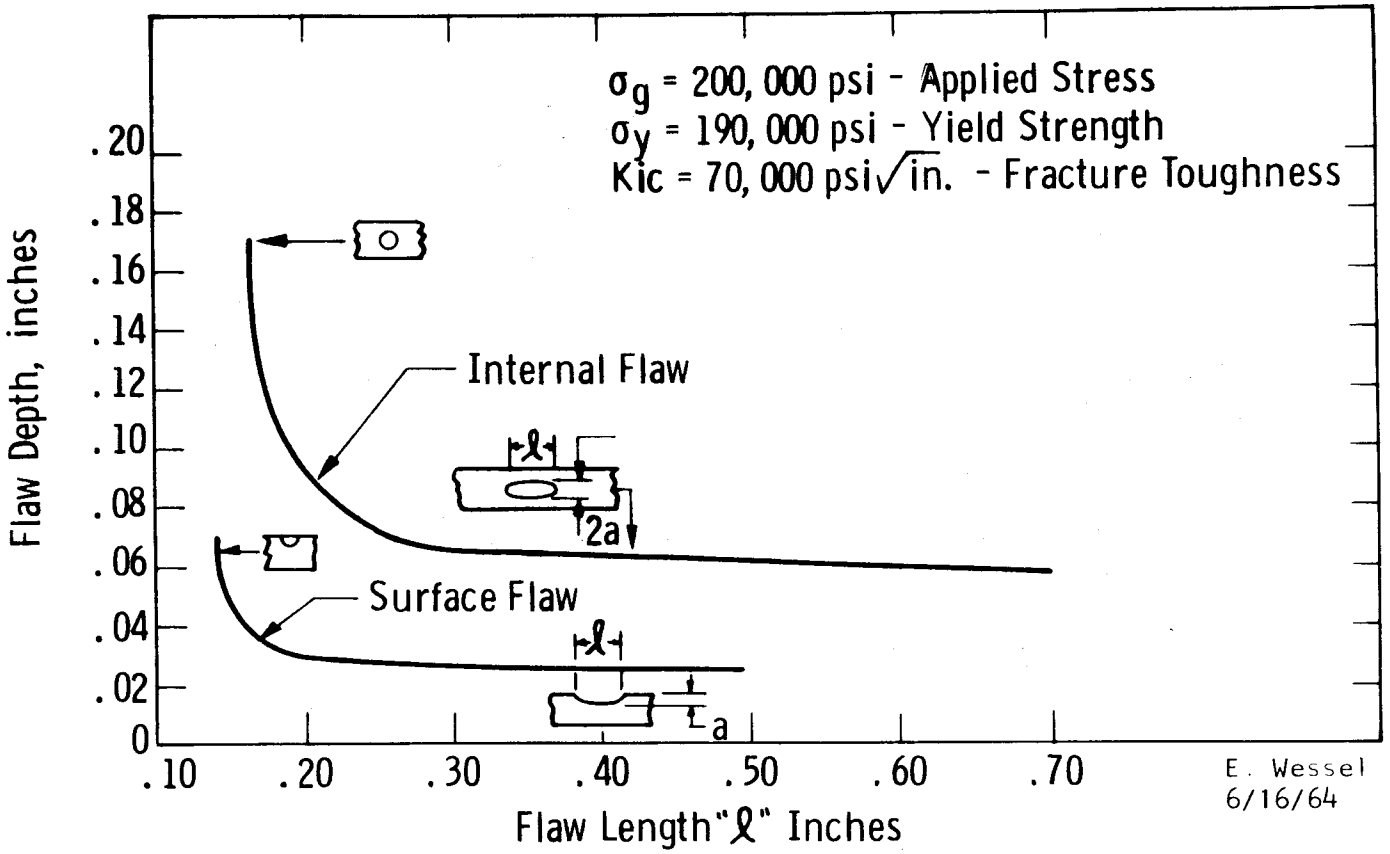

Fig. 7—Critical flaw sizes for D6 ac welds at an applied stress of 200, 000 psi

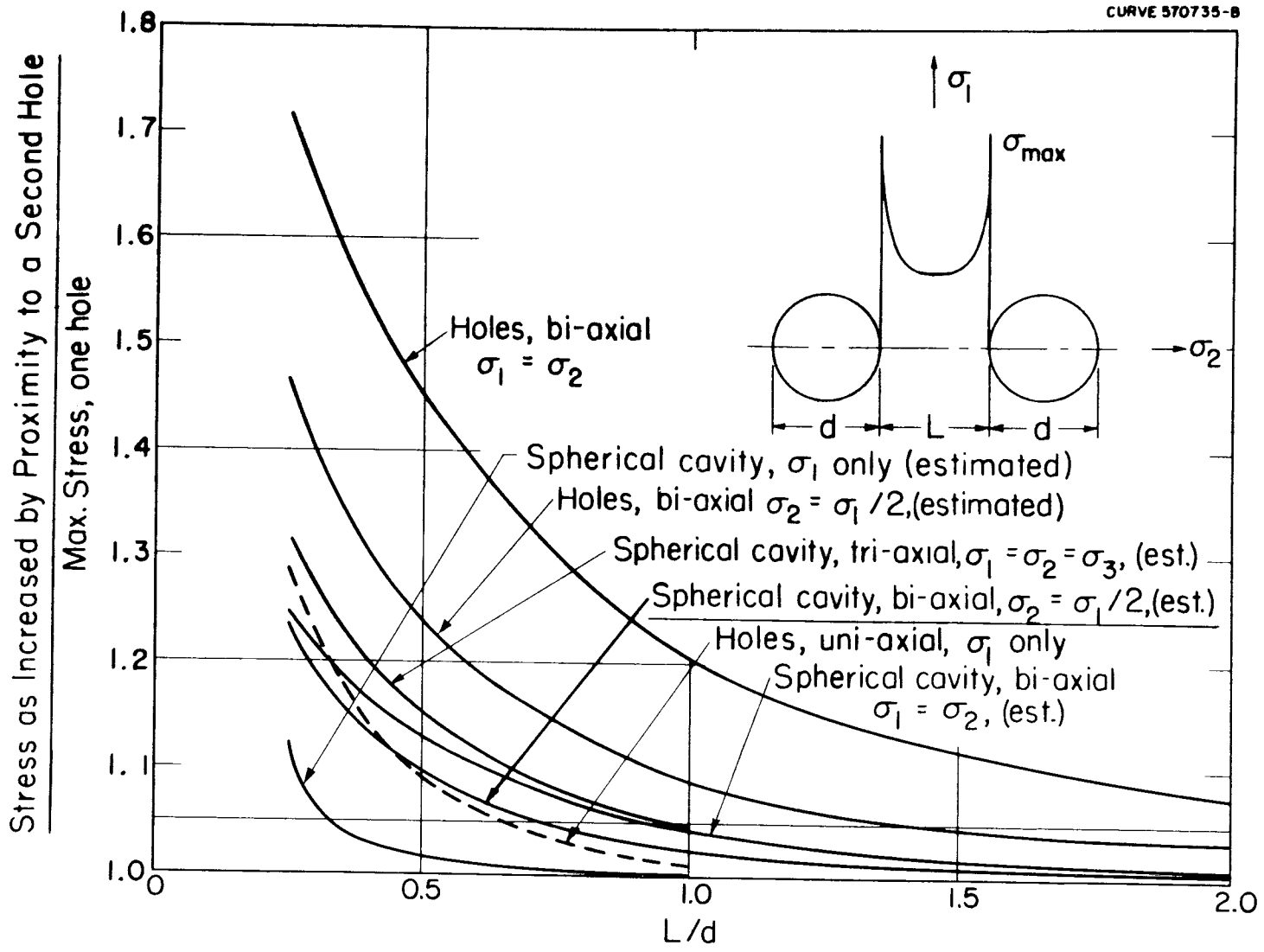

Fig.8-Interaction effect of two holes or cavities in an infinite plate or body. (PETERSON)[9]

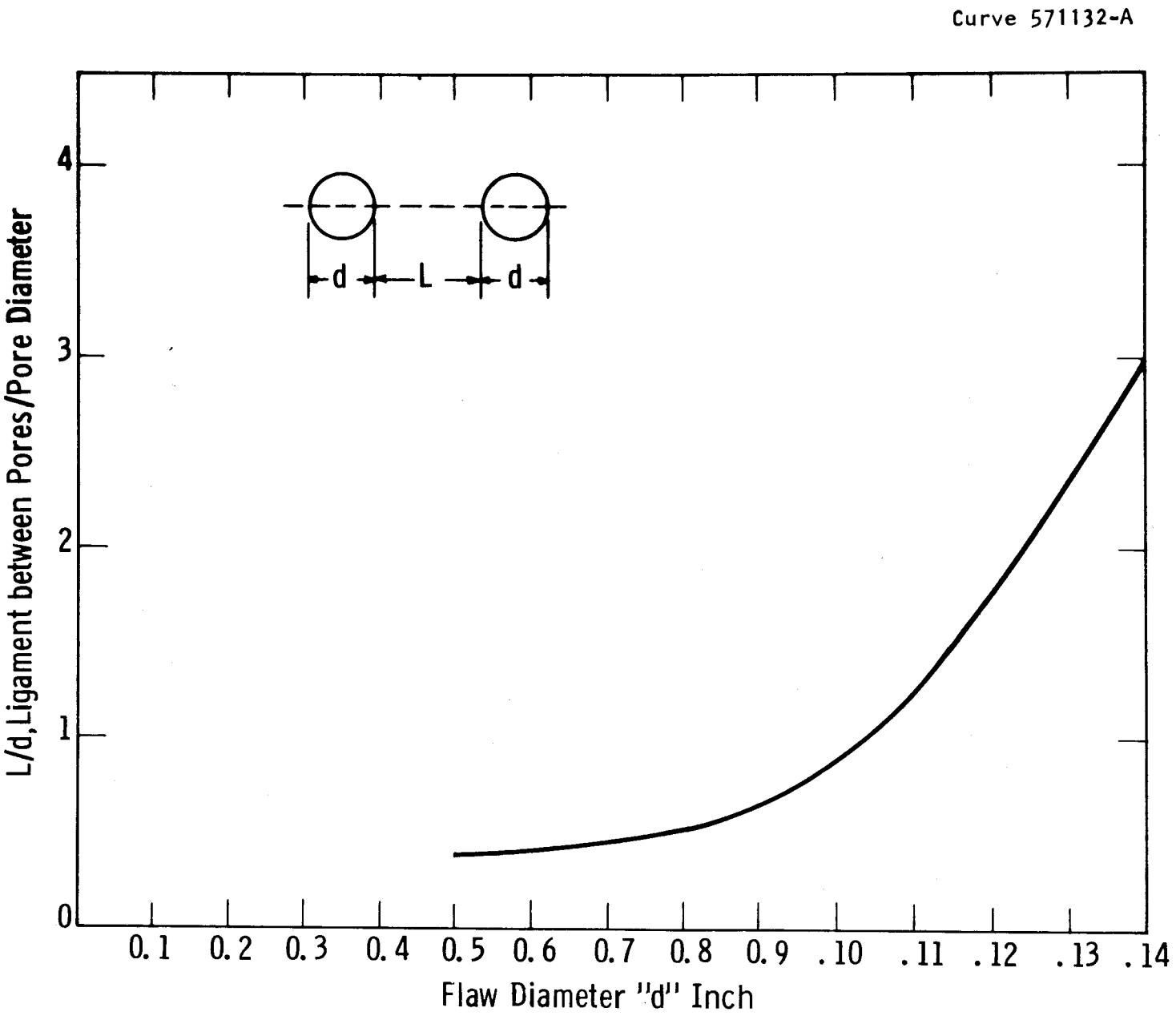

Fig. 9—Critical ligaments for pairs of various size flaws

NEW NDT TECHNIQUES FOR AEROSPACE MATERIALS AND STRUCTURES

E. J. Kubiak
General American Transportation Corporation
Niles, Illinois

Introduction

During the last few years, great strides have been made in developing new materials and new fabrication processes for aircraft and aerospace applications. These advances have resulted in materials and composite structures which have higher strength to weight ratios and greater environmental tolerance than was even thought possible not too many years ago. In particular, significant contributions have come in the area of refractory metals. Besides the many improvements which have been made in the refractory metals themselves, new fabricating techniques such as diffusion bonding and filament reinforcement have been developed and reduced to practice.

These latest developments in material and fabrication methods have in turn spotlighted the need for new and better ways to nondestructively inspect the structures resulting from them. The old, tried, and true NDT methods no longer are sufficient. Pressed by this urgent need for new nondestructive inspection methods, researchers have been working hard developing new techniques and applying known technology which has been laying dormant for years. Two NDT techniques which appear to have particularly good potential for inspecting modern day aircraft and aerospace materials and structures are: (1) FM Lamb waves and (2) dynamic infrared inspection. Let us take a brief look at each of these techniques to learn what they are and how they may be put to work.

FM Lamb Waves

The existence of the type of stress wave known as a Lamb wave was first established mathematically by Lamb[1] in 1916, but it was not until the mid-forties that their existence was verified experimentally by Firestone and Ling[2]. It is not necessary for us here to explore the theoretical aspects of Lamb waves since this has been covered quite extensively by both Worlton[3, 4] and di Novi[5, 6]. For our purposes, it will suffice to say that Lamb waves are the type of stress wave that may be propagated in a thin sheet with stress-free surfaces and that they consist of an infinite number of modes of vibration. In a given material, each Lamb wave mode has a different velocity of propagation. The phase velocity with which each mode travels is dependent on the thickness (d) of the sheet, the frequency (f) of the wave, and the order (n) of the mode. For a given frequency-thickness product (fd), there are a finite number of modes that can be generated,

and the number of possible modes increases as the fd product increases. This is illustrated in Figure 1 which is a theoretical plot of phase velocity versus frequency-thickness product for aluminum. At typical ultrasonic frequencies (above 1 megacycle), Lamb wave generation and detection is limited to thin sheets (0.100" and less) for most materials.

Lamb waves are generated by impinging a longitudinal sound wave with a speed V_L upon a sheet at an angle θ just as in shear wave testing. However, in contrast with shear wave testing, an interference pattern results throughout the sheet thickness because of the proximity of the surfaces. If the speed of the longitudinal wavefront moving along the sheet surface which is equal to $V_L/\sin\theta$ is the same as the phase velocity of the Lamb wave mode, constructive interference will occur giving rise to a standing wave across the sheet thickness which will the propagate parallel to the surfaces. Once a Lamb wave mode is generated, it will continue to travel down the length of a sheet, assuming the incident angle θ and the fd product are held constant, until it reaches a discontinuity such as the edge of the sheet or a flaw. Several effects can be observed as a result of a flaw or defect. First, the original Lamb wave mode will in part be reflected back towards the transmitting transducer where it will be received by the same transducer or a separate one inclined at the same incident angle θ. Secondly, the frequency-thickness product will no longer be satisfied over the discontinuity and that particular mode will not be present at that location. Thirdly, the discontinuity will cause mode conversion to occur and modes other than the original will be generated. Both of these latter effects can be detected with a receiving transducer inclined at a supplementary angle to the incident angle.

In recent years, several people have been experimenting with Lamb waves, and their work is cited in the references[7, 12]. For the past four years, the General American Research Division under contract to the Air Force Materials Laboratory has been investigating[13-17] nondestructive test methods for thin sheet evaluation. One development which has emerged during this work is an improved method of Lamb wave testing which has been called FM Lamb Waves. Previously Lamb wave testing had generally been accomplished by transmitting a single frequency longitudinal wave either in pulse or CW fashion. This procedure meant that precision adjustment of either the incident angle θ or the wave frequency was required in order to obtain a particular mode for even a slight change in sheet thickness or material properties. This can be seen from Figure 2 which is a plot of incident angle versus frequency-thickness product for aluminum. (The solid and dashed lines are theoretical solutions to the mathematical equations describing Lamb waves and the dots are experimental results.) This procedure makes inspection setup and data taking extremely slow and tiresome. Continuous wave (CW) systems have largely been used for Lamb wave inspection as they have the advantage that only a narrow bandwidth is required for reception. Unfortunately, CW systems introduce the disadvantage of standing wave effects.

To minimize these effects and facilitate setup,we have incorporated into our Lamb wave system: (1) a swept-frequency transmitter operating in the range of 2 to 25 MHz and (2) a heterodyning receiver which compares the received signal with the transmitted signal. The swept-frequency approach discriminates against standing waves, facilitates setup as frequency is not a parameter, and allows several Lamb wave modes to be simultaneously viewed in an amplitude versus frequency plot similar to that achieved with a spectrum analyzer. Thus it is possible to observe simultaneously the response of several modes to the same defect or discontinuity. By heterodyning the received signal with the transmitted signal, a difference frequency is obtained which is dependent upon the transit time of the Lamb wave through the sheet. Generally, this difference frequency is in the upper audio range. This is a very desirable feature for the detection of weak signals because it permits considerable bandwidth reduction. It also allows for the discrimination of signals due to spurious reflections.

Initially testing is normally performed in an immersion tank such as shown in Figure 3, because of the capability of being able to vary at will both transducer separation and angle of incident. For certain applications, a variable angle hand scanner, Figure 4, or a fixed angle hand scanner, Figure 5, can be used to overcome the water loading effect of the immersion test. A scanner for on-line work which features liquid filled rubber tires (for housing the transducers) and adjustable angle and separation distance is shown in Figure 6.

Figures 7a and 7b illustrate Lamb wave propagation in zirconium both in the direction of rolling and perpendicular to the direction of rolling. This data was taken from a .018" thick sheet of pure zirconium that had been annealed at 1250°F for two hours after rolling. Note the amplitude reduction of the two highest frequency modes (which are the 3A mode at 10.8 MHz and the 3S mode at 13.7 MHz) when the sample is inspected perpendicular to the direction of rolling. Figures 8a and 8b illustrate the effect of a laminar inclusion on Lamb wave propagation. This data was taken from a .028" sheet of titanium which contained small foreign inclusions which became laminar defects after rolling. Note the frequency shift and mode conversion occurring at the mode directly to the right of the 10 MHz marker.

Figures 9a and 9b illustrate the effect of lack-of-bond on Lamb wave propagation. The bond line being inspected was generated by rolling a .005" sheet of pure columbium between two sheets of zircaloy. The resultant structure was .080" thick,and the bonding defect has been verified by radiography. Note the loss of amplitude due to a poor bond and the apparent mode conversion.

The inspection and evaluation of thin sheet poses many unique problems not encountered with thicker materials. First, the inspection area per volume of material is large, requiring extensive scanning. If the inspection is accomplished at the mill, this must be done at high speeds with high response systems

in order that corrections or repairs can be made. The thinness of the material renders many of the approaches normally used ineffective or susceptible to variations proportional to thickness. In fact, some schemes take advantage of this effect to provide a measure of thickness; eddy current, gamma ray and beta backscatter gaging systems being typical. Voids or inclusions normally detectable by ultrasonic techniques are unperceptible at the operating frequencies of commercially available equipment. While these can be detected by nuclear radiation devices, the requirement for the high speed inspection of large areas presents many problems. FM Lamb waves, on the other hand, are capable of permitting flaw detection in thin sheets with a minimum amount of time per unit area and with a minimum number of sensors.

Dynamic Infrared Inspection

The basic concept of infrared inspection is predicated on the fact that flaws and defects within a body change the thermal characteristics of the body. If heat flow exists in the body and various other conditions are proper, this thermal characteristic change will manifest itself as a surface temperature difference or gradient. In other words, the body will exhibit a different thermal radiation signature if it contains flaws than it would if it contained no flaws. A high speed scanning infrared detection system can then sense these gradients or signatures and convert them into electrical signals which can be recorded and interpreted.

The important point to remember, however, is that heat flow must be present for infrared methods to detect flaws in materials and structures. This heat flow can be achieved either by action within the flaw or by injecting heat from an external source. These heat flow generation methods are known respectfully as passive and active systems. Some techniques which have been used or considered for heat injection sources are: (1) hot air jets, (2) plasma jets, (3) direct flames, (4) inductive heating coils, (5) contacting tape heating coils, (6) infrared and arc lamps, and (7) lasers.

Under contract[18, 19] to Air Force Flight Dynamics Laboratory, the General American Research Division has developed an automated infrared system for detecting surface or near surface fatigue cracks to be used in the Air Force Sonic Test Facility at Wright Patterson Air Force Base. This facility is capable of subjecting large aircraft or missile structures to the intense sound fields experienced in actual flight or launch. One of the primary instrumentation requirements of the facility is a noncontacting, nondestructive inspection system capable of rapidly locating, in real time, the position and extent of flaws or cracks which develop in the experimental structure during the course of the test. Earlier we had successfully applied IR techniques to the detection of voids and flaws buried in rubber and plastic structures. While metals, due to their higher thermal conductivity, present a much more difficult problem (as the rate of heat flow is faster and the thermal gradients that develop are smaller), analytical studies indicated that IR techniques should be applicable to the thin-metallic skin type

of construction normally used in aircraft and missiles. Analytical studies also showed that the amount of heat generated by an incident or propagating crack in metallic aircraft or missile structures was not sufficient in most cases to create a significantly different thermal signature. Therefore, the heat injection method, or active system, was chosen.

The best infrared detection method was found to be a system which injected heat into a small area or spot on the skin surface by means of a radiant heat source and which then measured the resulting temperature rise of the surface at or near that spot with a radiometer. To facilitate the rapid inspection of an aircraft structure, the source and radiometer spots are optically scanned in synchronism over a 10 x 10 degree field. Figure 10a shows schematically a plan view of a specimen with a fatigue crack being scanned by this technique and Figure 10b shows the resultant temperature versus position profile obtained for one scan.

By scanning at constant velocity, each point on the surface receives the same amount of energy over the same period of time. Therefore, the rise in surface temperature due to the injected energy will be the same unless something happens to disrupt the thermal characteristics of the surface. A fatigue crack open to the surface or near the surface will cause just such a perturbation of the thermal characteristics. As the heat source spot approaches the fatigue crack, heat flow away from the spot area will not be omnidirectional - the crack represents a restriction to heat flow. Therefore, the surface temperature will rise rapidly as the heat injection spot approaches the crack. This is shown graphically in Figure 10b. With the source and radiometer spots concentric as shown in Figure 10a, the surface temperature should theoretically drop back down to the level for "sound" material when the heat spot is centered over the crack because now heat flow is once again omnidirectional. And when the heat spot is just to the right of the fatigue crack, the surface temperature rises again because heat cannot flow back through the crack. This is shown graphically in Figure 10b, by the dotted lines. In practice, this effect is seldom observed - the actual measured temperature is more like the solid line. The primary reason for this is the resolution of the heat source and radiometer spots; they are of finite size and, therefore, some averaging is achieved. Also high scanning rates have a tendency to "smear" the temperature profile.

It should be pointed out that different effects can sometimes be achieved if the radiometer spot is located either ahead or behind the heat source spot. The best location depends upon scanning speed and the properties of the material being inspected. By performing multiple line scans an area of the specimen surface can be inspected. By employing a facsimile recorder of the type often used for ultrasonic scanning, a C-scan record of surface temperature changes versus x-y coordinates can be obtained which will graphically display the extent and location of fatigue cracks.

This technique of inspecting an area with moving source and radiometer spots has been termed dynamic infrared inspection by Levine and Johnson[20]. Maley[21] has also used the technique to inspect thin coatings for cracks and bonding defects and honeycomb composites for bonding.

Figure 11 illustrates shcematically the significant features of the infrared system for detecting fatigue cracks, and Figure 12 shows the actual system which was developed for the USAF.

Figure 13 is a 2X photograph of a .090 inch thick aluminum panel with fatigue cracks emanating from a 3/8 inch diameter hole. The location of the source and radiometer spots and the direction of scan are also shown in Figure 13. This particular orientation of the source and radiometer spots was chosen to illustrate several effects on the same test piece. Figure 14 is a 2X photograph of the facsimile recorder output for this specimen. There are several interesting points to note in Figure 14. Probably the most intriguing is that one of the cracks showed up lighter than "sound" material, and the other showed up darker. This effect is due to two factors: (1) the relative position of the radiometer spot with respect to the source spot and (2) the direction of scan relative to the inclination of the crack. Referring back to Figure 13, it can be seen that for the positive sloped (running from the third quadrant up to the first) crack, the radiometer spot crossed the crack ahead of the source spot. In so doing, the infrared detector "sees" a temperature change from that corresponding to "sound" material (because the source spot isn't close enough to the crack to cause a temperature rise) to a lower temperature (because the material on the other side of the crack has not as yet received any heat). Because our radiometer electronics performed a differentiation of the detector signal, this change was detected as a negative-going change and thereby printed lighter than the "sound" areas did. For the negative sloped (running from the second quadrant down to the fourth quadrant) crack, the radiometer and source spots cross the crack at approximately the same time. Under this condition, the infrared detector "sees" a temperature rise, the electronics interpret it as a positive-going change, and the result is an indication darker than that for "sound" material. The dark area following the hole (the white area) is due to the electronics being saturated by a large positive going signal at the top edge of the hole. This same effect is observed at the ends of a specimen. Changes in the electronics would minimize this effect.

Dynamic infrared inspection is capable of detecting and locating fatigue cracks in the metallic skin of aircraft and missile structures. However, in its present state of development the technique is limited to surface or near surface defects such as fatigue cracks. In lower conductivity materials, of course, the method will respond to defects further below the surface. In addition, the resolution of the system is not as yet maximized. The system as developed for the USAF will detect surface cracks that can also be found optically with a little magnification or by dye penetrants. Subsurface cracks that can be found with

this system can also be detected with eddy currents. Of course, none of these other methods are consistent with the requirements of the Sonic Test Facility for which this equipment was developed. However, this comparison with other techniques does illustrate the present capability of the technique.

The present capability is far from the ultimate which can be reached with the technique. With the rapid advances being made in gas lasers, the use of a CW laser in place of the arc lamp is an improvement worth investigating. Because of the laser's inherent high degree of collimation and higher energy density, the resolution of the present system can be increased. An added advantage of the laser that must not be overlooked is its capability to inject heat from longer distances. Just imagine the potential of a technique which could inspect a structure for defects from a distance of 30 feet of more.

The technique, of course, has applications other than the detection of surface or near surface fatigue cracks in this metals. In low conductivity materials, such as rubber, plastics, wood, and bonded fibrous materials, its advantages are particularly attractive for detecting debonds or buried voids or flaws. However, with the rate that power levels of gas lasers are being increased, it is also easy to visualize the technique becoming useful in more massive metal structures in the near future. Its inherent advantages of being noncontacting, and capable of permanent and instant record output are often (as was the case with detecting fatigue cracks in a sonic environment) just what the engineer or researcher requires in a NDT method.

REFERENCES

1. Lamb, Horace, On Waves in an Elastic Plate, Proc. Royal Society, London, A93, 114 (1917).

2. Firestone, F. A., and Ling, D. S., Report on the Propagation of Waves in Plates - Lamb and Rayleigh Waves, Sperry Products, Inc. Technical Report 50-6001 (1945).

3. Worlton, D. C., Ultrasonic Testing with Lamb Waves, HW-45649 (1956).

4. Worlton, D. C., Lamb Waves at Ultrasonic Frequencies, HW-60662 (1959).

5. di Novi, R. A., Theory of Lamb Waves, Symposium on Physics and NDT, ANL-6346 (Oct. 1960).

6. di Novi, R. A., Status Report on Lamb Waves, ANL-6329 (March 1962).

7. Worlton, D. C., Experimental Confirmation of Lamb Waves at Megacycle Frequencies, Symposium on Physics and NDT, ANL-6346, Oct. 1960.

8. Worlton, D. C., Thickness Measurements with Lamb Waves, Nondestructive Testing, 20, 2, (1962).

9. di Novi, R. A., Lamb Waves: Their Use in Nondestructive Testing, ANL-6630, March 1963.

10. Beauyard, L., Collette, G., and Drolut, C., The Effect of Dispersion and Velocity of Propagation of Lamb Waves during the Ultrasonic Testing of Mild Steel Sheet, Brit. J. of Nondestructive Testing, 1, 1, 50 (1959).

11. Grisby, T. N., and Tajhman, E. J., Properties of Lamb Waves Relevant to the Ultrasonic Inspection of Thin Plates, IRE Transactions on Ultrasonic Engineering, UE-8, 26 (1961).

12. Sawyer, W. A., Ultrasonic Testing of Thin Wall Zircaloy Tubing, Canadian General Electric Company Limited, Report No. R61CAP9 (1961).

13. Schmitz, G., Wieczorek, A., and Levine, M., Development of NDT Methods for the Evaluation of Thin and Ultra Thin Sheet Materials, ML TDR 64-278,

14. Wieczorek, A., and Schmitz, G., Development of NDT Methods for the Evaluation of Thin and Ultra Thin Sheet Materials, AFML-TR-75-320, Sept. 1965.

REFERENCES (Continued)

15. Kubiak, E., Hosek, R., Lichodziejewski, W., Development of NDT Methods for the Evaluation of Thin and Ultra Thin Sheet Materials, AFML-TR-66-304, July 1966.

16. Kubiak, E., and Frank, L., NDT Methods Development for the Evaluation of Thin and Ultra Thin Sheet Materials, Contract AF 33(615)-3567, Final Report to be released July 1967.

17. Wieczorek, A. B., Inspection of Thin Sheet Using Lamb Waves, 5th Symposium on Physics and NDT, Sept. 1965.

18. Shmitz, G., Levine, M., Investigation of Fatigue Failure Detection Systems Using Infrared Techniques, RTD-TDR-63, 4293, Oct. 1964, USAF Contract AF 33 (657)-8828.

19. Kubiak, E. and Frank, L., Development of Laboratory Model Fatigue Crack Detection Device Based on Infrared Techniques, AFFDL-TR-67-39, April 1967.

20. Levine, M. B., Johnson, B. A., Dynamic Infrared Inspection Techniques, 4th International Conference on NDT, London, England, September, 1963.

21. Maley, D. R., Maley, S. W., Applied Research to Establish Infrared Detection Methods for Nondestructive Analysis of Metallic and Ceramic Structures, ASD-TDR-62-385, March 1964.

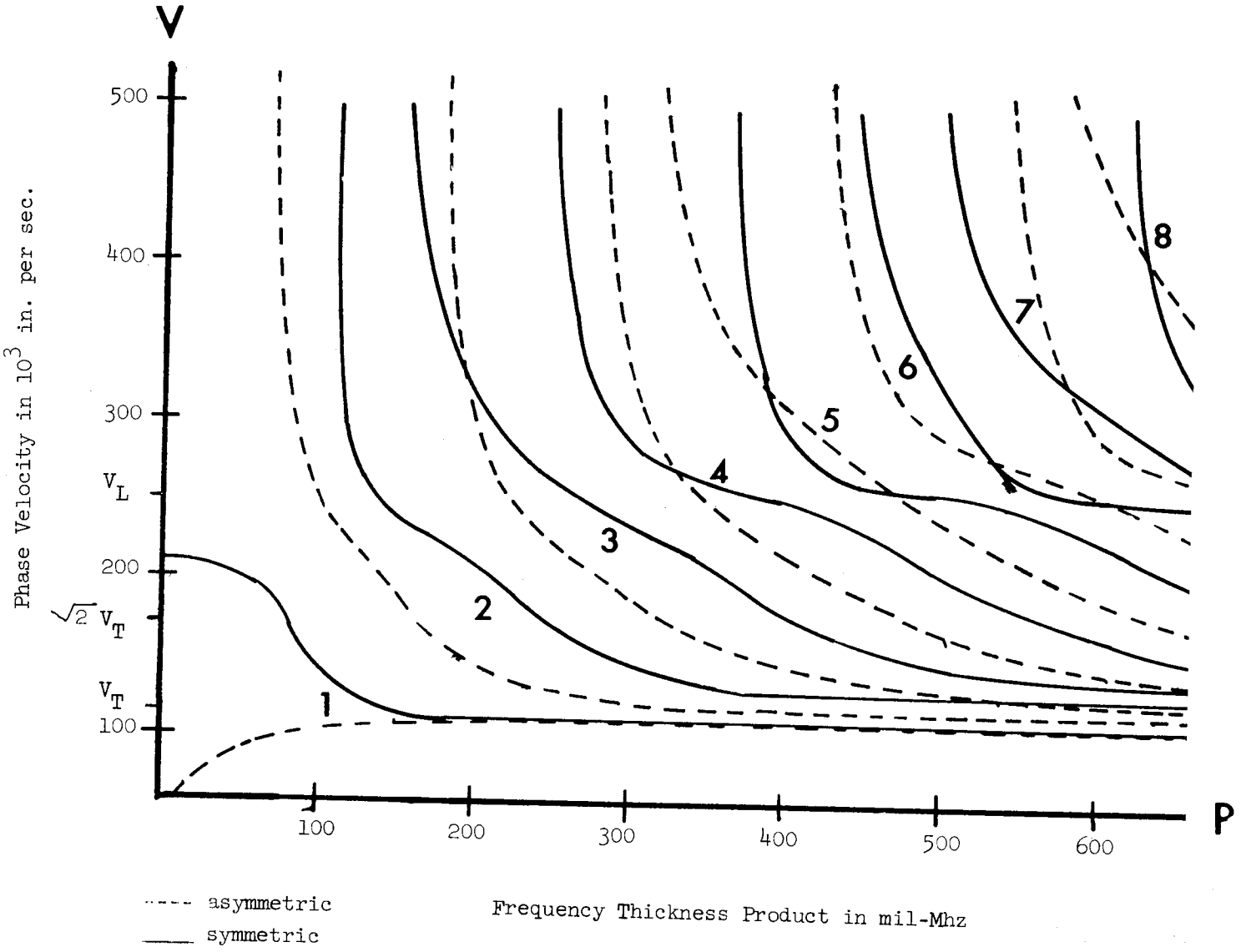

Figure 1 LAMB WAVE SPECTRUM IN ALUMINUM

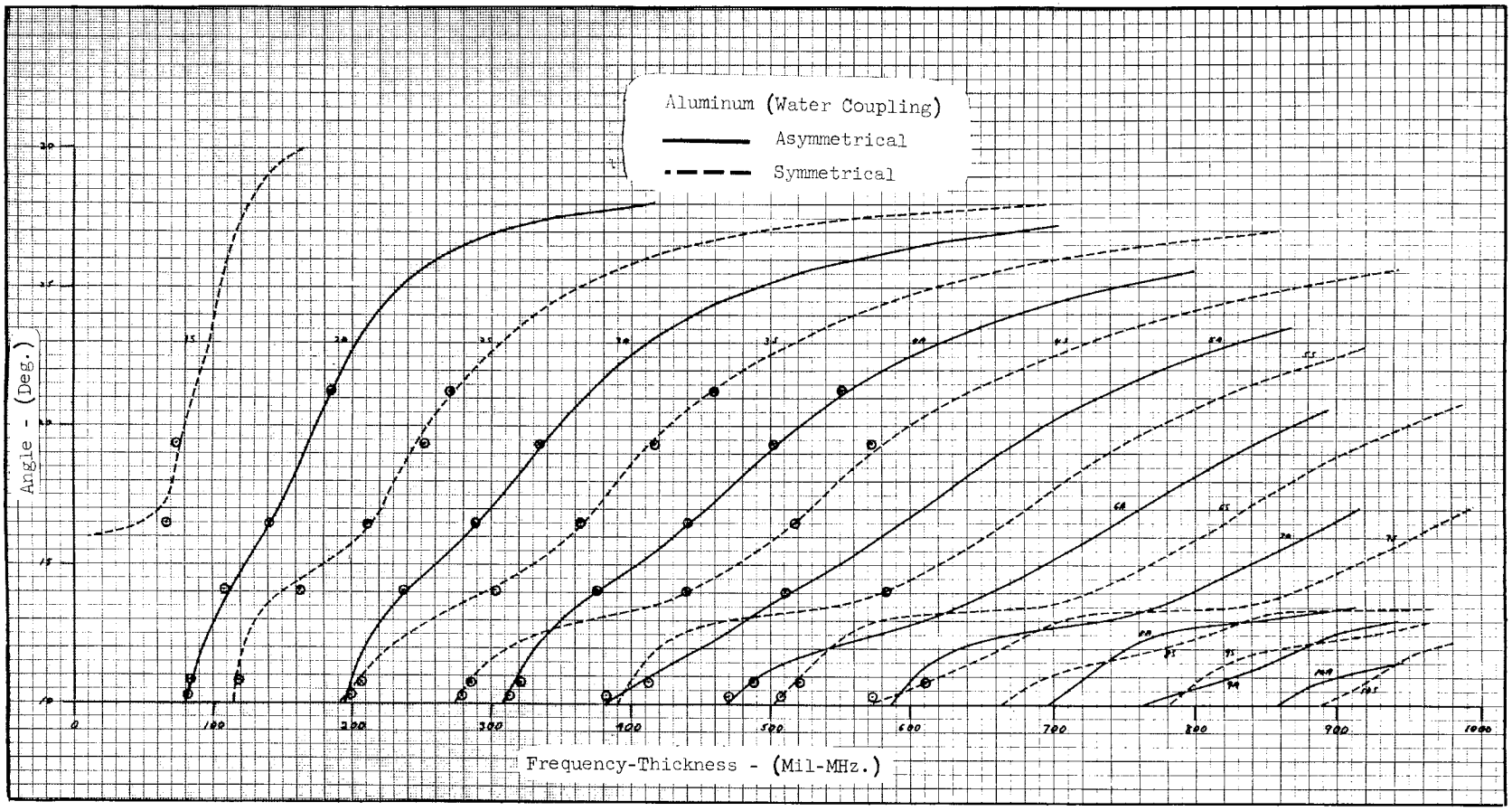

Figure 2 LAMB WAVE MODE IDENTIFICATION IN ALUMINUM

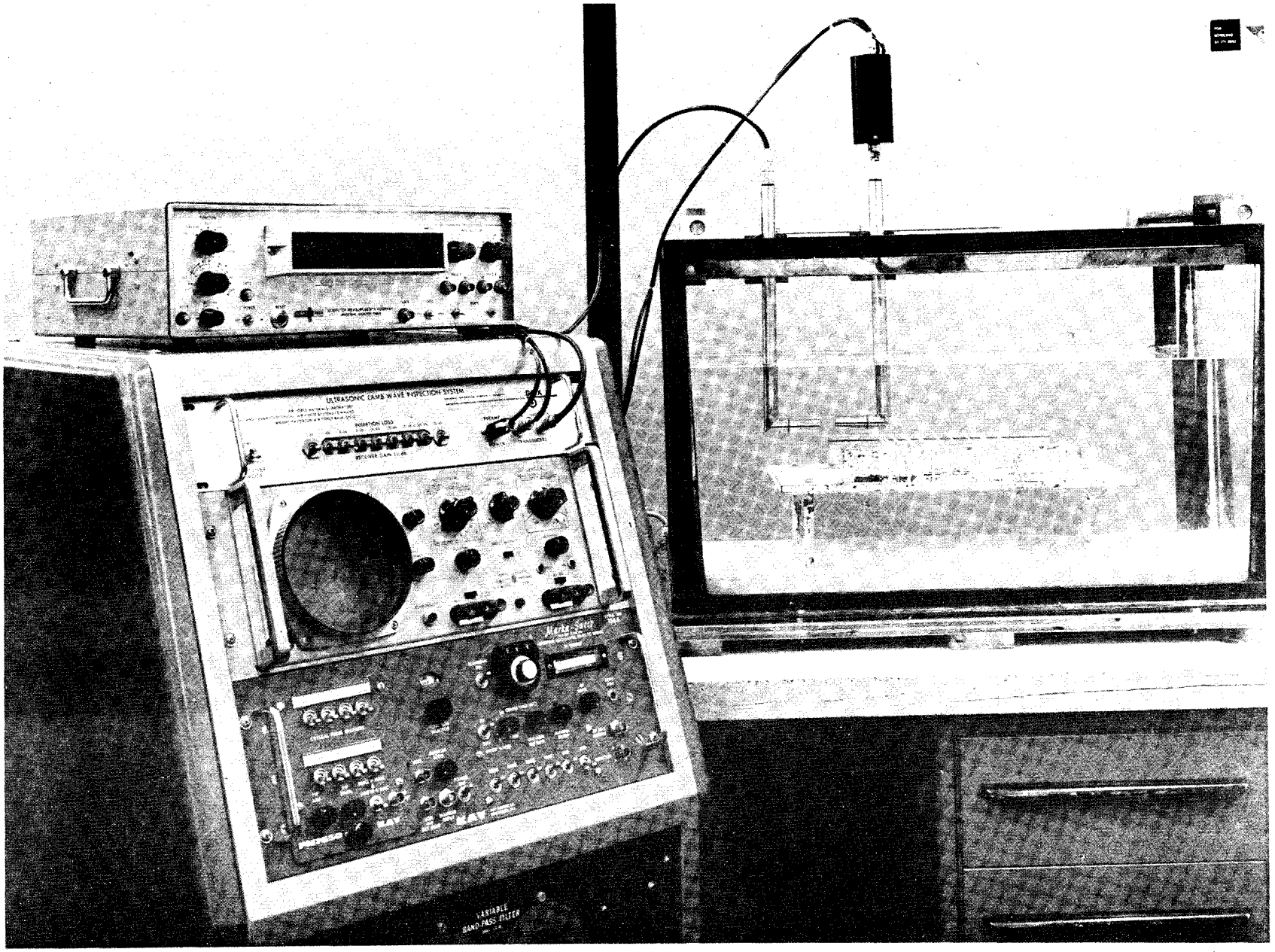

Figure 3 FM LAMB WAVE INSPECTION SYSTEM

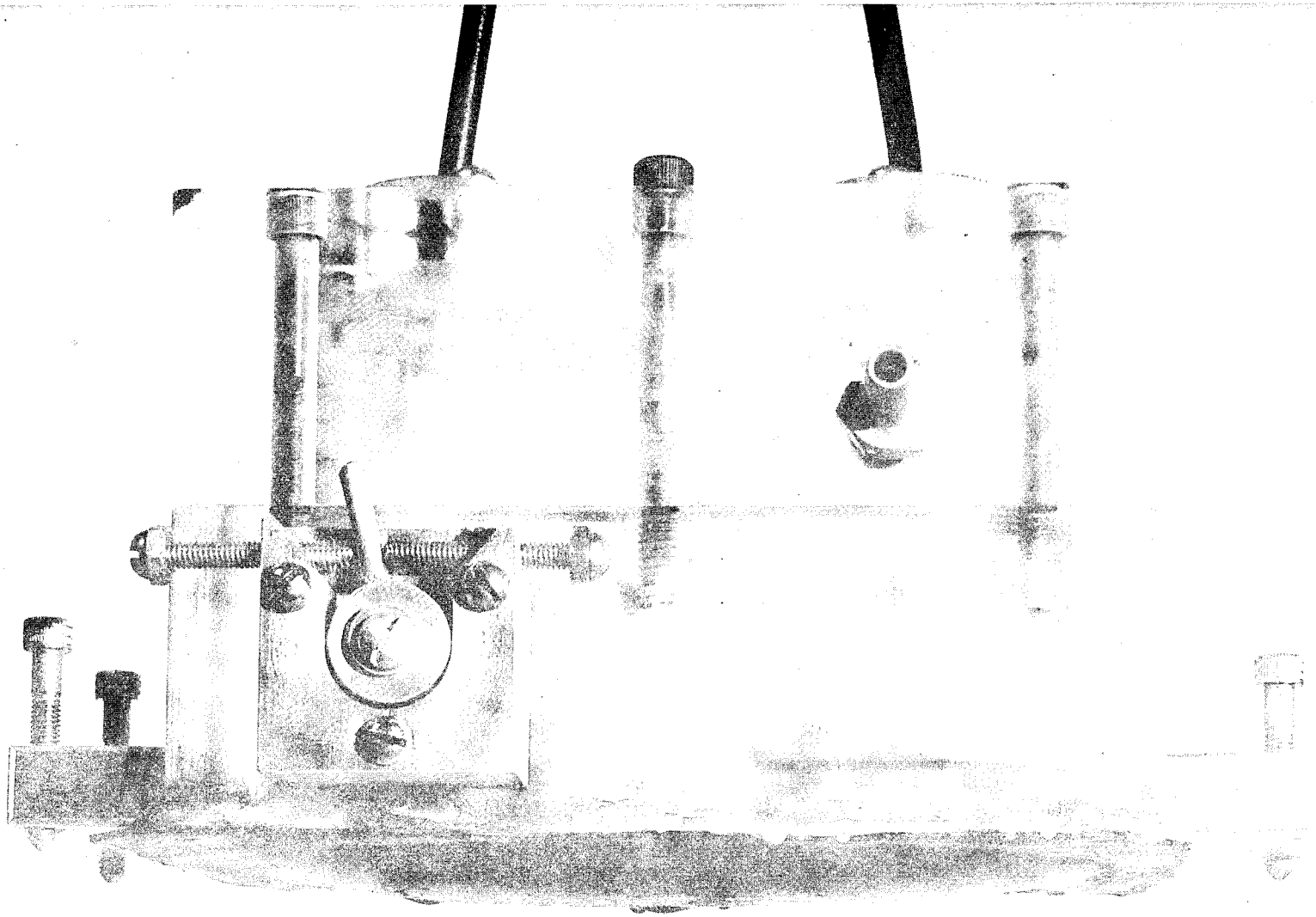

Figure 4 VARIABLE ANGLE HAND SCANNER

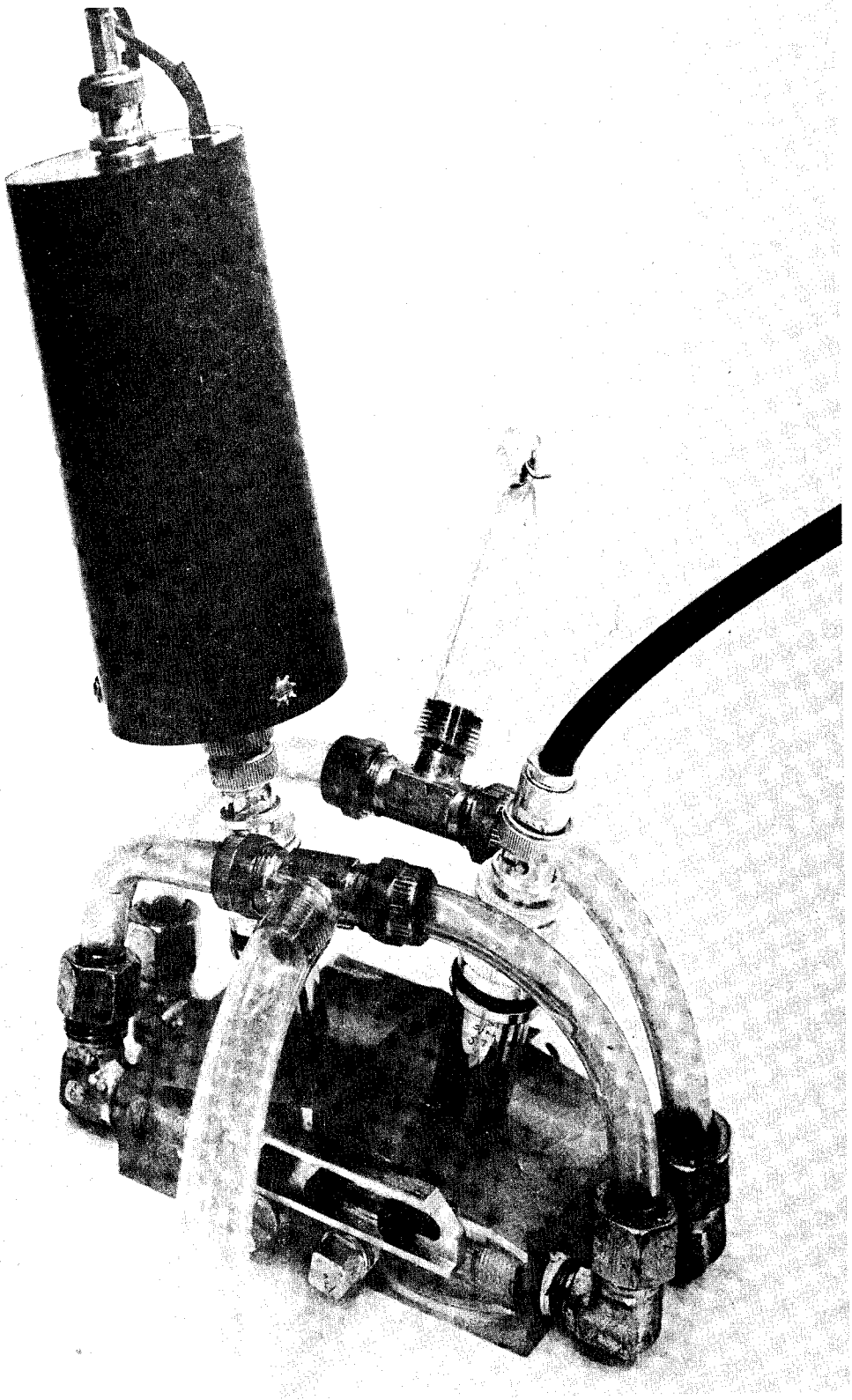

Figure 5 FIXED ANGLE HAND SCANNER

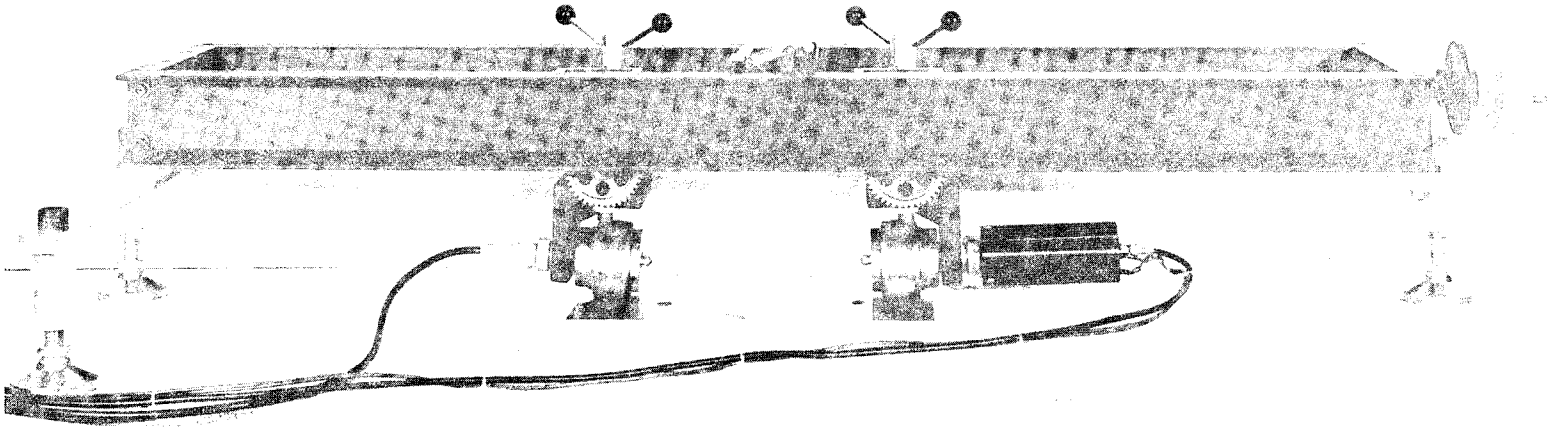

Figure 6 RUBBER TIRE SCANNER WITH ADJUSTABLE ANGLE AND SEPARATION DISTANCE

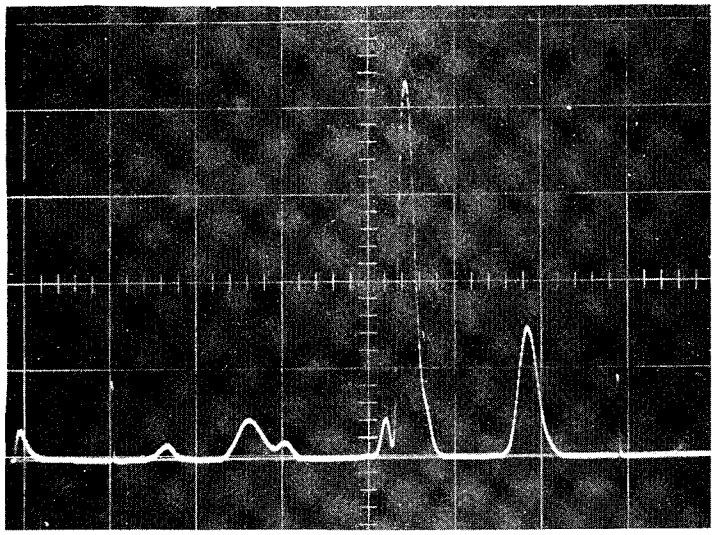

a) Direction of Rolling

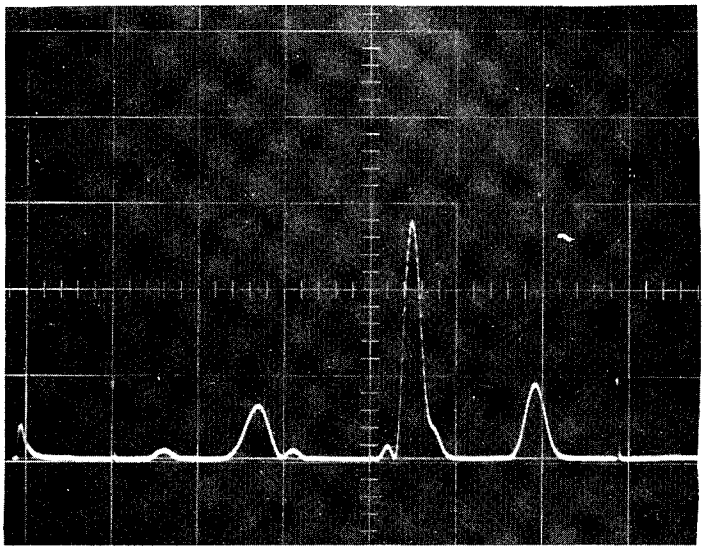

b) Perpendicular to the Direction of Rolling

2 MHz 16 MHz

Figure 7 LAMB WAVE RESPONSE DUE TO DIRECTION OF ROLLING (.018" Zirconium sheet)

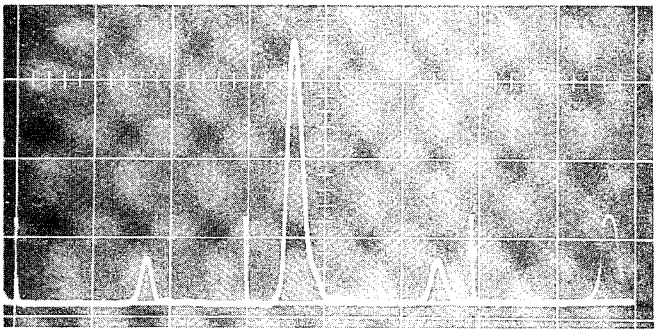

a) Defect free area

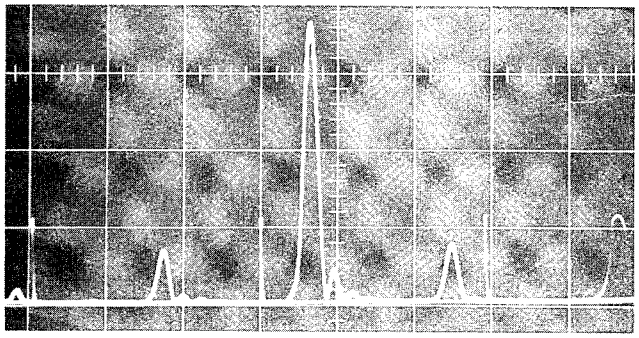

b) Laminar inclusion

4 MHz 10 MHz 16 MHz

Figure 8 LAMB WAVE RESPONSE DUE TO PRESENCE OF DEFECT (.028" Titanium)

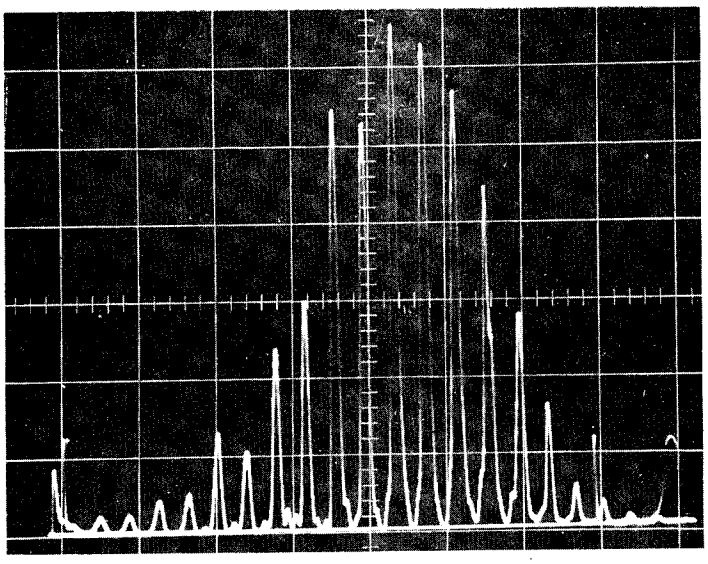

a) Good bond

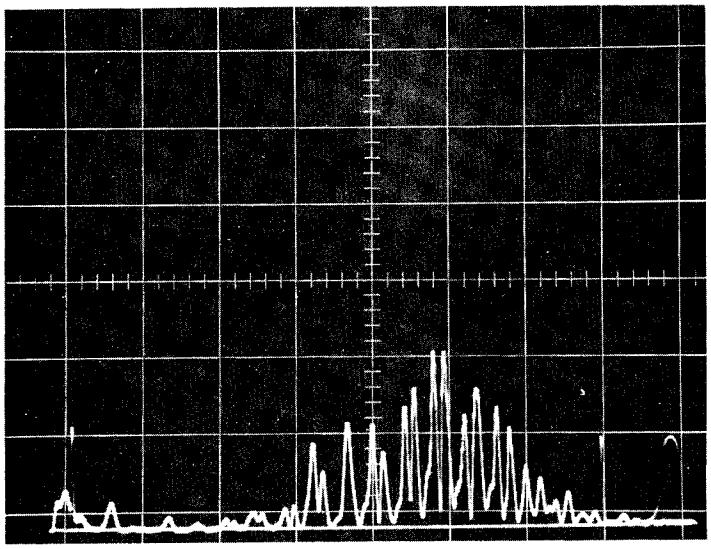

b) Poor bond

2 MHz 16 MHz

Figure 9 LAMB WAVE RESPONSE DUE TO LACK-OF-BOND (Zirconium)

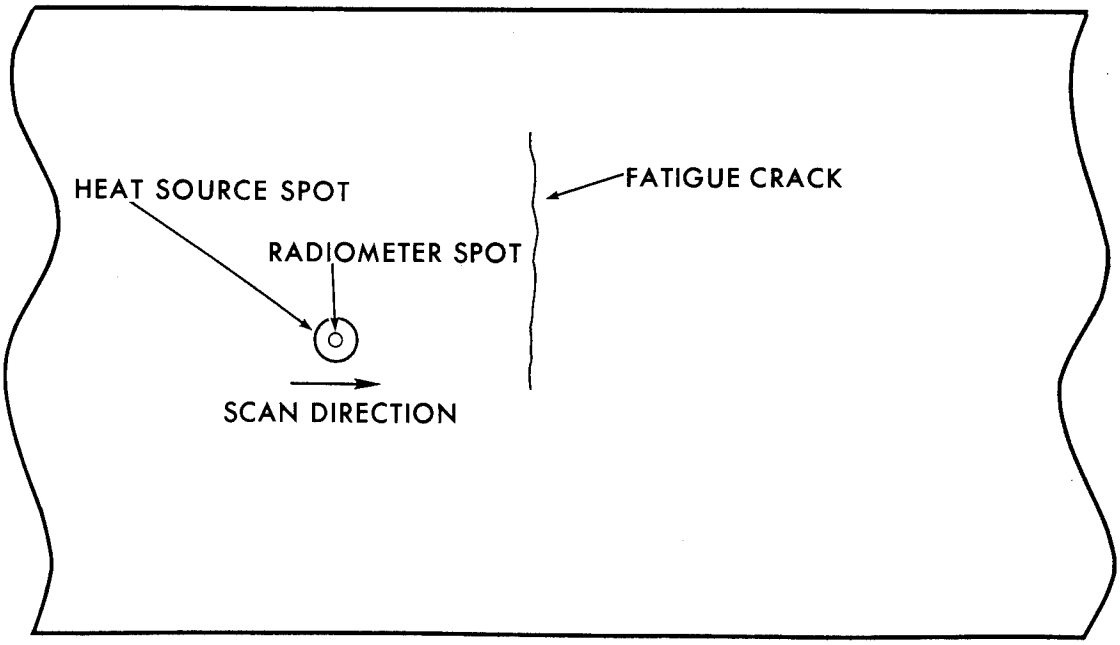

a. Plan View of Specimen Being Scanned

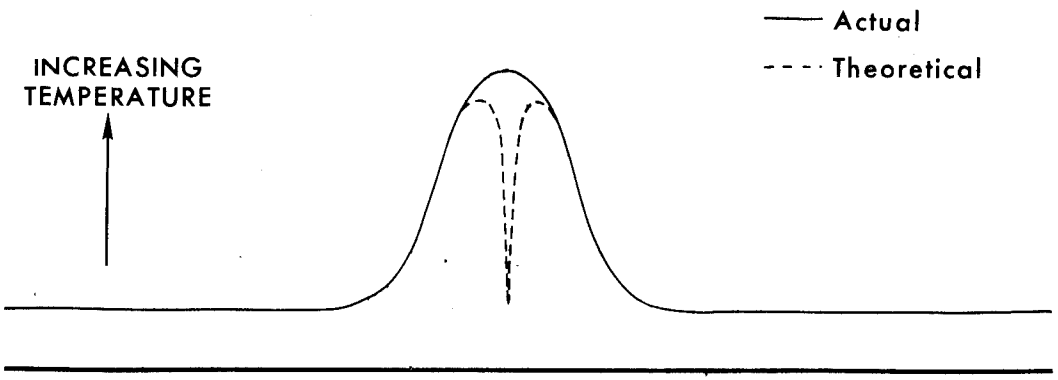

b. Surface Temperature vs. Position

Figure 10 MOVING HEAT SPOT GEOMETRY AND RESULTANT TEMPERATURE PROFILE

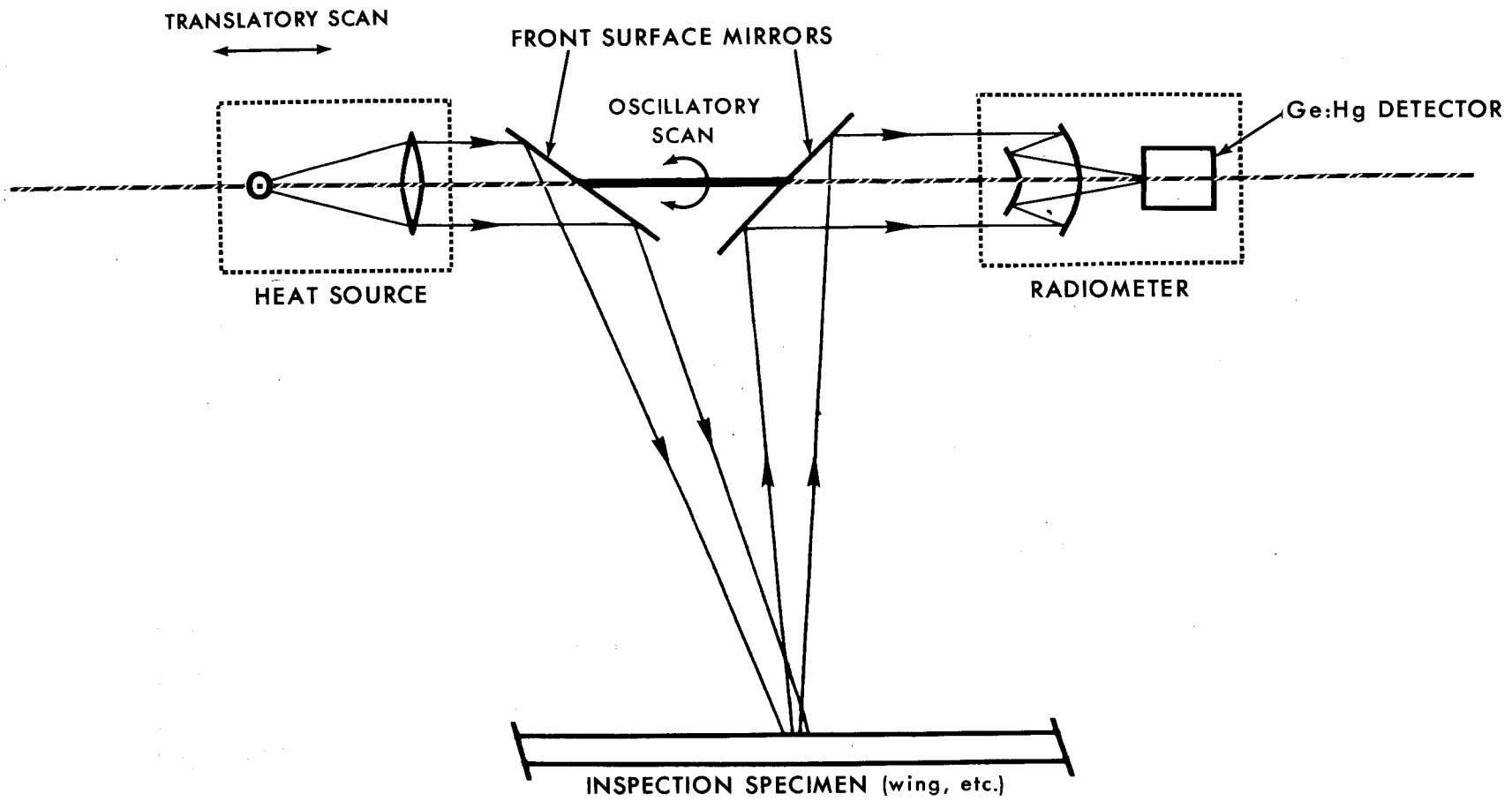

Figure 11 BLOCK DIAGRAM OF DYNAMIC IR SYSTEM

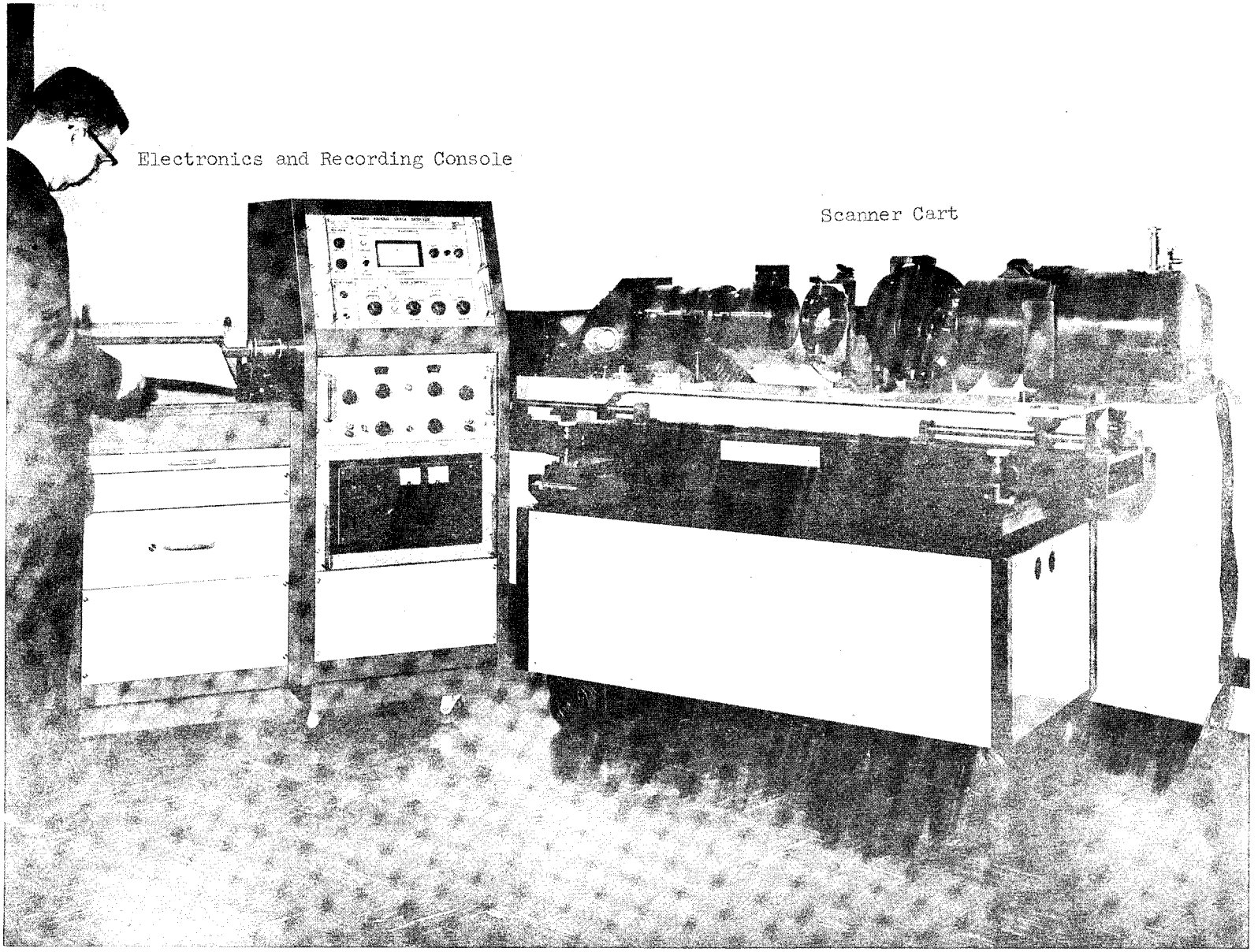

Figure 12 PHOTOGRAPH OF ACTUAL SYSTEM

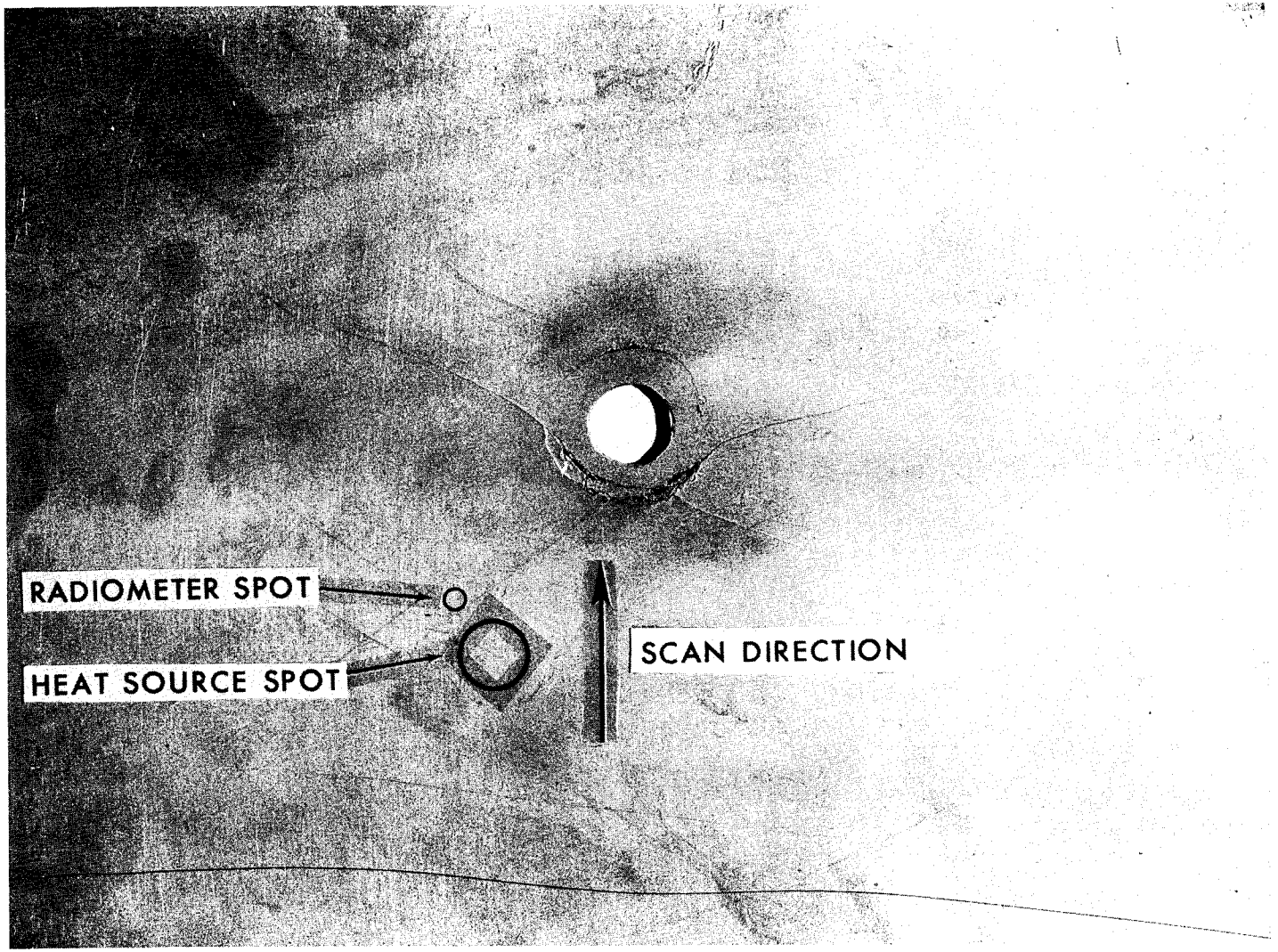

Figure 13 2X PHOTOGRAPH OF FATIGUE CRACKS AROUND HOLE

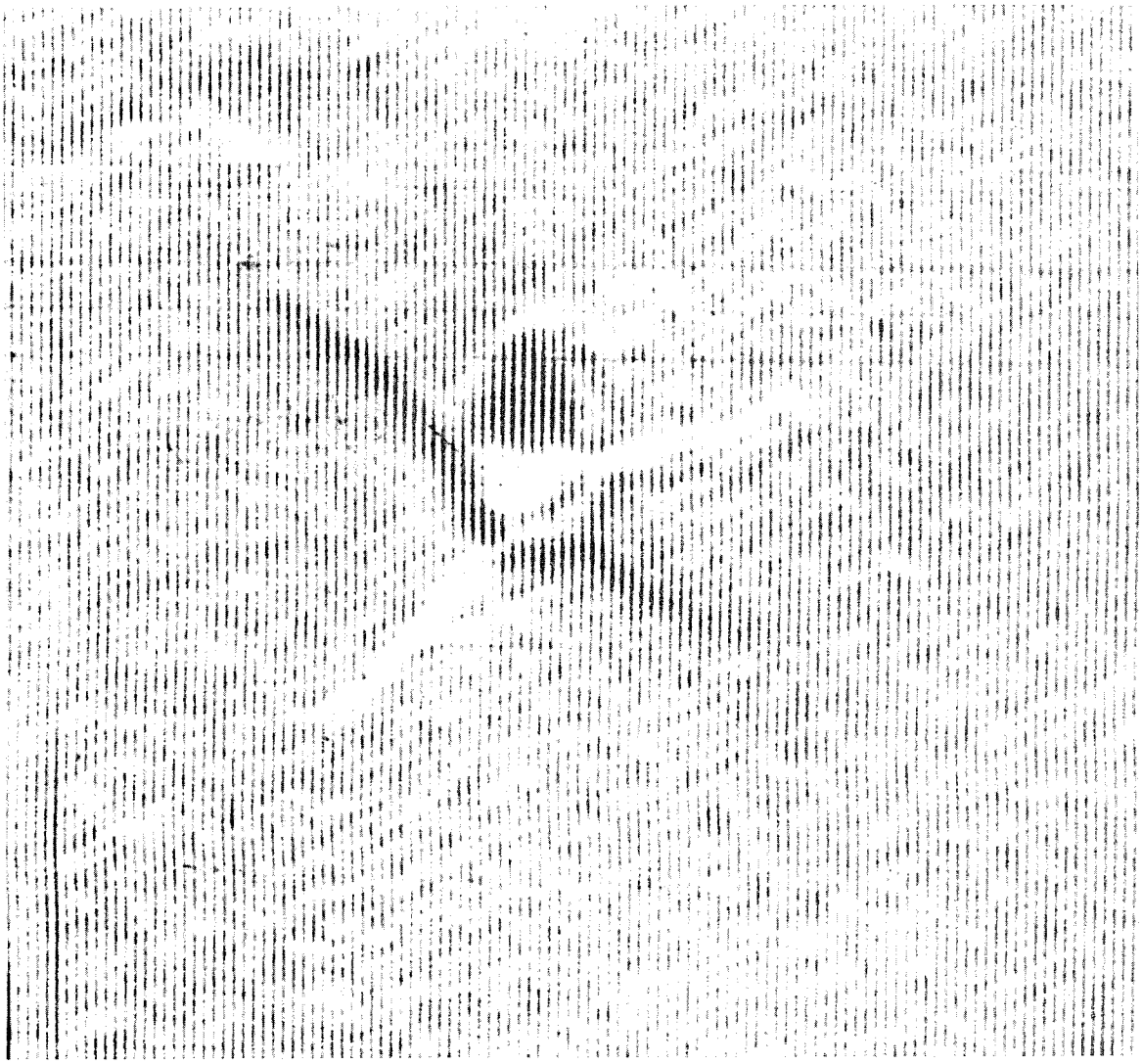

Figure 14 2X PHOTOGRAPH OF C SCAN RECORD FROM FACSIMILE RECORDER

PART I - A COORDINATIVE EFFORT TO SOLVE INDUSTRIAL N.D.T. PROBLEMS IN GREAT BRITAIN

and

PART II - A 31 MEV BETATRON STUDY OF THE PRODUCTION OF HIGH INTEGRITY STEEL CASTINGS

A. Nemet

Anthony Nemet Company

Richmond, Surrey, U. K.

Prior to 1955 there were two Societies exclusively concerned with non destructive testing in Great Britain, two further Societies which had main divisions concerned with this technique and some twenty other larger and smaller Institutions and Societies with a marginal interest. In that year, the first International Conference of N.D.T. was held in Brussels which ended in a resolution to delegates, asking them to take appropriate steps in their respective countries to set up a representative body, i.e. a National Committee, so that this single body should be empowered to co-ordinate the national effort and to negotiate and handle all international matters. As a result of this resolution the British National Committee for Non-Destructive Testing was formed in the summer of 1957. Subsequently, more than twenty Societies have taken up membership. All major engineering institutions are members.

The British National Committee is charged to promote discussions, to assist a co-operating Institution or Society in the presentation of N.D.T. papers and to undertake all international matters such as the nomination of members of the Standing Committee for International Co-operation. It meets five times a year and has turned out to be a really active body, the real drive coming, of course, from the four Societies intimately concerned with N.D.T. These are: The Society of Non Destructive Examination, The Non Destructive Society of Great Britain, The Institute of Physics and Physical Society and the Institution of Engineering Inspection. Apart from the activities mentioned, the British National Committee has set up a number of Panels, such as the Advisory Panel on Co-operation, the Advisory Panel on Education and Training, and the Working Party on the Needs of Industry. I am particularly

2./

concerned with this last named, and I want to say something about its origin and about our activities.

It was felt for some years that user industries - and this goes for both steel and aluminium constructors and foundries - have many non destructive testing problems which are insufficiently catered for by the equipment manufacturers. Some of these may well have been already solved, or on the way to be solved by one of the many laboratories, research departments or institutions somewhere in the country, about which there may be little or nothing known to the industry concerned. The first Working Party early in 1963, began by interviewing representatives of user industries and collected a considerable amount of material in the form of unsolved problems. It soon became clear that it was necessary to limit one's activities in various directions to avoid dilution of work, in particular, one was guided by the following three general considerations: Firstly, the problem had to be of interest to a number of firms or industries. Secondly, problems which were already well on the way towards a solution somewhere obviously did not need to be considered beyond putting the user interested in contact with the research centre concerned. And thirdly, one had to avoid fairly basic or fundamental research in order to make a real impact on the problem in a useful space of time. That is to say that the principles and the technology involved had to be fairly clearly known. Finally, activities which were important in themselves, but which had wider implications, far beyond the direct interest of the Working Party, were not considered as they were progressed by other bodies already. These included Codes of Practice, Standardisation, Acceptance Standards and Education. Direct consultancy service, that is to say, the solution of specific, narrower problems were also left out. Eventually, the following terms of reference for the Working Party have emerged: "The Working Party has firstly to decide that a problem exists and it is a common one in industry; secondly, it has to assess the state of existing knowledge; thirdly, to ascertain what information is still required and lastly, to review means of directing this information to the channels most appropriate to help in the solution of the problem. "

You can see from this that we had to steer a straight and narrow path between going after too much, which would have made us ineffective, and between just talking around a problem, bearing in mind that we are not a laboratory and cannot actually solve the problem by direct experiments or design. We have, however, collected

3./

a number of experts in the Committee - we are now fifteen people - who are sufficiently well connected in research and industry so that one can say that, after the problem had been thoroughly thrashed out by the Working Party, one had a pretty good idea who was working on a similar sort of task, how far he had got, and what he should do to solve the problem in question. Moreover, we can bring some gentle propaganda to bear on the people of the Laboratory or Research Association concerned and encourage them to take up contact with the industry interested and perhaps shape their work accordingly. This we do by various means, depending on the case. We either invite people to our meetings who have the problem together with representatives of laboratories who do such work, or we ask one of our members to call a specific meeting of invited representatives of industry and laboratories to discuss the question thoroughly.

In some cases, we have felt that, in spite of all the N.D.T. activity going on in the country, there was a need for a specific National Laboratory to investigate problems which are capable of solution by direct research, not otherwise catered for and to undertake longer term N.D.T. research. Over a year ago, therefore, the British National Committee have entrusted our Working Party to formulate the need for a British National Laboratory for Non Destructive Testing and I am glad to say that, after about a year's consideration, the Government agreed to this suggestion, through its Minister of Technology. It has now authorised the United Kingdom Atomic Energy Establishment at Harwell to widen the terms of reference of its Non Destructive Testing Laboratory to become a National Centre for N.D.T. I am very pleased to say that the head of this laboratory, Mr.R.S.Sharpe, is with us and is contributing a paper to this Conference.

After all this you may want to hear about some of the concrete problems with which we are concerned at the moment and what we are doing about them.

Well, there is the problem of speeding up ultrasonic scanning examination of large metal surfaces. Mr.F.Bareham of Aluminum Laboratories Ltd. organised a one day meeting on the speed of ultrasonic scanning. The Proceedings of this are being evaluated at the moment. Secondly, the field distribution of ultrasonic waves in various materials is being studied by the new National N.D.T. Centre

4./

Thirdly, X-ray fluroscopy of thick materials with a betatron and an image intensifier has been reported by Mr.R.Halmshaw - who is also with us at this Conference - and work has been put in hand as a result of this to develop screens which are more efficient for high energy X-radiation.

Further, the coupling of ultrasonic probes to hot surfaces has occupied the Working Party for a considerable time. This problem has come to us through the Oil Companies' Materials Association who are concerned with on-line testing of pipe welds, and corrosion testing of welds and pressure vessels. This problem can be conveniently split into two, that is to say up to about 600°C which is of interest to oil companies, power generating plants, etc. and from 600 to about 1100-1200°C which is of interest to steelmakers. We found that there is a great deal of interest in this particular problem, but little work has actually been done. We found some U.S., some Japanese[1] work, some work originating from the French Iron and Steel Research Establishment[2], some work in our own country carried out by the United Steel Companies[3]. After some deliberations we decided to hold a one-day symposium, and this took place on the 18th April. One of the difficulties was to limit the audience to such people who can actively contribute in the discussion from first hand experience, and who have direct interest in the problem, as the general interest is very wide. Here again the proceedings are being evaluated and, although there was a certain amount of reticence - due to commercial secrecy - of revealing experimental data, we feel that an open symposium helped all concerned in progressing towards the solution. The proceedings will be published, probably as separate papers.

A further problem is concerned with the examination of adhesive bonds between metals and non-metals. Eventually it was agreed that this could be part of a general conference on this subject which was held in the City University in London on the 5th and 6th April entitled "Fifth Annual Conference on Adhesion and Adhesives". The proceedings are to be published by University of London Press.

Another problem concerns the difficulties in ultrasonic examination of large grain columnar materials. This is a fundamental long term one and it will be attacked, we hope, in the new National Centre and perhaps also by the British Steel Castings Research Association.

Another problem brought to us is the detection and assessment of corrosion pitting. This is the concern of the oil companies and also of aircraft manufacturers. We have our teeth in this problem. We cannot say that we have chewed it yet. One of our

members has been entrusted with the organization of a conference on magnetic sub-surface defect detection. This reviewed several methods such as magnetic crack detection and magnetography. They issued a preliminary report and the work will have to be further progressed.

We held a one-day conference last November on :"Correlation of Tests, Defects and Service Life." This we did because it was felt in the National Committee that insufficient work was being done to follow up service experience on engineering parts which have failed after a known lifetime.

We were groping a little wildly through this difficult problem as we knew that many a tough conference had been held under the name "Significance of Defects" and we did not want to mix up this subject with Correlation of Defects and Service Life.

We invited a number of people from the aircraft industry and from the industries concerned with steel, and research in welding. An outstanding paper was delivered by Mr.A.J.Troughton[4] of Hawker Siddeley Aviation who discussed the philosophy of safe limit and fail-safe design. He showed how a load-probability curve leads to a crack-propagation/operating-time curve and so to a prediction of useful life. He gave an analysis of the main causes of failure in aircraft, based on analysing 52 different case histories. Eleven failures were due to the flight conditions being different from those assumed in the design, eighteen due to the test loading not being representative of those arising in practice and nine occurred because the test specimens used in laboratory work were not representative of the material under test. Most failures were due to bad detail design. There was little evidence of poor manufacture or faulty material being significant. Aircraft generally did better than test life predictions.

To follow up this meeting, the Society of Non-Destructive Examination will hold its Summer Meeting in July this year in Durham, England, on the same subject.

Mr.Newman and Mr.Young of the British Welding Research Association discussed the significance of defects in welds, based on work carried out on a magnesium bearing aluminum alloy and on pure aluminum. They pointed out that Commission 13 of the I.I.W.

6./

already collected and published case histories and Commission 9 did similar work on brittle failures. One of the difficulties in collecting and publishing case histories was due to commercial secfecy and the authors themselves were bound to keep a considerable proportion of the data collected by their member companies confidential.

In the discussion most speakers agreed that design factors were the prime cause of failures in practice, but that the influence of defects could not be neglected. Several speakers doubted if it were possible to generalise particularly as, in most cases, conditions of service were not known in detail nor were the design safety factors. In other words, general standards of acceptance are not possible but must be specific to the individual components. It was doubted by many speakers whether case histories of old components withdrawn from service would help much in the assessment on new stores, made in new materials and usually designed for higher performances.

In spite of these reservations many speakers suggested that an attempt should be made to collect case histories of failures, and the two special fields where this may be initiated were steel castings and the study of British Welding Research Association and I.I.W. failure reports. It was also suggested that the data could be supplied in a general manner on data cards and that this might overcome the problem of commercial secrecy. Much testing could be done on plant coming out of service and a Government Department might be persuaded to do some of this work, acting as an impartial body. The reports published by the British Engine Boiler and Electrical Insurance Co.[5] were cited as examples of the way in which this information might be presented. Other suggestions were made to the effect that defective materials should be introduced into service and monitored non destructively throughout their life. It was generally felt that Mr.Troughton's paper, though not directly applicable to other industries, nevertheless represented an excellent yardstick in the statistical and logical examination of designs with the aid of case histories and this symposium,by producing this paper and the associated discussion, has helped in clearing the air on this subject.

PART II

For the next part of my paper I am indebted to F.H.Lloyd & Co.Ltd. of Wednesbury, Staffordshire, which I believe is the largest steel foundry in Britain. They are using many types of non-destructive testing equipment and have installed a 31 MeV betatron[6)7)], made by the Swiss Brown Boveri Co. about three years ago. The Betatron contributed substantially, not in kind, but in order of magnitude to the knowledge of this foundry about casting techniques, and has had a direct influence on the acceptance standards of high integrity castings, such as steam turbine components and other pressure vessels.

It is true to say that N.D.T. has had a profound influence on the quality of high integrity steel castings and all phases of their manufacture.

The reason of defects in castings is, of course, well-known, i.e. the volume shrinkage amounting to nearly 10% between the molten metal and the solid casting. This shrinkage causes porosity and voids of various kinds which are often difficult to avoid.

It is clear that joint consultation between the designers of these castings, and the foundry, and also with the eventual user, e.g. the Power Generating Authority, is necessary at many stages throughout the design and manufacture, and it is most desirable that these consultations should begin well before the orders are placed. Information on similar components, derived from non-destructive testing, particularly from radiographs obtained with the betatron, is made available to all parties during these discussions and helps to shape design policy and standards. It is well-known that massive sections, away from feeder heads, are undesirable as they produce hot spots which cannot be refilled with molten metal and therefore lead to voids. Where there is an abrupt change of section, adequate fillet radius influences the stress concentration during solidification. The optimum fillet radius, i.e. a compromise between stress concentration and excess metal, which may lead to voids, is about three quarters of the wall thickness of the smaller member. This can be verified by radiographic tests.

Ultrasonic examination, supported by betatron radiography, leads to much useful information with regard to pattern making. For instance, hand made patterns often show the so-called heel

8./

effect, that is to say, thickening of metal in curvatures. The reason is simple: the pattern maker, in wishing to avoid reduction of metal thickness, often has no ready means of checking the pattern thickness and exceeds it. It has been shown that in such heel positions, due to a relatively small quantity of excess metal, voids are produced which can be shown up ultrasonically, but even more clearly with betatron radiography. As a result, some pressure is being brought to bear on designers to avoid shapes which cannot be generated, i.e. which have no axial symmetry. In this way, uniformity of wall thickness and uniform change of wall thickness can be ensured with the resulting improvement in casting quality. External chills are also well known, and they can be employed where large sections cannot be avoided. Thus foundry techniques are constantly being improved. Figure 1 shows the betatron room which is 100 ft. long by 36 ft. wide by 35 ft. high. Road and rail access is through an 18 ft. wide concrete sliding door, weighing about 34 tons. The crane handles 15 ton castings; heavier castings are handled on a special rail vehicle. To obtain economy in radiation protection of the building, it was found necessary to limit the betatron movement to 180° swing and 90° tilt with some restriction of the long travel; this means that neither the door area nor the corridor leading to the control room can be irradiated. The casting seen is on a 20 ft. turntable of 50 ton capacity and most of the work is carried out within the area of the turntable. This component, a stop throttle valve assembly for a 500 megawatt generating set, comprises castings welded together. Figure 2 shows an intermediate pressure outer case designed by one of the British turbine designers and Figure 3 another, similar, outer case by another turbine designer. Figure 4 shows the pipe leading from the turbine case of Figure 3, marked off for evaluation of defect size by ultrasonic inspection.

For the study of the problem arising from the design of the junction of the pipe leading from this turbine outer case, Figure 5 shows wooden slats made to correspond exactly to the cross section of the pipe junction shown on Figures 3 and 4. The heel effect mentioned earlier is clearly seen together with the centre-line shrinkage void found in this region. Figure 6 again shows the heel effect of a non-symmetrical pattern with the resulting shrinkage void. Figure 7 shows two pipe junction designs of a pressure vessel, of which one can be generated, that is, the symmetrical

9./

one around the straight axis, and another which cannot be generated and should be avoided.

Figure 8 shows two radiographs of a marine valve body, and is an example of the difference in appearance and quality between a betatron radiograph on the right and a Cobalt 60 radiograph on the left. Due to the small amount of forward scatter of the betatron the contrast is higher and the technique lends itself for testing widely varying cross sections. Figure 9 shows two betatron radiographs of a steam valve chest section. The void seen on the right hand radiograph disappeared due to re-design of the component by removing excess metal and thus a hotspot. Figure 10 is a header casting with a 4-8 in. wall. This component used to be produced by forging, but due to improved foundry technique it is found more economical to design it for casting. It can be produced practically without a defect.

Finally, I want to say something about the controversial subject of acceptance standards for high integrity castings. The simplest statement one can make is, of course, that, ideally, castings of this type should be completely free from any voids whatsoever and, theoretically, as far as I am informed, the American A.S.T.M. 71 Specification for grade 2 pressure vessels implies this sort of extreme requirement without saying it outright. Radiographs attached to this specification show little or no flaws of any kind. Now, whenever such extreme requirements are demanded by an Authority, which are very difficult, if not impossible to fulfil in practice, very often compromise solutions, dictated by common sense and design experience, are arrived at. This, however, is only another way of saying that not enough information was available when drawing up the acceptance standards, for instance, no account is taken of defect position in these standards. The British specification relating to turbine castings is somewhat more generous and more positive. It distinguishes between acceptable defects and non-acceptable defects. Acceptable defects are such which are of the rounded type, which will not interfere with machining. Further, porosity is acceptable, provided that it is not likely to cause a leakage path and finally a slight central line shrinkage is also accepted. You will notice that 'slight' is used, which is not a very accurate term. Non-acceptable defects are ragged defects from which cracks are likely to propagate during

10./

thermal cycling. Further, defects which reduce the effective thickness of the wall beyond the permissible stress limits are not acceptable. Cracks are never acceptable. Gross shrinkage is not acceptable. You will notice that the word 'gross' is again not very accurate. And, finally, through-porosity is not acceptable as it can lead to leakage.

Figure 11 shows a more recent approach which is finding its way into British acceptance specifications and aims at eliminating the vagueness of the terms mentioned. In the massive T-junction shown in Figure 11, referring to the upper part of the figure, the inscribed circle is taken as a measure of the junction volume, the dimension vertical to the plane of the figure is assumed as large compared with the diameter - and the small circle in the centre is, in this example, 20% of the diameter of the inscribed circle. The three legs of the voids are also shown to be 20% of the thickness of the legs of the casting. In the lower part of the figure the inscribed circle is the same, the T-junction is the same but the small circle as well as the width of the voids shown are $1\frac{1}{2}$ times as large as in the upper part of the figure, i.e. 30% of the diameter of the inscribed circle and 30% of the width of the casting legs respectively.

It is suggested that a reasonable acceptance standard for many high integrity components would be maximum tolerable defect size of 20% of the diameter of the inscribed circle, situated anywhere within the larger circle shown in Figure 11,below, which has 30% of the diameter of the inscribed circle. The actual figures may vary from component to component.

Figure 12 shows defects occuring outside these limits. These would have to be submitted to the Inspection Authority for a decision regarding acceptance or rectification.

Here are, thus some quantitative suggestions which are now being very closely considered in Great Britain by designers, users and the foundry and which are finding their way into acceptance standards for high integrity castings. This would have been very difficult, if not impossible, without such radiographic quality as obtainable from the betatron.

REFERENCES

1. See for instance British Patent 1057802 (Yawata)

2. L. Beaujard, J. Mondot, M. Kapluszak; Quelques Progres dans l'Examen Ultrasonore des Aciers a Haute Temperature

3. M. Atkins and M. Druce: Ultransonic probe system for the continuous inspection of hot steel. Journ. of the Iron and Steel Institute, June 1966.

4. A. J. Troughton, "The value of Non-Destruvtive Testing in the Aircraft Industry", Journ. Royal Aer. Soc. Vol 7, 675, March 1967

5. Br. Engine Boiler & El. Ins. Co. Technical Reports, New Series, Vols 1-7 (1952-1966)

6. A. Nemet and W. F. Cox, Non-Destructive Testing with the 31MeV Betatron, Br. Journ. of Non Destr. Testing Vol. 4, No. 1.

7. W. Bates, Examination of Heavy Steel Castings with the Betatron, Brit. Journ. of Non-Destr. Test., Vol 7, No. 3

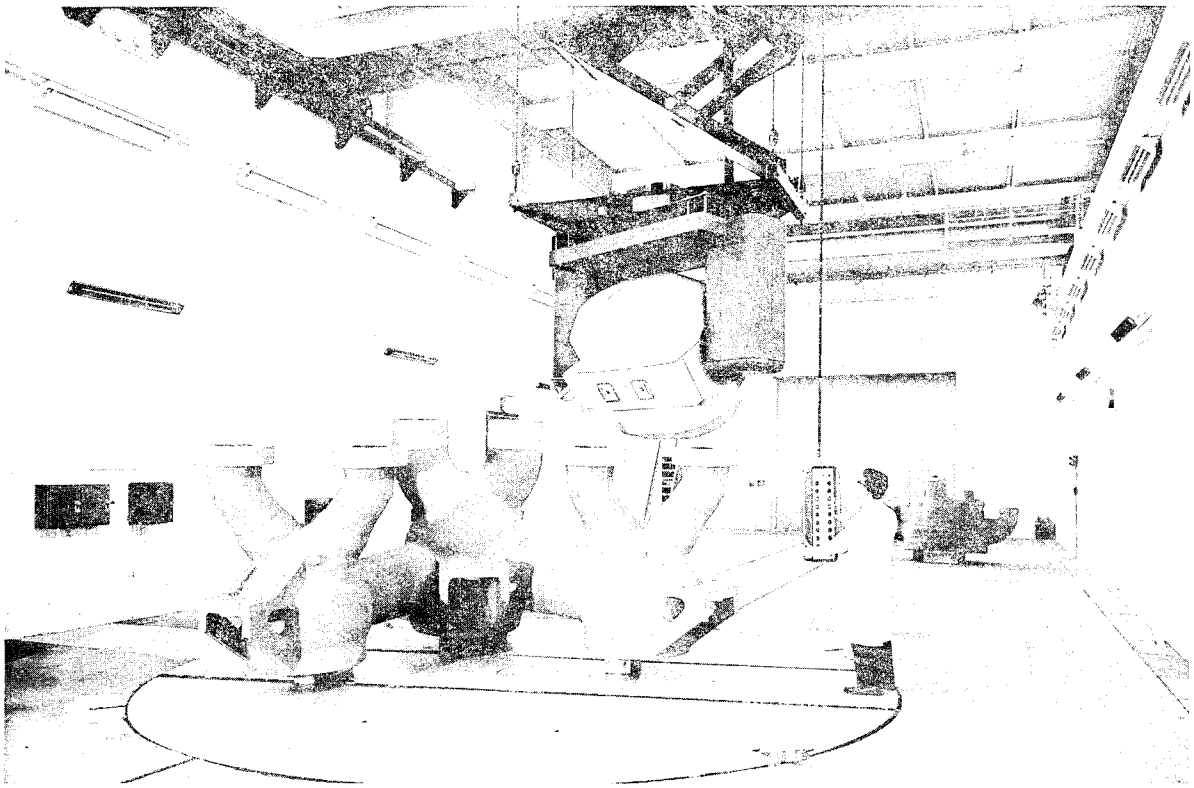

Figure 1. 31MeV Brown Boveri Betratron with Ceiling Suspension and Pendent Controls

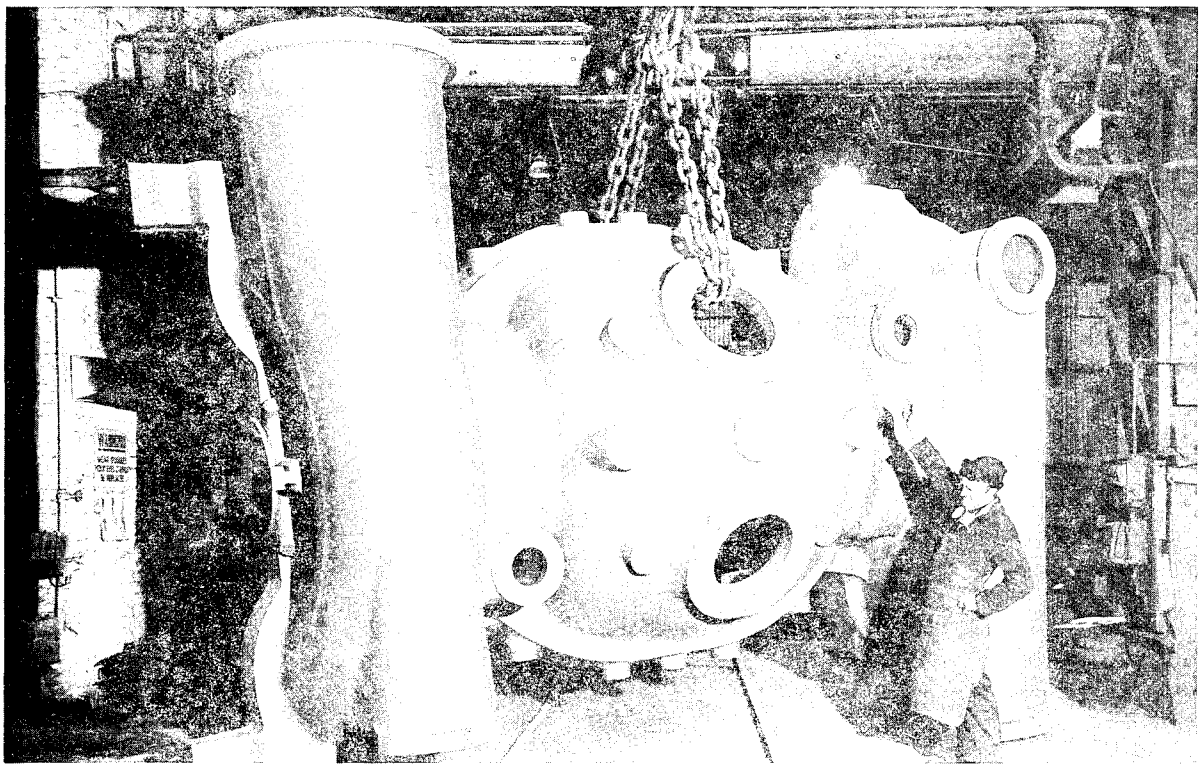

Figure 2. Intermediate Pressure Steam Turbine Casing for 500 MeV Generator Set (C.A.Parsons Ltd.)

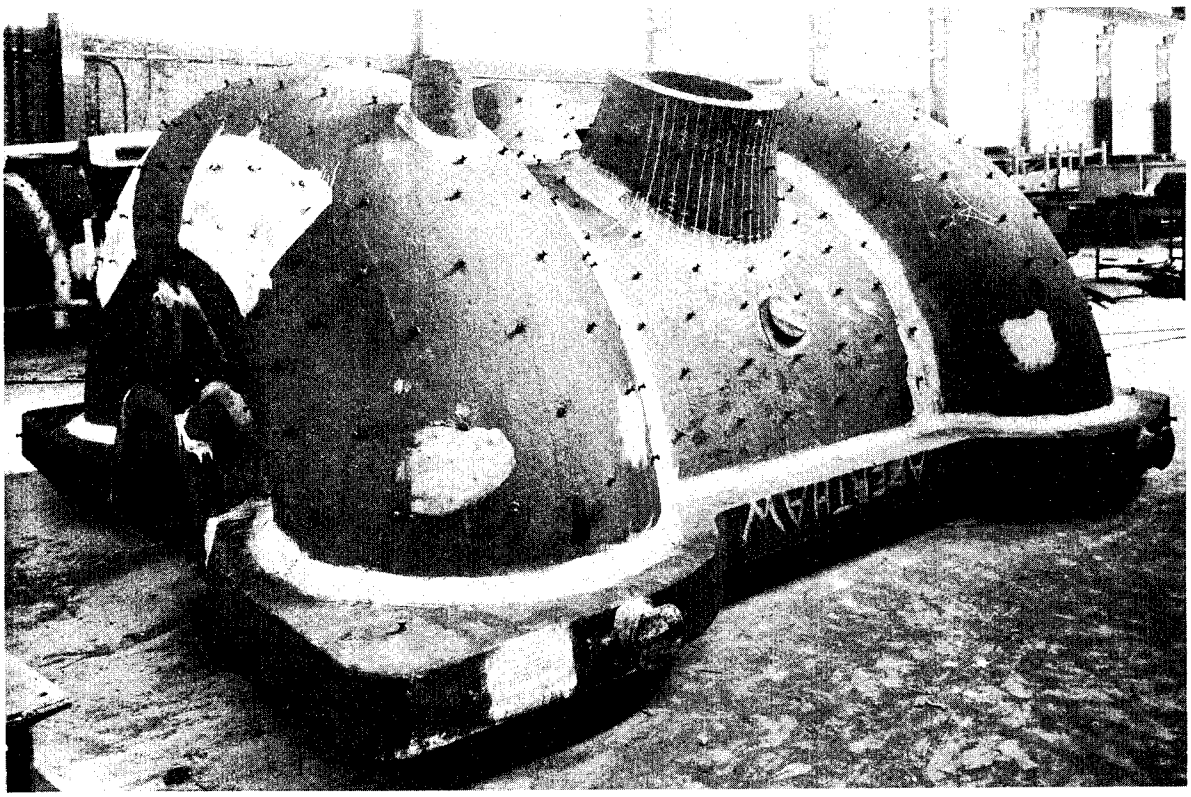

Figure 3. Intermediate Pressure Steam Turbine Casing for 500 MeV Generator Set (A.E.I. Ltd.)

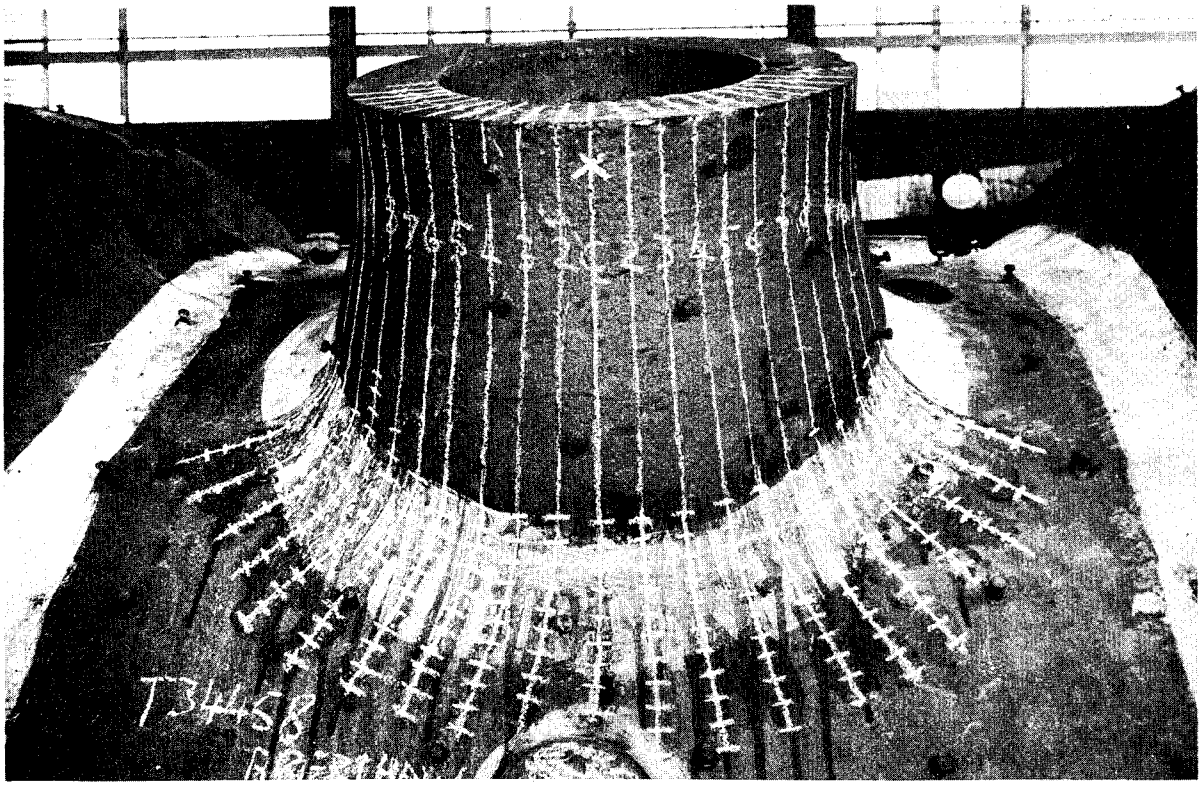

Figure 4. Pipe Connection to I. P. Turbine Casing

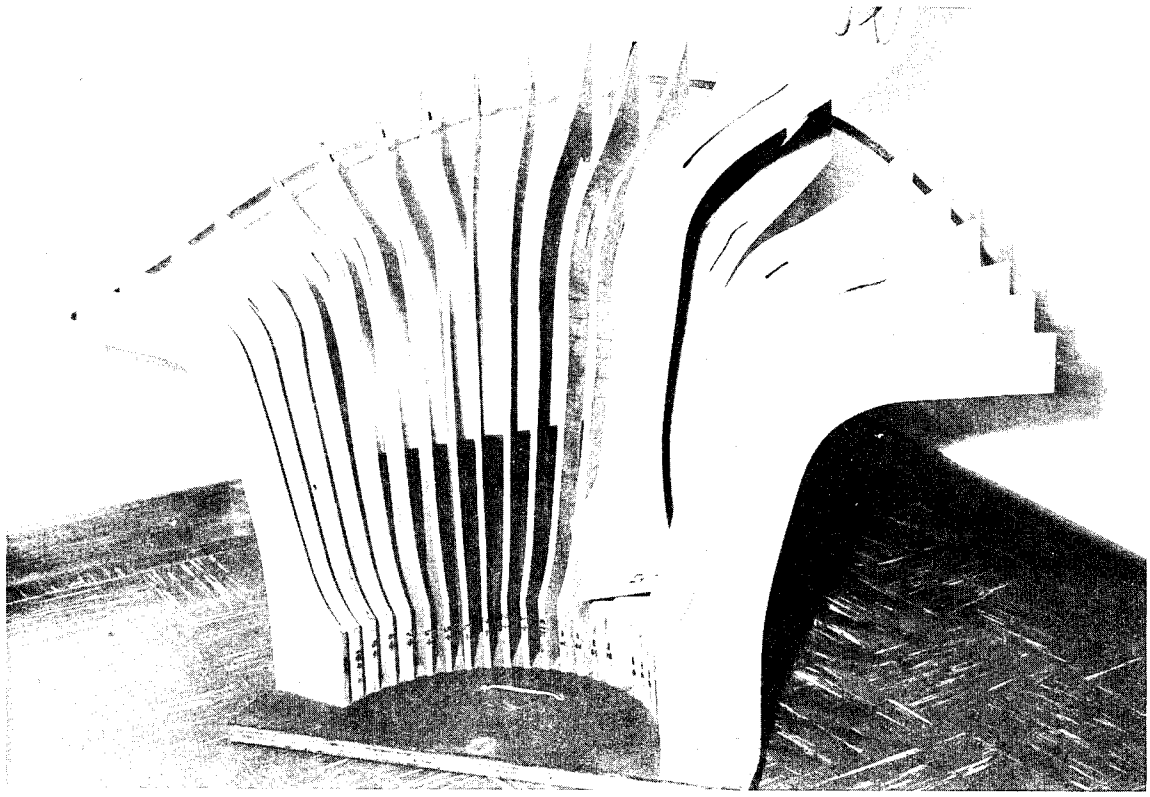

Figure 5. Wooden Cross-Section Model Slats of Pipe Connection to I. P. Turbine Casing

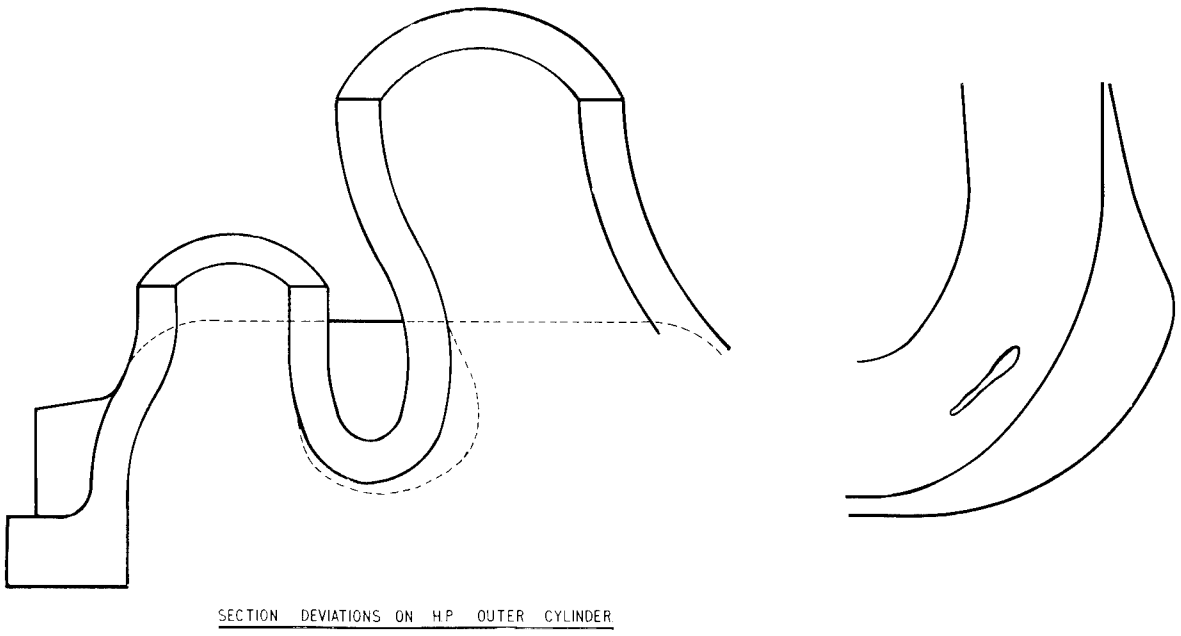

Figure 6. Section Deviation on H. P. Outer Cylinder

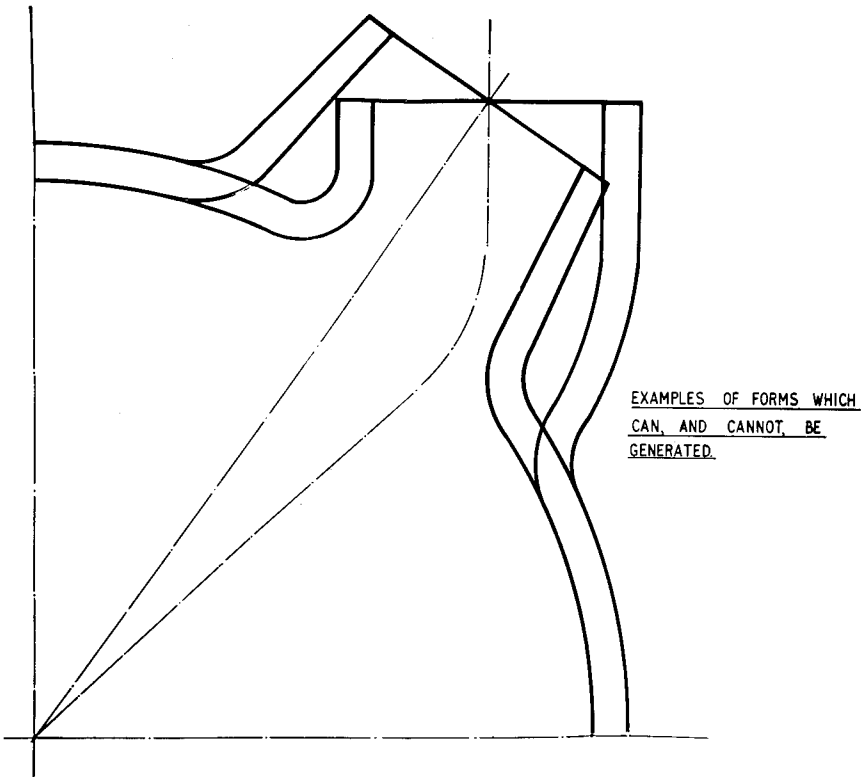

Figure 7. Two Pipe Junction Designs

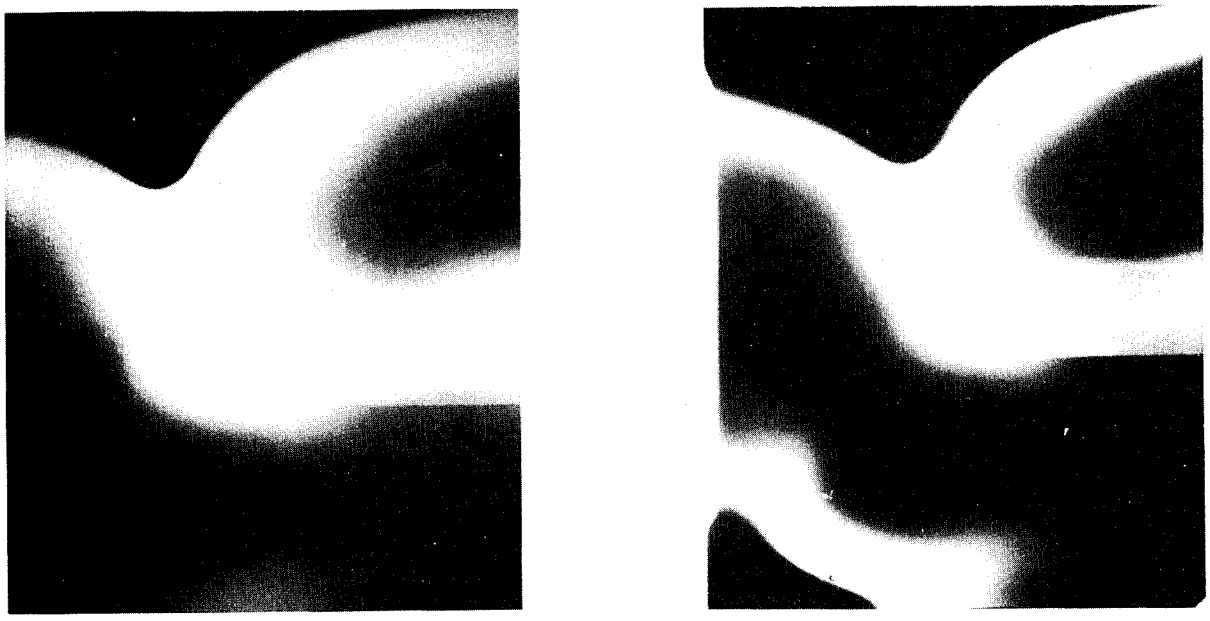

By Cobalt 60 By Betatron

Figure 8. Radiographs of a Marine Valve Body

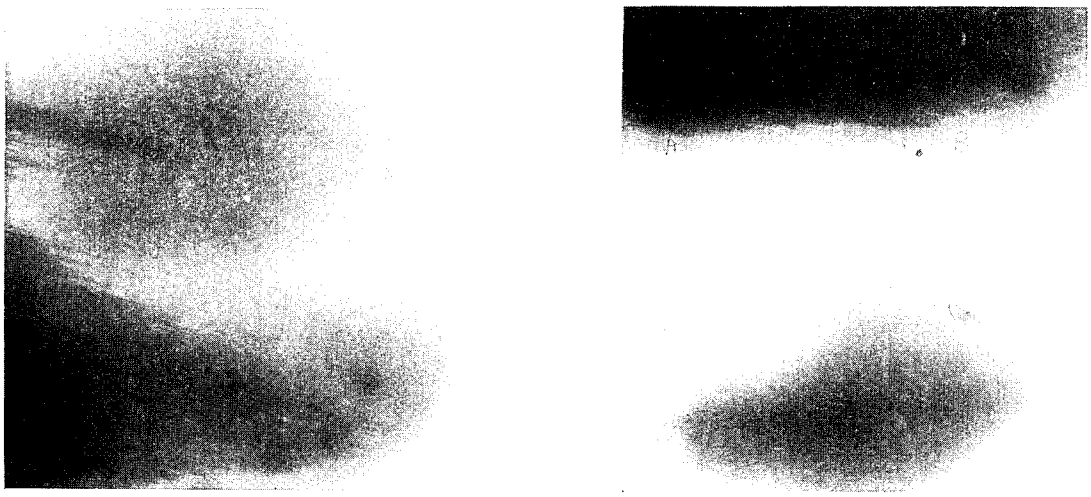

Figure 9. Betatron Radiographs of a Steam Valve Chest

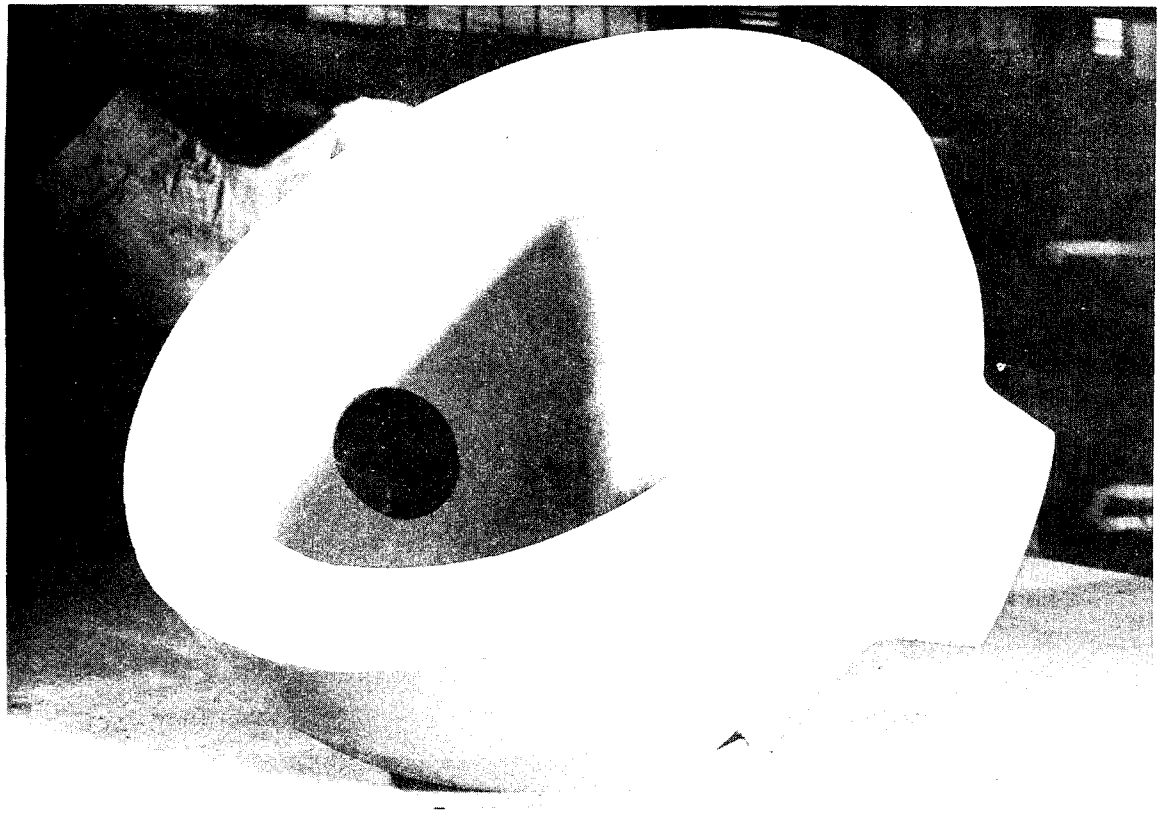

Figure 10. Valve Header Casting (Richardson and Westgarth Ltd.)

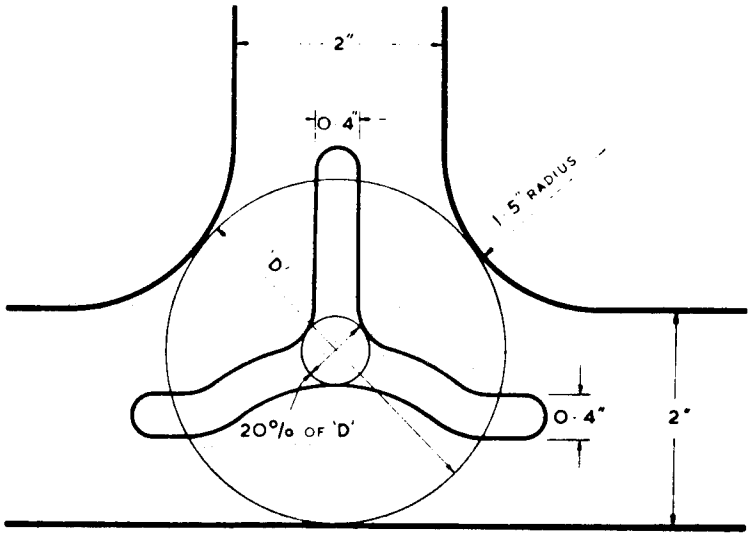

20% Tolerable Amount of Shrinkage Porosity

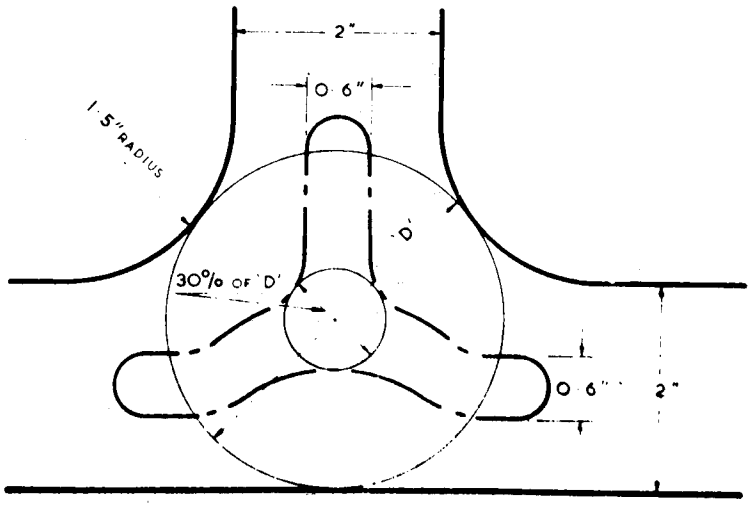

30% Boundaries within which Shrinkage Porosity Must be Contained

Figure 11. "20/30" System" of Acceptance Standard

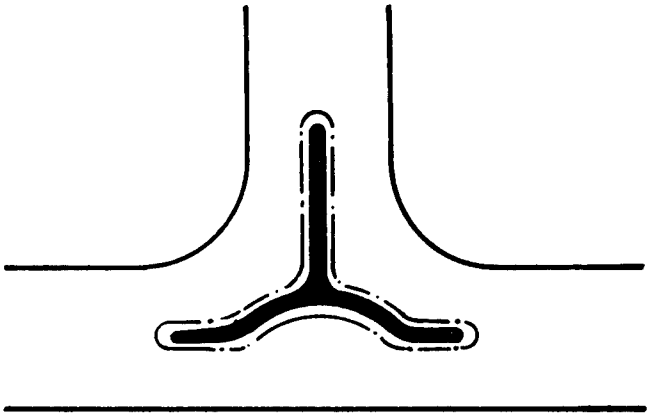

Acceptable without Submission

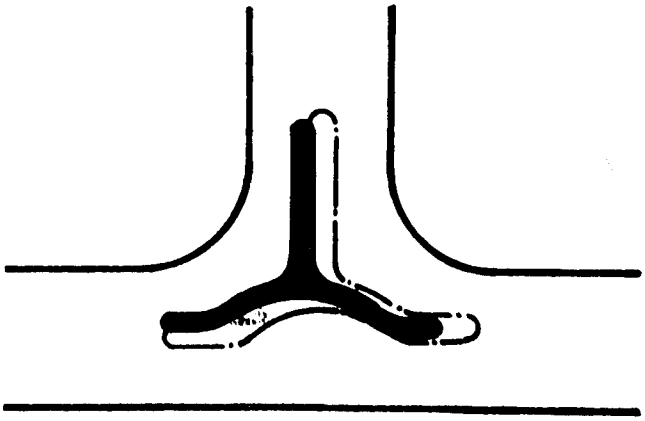

Unacceptable without Submission

Figure 12. Shrinkage Defect and Tolerable Shrinkage Position Envelop

EFFECTS OF MECHANICAL PROPERTIES ON THE VELOCITY OF ULTRASONIC WAVES

E. W. Kammer
Naval Research Laboratory
Washington D. C.

The initial motivation for the work described in this presentation was; to study the feasibility of using ultrasonic waves to detect and measure residual stresses. These stresses originate in many ways, being commonly "built-into" structures such as ship and submarine hulls, by the welding fabrication-sequence. Individual members, namely; plates, beams, and castings, may themselves be internally stressed as a result of rolling, heat treatment or inhomogeneity. Since the stressed member or structure is in static equilibrium the internal force pattern is not easy to evaluate by a nondestructive test. Furthermore this situation can seriously limit the load carrying capacity of a structure and hence means for detecting and measuring them are being sought.

Near-surface stress conditions have been successfully measured by hole drilling or trepanning methods, the edges of the excavated region being displaced by relaxation if a sufficiently large stress is present. Even though the amount of material removed is small this technique cannot strictly be termed nondestructive. X-ray measurement of average lattice parameter distortion has also proved useful but again yields information about the material near the surface.

Recent experimental results with ultrasonic waves offer no grounds for optimism that their practical application to this problem will mature in the immediate future. This is unfortunate because ultrasonics seemed to have certain initially attractive advantages, namely; it is truly nondestructive and it could probe into thick sections of material. These waves, particularly the shear modes, when traversing a uniformly stressed medium, experience a small change in velocity. If the velocity is known for the unstressed state of the same medium, some information can be inferred as to the state of stress. Since the change in velocity with stress is small, considerable instrumental difficulty arises when practical applications of this phenomenon are attempted. In most situations, sufficiently precise prior knowledge of the velocity in the identical unstressed medium is not available. Other factors, such as preferred orientation, temperature change, composition nonuniformity, to mention a few, confuse the interpretation of a single absolute velocity measurement intended to detect stress. Figure 1 illustrates some typical changes in transit time through a 1-in. thickness of sample observed for several structural aluminum alloys and a low carbon steel. The change in transit time is nearly a linear function of uniaxial tensile stress applied normal to the direction of wave propagation. These data concern simple shear modes only. Two orientations of the vibration plane are considered, namely parallel or perpendicular to the stress field, plotted above or below the axis respectively.

Although the velocity of shear waves is indeed slightly affected by stresses in the medium traversed, as shown in the figures, other uncontrollable factors are considerably more influential and make the interpretation of a single velocity determination ambiguous. For example; preferred orientation normally present in

commercially produced steel, could influence the change in transit time shown in Fig. 1 by factors of 3 or 4 times the magnitude shown for a 25,000 psi stress. Furthermore, the condition of uniform tensile or compressive stress examined in Fig. 1 does not prevail in the residually stressed material. Along a particular ultrasonic beam path through this latter medium, adjacent regions of compression and tension are traversed. For example, the $S_{//}$ polarized shear wave packet would increase in velocity while crossing a section in compression and slow down in the section under tension. The net change in velocity observed externally could be zero!

Partially compensating these negative conclusions, much has been learned of value to the ultrasonic art. These positive results will be helpful in guiding any future work on the detection of residual stress, which to be successful, must meet many exacting conditions not fully appreciated nor explicitly stated in previous contractual studies. One such condition concerns the magnetic-elastic coupling effects, displayed in Fig. 2, when the stressed medium is ferromagnetic. In this example HY-80 steel is the specimen material. The change in transit time over a 1-in. path length is plotted against uniaxial tensile stress. The letters L or S designate data for longitudinal or shear modes, respectively, and the subscripts or superscripts are intended to indicate the experimental conditions. For example, $S_{\perp}^{//}$ signifies that the polarization of the shear wave (S) was normal ($\perp$) to the stress and that the magnetic field was parallel ($//$) to the sonic beam path. The plots relating to the unmagnetized state have superscript zeroes.

Figure 2 shows that each mode behaves differently under the influence of the magnetic field. They have only one characteristic in common; namely, increase in velocity. In general, the longitudinal mode, $L^{\perp}$, changes the least and $S_{\perp}^{\perp}$ shear mode is displaced the most for the materials examined at this time. The relative positions of the other modes follow no simple pattern. These displacements on a transit time chart for steels like A212B or cold rolled types are about double the values shown for HY-80.

The data displayed in Fig. 2 were taken under conditions of a constant flux density. It is of interest to know how the displacement toward shorter transit times (or higher velocities) varies with changes in this magnetic state. A typical example is the $S^{\perp}$ mode in A212B steel at zero tensile stress. This is shown in Fig. 3 where the data have been plotted below the horizontal axis to be consistent with Fig. 2. Transit time decreases for either direction of the magnetic flux. Above the flux density of about 8000 gauss a marked enhancement of transmitted signal occurs. This can be attributed to the immobilization of the domain boundaries and the attendant reduction in eddy current energy losses supplied by the ultrasonic vibrations.

Instead of presenting the effects of stress on the ultrasonic waves as a change in transit time over a unit path length, it is sometimes preferred to compute a velocity ratio defined as follows:

$$\frac{\Delta V}{V} = \frac{V_S^{//} - V_S^{\perp}}{V_S},$$

in which the symbols $V_S^{//}$ and $V_S^{\perp}$ stand for the shear wave velocity when polarized parallel and perpendicular to a stress field of equal magnitude respectively. The term

V_S without superscript corresponds to the shear velocity in the unstressed medium. In an isotropic polycrystalline material considered here, V_S would be the same for both polarizations. A similar velocity ratio is used in the science of optics and termed "birefringence." Although not necessarily a stress related quantity in optics, the term has gained general acceptance in the art of ultrasonics as defined above.

In Fig. 4 the measurements of $\frac{\Delta V}{V}$ for several metals are plotted as a function of their Young's modulus. The trend exhibited suggests that a nearly linear relationship exists between the sonic birefringence coefficient and the simple tensile modulus. For this limited range of investigation the sonic velocity sensitivity to a given stress is greatest in the metals having the smallest Young's modulus. This could also be stated in terms of the inverse parameter, the lattice distortion, but its usefulness empirically favors the elastic constant as an independent variable. The modulus range recorded here covers most materials commonly used for structural purposes. Perhaps with this chart, when fully developed, one may be able to predict the sonic birefringence for any other material within this range if the modulus is known.

A more general way of classifying materials than that shown in Fig. 4 would be by ordering them according to their higher order elastic constants. The allotted space for this presentation does not permit inclusion of some results in this study field. It can also be appreciated that to obtain data, such as transit times, which have significant change of 10^{-10} second as quoted in the Figures implies fascinating advances in the art of ultrasonic measurements. Discussion of these also must be postponed for another day except perhaps to mention that true transit times can only be determined by taking into account the presence of the transducer also. This is particularly important when dealing with materials having acoustic impedances nearly the same as that for the piezoelectric element used in the transducers. In a recent "round-robin" interlaboratory "high precision" comparison of transit time measurements on the same silica block using quartz transducers the agreement between nine independent participants on the transit time was within 0.3% whereas it was possible to show with a recently devised data processing scheme that the extrapolated value of the transit time for a mass-less transducer was being overshot by 3%!

In summary then it must be concluded that the practical measurement of residual stress by ultrasonic means is not yet possible, but much has been learned of value to the ultrasonic art, and the experience will be helpful in guiding all future work. The cases studied here, which have a simple orthogonality between stress, magnetic fields and ultrasonic beam paths, rarely will be expected to occur in a practical problem. Yet these elementary configurations have fixed typical bounds for possible errors in transit-time determinations. They make abundantly evident the sobering complexity with which it is necessary to cope before the effects of residual stress on ultrasonic waves can be meaningfully interpreted.

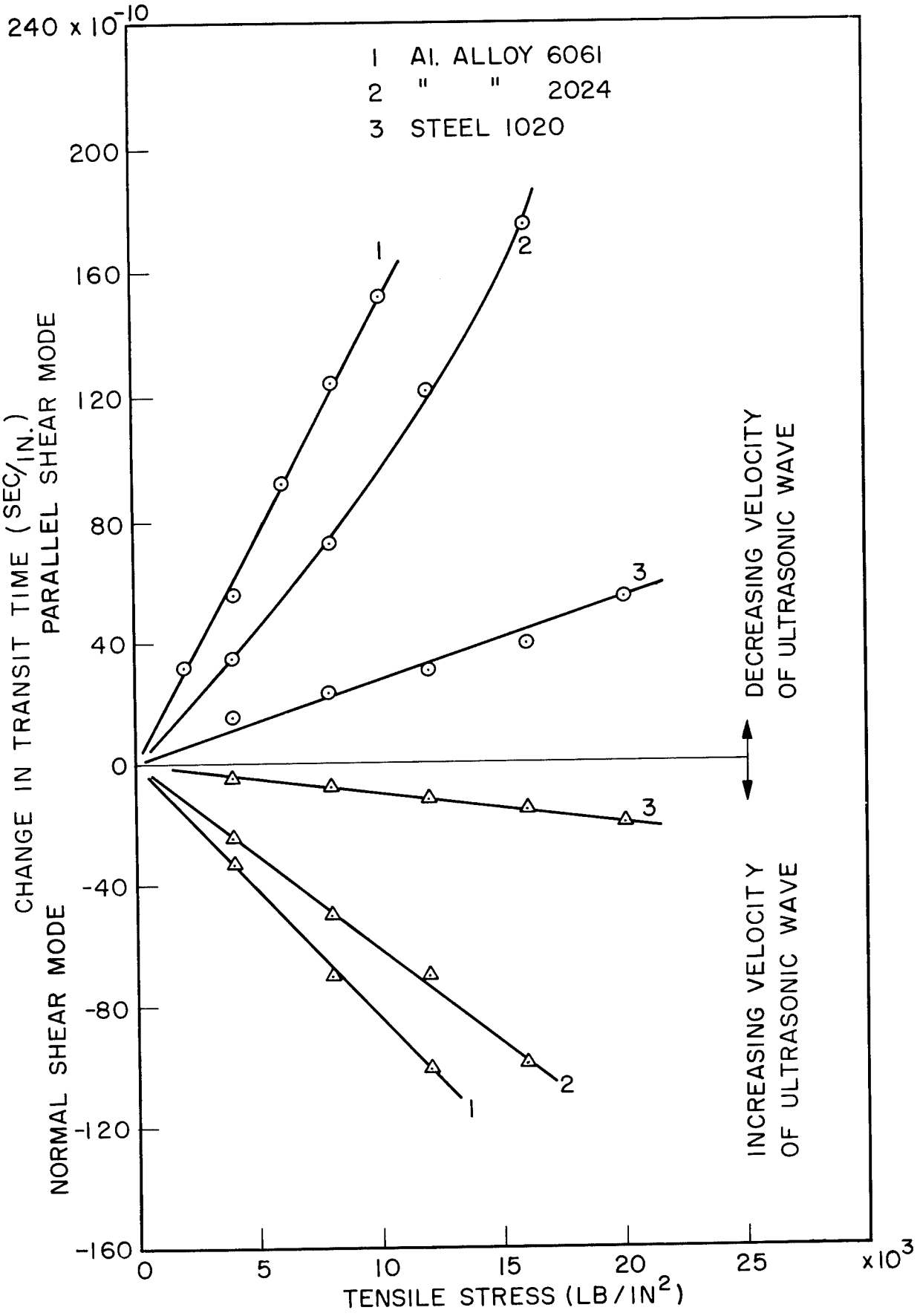

Figure 1. Effect of Stress on Transit Time for Various Materials

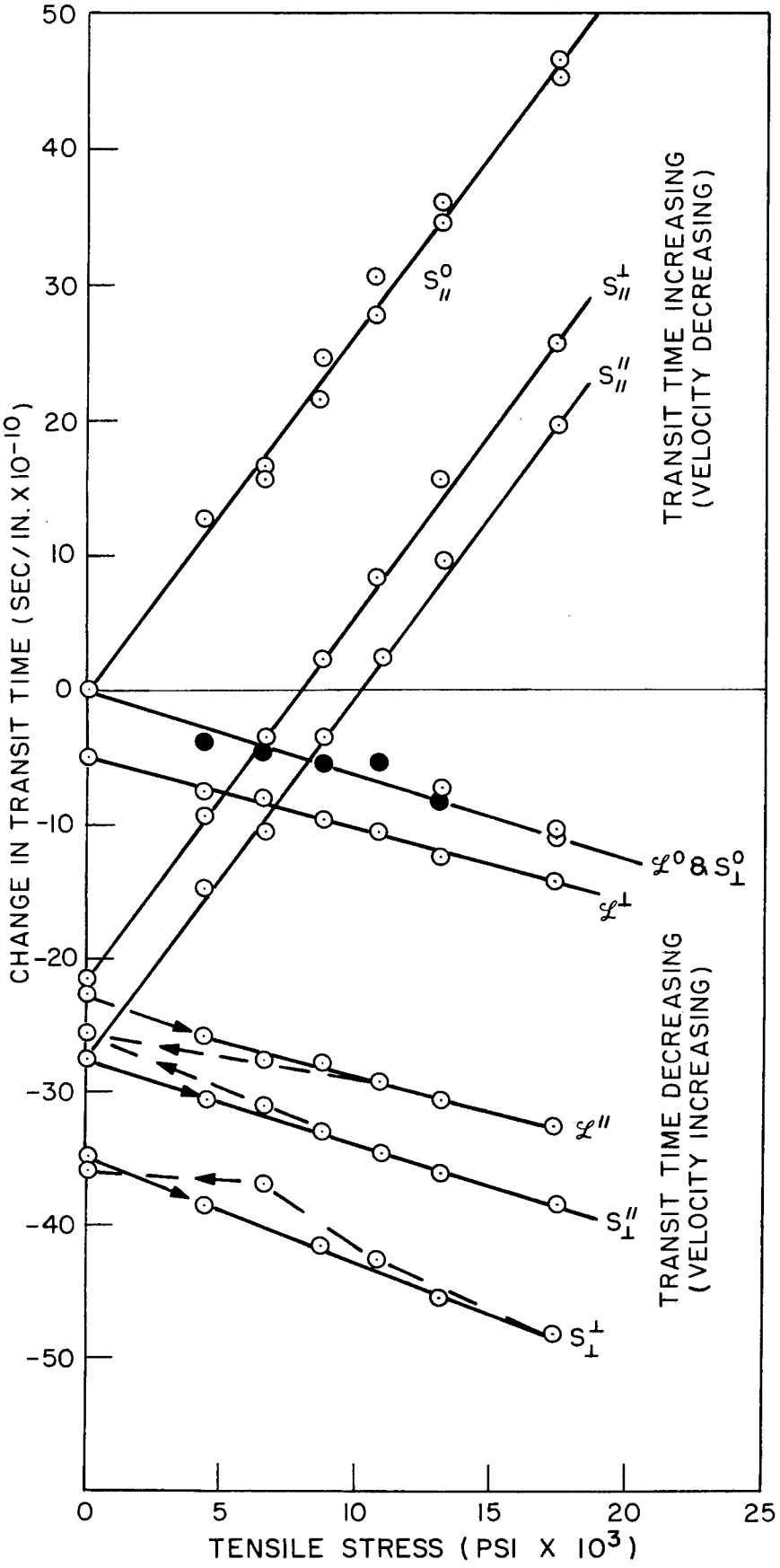

Figure 2. Effect of Stress and Magnetic Flux on Transit Time in HY-80 Steel

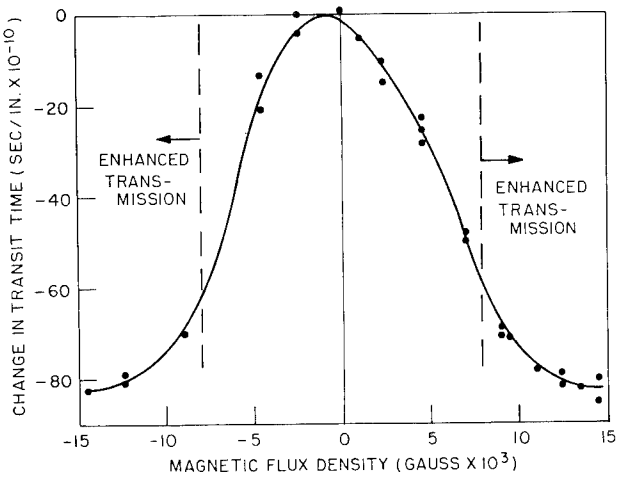

Figure 3. Effect of Magnetic Flux on Transit Time in A212B Steel

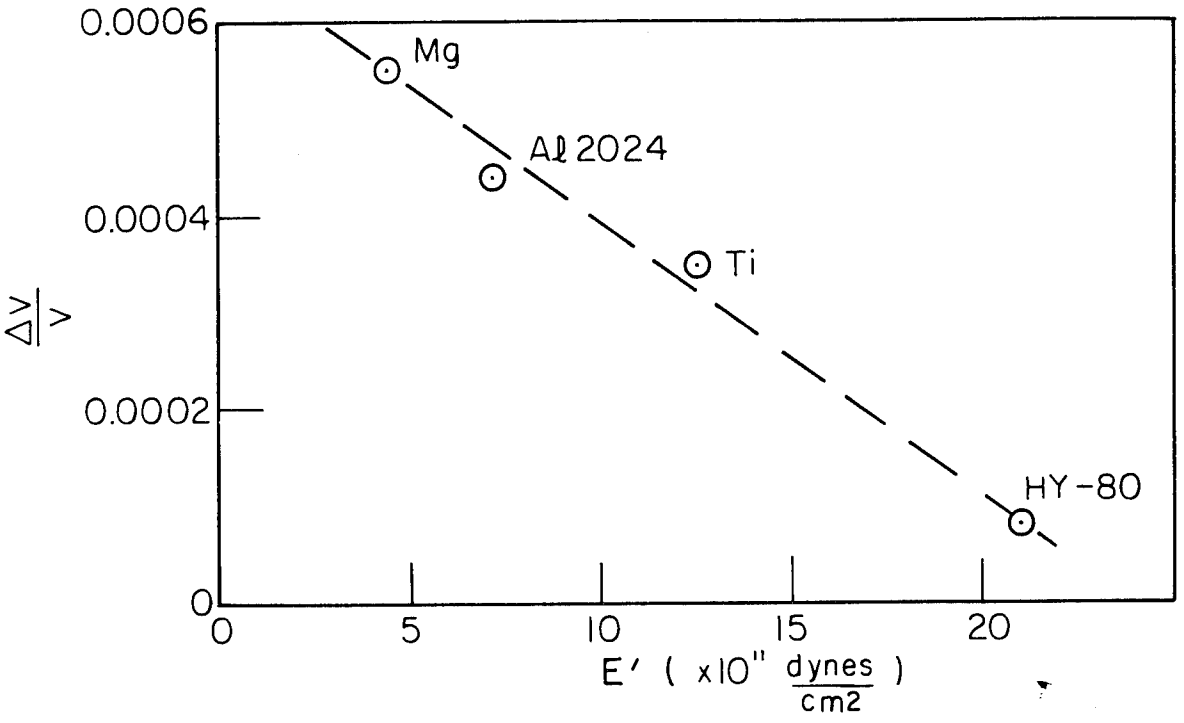

Figure 4. Ultrasonic Birefringence, $\frac{\Delta V}{V}$, as a Function of Young's Modulus under Conditions of Equal Stress (2000 psi)

CONFERENCE SUMMARY

F. H. Edwards

Bragg Laboratory, Sheffield, England

I understand it is your practice, at this late stage of a meeting, for someone to summarize or briefly highlight, each of the papers which have been presented. This in fact was my task.

However, I am sure quite a number of you would prefer to be off on their journeys and there is indeed a party, including myself, eager to take the opportunity of visiting Cape Kennedy and still to keep faith with their flight reservations in the late afternoon. So I would ask you to excuse my failure to complete this assignment in the conventional manner and accept a few remarks as an alternative. If anyone is dissatisfied, then please blame another of these "bloody" Englishmen.

I think you will agree that this has been a most successful conference in spite of the difficulties which apparently preceded it and which left us wondering "on the other side".

Although it was impossible to have the written papers in time for the meeting, the conference program provided abstracts of each paper furnished, I believe, by the authors themselves. So I am sure they have highlighted their own subject rather far better than I could do in the few minutes at my disposal.

However, the program under its title, "Correlation of Material Characteristics With Material Performance" has provided us with 24 papers, greatly varying in subject matter and content. In fact its diversity illustrates, I think, the perpetual dilemna which faces Panel 4 in its endeavor to cover the whole vast field of testing and its special assignment with respect to nondestructive methods.

Clearly, the symposium has brought together those who have been trained in many different disciplines or backgrounds who have shed refreshing new thoughts upon commonly accepted subject matter. Obviously, there has been a preponderance of papers concerned with metals but we welcome those others which remind us that engineering materials are also concerned with non-metallics of which rubber, cement, plastics and graphite are typical.

Now, no conference worthy of the name gets by without an element of controversy. The present meeting has indeed been stimulated by several speakers who have protested strongly that NDT, as an inspection tool, tends at times to be overplayed. This can lead to the expensive rejection of material

otherwise satisfactory, but which fails to satisfy some unnecessarily stringent limits derived, quite possibly, from the factor of ignorance which applied at the time. Certain speakers claimed that fracture mechanics, or preconsiderations such as LEO, could now produce more factual estimates of the size and number of defects which could be tolerated in a given instance. Obviously, this will lead to the drastic revision of standards of acceptance in the early future but if we can save upon labor and materials by such means, this conference will have done a pretty useful job.

On the contrary, there are problems in the engineering world which demand the application of very sophisticated methods of testing. Some of the latest developments have been described in the papers.

We had also an interesting second session devoted to "environmental effects" which included considerations of stress corrosion and cavitation erosion. Here again, an element of controversy enlightened the proceedings.

In fact so long as we are never satisfied with the state of Rome, there is hope for the future of testing.

SYMPOSIUM PARTICIPANTS

Adam, L. H.	Frankford Arsenal
Baker, G. S.	Aerojet General Corp.
Barer, R. D.	Pacific Naval Laboratory, Canada
Barrett, J. C.	Office, Director of Defense R & E
Benderly, A. A.	Harry Diamond Laboratories
Bennett, T.	Chanute Air Force Base
Birchon, D.	Admiralty Materials Lab., U. K.
Birk, A.	Automation Industries
Boisvert, Mr.	SAAMA, Kelly Air Force Base
Budnick, M. L.	U.S. Army Natick
Carman, C. M.	Frankford Arsenal
Carr, F. L.	Army Materials Research Agency
Colton, R. M.	Army Materials Research Agency
Coy, R.	University of Dayton, Research Institute
Darcy, G. A.	Army Materials Research Agency
Driscoll, D. E.	Army Materials Research Agency
Dukes, W. A.	Ministry of Aviation, U. K.
Dyer, C. H.	Navy Ordnance Lab.
Edwards, F. H.	Bragg Laboratory, U. K.
Forkas, L. L.	Martin-Marietta
Gardner, C.	Southwest Research
Goldstein, M.	Martin-Marietta
Greenberg, H.	Westinghouse R & D Center
Griggs, R. E.	DeLaval Turbine Inc.
Gross, R.	Marine Eng. Lab.
Halmshaw, R.	Royal Armament R & D Establishment, U. K.

Hastings, C. H.	AVCO Corp.
Hatch, H. P.	Army Materials Research Agency
Holloway, J. A.	Air Force Materials Laboratory
Kallas, D. H.	Naval Applied Science Laboratory
Klinker, L. G.	Army Research Office
Koster, W.	Metcut Research Associates
Kubiak, E. J.	General American Transportation Co.
Martin, G.	North American Aviation Inc.
Mather, B.	Army Engineer - Waterways Experiment Station
Mather, K.	Army Engineer - Waterways Experiment Station
McCauley, R.	Ohio State University
Miller, J. M.	Army Weapons Command
Mills, J.	Chanute Air Force Base
Moore, K. W.	Royal Canadian Navy
Nemet,A.	A. Nemet Co., U. K.
Peterson, M. H.	Naval Research Laboratory
Plexico, J.	Army Missile Command
Promisel, N. E.	Materials Advisory Board
Rodgers, E. H.	Army Materials Research Agency
Roffman, E.	Frankford Arsenal
Samuels, L. E.	Defence Standards Labs. Australia
Seltzer, D.	Martin-Marietta
Schroeer, R. M.	Arvin Systems, Inc.
Sharpe, R. S.	Nondestructive Testing Centre, U. K.
Socky, R.	General Electric
Sugiuchi, H.	Martin-Marietta
Todkill, P. J.	Dept. of Energy, Mines and Resources, Canada

Trapp, W. J.	Air Force Materials Laboratory
Van Arnhem, E. J.	Army Material Command
Wake, W. C.	Rubber and Plastics Research Association of Great Britain
Williams, F. S.	Naval Air Eng. Center
Whymark, R. R.	Tracor, Inc.

Appendix to Paper III-1

METALLURGY APPLIED TO THE SELECTION OF METALS*

D. Birchon

Admiralty Materials Laboratory, Holton Heath, U. K.

The optimum design of any structure can only be achieved by a judicious blend of experience, ingenuity, design philosophy, economics, materials selection and choice of fabrication processes. Each of these considerations is related to the others, and none can be properly discussed without reference to the others. Of these aspects, materials selection is sometimes treated lightly due to the complexity of the arguments involved. This is unfortunate, since the materials selected affect almost every aspect of subsequent design and construction, and the basis of their selection should therefore embrace every known mechanical and environmental condition to which they will later be subjected.

Design Philosophy

In each type of engineering there are overall design philosophies peculiar to that particular industry, and these have an important bearing upon the choice of materials and fabrication techniques.

In the automobile industry, the finished machine is required to be reasonably light and rigid, adapted to mass-production techniques and able to withstand the rigours of a fairly long life under widely varying climatic conditions, often in the face of indifferent and infrequent maintenance. The finished product must also have consumer appeal.

In the aeronautical industry, the structure must be very light, adaptation of the design for mass-production techniques and minimum cost is often less important than in the automobile industry, the required life in terms of hours of operation is generally shorter, and the structure and components are subjected to frequent and rigorous inspection and maintenance. However, there are wide extremes of temperature and loading, and stress levels are relatively high.

In marine and heavy engineering, very long lives are required. Structures are often very heavy and stress levels may be relatively low. These requirements are backed up by steady and maintained maintenance, though this is generally of less rigorous nature than that common in the aircraft industry. In marine engineering,

*Originally presented to Second International Engineering Materials and Design Conference, London, November 1961.

a further complication is provided by wide extremes of temperature and loading in a marine atmosphere and also, in many cases, by the presence of sea water, which is an effective electrolyte.

Within any given industry there are further variations in the design philosophy. This may be illustrated for marine engineering as follows.

In the Mercantile Marine the material is normally selected to be the most economic in terms of first cost (including fabrication, installation, etc.) and efficiency of function to give the required life. These considerations are assisted by the fact that loadings, voyage durations, repair facilities and schedules are generally fairly well established in advance. In naval applications, economy in cost is just as important, but there are often overriding requirements such as integrity under onerous conditions of loading and strain rate, often accompanied by low temperatures, and the necessity to be able to withstand the results of major damage to neighbouring, or even partially supporting structures. Materials likely to be in short supply in an emergency must be used as little as possible, and in some cases it is desirable to base the philosophy of design and materials selection upon easy replacement or repair of damaged components, under difficult conditions, in an emergency. In the case of materials for weapons of all types, the missile structure will finally be destroyed and we have the competing requirements of selecting the cheapest and most readily available material which must, at the same time, be capable of being stored for long periods without any deterioration in the efficiency of the weapon, yet it must withstand launching and flight loads and the inevitable rough handling prior to launching in action. In this type of application a proper consideration of alternative constructional methods is the only way in which the most intelligent and closely integrated design, material selection, construction and testing procedure can be evolved. This naturally requires the materials engineer to have a close appreciation of the function to be performed by the equipment and adequate knowledge and appreciation of the tolerances, both dimensional and functional, which can be accepted.

The necessity for close collaboration between the metallurgist, chemist, designer and user is not always fully appreciated, nor is this collaboration always easily achieved. Designers can only base their calculations upon firm figures, whereas the metallurgist is often painfully aware of the shortcomings of available information, and sometimes can only discuss things in terms of probabilities.

The most important role of the metallurgist in this context lies in ensuring that the whole basis of the design is not invalidated by some particular and unexpected deterioration in the integrity of the material, due to the operating conditions. For instance, he must ensure that there is no susceptibility to stress-corrosion cracking if the environment can give rise to suitable conditions for this form of attack. Or it may be that a particular manufacturing technique will lower the fatigue strength of the finished component below that to be expected from the intrinsic resistance of the bulk material. It is, therefore, important to note that the mechanical properties of materials are no more than a guide to their behaviour

in service, [1, 2] and it is only by the closest and most intelligent co-operation of designers, metallurgists, production engineers and users that the most efficient choice of metal may be made for the more difficult applications. One of the most important fruits of such collaboration lies in the fact that a change in the metal employed can often be combined with a simplified manufacturing process to produce a more efficient product, i. e. one which combines adequate strength, etc., with lower cost.

For the purposes of discussion we may consider the selection of a material for one of the more difficult applications, to be made up of the considerations set out in Table 1. These will now be discussed briefly, in turn, illustrated by some examples from service and supported by some references which may assist further reading.

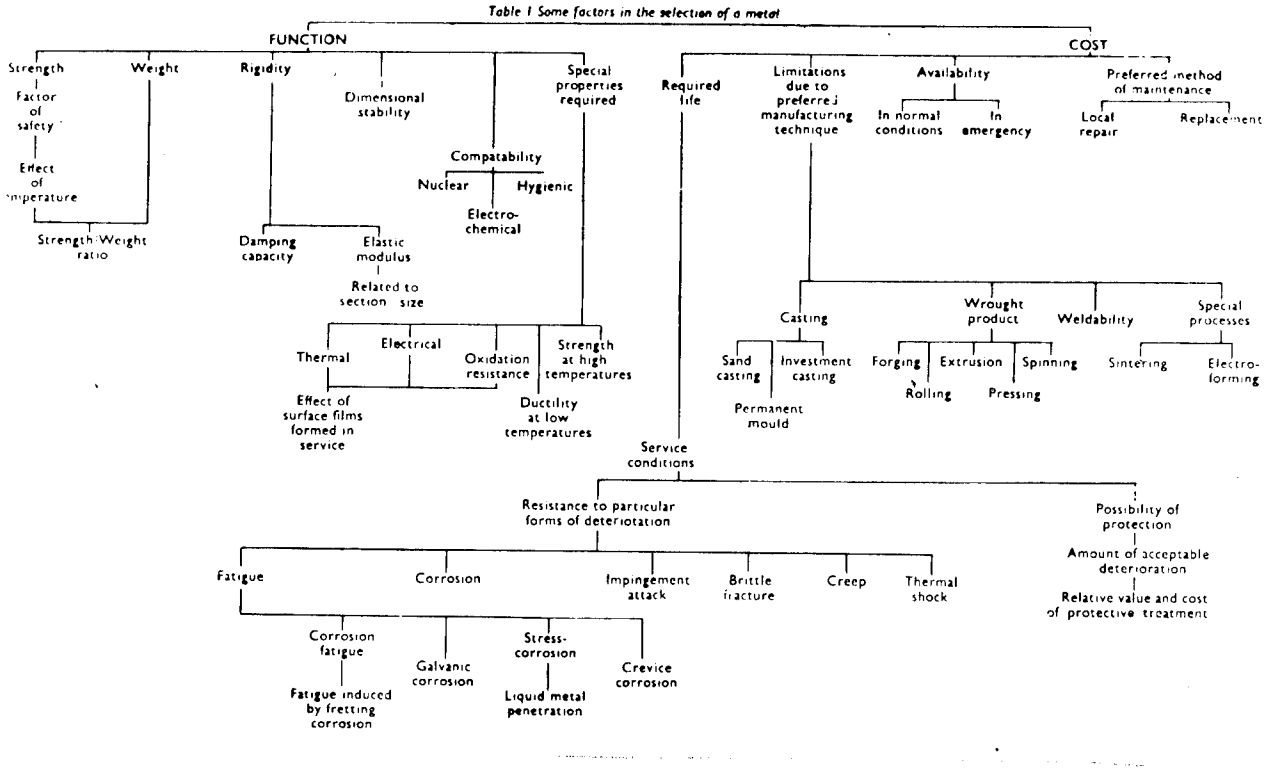

Strength and Weight

The necessary strength might appear to be the simplest consideration, since it may be based solely upon design loads. Unfortunately, this is not true, particularly when high strength materials are required and the structure is required to fail safe. [1, 2, 3] In steels, a high yield point/u. t. s. ratio is often associated with a high tensile strength and this may inhibit the ability of a component or structure to

deform sufficiently to redistribute peak stresses, with the result that fracture rather than distortion may follow an unavoidable overload. The choice of a metal of lower ultimate tensile strength may result in a safer structure because peak stresses can be reduced and distributed by local yielding. Again, a high tensile strength is accompanied by an increase in susceptibility to stress concentrations. For example the big-end bolts of a highly rated diesel engine were constructed of steel of 75 t. s. i. ultimate tensile strength in order to use the smallest practical size of bolt whilst still ensuring a reasonable factor of safety between the pre-stress in the bolt and the proof stress of the material. The inevitable minute relative movements between the central fitting portion of the bolt and the contacting surfaces in the bolt holes in the big ends when the engine was running caused fretting corrosion[4] of the bolts. Fatigue cracks were initiated from these areas and this resulted in fatigue failure of one bolt, followed by rapid tensile failure of the other and considerable damage to the engine from the disconnected connecting rod. When replacement bolts in the same material were tempered down to a tensile strength of 60 t. s. i. reducing the apparent factor of safety calculated on the proof stress/peak stress ratio, no further failures occurred, due to the reduced sensitivity of the steel to fatigue failure from the inevitable surface fretting which still occurred. Similar considerations apply with even greater force to large sections, in which surface notches may have a proportionally more damaging effect.

The concept of a factor of safety is vital in engineering design, yet it can be very misleading whenever complicating circumstances arise. A case of particular importance is whenever stress corrosion can take place. Cases sometimes arise in which a component can suffer from stress corrosion cracking, and an alternative material may be advised having lower tensile strength but immune to cracking under the particular conditions involved. In such cases the reduction in the apparent factor of safety should not be allowed to interfere with the selection of the better material.

Considerations of strength and weight are often closely linked, as in the case of rotating components in which the self-induced centrifugal stresses may represent a considerable proportion of the total stresses. Tabulated strength/weight data must be interpreted with caution, since high temperatures may be involved, as in gas turbines, steam generators, etc., and not only must the strength properties used relate to the temperature of operation, but resistance to creep must also be considered. This is often affected by orientation effects within the material, and care is then necessary in relating creep properties obtained in the longitudinal direction of the metal to the performance to be expected if the working stresses are in a different direction. In marine applications, the possibility of contamination by chlorides and the salt in the atmosphere must always be considered. Particles of chloride deposited on the surfaces of stainless iron turbine blades or light alloy compressor blades may cause pitting or cracking, which can then initiate fatigue or tensile failure. Selective deterioration of this type invalidates design calculations unless proper consideration is given to the initial selection of material and fabrication technique.

One of the most spectacular examples of weight saving in marine engineering is provided by vessels such as the 40,000-ton Oriana, which has the largest welded light alloy superstructure in the world. The weight of this superstructure is 1,040 tons, and represents a saving of approximately 1,500 tons compared with a similar structure in steel.

Less spectacular but very valuable weight-saving can be achieved in small pressure vessels, and strength members of aircraft and missiles by chemical or electrolytic machining procedures, in which metal is removed in a square grid or similar pattern, to provide maximum strength and stiffness with minimum weight.

Rigidity

The rigidity of a structure is a function of the elastic modulus of the material, the dimensions and sectional shape of the component, the way in which it is supported, and the relationship between the frequency of vibrations imposed upon it by external influences and the natural frequency of vibration of the structure. Large marine propeller and crank shafts provide examples of components in which there may be particular speed ranges, within the operational range, in which a resonant vibration can be excited. The large amplitude of these vibrations may not only be embarrassing from the point of view of noise, it may cause stresses large enough to initiate fatigue failure. Alternatively, a degree of elasticity, or even of plasticity, may be desirable to minimise peak stresses due to sudden overloads caused by external agencies. This is especially true of large bolts or studs required to retain structures subjected to occasional violent loads.

The degree of rigidity is largely a design matter, often involving a delicate compromise between what is desirable and what is attainable, as evidenced by final designs in which proper rigidity is secured for specified operating conditions, but limitations are imposed outside these conditions. For instance, large engines must sometimes be taken through particular speed ranges quickly during starting up to minimise the time available for the development of induced vibrations. Other large structures, such as bridges, must be protected from the influence of exciting vibrations at particular frequencies, as evidenced by speed limits on trains, disciplined groups of marchers breaking step, etc.

The amplitude of induced stresses may be reduced or limited by introducing damping into the structure. This can be done in one of two ways, either by introducing mechanical damping or by the use of materials of intrinsically high damping capacity. The inherent damping capacity of the majority of engineering materials is so low that it is usually swamped by the unavoidable structural damping due to friction at joints and in bearings and so on in the structure. However, materials such as cast iron have long been used because of their useful damping capacity, and new materials combining exceptionally high damping capacity with useful mechanical properties are now being developed. These materials must be selected and prepared with appropriate regard for their other properties, since their

resistance to corrosion or wear may be inferior to that of other materials of similar strength, but it is considered that recent developments will open up entirely new concepts in the application of high damping alloys in engineering design. This is illustrated by a comparison of the damping capacity of one of the recently developed alloys with that of some conventional metals in Fig. 1.

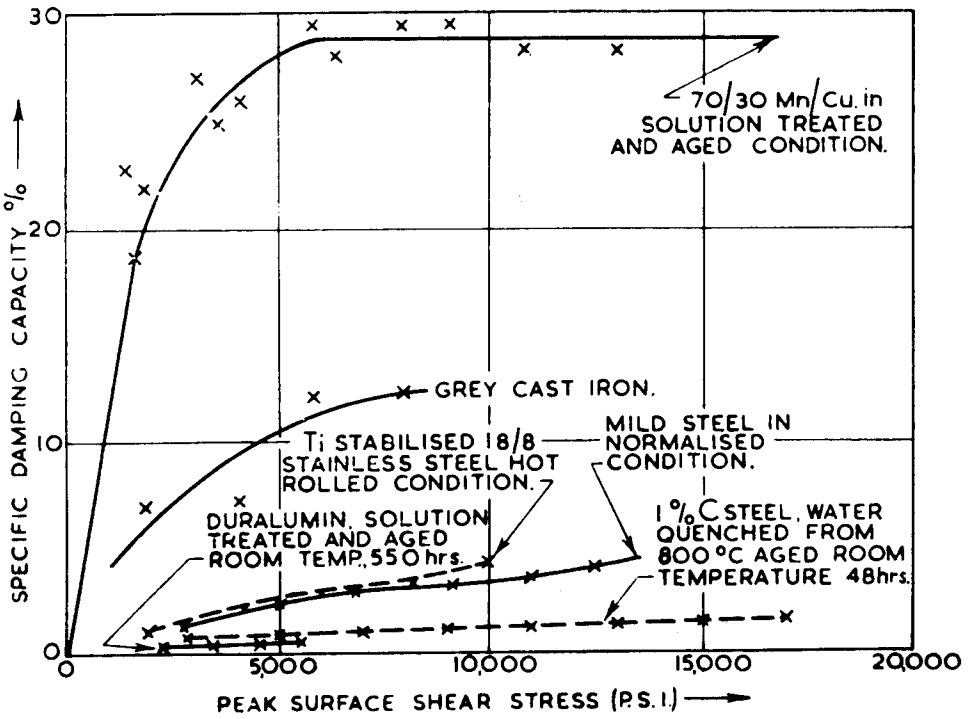

Fig. 1. Torsional damping capacity, at approximately 10 c/s, of a group of materials tested at room temperature.

Dimensional Stability

In large structures such as hulls, bridges, cranes, etc., small dimensional changes due to relief of residual stresses are unlikely to be of practical importance, but there are cases in which close dimensional stability must be maintained for prolonged periods of time. This is true of large turbine rotors and blades in which the tip clearance is necessarily small, small instrument components and structures such as waveguides for radar equipment, in which extremely close dimensional tolerances must sometimes be maintained in long, thin structures. In this type of application judicious selection of material and stress relieving-machining schedules may be essential. In welded structures the distortion resulting from welding must be allowed for. In general, a weld bead deposited on a fairly large component will be in a state of considerable longitudinal tension. In fact, welding is sometimes used as a means of correcting distortion, but this is a procedure which must be applied with caution. An example of unexpected contraction was provided when the damaged surface of a propeller shaft was repaired by welding and it was subsequently found that, due to the particular welding technique employed, the length of the shaft had decreased by 1 1/4 in.[6] In fact, a packing piece had to be inserted before it could be fitted back in the boat.

Compatibility

In nuclear reactors, the stringent precautions necessary to ensure compatibility between the fuel and canning materials and coolant has brought this term into prominence. Compatibility is also important in other parts of the circuit where corrosion, the ability to slide or rotate or the elimination of elements having long half lives following irradiation effects is essential.

In marine engineering one is always concerned with the effects of sea water. Sea water is an efficient electrolyte and electrically coupling dissimilar materials in the presence of sea water provides a familiar pattern of disaster as current flows from one material to the other, accompanied by dissolution of the anode. A classical case is that of a bronze propeller on a steel shaft fitted to a boat with a steel hull. Currents flow between the propeller and the neighbouring steel, and there is rapid pitting on the shaft and the hull unless suitable protective measures are employed. These may take the form of an efficient paint system on the hull and shaft, aided by local sprayed metal or glass cloth and resin protection of the shaft, cathodic protection from sacrificial zinc or magnesium anodes, or impressed current from carbon, platinum or lead-silver anodes.

Materials selection in cases where galvanic corrosion can occur is based mainly upon avoiding metallic contact between dissimilar materials which are both in contact with the water. This can sometimes be secured by avoiding dissimilar materials altogether, or by electrically insulating one from another, or by coating one material with another more compatible with the remainder of the structure, or by ensuring that the corrosion occurs in a place where it can be tolerated, or by selecting materials which are themselves mutually compatible.

Consideration of the relative potentials in sea water, as shown in Table 2,[7]

... potentials against saturated calomel electrode in sea-water at 25 deg C

(Abridged from DEF-5000)

Material	*Volts*
Magnesium and its alloys	−1 60
Zinc and its alloys	−1 05 to −1 10
Cadmium plate on steel	−0 80
Aluminium—alloy-clad DTD 687	−0 90
Cast aluminium (BS 1490, LM4, LM6, LM9)	
Wrought aluminium (BS 1470-11, 1C, NS3, N4, H10)	−0 75
Duralumin type (unclad) (BS 1470-77, H14-15)	−0 60
Iron and steel (not corrosion resisting)	−0 70
12% chromium BS 1630	−0 45
18% chromium 2% nickel BS 580	−0 35
18% chromium 8% nickel austenitic BS 970 En58, etc.	−0 20
Lead	−0 55
Terne plate	−0 50
Tin, tin-lead solders and tin plating on steel	−0 45 to 0 50
Chromium plating on steel or nickel-plated steel	−0 45 to 0 50
Copper and its alloys (brass, bronze, etc.)	−0 25
Nickel-copper alloys (BS 1526, 1529, 1532, 1535)	−0 25
Nickel plating on steel	−0 15
Silver solder BS 1485, Type 3	−0 20
Silver	0
Titanium	0

In the presence of an electrolyte, a material will corrode due to galvanic effects if it is electrically coupled to a metal listed below it in the above table

or some other appropriate environment, is of value in these cases, but it is not always possible to define a voltage bracket within which materials may safely be coupled together. This is due to a number of complicating factors, such as the effects of surface films and debris, polarisation phenomena and local variations in electrolyte composition. For instance, stainless steel and nickel may be active or passive, and their position in the table varies considerably between these conditions. Nevertheless, the table can be used as a basis for the intelligent selection of metals which must be coupled together and bridged by an electrolyte.

The ratio of the effective anode/cathode area is also important, since a small anode coupled to a large cathode may result in rapid and complete penetration at the anode. Similarly, the protection of a surface by a more noble material can be a dangerous practice if the surface is ever allowed to become wet. It is virtually impossible to ensure that the protective coating will never be locally penetrated and if this occurs the tiny anode exposed on the base material will suffer rapid corrosion stimulated by the large cathodic deposit on the surface. An example of this effect was provided by a propeller shaft in which a high strength hollow steel shaft was coated with a layer of electro-deposited nickel in a misguided attempt to prevent corrosion. Some fouling occurred and barnacles clinging to the surface of the nickel created local variations in oxygen concentration, setting up a galvanic cell between active and passive areas on the nickel, until it became perforated. These small holes, only 1/32 in. to 1/16 in. diameter, exposed the steel shaft to seawater, and the very small anode/cathode ratio between the small area of steel and the large surface area of the nickel resulted in rapid dissolution of the steel. Very large pits up to 1 in. in diameter and 1/4 in deep therefore developed underneath the nickel plating (Fig. 2) and no trouble was suspected until the shaft failed by fatigue (Fig. 3) from one of the larger pits. Similar effects can occur if noble hard facing alloys, such as those containing large quantities of nickel, chromium, cobalt and boron, are used to provide a hard

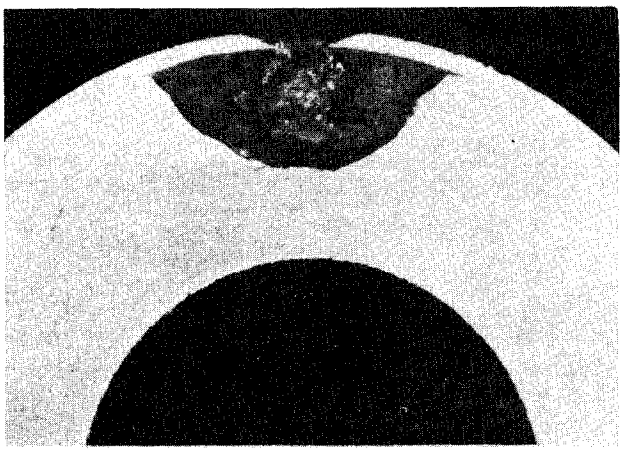

Fig. 2. Transverse section of shaft showing small hole in outer nickel plate which caused a large pit in the hollow steel shaft.

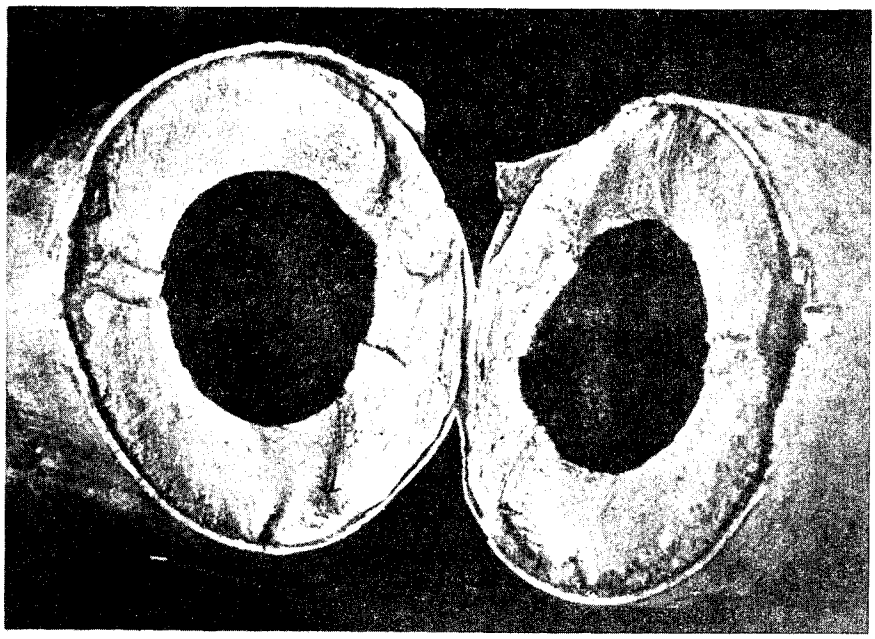

Fig. 3 (right). Fatigue failure of the nickel-plated shaft shown in Fig. 2. through one of the large pits.

surface on less noble metals such as steel. It is virtually impossible to ensure that such deposits will remain pore- and crack-free in service, and serious deterioration of the underlying metal is then inevitable if the surface operates in an electrolyte.

Compatibility is also important where materials must be in contact with food, and this factor must be considered in food factories, breweries, etc. The desirable conditions here are the elimination of widely dissimilar materials in situations in which they can be bridged by an electrolyte, and the elimination of toxic metals, contaminants and crevices. The design of containers with easily cleaned contours sometimes imposes particular manufacturing techniques and these, in turn, can exert an influence upon the selection of suitable materials, but in general problems of this sort are not particularly difficult.

Special Properties

These properties may be of minor importance, or they may form the corner-stone upon which the whole design must be based, as, for instance, if such attributes as the electrical properties or neutron transparency of the final component are of prime importance. The important considerations here are ensuring that the manufacturing technique, and forseeable deterioration effects in service, cannot destroy the vital functional properties of the component.

Cost Factors

An attempt to separate functional factors from those of cost must be artificial. But it does serve a useful purpose to attempt such a division, and for the purposes of this paper the following aspects are considered under the general heading of cost, since it is by control of these factors that the overall cost of a component or structure can be largely controlled.

Required Life

This is often a very delicate problem, in which the initial cost of the basic material and any protective treatments must be balanced against the cost of regular maintenance. Small components and relatively small assemblies may also be dealt with by designing for limited life and easy replacement, but large structures must be designed for long lives and easy repair of small areas as necessary. The most important considerations here are those concerned with the service conditions. Assuming that a material has been selected that will adequately meet the strength and similar functional requirements, its resistance to any particular forms of deterioration to which it may be subjected in service must now be assessed.

Fatigue

This is undoubtedly the most common single cause of failure in service and therefore justifies early mention. The important factors are that the choice of the material must be combined with design to eliminate stress concentrations, to ensure that the working stresses remain within safe limits, and to ensure that a minor unforseen mishap during fabrication or assembly cannot invalidate the safety of the component.

For instance, a large forging for a turbine rotor may be required in an alloy steel having considerable hardenability. If, somewhere between manufacture and final assembly, a stray weld flash is produced on the surface of such a rotor, a locally hardened zone, possibly cracked, and certainly with a most unpleasant local residual stress system will result, and this may well initiate fatigue failure. The responsibility of those concerned with design and materials selection therefore extends to safeguarding against accidents such as this.

Almost all fatigue failures start at the surface, and surface finish is therefore extremely important. This is related to the sensitivity of the basis material to stress concentrations, and therefore to the ultimate tensile strength of steels as illustrated in Fig. 4.[10] It is also related to the size of the section; in general, becoming more important as the size of the component increases.

Most engineering materials particularly steels, display an endurance limit (of the order of 50% of the ultimate tensile strength in rotating-bending) as shown in Fig. 5. This means that stress cycles below σ_L may be repeated indefinitely

Fig. 4 (below). Effect of surface condition on rotating-bending fatigue strength of steel. Polished 100

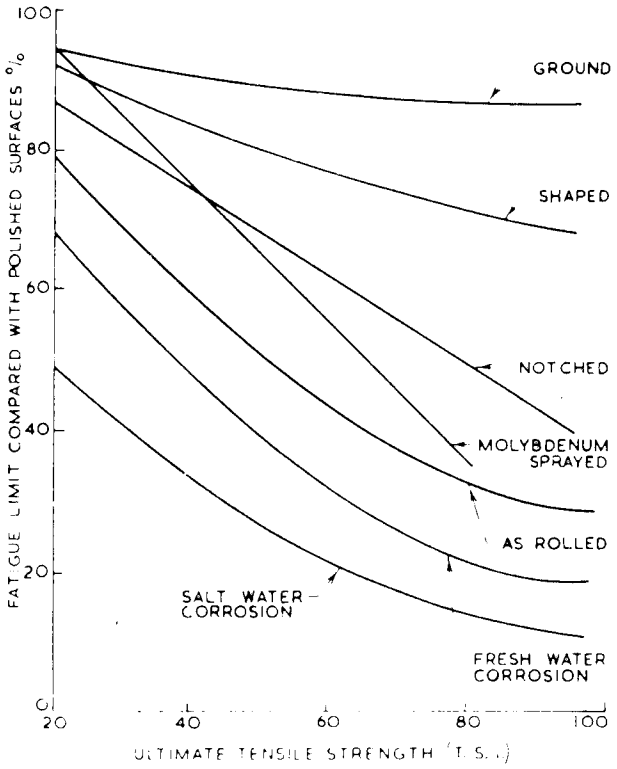

Fig. 5. Typical fatigue test characteristics.

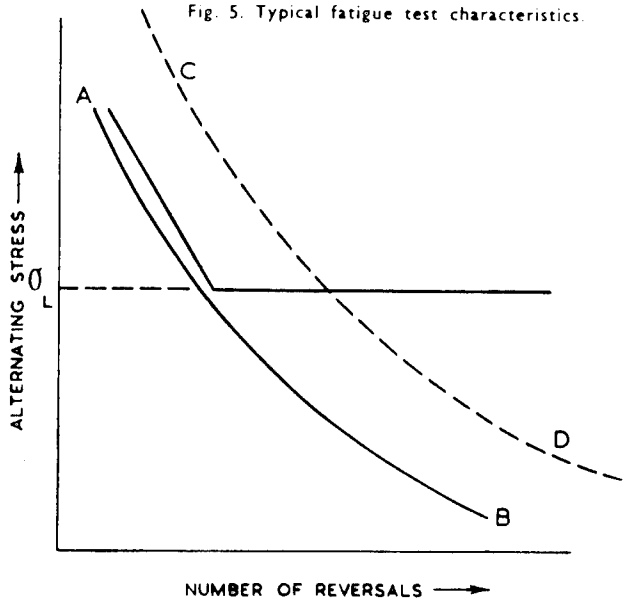

without causing failure. However, other materials, including many light alloys, display a dipping characteristic such as AB in Fig. 5, so that failure is inevitable in a finite time, even with very low stresses. A similar effect occurs when a material which normally exhibits an endurance limit is simultaneously cyclically stressed and exposed to a corrosive environment. Under these corrosion-fatigue

conditions there is no endurance limit, and the use of a material of higher intrinsic fatigue strength will only slightly improve the life as shown by CD in Fig. 5. The sort of damage which can be caused by corrosion-fatigue is illustrated in Fig. 6, in which a number of blunt fissures developed simultaneously

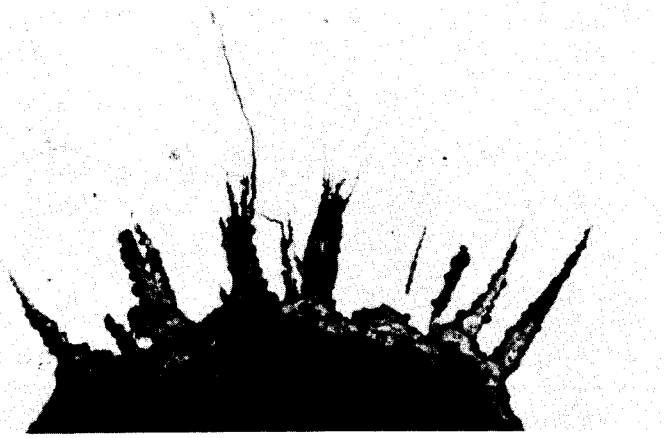

Fig. 6. Multiple corrosion-fatigue cracking at a thread root in a large stud.

at a thread root, until the stress-concentration conditions permitted a plain fatigue crack to develop and extend rapidly across the section. Failure under these conditions can only be prevented by preventing corrosion. It is most important to note that very minor corrosion effects can cause corrosion-fatigue failure, since it is only necessary for the corrosion to accompany the cracking, at the tip of the crack. Further information on fatigue is given in references 8, 9, 10 and elsewhere.

Corrosion

Corrosion is a major problem, particularly in marine and heavy process engineering, and it has been estimated that it costs £600,000,000 annually in the U.K. in damage, lost time and preventive measures. Much has been written on the subject [12, 13] and on preventive measures.

Corrosion may most easily be prevented by excluding the corrosive environment from the bare metal surface. In metals such as stainless steel, aluminum alloys and many copper-based alloys, the natural oxide film is sufficient protection for many applications; and, in the case of aluminum, can often be artificially thickened by anodising to resist more onerous environments. In more difficult cases an inert protective layer such as a properly applied paint system, or a mechanically strong glass fibre and resin system of protection, can often be used. Plastics coatings are also very useful, since they combine exclusion of the atmosphere and electrical insulation with abrasion resistance. Joints between dissimilar metals should be avoided, or insulated, or the electrolyte must be excluded from the surface of the anodic metal, if not from both surfaces. In any

protective system, the fail-safe philosophy must be observed in that it should be impossible for a small anodic area to be exposed (say as a result of mechanical damage to an inert protective coating) coupled to a large cathodic area, since this will cause very rapid pitting, and possibly perforation, of the anodic material.

Metallic coatings can be sacrificial, as in the case of Zinc on steel, so that local penetration is accompanied by corrosion of the coating instead of the substrate. But in cases such as this, electrode reversal effects must be borne in mind since, in hot water, the position is reversed for zinc on steel. Finally, cathodic protection[14] can be employed, either by using sacrificial anodes of zinc or magnesium, or impressed current from inert carbon or platinum or lead anodes.

Again, a judicious choice must be made between the initial material cost, the relative value and cost of protective treatments and regular maintenance, the frequency of repair and replacement and the amount of deterioration which can be accepted.

Corrosion is an aspect of materials selection in which it is remarkably easy to fall out of the frying pan into the fire. A simple example will serve to prove this point. Materials such as stainless steel rely upon an abundant supply of oxygen if they are to remain passive. The effect of marine fouling on a nickel-plated shaft has already been illustrated (Figs. 3 and 4), and in Fig. 7 the results of exposing a 1/8 in. thick sheet of austenitic stainless steel to sea water fouling for one year is displayed. Local fouling caused the perforation shown, and very severe wastage by crevice corrosion effects is evident across the line of the bolt holes, where the plate was in contact with its neighbour. Similar effects result wherever oxygen supply is restricted to such materials, as in glands and seals.

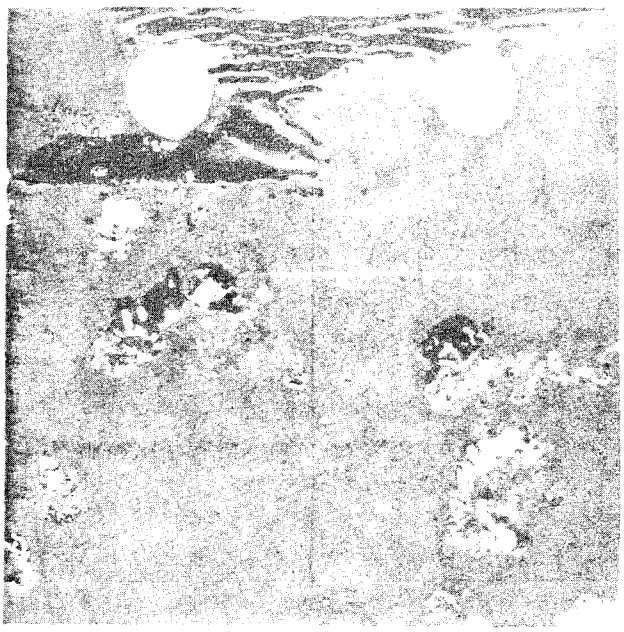

Fig. 7 (above). Severe wasting and penetration of a $\frac{1}{8}$ in. thick austenitic stainless steel after immersion in the sea for 12 months.

Stress Corrosion

Stress corrosion cracking, in which cracks develop with time in the presence of tensile stresses within the elastic limit of the material must also be considered, and typical failures are shown in Fig. 8. Caustic embrittlement is an example

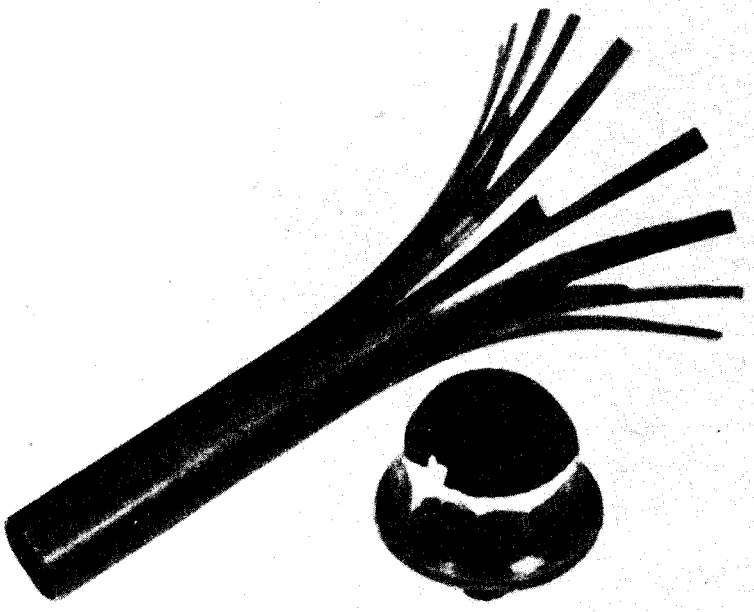

Fig. 8 (left). Typical stress-corrosion cracking in a brass tube and a brass lamp fitting.

often experienced in boiler drums. Interstices in riveted joints provide sites for the concentration of alkali to levels at which cracking occurs in the steel. This problem has now been almost eliminated by the adoption of welded steel drums. The season cracking of brass illustrated in Fig. 8 is another well-known example, but perhaps less is generally known of the stress corrosion cracking of stainless steels. Cracking associated with the grain boundary precipitation of carbides caused by welding non-stabilised stainless steels has been known for a long time, and this can be avoided by the selection of stabilised stainless steels containing titanium or niobium, or by heat treatment to ensure that the carbides are retained in solution. However, in the presence of high temperature and pressure water, a trace of chloride and oxygen can result in the cracking of stainless steels which are in no way sensitive to weld decay cracking and an example is shown in Fig. 9. This aspect is of obvious importance in the choice of materials for steam generating and associated machinery, whether conventional or nuclear, particularly for marine purposes, since it is virtually impossible to eliminate all traces of chloride contamination in plant required to operate for prolonged periods in a marine environment.

Brittle Fracture

With a decrease in temperature the mode of fracture of structural steels changes from an energy-absorbing tough and ductile fracture to a rapid brittle fracture of low energy absorption.[15] This may be demonstrated in a number of ways. One of these is illustrated in Fig. 10.

Fig. 9. Stress-corrosion cracking of austenitic stainless steel.

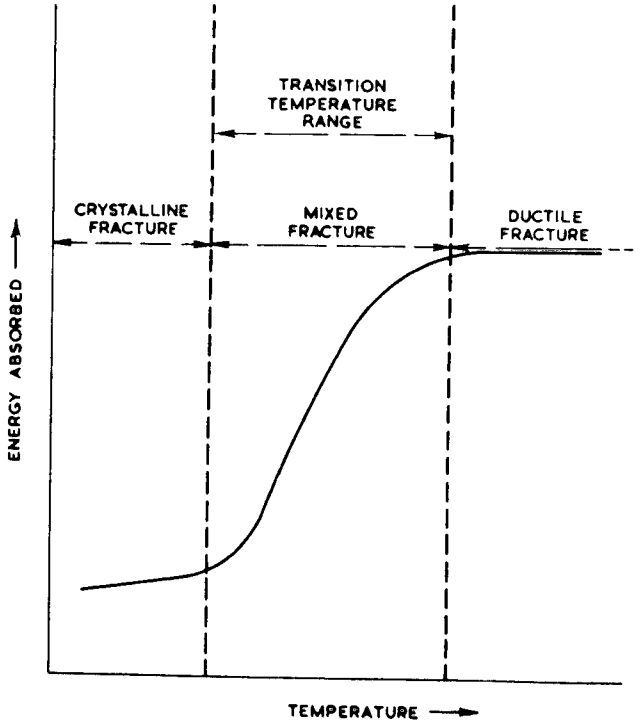

Fig. 10. Variation of energy absorption and fracture appearance with temperature of Izod or Charpy test.

These brittle failures may be catastrophic, and the failures of Liberty ships in the last war are well known.[16] Probably the best known of these is the U. S. S. Schenectady, which broke in half while fitting out in still water at an air and water temperature of 23 and 40 deg. F. respectively. The most recent case of disastrous failure in a ship by brittle fracture was that of the tanker World Concord built in 1952, which broke in half in the Irish Sea in 1954.

Despite publicity given to brittle fractures in ships, they are by no means confined to marine equipment, and an analysis presented by Boyd[17] listed the following known failures:

Type of Structure	Period	Number of Failures
Storage tanks	1919 to 1959	29
Bridges	1936 to 1951	21
Pressure vessels	1943 to 1958	10
Pipe lines	1950 to 1958	8
Turbo generators	1948 to 1958	13
Gas cylinders	1940 to 1943	58
Ships	1942 to 1946	32 major fractures
Ships	1946 to 1956	533 major and minor fractures in 182 ships

These fractures were usually associated with a low level of overall stress. In the case of the Schenectady the mean stress in the deck was only 4 1/2 t. s. i. The fractures were initiated from some kind of notch such as a sharp hatch corner, a weld defect or a metallurgical notch, and the fractures occurred instantaneously and with a loud report. These fractures are always characterised by lack of plastic deformation at the fracture and characteristic chevron markings which point to the origin or origins of failure. In selecting materials for use in applications where brittle fracture is a possibility, it is therefore necessary to integrate suitable design with materials of inherently low transition temperature. Difficulties sometimes arise when it is necessary for high-strength steels to be used in a welded structure, and special steels, electrodes and welding techniques have been developed for these purposes. Under irradiation by neutrons from a nuclear reactor considerable damage can be done to the structure of a metal and one effect of this is to raise the transition temperature of structural steels (Fig. 11). This aspect has therefore to be considered in the selection of materials

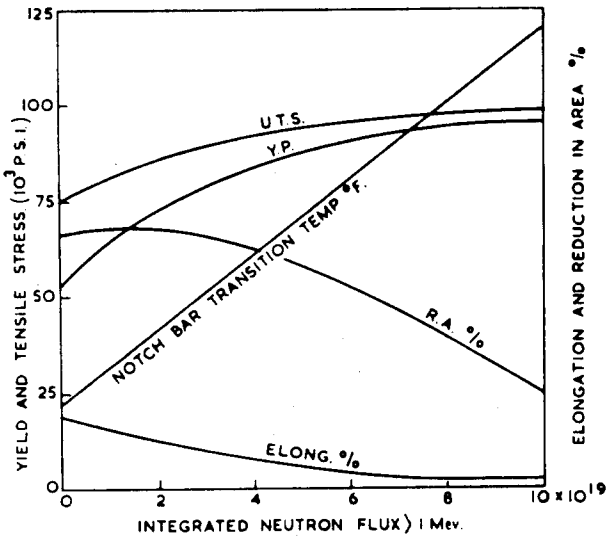

Fig. 11. Some effects of irradiation by fast neutrons on the properties of ASTM A212B steel (0·24% C, 0·81% Mn, 0·25% Si). ASTM grain size 5, irradiated at about 200 deg. F.[18]

for the pressure vessels of nuclear reactors. Plastic strain followed by ageing also raises the transition temperature of steel, and this can be important in the case of bolted assemblies in which the securing studs may be strained during tightening.

Creep

This may be defined as the continual deformation with time at constant stress and constant temperature, and a simple family of creep curves is illustrated in Fig. 12. At a given temperature, for any given material, the stress

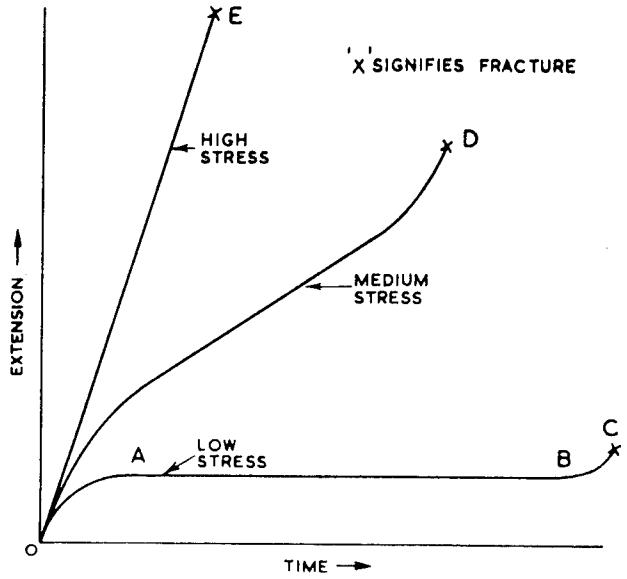

Fig. 12. Family of creep curves for a given material at a given temperature.

level will decide the creep rate. At low stresses this may fall essentially to zero, to give negligible creep rate over a long time as shown by AB, in which case fracture may finally occur at C with little total elongation. At higher stresses the creep rate will vary a little during the process, but never become zero, and failure will be accompanied by a shorter life time and greater elongation as the stress is increased.

Essentially therefore, in designing against creep, we are concerned with finite life, some deformation during service and the effects of excursions in temperature due to minor operational hazards, since a relatively small increase in temperature for a short time may produce a disproportionate creep extension in the component. It is also necessary to ensure that proper allowance is made for directional effects, since creep data are normally obtained and reported for tensile stress in the longitudinal direction of working of the material. Transverse creep properties are sometimes markedly inferior, and these properties are important in large rotor discs, internally pressurised tubes, and so on.

Thermal Shock

Thermal shock is a problem in components such as gas turbine blades, and is particularly difficult to combat with metals, due to their inherently high coefficients of expansion which set up correspondingly high strains under rapid temperature cycles. Fortunately, the ductility of metals permits much of these strains to be accommodated, with the result that brittle fracture is avoided, but repeated thermal shocks can cause thermal fatigue. Cermets and ceramics show promise in resisting thermal shock, due to their lower coefficients of thermal expansion, but pose other problems due to their brittleness. With the materials at present available the metallurgist can offer little solace to the designer beset by problems of thermal shock. The most effective remedy is to reduce the severity of the shocks by design, and forced slow heating and cooling before and after operation, in so far as this is possible.

Limitations due to Preferred Manufacturing Technique

The importance to be attached to manufacturing techniques varies enormously with the nature of the component involved and the quantities required. Common methods of fabrication involve casting, hot and cold working, welding and the use of pre-formed sections. In every case, full consideration of the problem should go beyond the facilities immediately available, and beyond previous practice. For instance, shell moulding and die casting can enable considerable savings to be made in machining, if the quantities involved justify the cost of the patterns and dies. Intricate yet lightly loaded components can often be produced as sintered metal compacts, with a spectacular reduction in cost. In one case known to the author, this method of manufacture reduced the cost of a component to 5.6% of the price of a similar component machined from a stamping.

The modern techniques of cold extrusion and ausforming also deserve to be more widely employed. The former enables mild steel and similar materials of moderate strength to be cold formed to intricate shapes and close tolerances, as in splined shafts, and also improves their properties to a point at which they can ometimes supplant low alloy steels. Ausforming, in which the steel is heavily deformed during an interrupted quench, whilst still in the austenitic condition results in an extremely fine martensitic grain size, enabling ultimate tensile strengths in excess of 150 t. s. i. to be achieved.

The major problems associated with choice of manufacturing technique are probably those of machinability and weldability. Difficulties are increased in both cases as the size of the component increases, especially if some of the fabrication must be conducted on site. It is a vital part of the initial materials selection procedure to anticipate these difficulties in advance and ensure that correct techniques are applied throughout all stages of fabrication and installation.

Availability and Preferred Method of Repair

These aspects often involve policy decisions, and may require to be considered under both normal and emergency conditions, depending upon the nature of the application. From a commercial point of view, direct replacement of all smaller items is normally the most efficient method. With larger components, however, and those performing a vital function in Service equipment, the ability for local emergency repair may be necessary. This usually influences materials selection through choice of suitable fabrication and assembly techniques.

Acknowledgement

This paper is published by permission of the Superintendent, Admiralty Materials Laboratory, but the views expressed are personal to the author.

References

1. D. Birchon, Engineering Materials & Design, 2, p. 417, 1959.
2. C. R. Soderberg, Metallurgical Reviews, Institute of Metals, 1, p. 31, 1956.
3. G. Gerard, Journal of Metals, 31, p. 201, 1961.
4. R. T. Allsop, Metallurgia, 60, p. 39, 1960.
5. N. L. Svenson, Engineering, 191, p. 154, 1961.
6. D. Birchon, Welding & Metal Fabrication, 27, p. 17, 1959.
7. DEF-5000 General Requirements for Service Telecommunication Equipment, H. M. S. O., London, 1955.
8. C. E. Phillips and A. C. Low, Trans. Inst. Mar. Engrs., 71, p. 357, 1959.
9. Metal Fatigue, J. A. Pope, Chapman & Hall, London, 1959.
10. Fatigue of Metals, R. Cazaud and A. J. Fenner, Chapman & Hall, London, 1960.
11. D. Birchon, Metallurgia, 58, p. 273, 1958.
12. R. W. Henke, Materials & Methods, 42, p. 119, 1955.
13. The Corrosion & Oxidation of Metals, U. R. Evans, Arnold, 1960.
14. Cathodic Protection, J. H. Morgan, Leonard Hill, London, 1959.
15. Brittle Behaviour of Engineering Structures, E. R. Parker, Chapman & Hall, London, 1957.
16. R. T. Young, Brit. Weld. Jnl., 8, p. 43, 1961.
17 G. M. Boyd, Conference on Brittle Fracture, Cambridge, September 1959.
18. J. C. Wilson and R. G. Berggren, Proc. A. S. T. M., 55, p. 689, 1955.

PROGRAM
Wednesday, May 10, 1967

8:00 Registration

8:30 Official Welcome
Mr. F. S. Williams
P-4 Chairman

Special Address
Mr. J. Barret J. C.
Executive Member Subgroup P

Introductory Lecture
Professor R. McCauley
Ohio State University

SESSION I
9:00-11:10 Case Histories
Chairman: P. J. Todkill, Canada-National Leader
Co-Chairman: J. A. Holloway, AF Materials Laboratory

(1) Selection/Development of NDT for Quantitative Prediction of Materials Performance
C. H. Hastings
AVCO, Space Systems Division

(2) Stress Wave and Fracture of High Strength Metals
G. S. Baker and A. T. Green
Aerojet-General Corporation

(3) Correlation of Testing with Service Behavior of Rubber Components
W. C. Wake
Rubber and Plastics Research
Association of Great Britain

(4) Nondestructive Techniques for Segregating 20MM Machine Gun Barrels Having Low Impact Qualities
E. H. Rodgers
U.S. Army Materials Research Agency

(5) Anisotropy Measurements and Their Relationship to the Deep Drawing of the Hawk Missile Oil Accumulator Housing
R. M. Colton
U.S. Army Materials Research Agency

11:10-11:30 Panel-Discussion

11:30-13:00 Lunch

SESSION II Environmental Effects
13:15-15:45 Chairman: D. A. Dukes, U.K.-National Leader
Co-Chairman: J. A. Kies, U.S. Naval Research Laboratory

(1) Stress Corrosion and Corrosion Fatigue Behavior of 250 KPSI Maraging Steel in Sea Water
R. D. Barer
Pacific Naval Laboratory
Canada

(2) Cavitation Erosion Facilities and Developments at the U.S. Applied Sciences Laboratory
J. Z. Lichtman, D. H. Kallas and A. Rufolo
U.S. Naval Applied Sciences Laboratory

(3) Unsolved Problems in Predicting the Behavior of Concrete
B. Mather
U.S. Army Engineer Waterway Experiment Station

(4) The Cantilever Beam Stress Corrosion Test - A New Philosophy in Corrosion Testing
M. H. Peterson
U.S. Naval Research Laboratory

(5) Catastrophic Failure of an Hydraulic Accumulator
F. R. Larson and F. L. Carr
U.S. Army Materials Research Agency

15:45-16:15 Session-Panel Discussion

Thursday, May 11, 1967

SESSION III — Structural Components and Composites
8:30-10:45

Chairman: G. A. Darcy
U.S.-National Leader
Co-Chairman: R. R. Whymark
Tracor Inc.

(1) Some Factors in the Selection and Correlation of Non-Destructive Testing Techniques
D. Birchon
Admiralty Materials Laboratory
Holton Heath, U.K.

(2) Relationships Between Specimen Performance and Structure Performance in Low-Cycle Fatigue
M. R. Gross
U. S. Navy Marine Engineering Laboratory

(3) Evaluation of High Performance Rocket Motor Cases Using Sub-Scale Precracked Models
C. M. Carman
Pitman-Dunn Research Laboratory
Frankford Arsenal

(4) The Characterization of Composite Material Defects to Allow Correlation of Nondestructive Testing with Systems Performance
G. Martin
North American Aviation
Los Angeles Division

(5) Low Voltage and Neutron Radiography Techniques for Evaluating Boron Filament/Metal Matrix Composites
J. A. Holloway and H. Berger
W. F. Sturke — Argonne National Laboratory
Air Force Materials Laboratory

10:45-11:15 — Session-Panel Discussion

11:30-13:00 — Lunch

SESSION IV — Methods, Techniques and Instrumentation

13:15-15:45

Chairman: N. E. Promisel
Materials Advisory Board

Co-Chairman: E. Roffman
Secretary-Panel 4
Frankford Arsenal

(1) Designing Nondestructive Tests to Define Material Characteristics
R. S. Sharpe
Nondestructive Testing Centre
Atomic Energy Research Establishment
U.K.

(2) Detection of Concealed Cracks Beneath Fasteners by Acoustic Means
R. M. Schroeer
ARVIN Systems Inc.

(3) Is There Any Correlation Between Flaws and Service Performance?
R. Halmshaw
Royal Armament Research and Development Establishment
U.K.

(4) An Engineering Basis for Establishing Radiographic Acceptance Standards for Porosity in Steel Weldments
H. Greenberg
Westinghouse Research Laboratories

(5) New NDT Techniques for Aerospace Materials and Structures
E. J. Kubiak
General American Transportation Corp.

15:45-16:15 — Session-Panel Discussion

S O C I A L H O U R
Thursday Evening

Time: 18:00 - Buffet Dinner - Officers Club

Speaker: Dr. J. B. Rhyne, Duke University

Friday, May 12, 1967

SESSION V — Workshop on Unsolved Problems and Novel Approaches

08:30-10:45

Chairman: L. E. Samuels
Australia-National Leader

Co-Chairman: C. H. Hastings
AVCO Space Systems
Division

(1) A Coordinative Effort to Solve Industrial N.D.T. Problems in Great Britain-A 31 Me V Betatron Study of the Production of High Integrity Steel Castings
A. Nemet
Anthony Nemet Company
U.K.

(2) Effect of Mechanical Properties on the Velocity of Ultra-Sonic Waves
E. W. Kammer
U. S. Naval Research Laboratory

(3) New Approaches for Studying Marine Fouling Using Laboratory Reared Organisms (Introduction and Movie)
A. Freiberger and D. H. Kallas
U. S. Naval Applied Sciences Laboratory

(4) Process Control of the Dynamic Crushing Stress Property of Expanded Paper Honeycomb
M. Budnick
U. S. Army Natick Laboratories

Short Prepared Discussions and Supplemental Statements

10:45-11:20 Conference Summary

11:30 Lunch

13:30 Adjournment

LIST OF SYMPOSIUM PARTICIPANTS

L. H. Adam	Frankford Arsenal
G. S. Baker	Aerojet General Corp.
R. D. Barer	Pacific Naval Laboratory, Canada
J. C. Barrett	Office, Director of Defense R & E
A. A. Benderly	Harry Diamond Laboratories
T. Bennett	Chanute Air Force Base
D. Birchon	Admiralty Materials Lab., U. K.
A. Birk	Automation Industries
Mr. Boisvert	SAAMA, Kelly Air Force Base
M. L. Budnick	U. S. Army Natick
C. M. Carman	Frankford Arsenal
F. L. Carr	Army Materials Research Agency
R. M. Colton	Army Materials Research Agency
R. Coy	University of Dayton, Research Institute
G. A. Darcy	Army Materials Research Agency
D. E. Driscoll	Army Materials Research Agency
W. A. Dukes	Ministry of Aviation, U. K.
C. H. Dyer	Navy Ordnance Lab.
F. H. Edwards	Bragg Laboratory, U. K.
L. L. Forkas	Martin-Marietta Corp.
C. Gardner	Southwest Research
M. Goldstein	Martin-Marietta Corp.
I. Greenberg	Westinghouse R & D Center
R. E. Griggs	DeLaval Turbine Inc.
R. Gross	Marine Eng. Lab.
R. Halmshaw	Royal Armament R & D Establishment, U. K.
C. H. Hastings	AVCO Corp.
H. P. Hatch	Army Materials Research Agency
E. Hoffman	Frankford Arsenal
J. A. Holloway	Air Force Materials Laboratory
D. H. Kallas	Naval Applied Science Laboratory
L. G. Klinker	Army Research Office
W. Koster	Metcut Research Associates
F. J. Kubiak	General American Transportation Co.
G. Martin	North American Aviation Inc.
B. Mather	Army Engineer - Waterways Experiment Station
K. Mather	Army Engineer - Waterways Experiment Station
R. McCauley	Ohio State University
J. M. Miller	Army Weapons Command
J. Mills	Chanute Air Force Base
K. W. Moore	Royal Canadian Navy, Canada
A. Nemet	A. Nemet Co., U. K.
M. H. Peterson	Naval Research Laboratory
J. Plexico	Army Missile Command
N. E. Promisel	Materials Advisory Board
E. H. Rodgers	Army Materials Research Agency
L. E. Samuels	Defence Standards Labs. Australia
D. Seltzer	Martin-Marietta Corp.
R. M. Schroeer	Arvin Systems, Inc.
R. S. Sharpe	Nondestructive Testing Centre, U. K.

R. Socky	General Electric Company
H. Sugiuchi	Martin-Marietta Corp.
P. J. Todkill	Dept. of Energy, Mines and Resources, Canada
W. J. Trapp	Air Force Materials Laboratory
W. J. Van Arnhem	Army Material Command
W. C. Wake	Rubber and Plastics Research Association of Great Britain, U. K.
F. S. Williams	Naval Air Eng. Center
R. R. Whymark	Tracor, Inc.